

VRIJE UNIVERSITEIT

**Modelling of fault reactivation potential and
quantification of inversion tectonics in the southern
Netherlands**

ACADEMISCH PROEFSCHRIFT

ter verkrijging van de graad van doctor aan
de Vrije Universiteit Amsterdam,
op gezag van de rector magnificus
prof.dr. T. Sminia,
in het openbaar te verdedigen
ten overstaan van de promotiecommissie
van de faculteit der Aard- en Levenswetenschappen
op donderdag 30 september 2004 om 13.45 uur
in de aula van de universiteit,
De Boelelaan 1105

door

Géza Wórum

geboren te Debrecen, Hongarije

promotor: prof.dr. S.A.P.L. Cloetingh
copromotor: dr. J.D. van Wees

*Egy fejezet sem lenne elég,
hogy megköszönjem Neki én
a kitartást és áldozatot,
mellyel támogatott Virikém.*

*Hogy is tudtam volna itt én
túlélni négy éven át
nélkülözve feleségem
szerelmét és támaszát.*

*Hisz vigasztalt ha búslakodtam,
örült Ő ha örültem,
rugdosott ha lustálkodtam,
s kiházott ha merültem.*

*Társam Ő, e kis leányka
mindenem e világon,
e könyvet Neked dedikálom
drága kicsi Virágom.*

The research reported in this thesis was carried out at:

Vrije Universiteit Amsterdam
Faculty of Earth and Life Sciences
Department of Tectonics
De Boelelaan 1085
1081 HV Amsterdam
The Netherlands

and

Nederlands Instituut voor Toegepaste Geowetenschappen TNO (TNO–NITG)
National Geological Survey
Department of Geo–Energy
Princetonlaan 6
3584 CB Utrecht
The Netherlands

Financial support was provided by TNO–NITG, National Geological Survey

The publication of this thesis was sponsored by:



TNO-NITG
National Geological Survey



Netherlands Research Centre
for Integrated Solid Earth Science



Vrije Universiteit
Amsterdam



Nederlandse Aardolie
Maatschappij BV

Netherlands Research School of Sedimentary Geology (NSG)
Publication no. 20040606

ISBN 90-9018395-7

© Copyright 2004, G. Wórum

Reading committee: dr. Ronald T. van Balen
dr. Fred Beekman
prof. dr. Harry Doust
dr. Matthias Gölke
dr. William Sassi
dr. Paul Reemst

Typeset with L^AT_EX 2_ε open source

Table of Contents

Acknowledgements	vii
Összefoglalás	ix
Summary	xiii
Samenvatting	xvii
1 Introduction and scope of the thesis	1
1.1 Tectonic evolution of the Netherlands	4
1.2 Scope and outline of the thesis	8
2 Tectonic stresses and fault reactivation: theory and modelling	11
2.1 Stresses in the lithosphere	12
2.1.1 Sources of tectonic stresses	12
2.1.2 Classification of tectonic stresses: the tectonic style	13
2.1.3 Depth dependence of the stress field in the upper crust	15
2.2 Reactivation of faults: theory	17
2.3 Reactivation of faults: modelling	18
2.3.1 The Wallace–Bott approach: an overview	19
2.3.2 A 3–D modelling approach	21
2.3.3 Synthetic examples of the slip tendency analysis	23
2.4 Discussion	27
2.4.1 Reliability of the calculated resolved stresses	27
2.4.2 Reliability of the prediction of fault reactivation	29
3 3–D slip tendency analysis in the Roer Valley Rift System (SE Netherlands)	31
3.1 Introduction	32
3.2 Modelling assumptions	33
3.2.1 Stress field	33
3.2.2 Mechanical parameters	34
3.3 Modelling results	35
3.3.1 Slip tendencies	37

3.3.2	Slip directions	39
3.3.3	Synthesis of the results	40
3.4	Discussion	40
3.4.1	Reliability of the results	40
3.4.2	Comparison of the results with observations	41
3.4.3	Comparison with other studies	44
3.5	Conclusions	45
4	Pre-Neogene controls on present-day fault activity in the southern Netherlands: role of variations in fault orientation in a uniform low-stress regime	47
4.1	Tectonic setting and evolution of the WNB–RVRS basin system . . .	49
4.1.1	Late Palaeozoic–Mesozoic	50
4.1.2	Tertiary	52
4.1.3	Quaternary	54
4.2	Comparison of fault patterns	54
4.2.1	Mesozoic fault pattern	54
4.2.2	Neogene–Quaternary	58
4.3	Neotectonic implications: slip tendency analysis	59
4.3.1	Input data	60
4.3.2	Analysis of the calculated slip tendency patterns	62
4.4	Discussion and conclusions	64
4.4.1	Possible causes of different stress fields	64
4.4.2	Possible causes of different slip thresholds	67
5	Quantitative reconstruction of Late Cretaceous–Tertiary erosion in the West Netherlands Basin	69
5.1	Methodology	71
5.2	Burial anomaly analysis in the West Netherlands Basin	74
5.2.1	Chalk (Houthem and Ommelanden Formations)	74
5.2.2	Holland Formation	78
5.2.3	Vlieland Claystone Formation	80
5.2.4	Lower Jurassic clays (Sleen and Aalburg Formations)	80
5.3	Geometric reconstruction of the amount of erosion	84
5.4	Discussion	88
5.4.1	Pattern of erosion	88
5.4.2	Magnitude of erosion	90
5.5	Conclusions	94
6	Implications of continuous structural inversion in the West Netherlands Basin for understanding controls on Palaeogene deformation in NW Europe	95
6.1	Data and methodology	97

6.1.1	Stratigraphy	97
6.1.2	Seismic data and mapping	98
6.1.3	Well data	99
6.2	Results	100
6.2.1	Spatio-temporal reconstruction of the Eocene tectonic movements	100
6.2.2	Quantitative reconstruction of the amount of erosion	105
6.3	Discussion	109
6.3.1	Differential subsidence vs. compaction	109
6.3.2	Characteristics and timing of inversion	111
6.3.3	Origin of the inversion	114
6.4	Conclusions	115
7	Synthesis and additional remarks	117
7.1	Fault modelling	117
7.2	Quantification of inversion tectonics	119
7.3	Future research perspectives	121
	Appendix A: Geometric modelling of faults	123
A.1	The midline method	125
A.1.1	Principles of the midline method	125
A.1.2	Implementation of the midline method	126
A.1.3	Disadvantages and errors of the midline method	127
A.2	The direct method	132
A.2.1	Principles of the direct method	133
A.2.2	Errors of the direct method	134
A.3	Summary, 3-D digital fault database of the Netherlands	136
	Appendix B: Colour plates	137
	References	147

List of Figures

1.1	Mapsheets of the “Atlas of the Deep Subsurface of the Netherlands” by TNO-NITG	2
1.2	Simplified litho-chronostratigraphic chart of the Netherlands	3
1.3	Late Palaeozoic geographical setting of NW Europe	5
1.4	Main Mesozoic tectonic features of the southern North Sea region	7
2.1	Andersonian classification of the stress regimes	14
2.2	Depth dependence of the principal stresses in the upper crust	16
2.3	Forces acting along a fault surface element	22
2.4	Reactivation analysis of a fictional fault system in a synthetic strike slip stress scenario	24
2.5	Sensitivity plot of a synthetic planar fault as the function of the σ_v/σ_H and σ_h/σ_H ratios	25
2.6	Sensitivity plot of a synthetic planar fault as the function of the σ_v/σ_H ratio and the orientation of σ_H	26
3.1	Main structural elements of the Roer Valley Rift System	33
3.2	Average calculated slip tendency as the function of the σ_h/σ_H ratio	37
3.3	3-D perspective view of the slip tendency patterns	38
3.4	3-D perspective view of the slip direction patterns	39
3.5	Depth map of the base Quaternary horizon and its gradient map	42
4.1	Main tectonic features of the Netherlands and its surroundings after the Variscan orogeny	48
4.2	Tectonic subsidence in the WNB–RVG system since the Late Palaeozoic	49
4.3	Thickness map of the lower Jurassic Altena Group	50
4.4	Thickness map of the Neogene	53
4.5	Depth map of the base Quaternary	55
4.6	Compiled map of the active Early–Middle Mesozoic faults	57
4.7	Map of the active Neogene and Quaternary faults of the study area	59
4.8	Available 3-D fault models in the study area	60
4.9	Calculated 3-D slip tendency patterns of the modelled faults	63
4.10	Tectonic features of the Rhenish Massif area since the Late Oligocene	66

5.1	Pre-Tertiary geological map of the onshore West Netherlands Basin	71
5.2	Evolution of interval velocity with burial/erosion	72
5.3	Interval velocity analysis of the Chalk Group	75
5.4	Comparison of chalk compaction trends	77
5.5	Interval velocity analysis of the Holland Formation	79
5.6	Interval velocity analysis of the Vlieland Formation	81
5.7	Interval velocity analysis of the Altena Group	82
5.8	Geometric restoration of the amount of erosion	85
5.9	Map of the amount of estimated erosion	88
5.10	General pattern of erosion in the West Netherlands Basin	93
6.1	Main Mesozoic and Tertiary tectonic features of the Netherlands and its surroundings	96
6.2	Palaeogene litho-chronostratigraphic chart for the West Netherlands Basin area	98
6.3	Characteristic seismic section through the northern flank of the Voorne Trough	101
6.4	Thickness analysis of the Lower Eocene and Middle Eocene Units	102
6.5	Tilting rate of the base Lower North Sea Group reflector throughout the Eocene	104
6.6	Burial anomaly analysis of the Landen Clay Formation	106
6.7	Geometric reconstruction of the Late Eocene erosion	108
6.8	Jurassic–Eocene tectonic subsidence of four synthetic wells	110
6.9	Location and main tectonic features of the Wessex- and Belgian Basins	113
A.1	The main steps of geometrical fault modelling in GOCAD	124
A.2	Principles of the midline method	126
A.3	Flowchart of the geometrical fault modelling	127
A.4	Example of an unrealistic fault model resulting from an inconsistent input data set	128
A.5	Uncertainty of the midline method	129
A.6	Artefacts of the calculated 3–D midlines of a branching fault system	130
A.7	Lateral smoothing of fault trace lines in ArcInfo	131
A.8	The effect of processing parameters on a 3–D midline	132
A.9	The main steps of fault modelling using the direct method	133
A.10	Errors of the direct method	134
A.11	Available 3–D fault models in the southern Netherlands	134

Acknowledgements

I hardly believe it. Here I sit, all the chapters are written and I am busy with the *Acknowledgements*. **My thesis is finished**. This success, however, is not only my own, since many people contributed enormously to this achievement. The next few paragraphs are dedicated to them and to those who made this four years unforgettable.

First and foremost, I would like to give my deepest gratitude to my promotor **Prof. Sierd Cloetingh** for providing me the opportunity to carry out this research in his “Tecto Group”. In addition, I owe him a confession: Sierd, I think you were right when you said “a healthy patient does not need surgery”. During these four, sometimes difficult years, I did find my way to be a capable researcher as you had foreseen it.

I am also very thankful to my supervisors at TNO–NITG, **Jan-Diederik van Wees** and **Henk Pagnier**, who came to my aid when the project was in trouble in the beginning of the research. The effort and ideas of the JD as well as his initiation of this project are very much appreciated. I am very grateful to Henk, who always gave me every possible scientific and bureaucratic assistance to keep the wheels turning. Henk, I consider him to be a very good boss and one of the best managers I have ever encountered.

The story of this Ph.D. started much earlier than April 2000. The whole idea of “Lets send another Hungarian into Amsterdam” came from **Prof. Frank Horváth**, to whom I am very grateful. The devotion of **Anco Lankreijer** to spin up the bureaucratic wheels of the VU and to provide a bridge between Budapest and Amsterdam is very much appreciated. Without him I could not even get close to Amsterdam.

This paragraph is dedicated to **Gábor Bada**, **Ronald van Balen** and **Laurent Michon**, who have enormously contributed to the scientific quality of this work. They spent significant amount of their valuable time to read, correct, and constructively criticize my work, as well as to initiate new ideas. I dare to say that they were my “second supervisors” and without their selfless assistance today I would be nowhere near here. I thank Ronald also for taking part in the reading committee and Gábor for keeping the contact with Anco in pre-Amsterdam times.

During these years in Holland beside the home, where I returned every day to sleep, I was also the resident of two other “homes”: the Tectonic Department of the VU and its “neighborhood” and the Geoenergy Department of TNO–NITG. The

fellow residents (both permanent and temporal) of these homes provided a very pleasant working atmosphere and significantly improved the quality of my being in Holland. From the VU my special thank goes to **Jorge, Stephanie, Tristan** (you always helped even when you couldn't), **Muriel, Jeroen** (thanks for letting us "living" at your place), **Liviu, Mihai, Daniel, Florian, Alex, Bri, Vale, Jurgen, Barbara, Glen, Heiko, Liesbeth, Sam, Lotte, Giovanna, Ute** and **Margot**, with whom the fun often continued even outside the gates of the VU. The "space party", the "80's borrel", the Bokbier festival, the 11 Kroegentocht-s, the birthdays, the Carnivals and the going-outs will never be forgotten. From the Tecto Group I have pleasant memories of **Alwien** and **Anna** (without you ladies I would have been lost in the bureaucratic dungeon of the VU), **Aline, Bernd, Cees, Charles, Christophe** (thanks for the fruitful discussions on the JGR paper), **Dick, Dimitrios, Ernst, Fred** (thanks for your contribution in the reading committee), **Harm, Harry D.** (your contribution in the reading committee is very much appreciated), **Harry S., Giovanni, Ingrid, Jolante, José, Karen** (thanks for being a helpful geological dictionary for the thesis), **Nico** (thanks for the rulers and calculators :-)), **Randall, Reini, Sevgi,** and **Stephan**.

Egy külön bekezdést szeretnék szentelni a magyar különítménynek. Bár nagyon jól éreztem magam a nemzetközi társaságban is, a magyaros főzések, a társalgás "feltétel nélküli megértése" nagyon hiányzott nekem is és Virágnak is. **Gábor, Windy, Zsófi, Laci** és kis családja felejthetetlen élményekkel (Queensday, Tikibad, Twiske) és estékkel (BBQ az erkélyen) gazdagítottatok bennünket, amiért nagyon hálás vagyok nektek. Felétek úgy hiszem nem hangzik közhelyként, hogy "majd még látjuk egymást". A kellemes esték és vacsik remélem folytatódnak.

From the staff of NITG I got enormous amount of help. I would like to mention **Hans Doornenbal, Ed Duin, Carla Elmers, Ben Wolters, Nora Parker, Eric Simmelink, Frank van Bergen, Ad Meinster** and **Robert-Jan van Leeuwen**, without whom I think this research would have been impossible. I have pleasant memories of **Bogdan, Cees, Cobie, Eric, Frank, Ipo, Jan, Joost, Lia, Manuel, Petra, Rob**, the fellow Ph.D. students **Allard, Iwan** and **Gesa** and of the other members of the Geoenergy group, many of whom unfortunately I did not get the chance to get more acquainted with.

Összefoglalás

A holland olajipar által mért és időközben nyilvánossá vált földtani adatok számos akadémiai illetve társadalmi fontosságú kutatási lehetőséggel kecsegtetnek. A Holland Geológiai Szolgálat által a rendelkezésemre bocsátott adatokat felhasználva a doktori dolgozatomban földtani vetők reaktivációjának három dimenziós modellezését, illetve Dél-Hollandia késő mezozoos-tercier inverziós/eróziós fejlődéstörténetének rekonstrukcióját tűztem ki célul.

A földtani kutatási adatokon alapuló 3-D geometriai vetőmodellek kiváló lehetőséget nyújtanak a vetők egy adott tektonikai feszültségtérben történő reaktivációjának tanulmányozására. A dolgozat első felében egy újonnan kifejlesztett numerikus módszer kerül bemutatásra, melynek segítségével földtani vetők reaktivációjának térbeli mintázatát határozhatjuk meg. A tektonikai feszültségtérre vonatkozó ismereteket figyelembe véve a modellezés során a vető geometriáját leíró 3-D felület mentén ébredő nyíró- és nyomófeszültségek hányadosa (csúszási tendencia) illetve a nyírófeszültség iránya kerül kiszámításra. Habár a számított feszültségek a valós feszültségeket csak első rendben közelítik, a 3-D csúszási tendencia mintázatnak valamint a vető mentén uralkodó súrlódási együtthatónak az összehasonlítása fontos információkat szolgáltat az adott vető reaktivációjának valószínűségéről.

A bemutatott új módszert az aktív tektonikai mozgásokkal jellemzett Ruhr-völgyi Rift Rendszer (Roer Valley Rift System: RVRS) területén térképezett vetőkre alkalmazom. A modellezési eredményekből kitűnik, hogy a vizsgálati területen észlelt jelenkori vetőaktivitás (földrengések, negyedidőszaki deformáció) megmagyarázható a súrlódási együtthatók és a tektonikai feszültségnagyságok egy ésszerű tartományán belül is. Ezen felül, megfelelő egyezés adódott a modellezett illetve a földrengés fészekmechanizmusokból számított csúszási irányok között. Ezek az eredmények arra utalnak, hogy a földkéreg legfelső tartományában észlelt vetők alkalmasak a reaktivációs paraméterek meghatározására még a szeizmogén zóna alsóbb tartományaira vonatkozóan is. Az eredmények arra is rámutatnak, hogy a vetők hierarchiája és a regionális tektonikai viszonyok a vetőreaktivációban nagyon fontos szerepet játszanak.

A Nyugat Holland Medence (West Netherlands Basin: WNB) a RVRS-től északnyugatra helyezkedik el, melyek együtt Hollandia legjellegzetesebb tektonikai egységét alkotják. A két medencének közös tektonikai eredete és nagyon hasonló Meozoos fejlődéstörténete van. A neogén-kvarter fejlődéstörténetük azonban szembetűnően különböző. Míg a WNB tectonikusan/szeizmikusan inaktív és egyenletes neogén-

kvarter sülyedéssel jellemzett, addig az RVRS területén a késő oligocén óta vetőreaktivációval illetve intenzív szeizmicitással járó lemezen belüli deformáció zajlik. Figyelembe véve a jelenlegi ÉK-DNy-i extenziót valamint a két medence hasonló orientációját és mezozoós fejlődéstörténetét, szembetűnően különböző neotektonikai mozgások jelenléte nem lenne várható. Részletes tektonikai vizsgálatok azonban rámutatnak, hogy (1) a palaeozoós-mezozoós tektonikai szerkezetek jelentős hatást gyakorolnak a medencerendszer harmad- és negyedidőszaki deformációjának stílusára; (2) az RVRS-ben a jelenlegi vetőaktivitás már korábban kialakult vetők reaktivációjához köthető; (3) a mezozoós vetőirányok kis mértékben eltérnek a két medencében. Felhasználva az új vetőmodellezési módszert arra keresem a választ, hogy a vetők orientációjának különbözőségei eléggé nagyok-e ahhoz, hogy azok mentén jelentősen különböző erők ébredjenek egyazon feszültségtér hatására. A modellezési eredmények fontos információkat szolgáltatnak az RVRS területén található aktív törérendszer eredetére vonatkozóan is. A vizsgálat a medencerendszer területén térképezett vetők hasonló viselkedését valószínűsíti laterálisan homogén regionális feszültségtér esetén. Mindez ellentmondásban van az észlelt vetőaktivitás térbeli eloszlásával. Másfelől viszont kiderült az is, hogy a csúszási tendencia nagyon érzékeny a kisebbik horizontális illetve a vertikális főfeszültség hányadosára. Az RVRS-ben tapasztalt intenzív vetőaktivitás illetve a WNB-ben tapasztalt tektonikai nyugalom lehetséges magyarázata vagy az, hogy a regionális extenzió gyengébb a WNB-ben mint az RVRS-ben (inhomogén feszültségtér), vagy pedig az hogy a vetők reaktivációval szembeni ellenállása különböző e két medencében (eltérő kőzetmechanikai viszonyok). A vizsgálatok alapján hangsúlyozni kell, hogy a tektonikai fejlődéstörténet differenciálódása már a korai terciér során megkezdődött, ezért ésszerű feltételezni, hogy a különböző feszültségtér és/vagy csúszási határérték kialakulása közvetlenül kapcsolatba hozható az RVRS kainozoós riftesedésével. E két lehetőség bekövetkezésének igazolásához számos hipotézis kerül ismertetésre figyelembe véve a litoszféra szerkezetét valamint a két medencének illetve tágabb környezetüknek harmadidőszaki fejlődéstörténetét.

A késő kréta-terciér időszakban Hollandia üledékes medencéinek egész sora invertálódott az alpi kollízióból eredő kompressziós feszültségek hatására. Az egymást követő inverziós fázisok kumulatív eredményeként ezen medencék üledékes összelete deformálódott és jelentős mértékben lepusztult. A WNB-ben jó minőségű 3-D szeizmikus adatok illetve nagy mennyiségű fúrási adat áll rendelkezésre, amely kiváló alkalmat nyújt a lepusztult üledékösszlet mennyiségének becsléséhez. A doktori értekezés második felében egy olyan eljárás kerül ismertetésre, amely a WNB inverziós tektonikájának kvantitatív rekonstrukcióját célozza. A vizsgálat során szeizmikus reflektorok illetve intervallum-sebességeken alapuló kompaktációs trendek analízisét végeztem el, melyek között a megbecsült erózió mennyiségét illetően nagyon jó egyezés mutatkozik. Az eredmények kelet felé növekvő mértékű lepusztulást mutatnak, mely 1500-1700 *m* maximális értéket ér el. Erre a regionális trendre egy másik, gyorsan változó lokális komponens szuperponálódik, melynek analíziséből arra következtethetünk, hogy a normál vetők inverz módon történő reaktivációja

nagyon fontos szerepet játszott az inverzióban illetve az üledékek lokalizált eróziójában. Erre utal egyrészt, hogy egyes vetők két oldalán több száz méteres különbségek adódtak a differenciális erózió mértékében. Az erózió helyi maximumai és minimumai vetők reaktivációjához kapcsolódó antiklinálisokban és szinklinálisokban jelentkeznek.

A deformáció illetve az erózió mértékének tekintetében a késő eocén tektonikai fázis a WNB-ben illetve az Északi-tenger más medencéinek területén is másodrendűnek tekinthető a késő kréta inverziós fázishoz képest. Emiatt a megőrződött és szeizmikus szelvények által leképzett paleogén üledékösszlet részletes analizésére nyílik lehetőség, amely betekintést nyújt a WNB paleogén fejlődés- és inverzió történetébe. Ezen inverziós fázis jellemvonásai a régió más medencéinek inverziójával kerülnek összevetésre, mely új információkat szolgáltat a paleogén kompressziós mozgásokról ÉNy-Európában is. Az analizis rámutat, hogy a WNB paleogén inverziója, amelyet a medence központi részének felboltozódása illetve a vetők reverz módon történő reaktivációja jellemez, egy folyamatos, hosszú távú inverziós folyamatnak, semmint egy pulzus-szerű inverziós fázisnak az eredménye. A tektonikai mozgások intenzitása azonban nem volt egyenletes az eocén folyamán, hanem az eocén végén volt a legerősebb. Ezek a jellegzetességek hasonlóak más északi-tengeri illetve a La Manche Csatorna területén található mezozoos medencék inverziós képéhez. Ezen felül jó egyezés mutatkozik a paleogén inverziós fázisok és az alpi orogén események között. Az intenzív késő eocén inverziós fázis az Északi-tenger déli területein az alpi kollízió által indukált hosszú távú inverziós folyamat egyfajta betetőzésének tekinthető.

Summary

Publicly available geological exploration data obtained by the petroleum industry in the Netherlands bear numerous research possibilities both of academic and of societal importance. Using such data sets provided by TNO–NITG (National Geological Survey) this Ph.D. thesis focuses on the 3–D modelling of fault reactivation and on the reconstruction of the Late Mesozoic–Tertiary inversion/erosion history of the Netherlands.

3–D geometrical fault models revealed by geological data provide an excellent opportunity to study the reactivation of faults in a certain tectonic stress field. In the first part of this thesis I describe a newly developed numerical approach to constrain the three–dimensional pattern of fault reactivation. Taking advantage of the knowledge of the tectonic stress field, I calculate the ratio of the resolved shear and normal stresses (slip tendency) as well as the direction of the shear stress at every location on the faults modelled by triangulated surfaces. Although the calculated contact stresses represent only a first order approximation of the real stresses, comparison of the 3–D pattern of slip tendency with the frictional resistance of the fault can provide useful constraints on the probability of fault reactivation.

The method is applied to 3–D geometrical fault models of the Roer Valley Rift System (SE Netherlands), which is presently characterised by pronounced tectonic activity. The analysis demonstrates that the observed fault activity can be explained within a reasonable range of frictional parameters and input stress magnitudes. In addition, a fairly good correlation exists between the predicted slip directions and the focal mechanisms of local earthquakes. This suggests that in the study area, fault models that are valid in the uppermost part of the crust are also suitable to constrain fault reactivation even in the deeper parts of the seismogenic layer. Further, the analysis demonstrates that fault hierarchy and the regional tectonic context of the fault system are important factors in fault reactivation. Therefore, they always should be taken into account during evaluation of the calculated slip tendency and slip direction patterns.

The West Netherlands Basin is located north–west of the Roer Valley Rift System (RVRS). Together they form the most prominent tectonic features of the onshore Netherlands. The two basins have a common tectonic origin and a similar Mesozoic evolution. Their Neogene–Quaternary evolution, however, is markedly different. While the West Netherlands Basin is tectonically/seismically inactive and is characterised by uniform Neogene–Quaternary subsidence, in the Roer Valley Rift System

fault-controlled, intra-plate deformation has been taking place since Late Oligocene times with pronounced seismic activity. Considering the present-day NE–SW regional extension as well as the similar basin orientation and Mesozoic evolutions one would not expect strikingly different neotectonic activity in the two basins. However, a detailed structural analysis reveals that (1) the Palaeozoic–Mesozoic tectonic fabric has great influence on the Cenozoic deformation style of the basin system; (2) present-day faulting in the Roer Valley Rift System is related to the reactivation of pre-existing faults and (3) the Mesozoic fault pattern is slightly different in the two basins. Using the new fault modelling technique I determine whether these differences in fault orientation are substantial enough to produce significantly different resolved stresses along the faults. This modelling not only tests a common geological phenomenon but indirectly also delivers important constraints regarding the origin of faulting in the study area. The modelling results reveal that the faults in both basins should behave similarly under conditions of a laterally homogeneous regional stress field — which is in disagreement with the present-day tectonic activity of the region — and, on the other hand, that the predicted tendency of slip is very sensitive to the ratio of the minimum horizontal and the vertical stress (S). As an explanation for the pronounced fault activity in the Roer Valley Rift System and the tectonic quiescence of the West Netherlands Basin it is proposed that either the regional extension in the West Netherlands Basin is “weaker” (in term of higher S ratio) than that in the Roer Valley Rift System or that the slip thresholds in the two basins are different. The study emphasises that differentiation in the tectonic evolution already started in the Tertiary, and therefore it is reasonable to assume that the different tectonic stress field and/or slip threshold between the two areas is directly related to the origin of the Cenozoic rifting in the RVRS. Several hypotheses are discussed to account for these two possibilities, taking into account the lithospheric structure and the Cenozoic tectonic evolution of the two basins as well as that of surrounding areas.

During the Late Cretaceous–Tertiary period compressional stresses originating from the Euro–African collision inverted various sedimentary basins in the Netherlands. As the cumulative result of these inversion phases, the basin-fills were deformed and deeply eroded. In the West Netherlands Basin high quality 3–D seismic surveys and a large amount of borehole data are available, providing an excellent opportunity to determine the amount of eroded sediments. In the second part of the thesis a multidisciplinary study is carried out in order to quantitatively reconstruct the inversion tectonics in the West Netherlands Basin. The approach consists of the analysis of seismic reflectors and interval velocity-based compaction trends. The study demonstrates that very good consistency exists between the different methods, and indicates that an increasing amount erosion took place towards the East, reaching 1500–1700 *m* as maximum. Onto this regional trend of erosion a high frequency local trend is superimposed. This local component implies that reactivation of faults played a major role in the inversion and localised erosion of the basin fill: across major faults several hundreds of meters of difference can be observed in the

magnitude of erosion, while the local maxima and minima of erosion can be related, respectively, to fault-related anticlines and synclines.

Considering the amount of deformation and erosion, the Late Eocene tectonic phase in the West Netherlands Basin and in other basins of the southern North Sea region is of secondary importance compared to the Late Cretaceous inversion. Because of this, a detailed analysis of the preserved Palaeogene sediments revealed by 3-D seismic surveys is possible, which offers new insights into the Palaeogene tectonic history and inversion of the West Netherlands Basin. The inversion characteristics are compared to those of other basins in the region, which provides constraints on the Palaeogene compressional tectonic movements in NW Europe. The inversion of the West Netherlands Basin, which is characterised by the doming of the basin centre and by the reactivation of pre-existing faults in a reverse mode, was found to be the result of a continuous inversion process rather than a distinct tectonic pulse. The intensity of the tectonic movements was not uniform throughout the Eocene and was strongest during the latest Eocene. These characteristics are similar to those of other basins in the southern North Sea region and in the English Channel area. In addition, a good correlation exists between Alpine tectonic events and the Palaeogene inversion phases. In the light of these observations the latest Eocene inversion pulse in the southern North Sea region can be considered as the culmination of a long-term inversion process originated from the Alpine collision.

Samenvatting

Publiek beschikbare geologische exploratie gegevens, verkregen door de olie industrie in Nederland bevatten talloze onderzoeksmogelijkheden, die zowel van academische als maatschappelijk belang kunnen zijn. Gebruikmakend van dergelijke gegevens, is dit proefschrift gericht op de 3-D modellering van breukreactivatie en op de reconstructie van de laat Mesozoïsche–Tertiaire inversie en erosie geschiedenis van de Nederlandse ondergrond.

3-D geometrische breukmodellen, die gebaseerd zijn op geologische gegevens, bieden een uitstekende mogelijkheid om reactivatie van breuken in relatie tot bepaalde tektonische spanningsvelden te bestuderen. In het eerste deel van dit proefschrift beschrijf ik een nieuwe numerieke methode om het drie dimensionale patroon van breukreactivatie te bepalen, gebruikmakend van de beschikbare kennis van het tektonische spanningsveld en de ratio van de berekende schuif en normaal spanning op de breukvlakken (slip tendency), alsmede de richting van de schuifspanning, die berekend worden op ieder punt van de breuken, die gerepresenteerd zijn door getrianguleerde vlakken. Hoewel de berekende spanningen niet meer dan een eerste benadering zijn van de werkelijke spanningen, geeft het berekende drie dimensionale patroon van slip tendency in samenhang met de schuifweerstand van breuken belangrijke randvoorwaarden voor de waarschijnlijkheid van breukreactivatie.

De methode is toegepast voor de 3-dimensionale reconstructie van breukmodellen in de Roerdal Slenk (Zuid-Oost Nederland), die gekenmerkt wordt door actieve tektoniek. De analyse laat zien dat de geobserveerde breukactiviteit verklaard kan worden met een realistische reikwijdte van schuifweerstand van de breuken en de oriëntatie en magnitude van het huidige stress veld. Bovendien bestaat er een goede correlatie tussen de voorspelde schuifrichtingen en de geobserveerde haardmechanismen van lokale aardbevingen. Dit geeft aan dat in het studiegebied de breukmodellen niet alleen gelden voor de bovenste deel van de korst maar ook breukreactivatie beschrijven in diepere delen van de seismogene korst. De analyse laat verder zien dat de breukhierarchie en de regionale tektonische context een belangrijke rol spelen in breukreactivatie. Deze aspecten dienen altijd meegewogen te worden in studies naar slip tendency en schuifrichtingen.

Het West-Nederlands Bekken (WNB) is gelegen ten noord westen van de Roerdal Slenk (RDS). Samen vormen ze de meest prominente tektonische bekkenstructuren in onshore Nederland. De twee bekkens hebben een gemeenschappelijke tektonische origine en een vergelijkbare Mesozoïsche bekkenevolutie. Echter, de Neogene en

Kwartaire evolutie van de bekkens zijn sterk verschillend. Het West-Nederlands Bekken is tektonische en seismisch inactief en is gekenmerkt door een uniforme bodemdaling. De Roerdal Slenk daarentegen is gekenmerkt door sterke differentiële bewegingen langs tektonische actieve (rand)breuken sinds het Laat- Oligoceen. Gezien de NW-ZO oriëntatie van beide bekkens en hun vergelijkbare Mesozoïsche bekkenevolutie, zou men niet een zeer verschillende neo-tektonische evolutie verwachten. Een gedetailleerde structurele analyse van de bekkenstructuren laat zien dat (1) Het Paleozoïsch-Mesozoïsch tektonisch raamwerk van de bekkens een grote invloed heeft op de Cenozoïsche stijl van deformatie; (2) de huidige breukbewegingen in de Roerdal Slenk gerelateerd zijn aan reactivatie van bestaande breuken; (3) het Mesozoïsche breuksysteem in de bekkens enige onderlinge verschillen vertoont. Gebruikmakend van de breuk modelleringstechniek beoog ik te bepalen of de verschillen in breuksystemen voldoende groot zijn om te verklaren dat breuken in het WNB niet en in de RDS wel gereactiveerd worden. Deze modellering test niet alleen een hypothese voor de huidige reactivatie, maar geeft ook belangrijk inzicht in de oorsprong van breukbewegingen en patronen van breukreactivatie in beide bekkens. De modelresultaten tonen aan dat de breuken in beide bekkens een vergelijkbaar reactivatiegedrag zouden moeten weerspiegelen onder een homogeen spanningsveld. Dit is in tegenspraak met de huidige verschillen in neo-tektonische activiteit. Echter de modellering laat ook zien dat het optreden van reactivatie zeer gevoelig is voor de ratio van minimale horizontale spanningen en de verticale spanning (S). Mogelijke verklaringen voor de relatieve tektonische rust in het WNB zijn daarom (1) de extensie spanningen in het WNB (S hoger) zijn lager dan in de RDS; of (2) de schuifweerstand van breuken in het WNB is hoger dan in de RDS. Aangezien de differentiatie in tektonische activiteit optreedt vanaf het begin van de Cenozoïsche rifting in de RDS in het Laat-Oligoceen, kan verondersteld worden dat het onderliggende mechanisme vanaf dat tijdstip actief is geweest. In mijn proefschrift ga ik verder in detail in op de bovengenoemde twee verklaringen voor de differentiatie, waarbij ik de structuur van de lithosfeer en de Cenozoïsche tektonische evolutie van beide bekkens en omliggende gebieden meeweeg.

Gedurende het Laat-Krijt en Tertiair, hebben compressieve spanningen, veroorzaakt door de Alpiene orogenese, geleid tot inversie van sedimentaire bekkens in de Nederlandse ondergrond. Ten gevolge van meerdere opeenvolgende inversiefases is de bekkenvulling van de geïnverteerde bekkens sterk gedefformeerd en geërodeerd. In het WNB zijn hoge resolutie 3-D seismische surveys en een grote hoeveelheid boorgatgegevens beschikbaar. Deze bieden een excellente basis voor het vaststellen van de hoeveelheid geërodeerde sedimenten. In het tweede deel van mijn proefschrift is een multi-disciplinaire aanpak gebruikt om kwantitatieve reconstructies te maken van de inversie tektoniek in het WNB. De aanpak omvat enerzijds erosieschattingen op basis van de analyse van seismische reflectoren en anderzijds erosieschattingen op basis van anomale compactietrends verkregen uit intervalnelheden uit sonic logs. De onafhankelijk bepaalde erosieschattingen laten een duidelijke samenhang zien. De resultaten tonen een toename van erosie naar het oosten van het bestudeerde gebied,

tot een maximum van 1500–1700 *m.* Op deze regionale trend zijn lokale variaties gesuperponeerd, ten gevolge van breukbewegingen en plooiing tijdens inversie. De studie laat zien dat breukbewegingen een belangrijke rol speelden tijdens de inversie en hebben geleid tot sprongen in erosie langs breuken van ca. 300 *m.* Lokale minima en maxima van erosie hangen samen met de breukgerelateerde plooi-assen van de inversie.

De Laat-Eocene tektonische fase van inversie in Nederland is van tweede orde belang vergeleken met de Laat-Krijt inversie in het WNB en andere bekkens in de Zuidelijke Noordzee. In dit proefschrift is deze fase bestudeerd aan de hand gepreserveerde Paleogene sedimenten, waarvan de opbouw bestudeerd is met hoge resolutie 3-D seismische surveys. Deze analyse geeft nieuw inzicht in de Paleogene tektonische geschiedenis en inversie van het WNB. De inversie karakteristieken zijn vergeleken met andere bekkens in de regio, welke nieuwe inzichten geeft in de Paleogene compressieve tektoniek in NW Europa. De inversie van het WNB, welke is gekarakteriseerd door een opwelling van het bekkencentrum en opschuivingen langs bestaande breuken, blijkt het resultaat van een continue proces van deformatie in plaats van een enkele tektonische puls. De intensiteit van de tektonische bewegingen was niet gelijk gedurende het Eoceen, opbouwend tot een piek in het laatste Eoceen. Deze karakteristieken zijn vergelijkbaar met andere bekkens in de regio van de Zuidelijke Noordzee en het Engelse Kanaal. Voorts bestaat er een duidelijke samenhang tussen de Alpiene tektonische fases en de Paleogene inversie fases in het WNB. In het licht van deze observaties is de laatst-Eocene piek in deformatie te beschouwen als de culminatie van een langdurig inversie proces als gevolg van de Alpiene orogenese.

Chapter 1

Introduction and scope of the thesis

Deep under the flat, monotonous surface of the Netherlands a diverse geological landscape is buried resulting from an exciting geological history. The geological history recorded in the subsurface of the Netherlands bears numerous research possibilities not only of academic but also of societal and of economical importance (e.g., Cloetingh, 2000). The economically important oil and gas exploration, for example, is one of the leading geological research activities in the Netherlands. Exploration and mining of coal also significantly contributed to the geological knowledge of the Netherlands. Furthermore, tectonic and seismological studies have revealed significant recent intra-continental tectonic activity in the south-eastern part of the country, which has manifested itself in numerous historic and instrumentally recorded earthquakes. The most severe occurred on 13th of April 1992 near the city of Roermond, causing landslides and significant property damage (e.g., Camelbeeck and Van Eck, 1994; Camelbeeck et al., 1994). Better understanding of the past and present-day geological processes of the Netherlands therefore is important not only from academic, but also from economical and societal point of view.

As the largest part of the Netherlands is covered by Quaternary sediments, access to the geological past can only be achieved by expensive field campaigns such as seismic surveys and boreholes. These data are generally obtained and owned by profit-oriented companies of the petroleum industry and often are not available for academic research. However, the Netherlands Institute of Applied Geosciences TNO — National Geological Survey (TNO–NITG) has obtained access to these data in order to integrate the geological knowledge into a national scale database (Atlas of the Deep Subsurface of the Netherlands).

A large part of the data set managed by TNO–NITG has become available recently to the public by the new mining law. The availability of subsurface data on a regional as well as national scale opens new academic research possibilities. With this in mind, four years ago a research co-operation called the Knowledge Center was initiated between TNO–NITG and the Vrije Universiteit Amsterdam. The aim was to bring together the data and infrastructure of TNO–NITG with the modelling techniques, software and research personnel of the Tectonic Department of the Vrije

Universiteit to achieve a common goal, which is the better understanding of the sub-surface, geological history and present-day geological processes of the Netherlands. The co-operation concerns mainly three disciplines: tectonics, sedimentology and geo-engineering. This Ph.D. thesis was initiated in the context of this co-operation and focuses on the modelling of fault reactivation and on the reconstruction of the Late Mesozoic–Tertiary erosional history of the Netherlands.

The data set available for this Ph.D. research can be subdivided into two main groups. The first group consists of the products of the geological mapping campaign (dinoloket.nitg.tno.nl), which subdivides the onshore Netherlands into 15 mapsheets (Fig. 1.1). Every mapsheet consists of a digitally available topographic map, the depth maps of eight stratigraphic horizons and the corresponding maps of subcrop- and fault-trace lines. The stratigraphic horizons represent the boundaries of geolog-

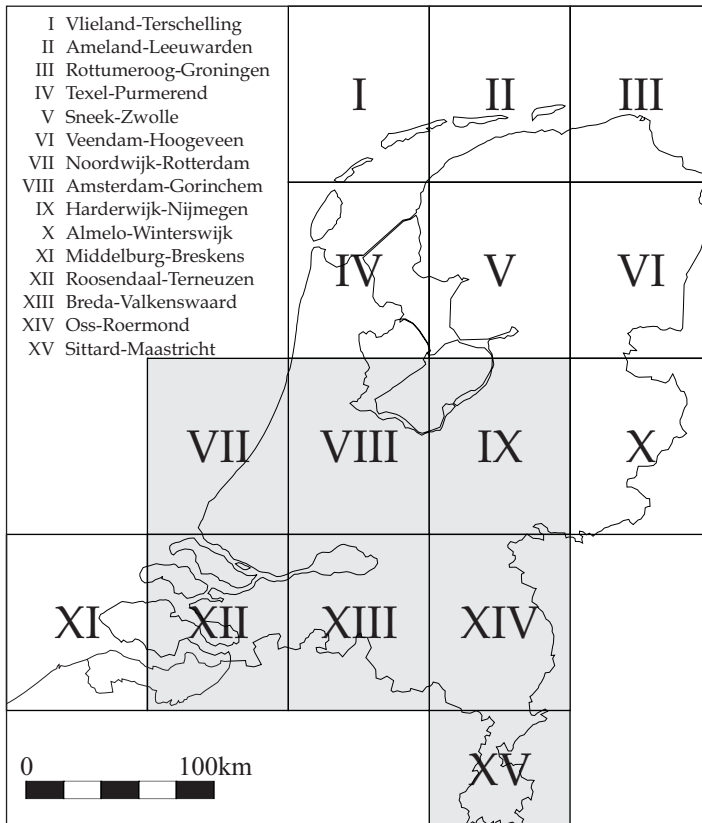


Figure 1.1: Mapsheets of the “Atlas of the Deep Subsurface of the Netherlands” by TNO–NITG. Grey-shaded mapsheets cover the area of interest in this thesis.

ically important litho- and chronostratigraphic units (Fig. 1.2): (1) base Rotliegend Group; (2) top Zechstein Group; (3) base Triassic; (4) base Jurassic; (5) base Schieland Group; (6) base Rijmland Group; (7) base Chalk Group; (8) base North Sea Supergroup. In addition, on some mapsheets the base Upper North Sea Group- and the base Quaternary horizon are also available.

The regional mapping is based on high quality 2-D and 3-D seismic surveys and an enormous amount of well data. The latter include not only the lithostratigraphic subdivision of the succession, but also cores, cuttings, laboratory measurements and wire-line logs from various depth intervals. A typical log suite consists of gamma ray-, sonic-, density and resistivity logs. The part of this data set forms the other group of data used during this Ph.D. research. Access to the raw seismic and well data has made it possible to perform an analysis having higher resolution than that of the data provided by the regional mapping alone.

Before presenting the scope and outline of this thesis, a short overview of the

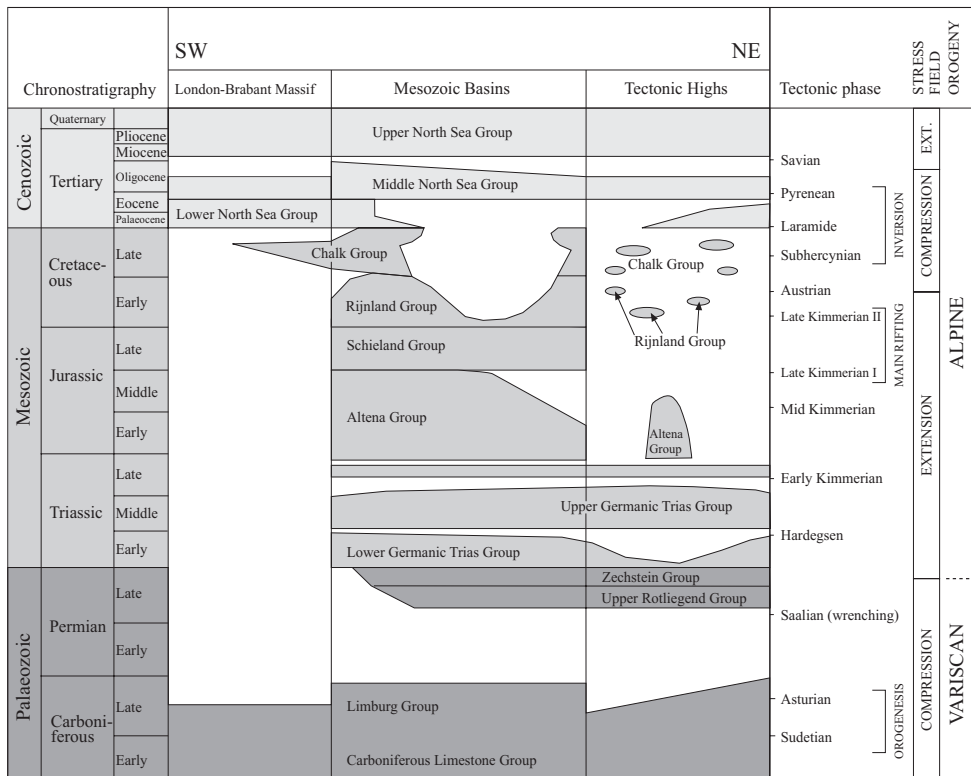


Figure 1.2: Simplified litho-chronostratigraphic chart of the Netherlands (modified after TNO-NITG, 2002).

most important events in the geological history of the Netherlands is presented. Placing the scope of the research into a broader geological context may provide better understanding of the main goals of this thesis.

1.1 Tectonic evolution of the Netherlands

The present-day structural framework of the Netherlands reflects a complex tectonic history (Fig. 1.2). The oldest rocks found in the Netherlands and surrounding areas indicate that in Early Devonian times the Netherlands formed the southern part of the Caledonian deformation zone, a trend that marks the east–west collision of Baltica and Laurentia as well as the north–south convergence of Gondwana and Laurasia (e.g., Ziegler, 1990). After the closure of the Iapetus ocean the southern Netherlands became part of the 2500 *km* long Variscan Foredeep Basin in the area of the rapidly degrading Mid European Caledonides (Fig. 1.3). Devonian–Early Carboniferous sediments in the Netherlands mainly originate from the erosion of this mountain chain. In the meantime the north–south convergence between Laurasia and Gondwana continued, which resulted in a continent–continent collision and intensive deformation in the Variscan fold-and-thrust belt in the Middle Carboniferous. As the Variscan mountain chain was evolving, strong subsidence occurred in the foredeep basin due to the flexural load of the orogen, resulting in the deposition of a more than 5000 *m* thick marine and continental succession in the Netherlands (Limburg Group). This succession contains several economically important coal beds and forms the most important hydrocarbon source rock in the Netherlands (Bodenhausen and Ott, 1981; De Jager et al., 1996; Gerling et al., 1999; Van Balen et al., 2000; De Mulder et al., 2003).

Following the latest phases of the Variscan orogeny (Late Carboniferous) the megacontinent of Pangea was sutured, which had large impact on the climate of NW Europe. North of the Variscan mountain chain an arid climate prevailed and an isolated basin developed (Southern Permian Basin Fig. 1.3). In this basin continental sandstones, clays and halite sequences were deposited in the Middle–Late Permian under desert and desert-lake conditions (Rotliegend and Zechstein Groups (Fig. 1.2); e.g., Van Wijhe et al., 1980; Ziegler, 1990; Geluk et al., 1996). These rocks form excellent reservoir and cap rocks throughout the entire Netherlands (e.g., Winstanley, 1993; Geluk et al., 1996; Gerling et al., 1999). Sedimentation in this isolated basin continued during the Triassic, although, from time to time marine connections were established with the Tethys Ocean in southern Europe through seaways across the rapidly eroding Variscan chains (e.g., Ziegler, 1990). By the Early Jurassic an open marine environment, in which clays with high organic content were deposited (Altena Group, Fig. 1.2) became dominant in the Netherlands. These clays form the source rock for many oil and gas fields in the West Netherlands Basin and Broad Fourteens Basin (e.g., Bodenhausen and Ott, 1981; De Jager et al., 1996; Van Balen et al., 2000).

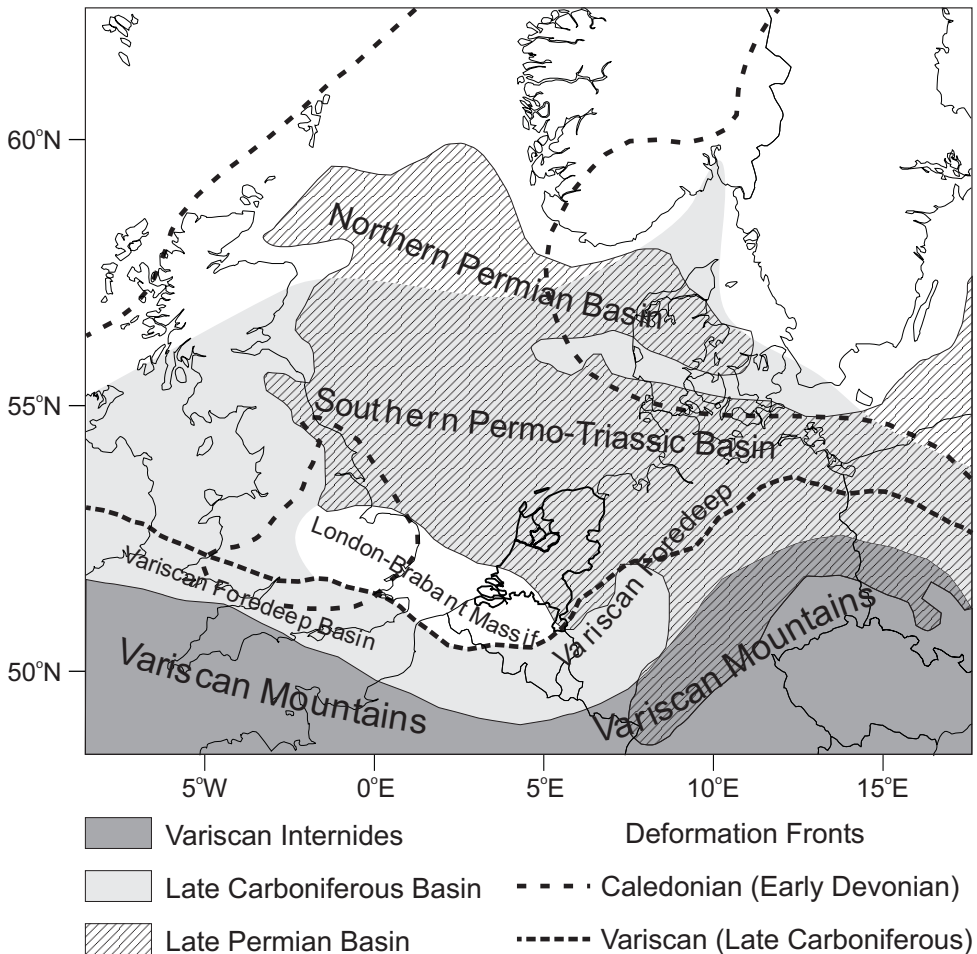


Figure 1.3: Late Palaeozoic geographical setting of NW Europe (modified after Ziegler, 1990).

In contrast to the Permian, during which only mild tectonic movements occurred, the Triassic–Mid Jurassic period in the Netherlands was characterized by intensified tectonic activity. Extensional movements related to the complex disintegration of Pangea in the Tethys- and North Atlantic region started in the Early Triassic and resulted in the development of several NW–SE oriented tectonic highs and lows in the Netherlands (e.g., De Mulder et al., 2003). The orientation of these tectonic features was controlled by the pre-existing Variscan fault pattern (e.g., Ziegler, 1990; Oudmayer and De Jager, 1993). Following the Mid Jurassic crustal separation in the western Tethys (e.g., Biju-Duval et al., 1977) the dominant tectonic force in north-

west Europe became an east–west oriented extension originating from the Arctic–North Atlantic rift system (Ziegler, 1990; 1992). Intensified crustal extension in the North Sea region was taken up at its southern end by right-lateral movements between the tectonic highs, which ultimately resulted in the development of a series of rapidly subsiding transtensional basins during the Late Jurassic–Early Cretaceous period (Fig. 1.4). In the Dutch part of the system the Roer Valley Graben, the West Netherlands Basin, the Central Netherlands Basin and the Broad Fourteens Basin were developed, where thick successions of continental and shallow marine sediments (Schieland and Rijnland Groups, Fig. 1.2) were deposited (e.g., Heybroek, 1974; Van Wijhe, 1987; Ziegler, 1990; 1992; Dronkers and Mrozek, 1991).

A broad, uniform subsidence in the North Sea region indicates that tectonic movements slowed down in the Middle–Late Cretaceous. This, together with the high eustatic sea level favored the deposition of open marine chalks, which can be found over the whole NW Europe. Deposition of the chalk in the Late Cretaceous, however, was interrupted by a series of tectonic events, which had large impact on the present-day subsurface topography of the Netherlands. Alpine orogenic events related to the convergence between Eurasia and Africa generated compressional stresses, which — transmitted deep into the European plate — inverted the Late Jurassic basins of the Netherlands and adjacent areas (e.g., Ziegler, 1987; 1990; Van Wijhe, 1987; Van Hoorn, 1987; Dronkers and Mrozek, 1991; Nalpas et al., 1995; De Jager et al., 1996; Racero-Baena and Drake, 1996). During inversion the normal faults were reactivated in a transpressional manner, while the basin fill was folded, uplifted and deeply eroded. The inversion of these basins occurred in several phases (e.g., Ziegler, 1987), between which calmer tectonic periods prevailed. The most important inversion pulses occurred in the Late Cretaceous, Middle Paleocene and in the latest Eocene.

In the Tertiary the megatectonic setting of Western and Central Europe underwent fundamental modifications. With the onset of sea-floor spreading in the North Atlantic in the Palaeogene active rifting was abandoned in the North Sea region and large-scale regional subsidence occurred, affecting also a large part of the Netherlands (e.g., Letsch and Sissingh, 1983; Zagwijn, 1989; Ziegler, 1990). The main depocentres of Palaeogene shallow marine sedimentation were located on the flanks of the inverted basins. In the Middle Oligocene a rift arm related to the Northwest European Rift System reached the southern Netherlands from the southeast. Pre-existing faults in the Roer Valley Graben were reactivated in a normal manner allowing the accumulation of shallow marine sediments with a significant thickness (e.g., Letsch and Sissingh, 1983; Zagwijn, 1989; Zijerveld et al., 1992; Ziegler, 1994; Michon et al., 2003). The seismicity record of the last 100 years as well as numerous geological, morphological and geophysical studies indicate that the fault controlled intraplate deformation in the SE Netherlands continues even today (e.g., Groenewoud et al., 1991; Camelbeeck et al., 1994; Van den Berg, 1994; Ziegler, 1994; Kooi et al., 1998; Houtgast and Van Balen, 2000; Michon et al., 2003; Michon and Van Balen, 2004; Van Balen et al., 2004). Faults and tectonic basement blocks of Mesozoic and Palaeo-

zoic origin play a major role in the neotectonic activity of this region. Other areas of the Netherlands, even those areas in the direct NW continuation of the Roer Valley Graben, are tectonically inactive.

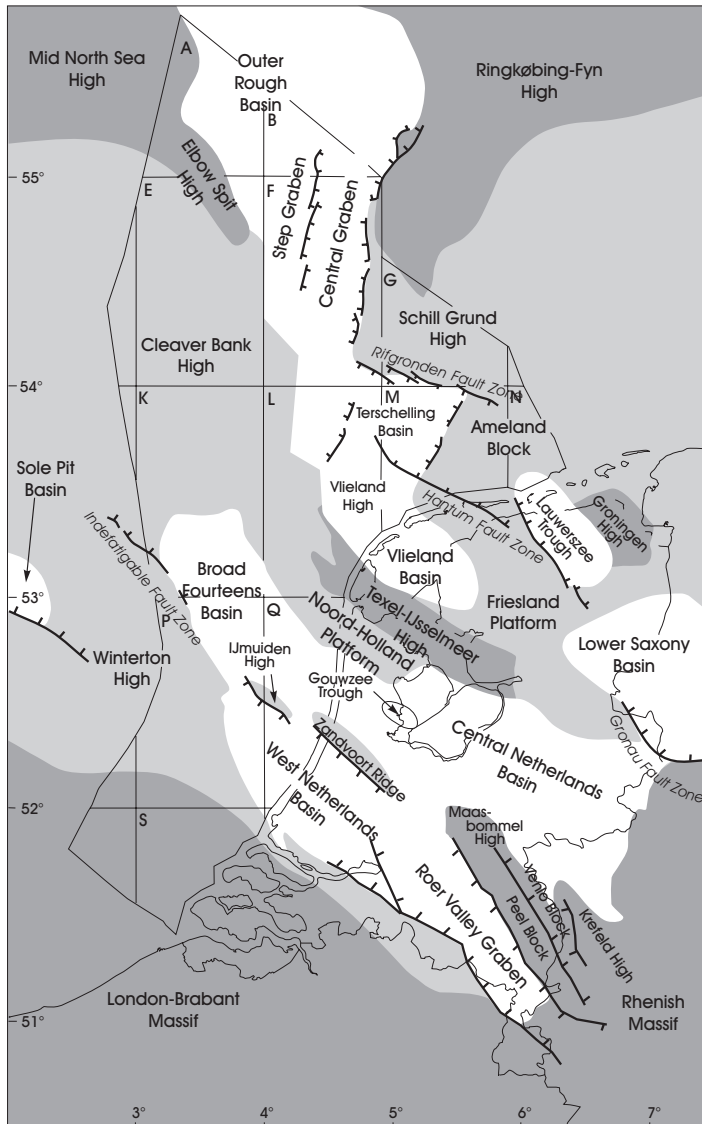


Figure 1.4: Main Mesozoic tectonic features of the Netherlands and surrounding areas (after TNO-NITG, 2002).

1.2 Scope and outline of the thesis

This Ph.D. research has focused on the modelling of fault reactivation and the quantitative reconstruction of the inversion tectonics in the southern Netherlands. Although the data available from TNO–NITG cover the entire onshore Netherlands, the focus of this research has, for several reasons, been put on the southern part of the country. One of the reasons is that the most prominent geological feature (the Roer Valley Graben–West Netherlands Basin system) of the onshore Netherlands is located in this area. Although its history is well known, many questions remain. The second reason is that in the West Netherlands Basin, being an important hydrocarbon province of the country, large amounts of high quality data (2–D and 3–D seismic surveys, well data) are available. This makes it possible to perform tectonic modelling studies of high resolution in both space and time.

One of the main goals addressed at the commencement of this Ph.D. research was the development and implementation of a method to provide detailed 3–D geometrical models of faults in the subsurface of the Netherlands. Digital 3–D fault models open new possibilities for future research, such as the evaluation of fault reactivation potential, as well as finite element geomechanical or reservoir modelling. In the framework of this Ph.D. research two fault modelling techniques were developed (the so-called midline- and direct methods). The midline method uses classical mapping data as inputs (fault trace lines and geological horizons), while using the direct method the fault models are extracted directly from 3–D seismic surveys. The technical details of these modelling techniques as well as their advantages and drawbacks are discussed in *Appendix A*.

In *Chapter 2* fault reactivation modelling, which is one of the most important applications of the 3–D fault database, is discussed. Estimation of fault reactivation potential has not only academic but also societal importance, especially in the south-eastern Netherlands. *Chapter 2* comprises a short overview of the origin of tectonic stresses with special reference to NW Europe, then the theory and modelling possibilities of fault reactivation are presented and discussed. Special emphasis is put on the Wallace–Bott or far-field stress approach (e.g., Wallace, 1951; Bott, 1959, Pascal et al., 2002; Pascal and Angelier, 2004), the applicability of which was justified by many numerical and field studies. Finally, a newly developed approach is presented (3–D slip tendency analysis), which implements the Wallace–Bott approach into three dimensions. The aim is to model the 3–D pattern of fault reactivation (potential and direction) using the full 3–D geometry of faults revealed by geological data. The inputs to the method are 3–D geometrical fault models and parameters describing the regional stress field. Drawbacks and the reliability of this new method are also discussed.

In *Chapter 3* the 3–D slip tendency modelling technique is applied in the tectonically most active south-eastern part of the Netherlands (Roer Valley Rift System). In this area valuable constraints are available on the activity of the fault system, making it an ideal case study area. The research efforts presented in *Chapter 3* focus

on (1) testing the applicability and limitations of the new 3-D approach by comparing the modelling results with observations on recent fault activity in the region and (2) by doing so obtaining important knowledge about the fault reactivation pattern, faulting mechanism and the regional stress field in the Roer Valley Rift System.

The present-day tectonic activity in the West Netherlands Basin and Roer Valley Rift System is markedly different despite the fact that they have a common tectonic origin and similar structural composition. In the Roer Valley Rift System fault-controlled intra-plate deformation is taking place, while the West Netherlands Basin, although located in the direct NW continuation of the Roer Valley Rift System, is tectonically inactive. In *Chapter 4* the present-day tectonics and fault behaviour of these two basins are compared and modelled using their three-dimensional pre-Tertiary fault pattern. Integration of the subsurface data provided by TNO-NITG gives an excellent opportunity to investigate the structural development of the basin system on a regional scale. The structural analysis of the two basins reveals slightly different fault orientations. Using the technique presented in *Chapter 2* it is to be determined if these differences in fault orientation are substantial enough to produce significantly different resolved stresses along the faults in uniform regional stress field. The modelling results are discussed in the light of the pre-Quaternary evolution of the basin system. Processes and tectonic models, which could explain the observed neotectonic differences, are also discussed.

During the Late Cretaceous-Tertiary inversion phases a significant amount of sediment was eroded from various sedimentary basins in the Netherlands. Quantification of erosion is important, since it provides constraints on the pre-inversion tectono-sedimentological setting of the study area. Erosion estimates can also be used to determine and model the maximum depth of burial of the sediments and, by implication, the amount of expelled hydrocarbons. In addition, during basin inversion meteoric waters can flush even the deeper parts of the sedimentary succession, which is assumed to be the main reason of the severely biodegraded hydrocarbons in some parts of the West Netherlands- and Broad Fourteens basins (Bodenhausen and Ott, 1981; Bouw and Oude Essink, 2003; Verweij, 2003). In order to estimate the degree and area of biodegradation a knowledge of paleo-topography and the amount and pattern of removed sediments are essential. In *Chapter 5* a quantitative analysis, carried out in the West Netherlands Basin is presented, which aims to determine the amount of eroded sediments. The West Netherlands Basin was selected as a study area because of the abundance of top-quality borehole and seismic data in this region. Interval velocity data measured in boreholes located in the central part of the basin are compared with those obtained from the margin of the basin, where significant erosion did not occur. In addition, high quality 3-D seismic data are analyzed in order to determine the pattern of erosion, which provides important constraints on the deformation kinetics during the Late Cretaceous-Mid Paleocene inversion phase in the West Netherlands Basin.

In *Chapter 6* a detailed analysis of high quality 3-D seismic and borehole data is carried out to characterise and reconstruct the Palaeogene tectonic inversion in the West Netherlands Basin. In terms of the amount of removed sediment the Palaeogene inversion phase has always been considered as of secondary importance compared to the Late Cretaceous event. Because of this, however, a detailed analysis of the preserved Palaeogene sediments is possible, which can help to characterise and better understand the Late Eocene tectonic movements in the West Netherlands Basin. Moreover, it can also provide useful constraints on syn-sedimentary inversion processes. The obtained characteristics of basin inversion are compared to those of other basins in the southern North Sea region and in the English Channel area, which highlights important aspects of basin inversion in NW Europe during the Palaeogene.

Chapter 2

Tectonic stresses and fault reactivation: theory and modelling

It has been long known that tectonic stresses generated by various geological processes induce contact forces along pre-existing fractures in the Earth's lithosphere (e.g., Wallace, 1951; Bott, 1959; Sibson, 1985). If the contact forces meet certain criteria, slip can occur along the given plane of weakness. Understanding and predicting the behaviour of pre-existing faults, therefore, is crucial and has not only scientific but also economical and societal importance. For example, adequate estimation of the resolved stresses along known or suspected faults is very important in exploring high-risk and earthquake-prone faults and ultimately in assessing tectonic stability and seismic hazard. Seismic hazard assessment is one of the key societal issues in areas where earthquakes frequently occur. Another example is the oil industry, where the effect of faulting on the geometry of traps is important. However, using classical exploration methods (seismic surveys) only the dip-slip component of the displacement field can be observed. The sense and relative magnitude of the lateral component remain undetected and can only be estimated using indirect observations. Furthermore fault sealing, which is also of crucial importance in hydrocarbon trapping and reservoir geology, depends also on the displacement and the actual stresses on the faults (e.g., Grauls and Baleix, 1994; Sibson, 1994; Skar, 2000).

In this chapter the theory and the modelling possibilities of fault reactivation are discussed. A new approach is also presented, which uses the 3-D geometry of the faults to constrain the likelihood and style of reactivation. A detailed discussion of this modelling technique is essential, since in the following chapters it will be applied on seismically active areas in the Netherlands. Firstly, the sources, classification and characteristics (depth dependence) of tectonic stresses in the lithosphere are discussed briefly. Then the theory, the mathematical background and the modelling

This chapter is partly based on: Worum, G., Van Wees, J.D., Bada, G., Van Balen, R.T., Cloetingh, S. and Pagnier, H. 2004 Slip tendency analysis as a tool to constrain fault reactivation: A numerical approach applied to 3D fault models in the Roer Valley Rift System (southeast Netherlands). *Journal of Geophysical Research* (109), B02401, doi:10.1029/2003JB002586

possibilities of fault reactivation are presented. Special emphasis is put onto the newly developed 3-D technique, which uses the 3-D fault models presented in *Appendix A*.

2.1 Stresses in the lithosphere

Each part of the Earth's lithosphere is constantly subjected to various internal and external forces. In response to, and to compensate for these forces, the given plate builds up excess mechanical stresses in addition to those arising from its own weight. These stresses, which can have considerable magnitude, are the primary sources of the failure and deformation of the lithosphere and are also the source of reactivation of pre-existing weakness zones. The nature, magnitude and distribution of the lithospheric stresses exhibit great vertical and horizontal variability, since neither the mechanical properties of the deforming medium (e.g., composition, density, strength), nor the physical conditions within the lithosphere (e.g., pressure, temperature etc.) are uniform. For example, high permanent stresses are not present in the lower part of the crust and in the deeper mantle lithosphere since at these depth intervals the material is weak and the process of ductile creep relieves any differential stress (e.g., Ranalli, 1995). Stress amplification in the upper crust and in the uppermost mantle (e.g., Kuznir and Bott, 1977) and the highly variable lithospheric deformation patterns induced by the same external forces (i.e., coupled/decoupled deformation, e.g., Buck, 1991; Cloetingh et al., 1999) are all the results of the mechanical stratification of the lithosphere. Laterally the mechanical and physical properties of the lithosphere do not change dramatically — especially in intra-plate conditions — resulting in similar stress conditions over large areas (e.g., Cloetingh and Wortel, 1986; Müller et al., 1992). This large-scale stress pattern is called the regional stress field, on which secondary perturbing stresses originating from local effects (local stress field) are often superimposed.

2.1.1 Sources of tectonic stresses

Below, the most important sources of tectonic stresses are discussed, with special reference to NW Europe. Providing a complete list of stress sources and a detailed explanation about the stress-inducing mechanisms is beyond the scope of this thesis; they however can be found in other works (i.e., Gölke, 1996; Bada, 1999 and references therein).

Numerous analytical and numerical studies have demonstrated that one of the most important sources of tectonic stresses is gravity- i.e., buoyancy-related (e.g., Dahlen, 1981; Fleitout and Froidevaux, 1982; Ranalli, 1992; Richardson and Coblenz, 1994; England, 1996; Gölke and Coblenz, 1996). Lateral density and thickness variations of the lithosphere are normally compensated at the base of the lithosphere by the process of isostasy. At shallower levels, however, there is often a gravitational

potential energy difference between the “normal” and the perturbed areas inducing a lateral pressure gradient, that is compensated by excess tectonic stresses. The best-known manifestations of these types of stresses are the *ridge-push* forces directed normal to mid-ocean ridges and the force associated with the differential gravitational loading across passive margins (e.g., Lister, 1975; Bott, 1991). These forces were determined to be the primary source of the present-day plate-wide (regional) stress field in NW Europe (Gölke and Coblenz, 1996).

Another important stress source is the so-called *collisional resistance*, which is associated with convergent plate boundaries, including continent–continent collisions. If the collisional stresses are not accumulated by deformation within the orogen or the foreland basin, then they can be transmitted deep into the two colliding plates. In the present day stress field in NW Europe this type of stress is of secondary importance compared to the *ridge-push* stress (Gölke, 1996; Gölke and Coblenz, 1996). In the geological past, however, it played a key role. The inverted sedimentary basins in the southern North Sea region located more than 1000 km from the orogen demonstrate this (e.g., Ziegler, 1987).

The *slab-pull* and the *trench suction* stresses are also associated with convergent plate boundaries. The *slab-pull* is a tensional force generated in the subducting plate and is caused by the sinking of the dense oceanic lithosphere into the lighter asthenosphere. The *trench suction* force is generated in the overriding plate and plays a key role in the evolution of back-arc basins. This is also a tensional force and is caused either by an induced asthenospheric corner flow between the overriding and subducting plates or by the suction force generated by the vertical sinking of the subducting slab (e.g., Richardson and Solomon, 1979; Cloetingh and Wortel, 1986).

The main source of *flexural stresses* are loads applied to the Earth surface, such as the sedimentary load, erosion, the load of an ice sheet or a sea mount (e.g., Bodine et al., 1981; Cloetingh et al., 1982). Another source of this type of stress is the so-called bending stress associated with horizontal force-induced lithospheric folding (e.g., Cloetingh et al., 1999). Although flexural stresses can have significant magnitude they are only of local importance, since the flexure does not have very large lateral range, which could influence the large-scale regional stress pattern (e.g., Van Wees and Cloetingh, 1996).

2.1.2 Classification of tectonic stresses: the tectonic style

The state of stress in an elastic medium can be represented by three mutually orthogonal compressional or tensional stresses (the principal stresses ($\sigma_1 > \sigma_2 > \sigma_3$)). In geology, Anderson’s theory, which suggests that tectonic forces are dominantly horizontal resulting in one principal stress being vertical, is generally accepted. Thus, the maximum horizontal (σ_H), the minimum horizontal (σ_h) and the vertical stresses (σ_v) are suggested to coincide with the principal stresses. This assumption is usually valid in the uppermost part of the crust, however, in the deeper parts or close to faults and mechanical inhomogeneities there can be significant deviations. Based on

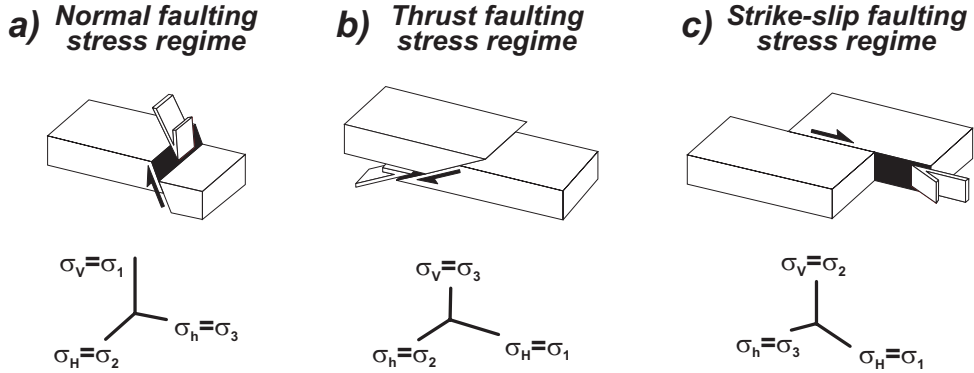


Figure 2.1: Anderson's (1951) traditional classification of the stress regimes and their characteristic deformation patterns. σ_H , σ_h and σ_v represent the maximum horizontal, the minimum horizontal and the vertical stresses, respectively. σ_1 , σ_2 and σ_3 are the principal stresses, where $\sigma_1 > \sigma_2 > \sigma_3$ (modified after Bada, 1999).

the orientation of the largest and the smallest principal stress (σ_1 and σ_3) Anderson (1951) established the traditional classification of the stresses, which rank the stresses into normal faulting-, thrust faulting- and strike-slip faulting stress regimes. Every stress regime has its own characteristic deformation style (Fig. 2.1).

The state of stress can also be classified according to the relative magnitude of the principal stresses. For this classification the so-called shape ratio is defined (e.g., Gephart and Forsyth, 1984; Angelier, 1984; Suppe, 1985):

$$R = \frac{\sigma_2 - \sigma_1}{\sigma_3 - \sigma_1} \quad (2.1)$$

where the R -value may range between 0 and 1. The shape ratio is a frequently used parameter, since this is the maximum information regarding the magnitudes of the principal stresses, which can be gained from stress inversion studies (e.g., Gephart and Forsyth, 1984; Angelier, 1984; Plenefisch and Bonjer, 1997).

The stress regime identified in terms of Andersonian state of stress can vary both horizontally and vertically (Bell and Babcock, 1986; Rebaï et al., 1992; Brudy et al., 1997, Sassi and Faure, 1997). This variation may be related to variations in the structural setting, the presence of faults, inhomogeneous rock properties or abnormal fluid pressures (e.g., Cornet and Burlet, 1992; Grauls and Baleix, 1994; Hardebeck and Hauksson, 2001). The transition from one regime to another can be both continuous and abrupt (e.g., Sassi and Faure, 1997).

The stress regime has important impact on the style of deformation. After the pioneering work of Anderson (1951), Wallace (1951) and Bott (1959) several authors established kinematical relationships between the type of a stress regime and faulting-fracturing processes. The knowledge of the stress regime allows determination not only of the orientation of newly formed shear fractures but also of the

kinematics of movement on any pre-existing planar fracture (e.g., Sibson, 1974, 1985; Yin and Ranalli, 1992; Sassi et al., 1993; Sassi and Faure, 1997). This kinematical relationship has been successfully used by several authors (e.g., Nieuwland and Walters, 1993; Beekman et al., 2000) to predict the macroscopic deformation style using the detailed knowledge of the stress pattern revealed by numerical modelling.

In the case when the tectonic stress field is not invariable, the “stability” of the state of stress can be evaluated in terms of the R -value. For example, considering σ_1 being vertical, an R -value of 0.5 means that σ_2 is exactly between σ_1 and σ_3 ($\sigma_2 = (\sigma_1 + \sigma_3)/2$). The dominating fault pattern in this case would be pure normal faulting with strike directions perpendicular to σ_3 , that is uniform over large areas even if the magnitude of σ_2 is slightly fluctuating. In this case the stress field is called stable. If, however, the R -value is close to 1 ($\sigma_2 \sim \sigma_3$) then there is no distinctive direction for the strike of the developing normal faults: every direction is equally possible. In case of $R \sim 0$ ($\sigma_2 \sim \sigma_1$) small disturbances in σ_2 can easily “flip over” the stress field into another stress regime. In $R = 1$ and $R = 0$ cases, therefore, the stress field is called unstable.

2.1.3 Depth dependence of the stress field in the upper crust

In order to accurately estimate the likelihood and style of fault reactivation a detailed knowledge about the confining tectonic stress field is needed. Below, the general patterns of the depth dependence of the stress field are discussed. These patterns allow certain assumptions to be made with respect to the regional stress field, which are very important regarding fault reactivation modelling, since they make the procedure simpler without violating its validity.

Hydraulic fracturing measurements performed in the uppermost part of the crust provide detailed information about the magnitudes of tectonic stresses (e.g., Haimson and Fairhurst, 1967; Zoback and Haimson, 1983; Rummel, 1986; Zoback and Healy, 1992; Brudy et al., 1997; Cornet and Hudson, 2003). By combining the results of this technique with borehole breakout- and drilling-induced tensile fracture data, it is possible to determine the tectonic stress magnitudes even at greater depth (Brudy et al., 1997). The stress magnitudes generally follow steadily increasing patterns with depth, across faults and interfaces of mechanical properties, however, they often change abruptly (e.g., Cornet and Burlet, 1992; Sassi and Faure, 1997; Beekman et al., 2000). Under undisturbed, intra-plate conditions the observed depth-dependence of the principal stresses can be summarised by the following dimensionless functions (after Rummel (1986), Fig. 2.2):

$$\begin{aligned}
 R_h(z) &= \frac{\sigma_h(z)}{\sigma_v(z)} = \frac{\gamma_h}{z} + \beta_h \\
 R_H(z) &= \frac{\sigma_H(z)}{\sigma_v(z)} = \frac{\gamma_H}{z} + \beta_H
 \end{aligned}
 \tag{2.2}$$

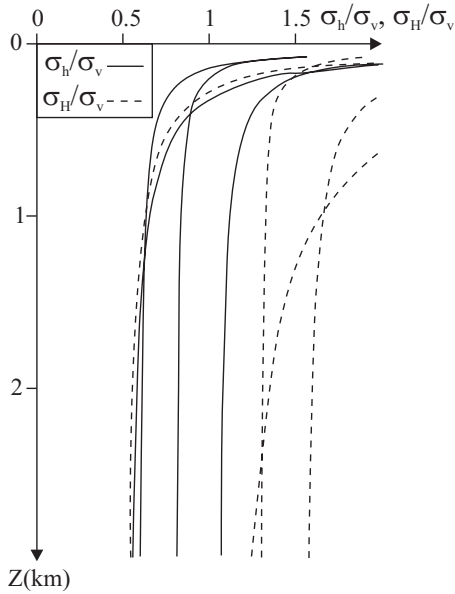


Figure 2.2: Depth dependence of measured horizontal principal stresses (σ_h and σ_H) normalised with respect to the vertical principal stress (σ_v) for hydrofrac tests in different boreholes with depth $z > 500$ m (after Rummel, 1986).

The ratios of the principal stresses in stress fields described by equation (2.3) are the same at every depth. Therefore this state of stress can be represented by a uniform stress tensor, which has three independent parameters: the orientation of σ_H and the σ_h/σ_H and σ_v/σ_H ratios, respectively. The form of this reduced stress tensor is:

$$\underline{\underline{\sigma}} = \begin{pmatrix} 1 & 0 & 0 \\ 0 & \sigma_h/\sigma_H & 0 \\ 0 & 0 & \sigma_v/\sigma_H \end{pmatrix} \quad (2.4)$$

This representation of the principal stresses is ideal for the fault reactivation analysis, since, as it will be shown later, neither the direction nor the likelihood of the fault reactivation depends on the absolute magnitude of the stress tensor. It has to be emphasised that with respect to fault reactivation modelling, the tensor form of equation (2.4) is equivalent to equation (2.3), and, at greater depth, to the observed stress pattern of figure 2.2. In other words, the stress model of equation (2.4) not only significantly simplifies the calculation of the fault reactivation parameters during the modelling procedure, but also is in accordance with the observed pattern of tectonic stresses.

where γ_h , γ_H , β_h , β_H are constants (for case studies and values see Rummel (1986), Brudy et al. (1997), Cornet and Hudson (2003) and references therein). σ_H , σ_h and σ_v represent the maximum horizontal, the minimum horizontal and the vertical stresses, respectively, which are assumed to be equal to the principal stresses. Figure 2.2 reveals that below a certain depth (~ 0.3 – 1 km depending on the β and γ values) the σ_h/σ_v and σ_H/σ_v ratios can be considered as being depth-independent values. This means that the linear depth dependence of the principal stresses having the following form adequately describes the stress field at greater depth (e.g., Jaeger and Cook, 1976; Ito and Zoback, 2000):

$$\sigma = K \cdot z \quad (2.3)$$

where σ is one of the principal stresses in general and K is constant. Equation (2.3) is extensively used in the mining industry and its validity has been justified by numerous successfully solved engineering problems.

2.2 Reactivation of faults: theory

It is generally accepted that slip occurs in the direction of the resolved shear stress (e.g., Wallace, 1951; Bott, 1959; Angelier, 1984; Pascal et al., 2002). This assumption, which is extensively used in stress inversion techniques, was found to be valid in most geological situations in several numerical studies (e.g., Dupin et al., 1993; Pollard et al., 1993).

Regarding the conditions of slip along a fracture the simplest criterion is provided by the law of friction (Amonton’s law):

$$\begin{aligned} \tau &\geq \mu_{slide} \cdot \sigma_n \\ \frac{\tau}{\sigma_n} &= ST \geq \mu_{slide} \end{aligned} \quad (2.5)$$

where τ and σ_n are the shear and normal components of the force acting between the two sides of the fracture, respectively, while μ_{slide} is the coefficient of frictional sliding along the fault. The ST parameter is called **slip tendency** (after Morris et al., 1996), which is a quantitative measure of the likelihood of fault reactivation: higher slip tendency implies that the state of stress along the given fault is “closer to failure” and consequently that the possibility of slip is higher.

In rock mechanics sometimes another approach being more realistic than Amonton’s law is used. In this the frictional resistance of the fault is estimated taking into account additional factors (Jaeger and Cook, 1976):

$$\begin{aligned} \tau &\geq S_0 + \mu_{slide} \cdot (\sigma_n - P_{Hidr}) \\ ST &\geq \frac{S_0}{\sigma_n} + \mu_{slide} \cdot \left(1 - \frac{P_{Hidr}}{\sigma_n}\right) \end{aligned} \quad (2.6)$$

In equation (2.6) τ and σ_n are defined as respectively the shear and normal stress magnitudes under **normal pore pressure** conditions, S_0 is the cohesion of the fault and P_{Hidr} is the overpressure of the pore fluid.

In-situ quantification of the parameters on the right-hand side of equation (2.6) is difficult, however field studies and laboratory experiments can provide information regarding their values. Knowledge of the typical range of these parameters is very important with respect to the evaluation of tectonic stability. Laboratory experiments indicate that cohesion between two sliding surfaces depends on the normal stress (e.g., Byerlee, 1978) and is found to range between 300–1100 *KPa* (Jaeger and Cook, 1976). As other experiments have shown (Krantz, 1991), cohesion along fractures generally decreases as subsequent slip occurs (e.g., large faults), but it can also be “healed” by, for example, rock–fluid interactions (e.g., Tenthorey et al., 2003). Several field studies have shown however, that neglecting cohesion along pre-existing faults is a realistic assumption (e.g., Brace and Kohlstedt, 1980; Reches, 1987; Twiss and Moores, 1992; Zoback, 1992; Plenefisch and Bonjer, 1997). This

assumption reduces equation (2.6) to a simpler form:

$$\begin{aligned}\tau &\geq \mu_{slide} \cdot (\sigma_n - P_{Hidr}) \\ ST &\geq \mu_{slide} \cdot \left(1 - \frac{P_{Hidr}}{\sigma_n}\right) = \mu_{eff}\end{aligned}\tag{2.7}$$

where μ_{eff} is the “effective” frictional coefficient. Considering constant shear and normal stress magnitudes, slip occurrence is more likely if μ_{eff} is low. This may result either from elevated pore pressure or from a reduced frictional coefficient (μ_{slide}), but in reality, slip may result from the combination of both factors. In studies evaluating earthquake focal mechanism data (Zoback, 1992; Plenefisch and Bonjer, 1997), generally the two end-members are considered: (1) pore pressure is assumed to be hydrostatic allowing the frictional coefficient to be determined or (2) frictional coefficient is assumed to be in agreement with laboratory measurements ($\mu_{slide}=0.6-1.0$ Jaeger and Cook, 1976; Byerlee, 1978) and the elevated pore pressure is determined. Using the first assumption $\mu_{slide}=0.3-0.6$ range was determined (Zoback, 1992; Plenefisch and Bonjer, 1997). Other studies also found frictional coefficients lower (0.2–0.6) than those measured in laboratory (e.g Reches, 1987; Martinez-Diaz, 2002). A decreased frictional coefficient along large faults was found to be reasonable and was explained by sliding on a gouge layer and/or the lubricating effect of clay and water (Brace and Kohlstedt, 1980; Hobbs et al., 1990).

Thus, comparison of slip tendency values with a reasonable range of frictional coefficients is a good approach to determine those faults or fault segments, that are likely to be active in a given stress field. In this idealised case, if the slip tendency overcomes the frictional coefficient of the fault, the probability of slip is high. If overpressure is not negligible then the “effective” frictional coefficient should be considered as the threshold of slip. In this case, however, the absolute magnitudes of the resolved normal stresses have to be estimated (e.g., Zoback, 1992; Plenefisch and Bonjer, 1997).

2.3 Reactivation of faults: modelling

Accurate prediction of the stresses along pre-existing faults can only be provided using sophisticated methods such as the 3-D finite element modelling method. This method however, is not ideal for a quick evaluation of the fault behaviour, since it is robust and time consuming in terms of both preparation and computation. In addition, complex models containing many faults have enormous demand on computation power and, worse, tend not to converge. Using coarser models in these situations could speed up the calculation, but with this the advantage of the fault models being detailed and three-dimensional is often lost.

2.3.1 The Wallace–Bott approach: an overview

Several frequently used forward modelling methods have been developed, which aim to quickly model the fault behaviour in a certain tectonic stress field. These methods estimate the probability and/or sense of reactivation using either a graphical approach (Mohr circles; e.g., Jaeger and Cook, 1976; Ranalli, 1987; Twiss and Moores, 1992) or an analytical approach (Sibson, 1985; Yin and Ranalli, 1992; Van Wees and Stephenson, 1995; Morris et al., 1996; Pascal, 1998; Alaniz-Alvarez et al., 2000; Pascal et al., 2002). Of these, the graphical Mohr approach is of “historical” importance, since it is simple, clear and therefore was extensively used for many years to model fault reactivation. Many successfully solved engineering problems justify the validity of this approach.

All of these techniques use the Wallace–Bott hypothesis (Wallace, 1951; Bott, 1959) which follows five main assumptions: (1) faults are planar and infinite; (2) displacement along the faults is small; (3) fault blocks are rigid and no block rotation occurs; (4) displacement is independent from displacement on other faults (no fault interactions) and (5) a single homogeneous stress field is considered responsible for the displacements. It is important to note that these forward approaches are the opposite of the more popular and widely used stress inversion methods, which use the same Wallace–Bott assumption (e.g., Angelier, 1984; Gephart and Forsyth, 1984; Reches, 1987; Gephart, 1990; Yin and Ranalli, 1995; Yamaji, 2000). The disadvantage of these either forward or backward techniques is that the calculated contact forces are based on significant simplifications of reality, neglecting many important factors such as fault interaction, fault block rotation and fault block deformation. Numerous fault reactivation studies were performed in the past using the Wallace–Bott hypothesis. None of these however, suggested that the deviation between the calculated and actual stresses along the faults would be statistically significant, since the predicted fault behaviour was always found being consistent with the Wallace–Bott approach (e.g., Zoback and Zoback, 1980; Zoback et al., 1981; Gephart and Forsyth, 1984; Bergerat, 1987; Rebaï et al., 1992; Dupin et al., 1993; Pollard et al., 1993). Thus, it has been both empirically and quantitatively demonstrated that the Wallace–Bott hypothesis is applicable to model fault reactivation as a first order approximation.

Mathematical principles

Let us assume a stress field, where one of the three static principal stresses is vertical (Andersonian). This stress tensor in its eigensystem has the following, diagonal form:

$$\underline{\underline{\sigma}}_E = \begin{pmatrix} \sigma_H & 0 & 0 \\ 0 & \sigma_h & 0 \\ 0 & 0 & \sigma_v \end{pmatrix} = \sigma_H \cdot \begin{pmatrix} 1 & 0 & 0 \\ 0 & \sigma_h/\sigma_H & 0 \\ 0 & 0 & \sigma_v/\sigma_H \end{pmatrix} \quad (2.8)$$

where σ_H , σ_h and σ_v represent the maximum horizontal, the minimum horizontal and the vertical principal stresses, respectively. This stress field in the reference

geological co-ordinate system (O, East, North, Up) has the tensor form of:

$$\underline{\underline{\sigma}} = \underline{\underline{\Omega}} \cdot \underline{\underline{\sigma}}_E \cdot \underline{\underline{\Omega}}^T \quad (2.9)$$

where $\underline{\underline{\Omega}}$ is the matrix describing the transformation between the geological co-ordinate system and the eigensystem of $\underline{\underline{\sigma}}_E$. $\underline{\underline{\Omega}}$ is a rotational matrix and can be written as:

$$\underline{\underline{\Omega}} = \begin{pmatrix} \cos \Theta & \sin \Theta & 0 \\ \sin \Theta & -\cos \Theta & 0 \\ 0 & 0 & 1 \end{pmatrix} \quad (2.10)$$

where Θ is the azimuth of σ_H . Θ is measured clockwise from north (y axis).

The normal unit vector of the surface is denoted by \underline{n} . The \underline{F} force, which acts along the surface as it is subjected to the $\underline{\underline{\sigma}}$ stress field as well as its normal and shear components respectively, are given by the following vector operations:

$$\underline{F} = \underline{\underline{\sigma}} \cdot \underline{n} \quad (2.11)$$

$$\underline{\sigma}_n = (\underline{n}^T \cdot \underline{F}) \cdot \underline{n} = (\underline{n}^T \cdot \underline{\underline{\sigma}} \cdot \underline{n}) \cdot \underline{n} \quad (2.12)$$

$$\underline{\tau} = \underline{F} - \underline{\sigma}_n \quad (2.13)$$

where $\underline{\sigma}_n$ and $\underline{\tau}$ denote the normal and shear component of the \underline{F} force, respectively. The slip tendency is defined by the ratio of the shear and normal stress magnitudes:

$$ST(x, y, z) = \frac{\|\underline{\tau}\|}{\|\underline{\sigma}_n\|} \quad (2.14)$$

In the eigensystem of the stress tensor (x', y', z' co-ordinate system) where $\underline{\underline{\sigma}} = \underline{\underline{\sigma}}_E$, by combining (2.8), (2.12), (2.13) and (2.14) the slip tendency yields the following form:

$$ST(x', y', z') = \frac{\sqrt{\left[n_x^2 + \left[\frac{\sigma_h}{\sigma_H} \right]^2 n_y^2 + \left[\frac{\sigma_v}{\sigma_H} \right]^2 n_z^2 - \left[n_x^2 + \left[\frac{\sigma_h}{\sigma_H} \right] n_y^2 + \left[\frac{\sigma_v}{\sigma_H} \right] n_z^2 \right]^2}}{n_x^2 + \left[\frac{\sigma_h}{\sigma_H} \right] n_y^2 + \left[\frac{\sigma_v}{\sigma_H} \right] n_z^2} \quad (2.15)$$

where n_x , n_y and n_z denote respectively the x , y and z components of the normal vector of the surface element described in the eigensystem of the stress tensor. It is important to note that the slip tendency does not depend on the absolute magnitude of the principal stresses. It depends only on the ratios of the principal stresses and on the relative orientation of the fault.

As discussed by Wallace (1951) and more recently by Pascal and Angelier (2003), the direction of the shear vector also depends only on the relative magnitude of the principal stresses and the orientation of the fault. Since the direction of the shear vector is associated with the direction of slip, the absolute magnitude of the stress tensor is irrelevant regarding fault reactivation. In other words, using the normalised form of the stress tensor (equation (2.4)) to evaluate fault reactivation is sufficient if the calculation is based on the Wallace–Bott approach.

For evaluation and visualisation purposes, the shear direction often has to be represented by a scalar value. This can be defined by the α angle between the dip direction (parallel to the dip-line and pointing downwards) and the direction of the shear vector. The crossproduct of the unit dip-line vector and the normalised shear vector enables one to determine the α slip direction in the full 0° – 360° range:

$$\alpha = \begin{cases} \sin^{-1} \left(\left\| \frac{\underline{dip}}{\|\underline{dip}\|} \times \frac{\underline{\tau}}{\|\underline{\tau}\|} \right\| \right) & \text{if } \left(\frac{\underline{dip}}{\|\underline{dip}\|} \times \frac{\underline{\tau}}{\|\underline{\tau}\|} \right) \cdot \underline{n} > 0 \\ 180 + \sin^{-1} \left(\left\| \frac{\underline{dip}}{\|\underline{dip}\|} \times \frac{\underline{\tau}}{\|\underline{\tau}\|} \right\| \right) & \text{if } \left(\frac{\underline{dip}}{\|\underline{dip}\|} \times \frac{\underline{\tau}}{\|\underline{\tau}\|} \right) \cdot \underline{n} < 0 \end{cases} \quad (2.16)$$

α values of 0° and 360° represent normal, while 180° , 90° and 270° represents pure reverse, left- and right lateral movements, respectively.

2.3.2 A 3–D modelling approach

In agreement with the Wallace–Bott hypothesis, the forward techniques mentioned above always use 2–D or planar fault geometries to estimate fault behaviour in a certain stress field, even if the detailed 3–D geometry of the fault system is available (typically in the case of subsurface exploration by the petroleum industry). By doing so some important aspects of fault reactivation related to changing fault shape/orientation could remain undetected.

In the following section a new analytical technique is presented, which aims to simulate the 3–D pattern of contact forces arising along faults in a certain tectonic stress field, in order to provide constraints on the 3–D pattern of fault reactivation. The method utilises the full 3–D fault geometry revealed by geological data. The calculation of the resolved stresses is based on the Wallace–Bott hypothesis: at every location on the 3–D fault surface the resolved shear and normal stresses are calculated using the local normal vector of the fault at the given location and the regional tectonic stress field. In a dynamic way local distortions of the stress field due to fault interaction, fault shape and fault block rotations are not taken into account. As mentioned in the previous section this approach is reverse of the more widely used stress inversion methods, which use kinematic data collected in the field or focal mechanism solutions of earthquakes to reconstruct the paleo- or recent stress field (e.g., Angelier, 1984; 1990; 2002; Reches, 1987; Gephart and Forsyth, 1984; Gephart, 1990; Yin and Ranalli, 1995; Yamaji, 2000). The technique presented here works the opposite way: it takes advantage of the knowledge of the regional/local stress

field and of the detailed fault shape in order to estimate the stress pattern along pre-existing faults. The calculated force pattern is used to provide constraints on fault reactivation. Faults, or fault regions, where the calculated shear forces overcome the frictional resistance of the fault are considered to be a probable location of fault reactivation.

Modelling procedure

The presented numerical analysis follows three major steps. During the first step, the 3-D geometrical model of the fault pattern is prepared and the confining stress field is determined. It must be emphasised that the method yields reliable results only if *both* the 3-D fault geometry and the recent stress field in the study area are well constrained. The 3-D fault models are represented mathematically by triangulated surfaces and are created using the techniques discussed in *Appendix A*.

During the second step the magnitudes of the contact stresses, the direction of the shear stress and the slip tendency parameters are calculated at every location of

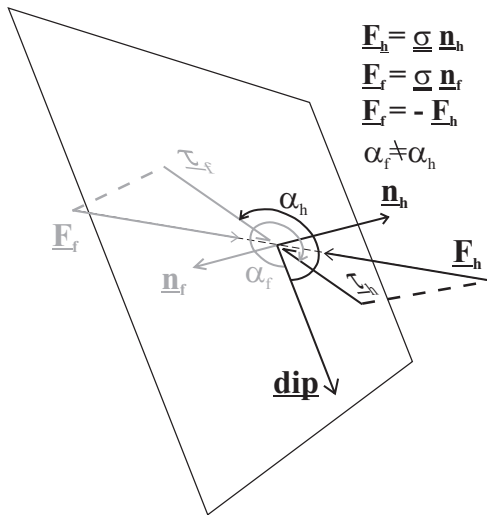


Figure 2.3: Forces (\underline{F}_f and \underline{F}_h) and their shear components ($\underline{\tau}_f$ and $\underline{\tau}_h$) acting between the two sides of a fault surface element in a stress field represented by the stress tensor $\underline{\sigma}$. The shear direction (α) is defined by the angle between the dip-line and the shear vector (equation (2.16)). See text for further discussion.

the 3-D fault models using equations (2.8)–(2.16). The calculations are performed using a Java2 computer tool, which was developed during this Ph.D. research. The inputs for the software are the 3-D fault models as well as the parameters describing the stress field. The input stress field is assumed to be Andersonian, laterally invariable and linearly depending on depth in agreement with the general observations (equation (2.2) or equation (2.4)).

From a mathematical point of view, the definition of the slip direction raises a problem, which is related to the chosen normal vector (Fig. 2.3). The same fault can be oriented either by a normal vector pointing towards the interior of the hangingwall block (\underline{n}_h) or by \underline{n}_f , which is the normal vector oriented oppositely. In case of shear faulting \underline{F}_h (\underline{F}_f) represents the pushing force of the hangingwall (footwall) block acting on the hangingwall (hangingwall) block. The relative movements of the two blocks along the fault, which are represented by the shear components of \underline{F}_h and \underline{F}_f ,

are parallel but have opposite direction. However, since α is defined as in equation (2.16), α_h does not equal α_f . This can lead to confusion if one wants to compare slip directions on faults oriented by the opposite normal vector. To avoid this confusion both α_h , representing the slip direction of the hangingwall block relative to the footwall block and α_f , representing the slip direction of the footwall block relative to the hangingwall block are calculated. As outputs, the software provides the fault surfaces with calculated shear stress vectors, slip tendencies and slip directions (α_h and α_f) as properties stored by the fault nodes.

During the third step in the numerical analysis, the statistical and/or visual evaluation of the computed parameters is carried out. For this purpose the commercial software GOCAD is used, which is also suitable for any further processing of the output parameters (e.g., corrections). Analysis of the resolved stresses in order to constrain the reactivation pattern of the faults is performed during this step.

2.3.3 Synthetic examples of the slip tendency analysis

In order to demonstrate the practical application of the fault reactivation analysis, two synthetic examples are presented. In both examples a laterally homogeneous, depth dependent stress field, described by equation (2.4), was chosen as input. Although the examples are purely synthetic, both the fault orientations and the stress ratios are realistic enough to simulate a real world scenario.

3-D example

In this example slip tendency and slip directions were calculated for three faults subjected to a stress field, whose maximum horizontal principal stress is approximately parallel to fault A (Fig. 2.4). The stress tensor describes a strike-slip faulting regime. The calculated slip tendency and slip direction values are represented as scalar patterns displayed along the faults in GOCAD. For ease of interpretation, the slip trajectories of the hangingwall blocks are also displayed.

The example demonstrates the impact of changing fault orientation on the reactivation pattern along the faults. The high slip tendency values on the upper part of Fault A (listric fault) and on the left-hand side of fault B indicate that these locations are optimally oriented to the confining stress field. For example, if the faults were cohesionless with a frictional coefficient of 0.3 (realistic value), then the upper part of fault A and the left-hand part of fault B would be predicted to more likely slip than those parts of these faults that are characterised by lower slip tendency values. The very low calculated slip tendency on fault C indicates that it is not optimally oriented to the stress field, and therefore reactivation is unlikely to occur.

The resolved shear directions show how the direction of possible slip varies along the faults as the relative orientation between the fault and the stress field varies. A nice example is fault A, which experiences pure dip slip forces in the left hand side and oblique slip forces at the right hand side.

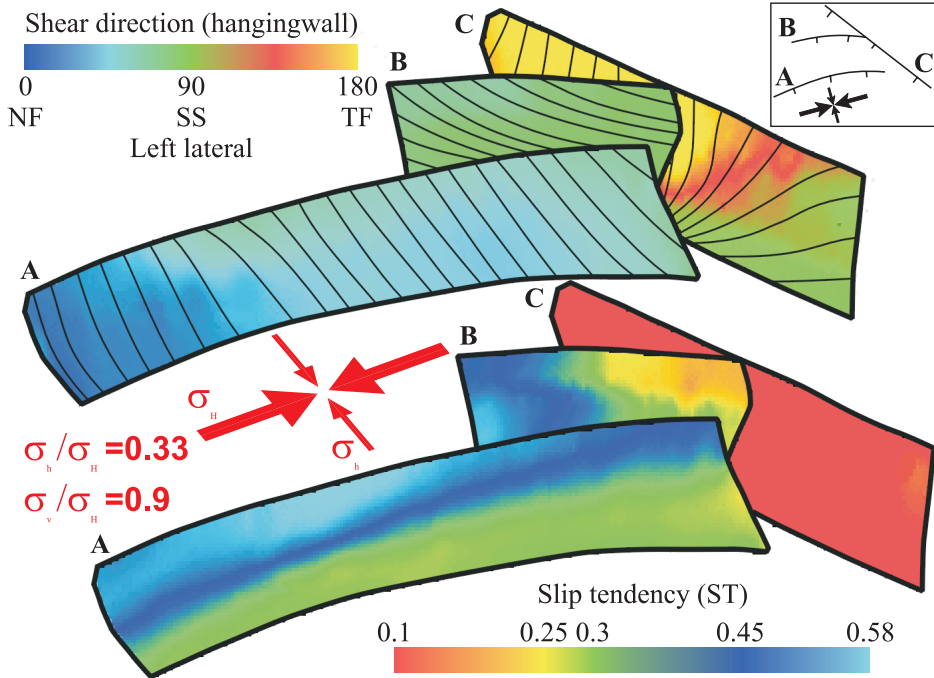


Figure 2.4: Reactivation analysis of a fictional fault system in a synthetic strike slip stress scenario. The inset shows the map view of the modelled faults A, B and C. The lower and upper panel shows the calculated slip tendency and shear directions, respectively. Shear trajectories are also shown (thin lines). NF, SS and TF denote normal faulting, strike slip faulting and thrust faulting, respectively. See text for further discussion. *Colour plate in Appendix B (p. 137).*

“2.5–D” example

In many tectonic studies a 3–D slip tendency analysis cannot be performed due to the lack of detailed 3–D fault models. Often only the average fault orientation (strike and dip angles) rather than the detailed 3–D shape of the fault is known (hence “2.5–D”). Performing a slip tendency analysis on a fault model represented by a plane is also very instructive, since it provides useful constraints on fault behaviour as a whole in the given stress field. In fact, if the approach is computerised, fault behaviour can be easily evaluated in a wide range of stress scenarios using one plot (sensitivity plot). In these plots one of the three independent stress parameters influencing the reactivation of faults (the orientation of σ_H , and the σ_h/σ_H and σ_v/σ_H ratios) is fixed and the ST as well as the shear direction parameters are displayed as the function of the other two. A given point within the sensitivity plot represents a particular tectonic stress field. The corresponding ST and shear direction values,

which represent the generated state of stress *along the fault* and consequently the fault behaviour, can be easily determined.

Many field examples have demonstrated that the regional stress field often changes its magnitude both horizontally and vertically, without changing its orientation (e.g., Rebař et al., 1992; Sassi and Faure, 1997). The sensitivity plots are very useful to monitor the changing deformation style in such scenarios. Namely, a changing stress regime on the sensitivity plot is represented by a line, along which fault reactivation parameters as well as the “moment” of fault reactivation (i.e., critical stress tensor) can be easily determined.

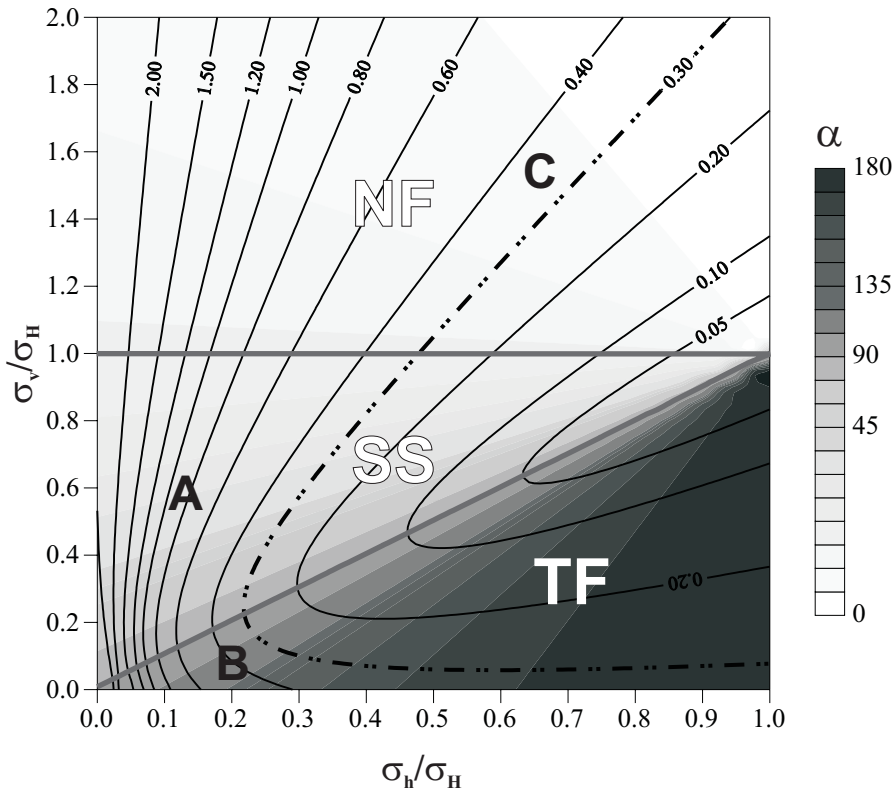


Figure 2.5: Sensitivity plot of a synthetic planar fault (N130° strike, 60° dip) as the function of the two stress-ratios. The orientation of σ_H is fixed as N135°. Slip tendency is shown as contour lines. ST values larger than 0.3 indicate fault activity. α values of 0°, 90° and 180° represent pure normal strike-slip and reverse faulting, respectively. Transitions between the three fundamental stress regimes are shown by thick lines. NF, SS, TF: normal-, strike slip- and thrust faulting stress regimes. See text for discussion.

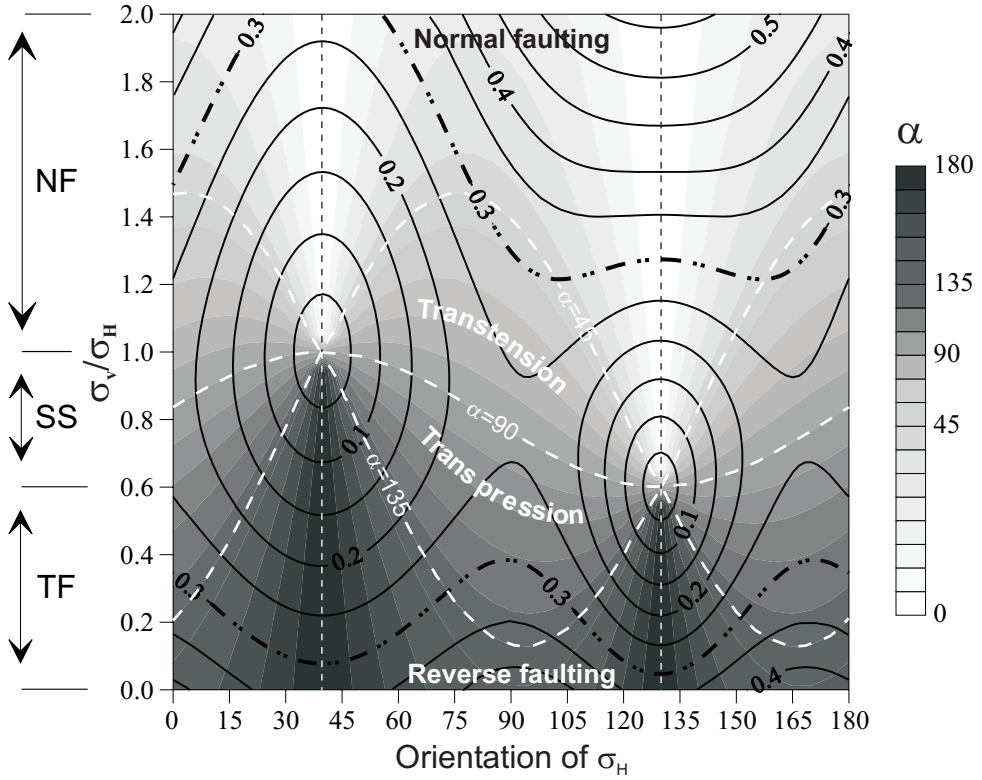


Figure 2.6: Sensitivity plot of a synthetic planar fault as the function of the σ_v/σ_H ratio and the orientation of σ_H (same fault as in figure 2.5). The σ_h/σ_H ratio is fixed as 0.6. Contours and abbreviations are the same as in figure 2.5. The two vertical dashed lines indicate stress fields with one of the horizontal principal stresses being parallel with the fault strike. Note that in these cases only dip-slip reactivation is possible.

Below, two sensitivity plots of a synthetic fault are presented. The fault has a strike direction of N130° and a dip angle of 60°. In the first plot the direction of the maximum horizontal stress is fixed at N135°, leaving the principal stress ratios to cover a wide range (Fig. 2.5). In case of the other plot a constraint regarding the ratios of the principal stress magnitudes was applied ($\sigma_h/\sigma_H=0.6$). The ST and the slip/shear direction parameters are evaluated as the function of σ_v/σ_H ratio and the orientation of the σ_H (Fig. 2.6). In both figures ST value of 0.3 is assumed to represent the slip threshold (dashed-dot-dot lines). ST values larger than 0.3 indicate that the fault is critically stressed and is prone to reactivation. In this case the calculated shear direction is assumed to be equal to the direction of slip.

Figure 2.5 demonstrates that in the largest part of the thrust faulting and strike-slip faulting regimes the ST values are not high enough to reactivate the fault (ST is lower than 0.3). Reactivation in these regimes is likely only if the σ_h/σ_H ratio is very small (lower left corner of the plot, indicated by A and B). In a more realistic range of the σ_h/σ_H ratio (0.5–1) the threshold of reactivation is reached only if the stress tensor describes a normal faulting regime (location C). It is worth mentioning that in this part of the plot (around C) the ST and α parameters are not very sensitive to the changes in the two stress ratios. This means that the reactivation parameters can be reliably estimated even if the tectonic stress field is only approximately known (i.e., only the ranges of the two stress ratios are constrained).

From figure 2.6 it is also concluded that the investigated fault “prefers” reactivating in a normal manner (slip parallel to the dip-line). Namely, in those σ_v/σ_H ratio— σ_H orientation combinations, where the calculated shear direction is transtensional, transpressional or thrust faulting ($\alpha > 45$) the ST values are below the slip threshold. Reactivation is predicted to occur only if the vertical principal stress is either very large or very small (trivial solutions) or if the orientation of σ_H is in the range of N110–150°. In other words, for easiest reactivation the direction of σ_H should be approximately parallel to the fault (this is the optimal situation for normal faults). In this range a σ_v/σ_H ratio of 1.4 or larger is needed for reactivation. It is also important to remark that forces parallel to the dip-line also arise if the orientation of the stress field is ~ 20 – 50° (σ_H is perpendicular to the fault). In this range, however, the ST is not high enough to produce slip.

2.4 Discussion

2.4.1 Reliability of the calculated resolved stresses

Several field and numerical examples have proved that the “regional stress field” at a given scale is consistent with the kinematics of faults (or fault parts) of the same scale (Rebaï et al., 1992; Dupin et al., 1993; Hardebeck and Hauksson, 2001; Martinez-Diaz, 2002). The stress tensor that is called regional is scale-dependent and can be different at different scales. Therefore, in order to adequately approximate the resolved stresses along mapped faults using the Wallace–Bott hypothesis the confining stress field at the scale of the spatial resolution of the fault models has to be known. If this condition is met, the calculated resolved stresses are reliable. Depending on the number and spatial distribution of the faults this would require stress indicators (borehole breakout, hydrofrac, overcoring etc.) to be available with high spatial density. Since this is seldom the case the input stress field is always “more regional” than would be required, resulting in different degrees of discrepancy between the calculated and the actual resolved stress pattern.

Several numerical and analytical studies have been carried out in order to quantify the uncertainty of the Wallace–Bott approach (Dupin et al., 1993; Pollard et al., 1993; Cashman and Ellis, 1994; Nieto-Samaniego and Alaniz-Alvarez, 1997). The uncertainty was evaluated in terms of deviation between the calculated and the actual slip directions. The studies show that the effect of the fault length-to-width ratio and the fault depth is negligible (less than 6° deviation). The effect of displacement along a fault on other nearby faults, however, can sometimes be significant. For example, Pollard et al. (1993) found that around a transfer fault connecting two strike-slip faults, the real stress pattern was considerably different from the regional one ($\sim 40^\circ$ deviation in slip direction). Dynamic interaction between two, non-intersecting faults was found to be dependent on the distance between them as well as on the style and amount of displacement. If the displacement is small or the distance is large the deviation between the slip directions was found to be acceptable (less than 10° deviation). In case of large displacement (due to for example a large earthquake (Cashman and Ellis, 1994)) or small distance, the discrepancy was determined to range between $20\text{--}30^\circ$ (Dupin et al., 1993; Pollard et al., 1993). As it turns out from these studies, the effect of dynamic interaction between two faults forming a transfer zone is smaller if the fault displacement contains less of a strike-slip component. As Pollard et al. (1993) pointed out, conjugate faults, which are interpreted as forming in one episode of deformation, can also interact: “If their spacing is wide relative to their length, interaction is weak, so slip direction is controlled by the regional stress field. However, for closely-spaced conjugate faults, interaction may be significant.” Faults can also interact with themselves: displacement along one part of the fault can distort the regional stress pattern on another part, especially around irregularities such as bends and bulges (Hardebeck and Hauksson, 2001). These features, which are not uncommon along faults, may be located far from the site where the initial displacement occurred.

The significance of these dynamic stress distortions is thought to depend not only on the fault geometry but also on the deformation rate (Dupin et al., 1993; Hardebeck and Hauksson, 2001). As has been suggested by Hardebeck and Hauksson (2001), if the deformation rate is slow then the tectonic loading driven by far field processes is expected to cancel out these stress variations in the long term. However, in areas characterised by high strain rates and frequent slip periods (e.g., plate boundaries such as southern California; Hardebeck and Hauksson, 2001) there may not be enough time between two subsequent earthquakes to cancel out the stress distortion caused by the previous slip episode. This could result in a very heterogeneous stress field in the long term.

Kinematic interaction between faults occurs in zones where faults intersect, since the slip direction is constrained by the geometry of the intersection line. Around the intersection line the deviation between the resolved stresses calculated using the Wallace–Bott hypothesis and the actual stresses can be significant. This distortion however was estimated to decay rapidly away from the intersection line (Dupin et al., 1993; Nieto-Samaniego and Alaniz-Alvarez, 1997).

Besides the mentioned numerical studies, numerous field studies (Zoback and Zoback, 1980; Zoback et al., 1981; Gephart and Forsyth, 1984; Bergerat, 1987; Rebaï et al., 1992; Zoback, 1992) also demonstrated that the observed slip data was consistent with the “far-field approach” and that the uncertainties were acceptable. These authors have justified that as a first order approximation the stress pattern calculated using the Wallace–Bott hypothesis is appropriate for modelling the actual stresses along faults. The 3–D approach presented in this chapter, which is also based on the Wallace–Bott approach, does not and can not take dynamically into account phenomena that deviate the local stress field from the regional one (e.g., fault interaction). In situations when the distortion is expected to be significant (some of them have been mentioned earlier) higher uncertainties should be considered in the calculated stress pattern or, if there is available data, the resolution of the input stress field should be increased. Several authors using a similar approach to the one described in this chapter have used the first order approximation of the resolved stresses to estimate fault behaviour on different scales (Morris et al., 1996; Pascal et al., 2002; Ferrill and Morris, 2003).

2.4.2 Reliability of the prediction of fault reactivation

The method presented in this chapter uses the 3–D pattern of calculated resolved stresses to constrain the probability and direction of possible fault reactivation. Providing accurate predictions of the three–dimensional pattern of fault reactivation is not easy. On one hand, the calculation of the resolved stresses is based on simple assumptions, and on the other hand the parameters on the right hand side of equation (2.6) and (2.7), describing the reactivation criterion, are generally poorly constrained. The frictional coefficient and the cohesion of the faults for example are impossible to measure *in-situ*, and they may vary from fault to fault and even along one particular fault. In addition, several earthquake studies have shown that slip on one part of the fault is often the result of displacement on another segment of the same fault (e.g., Camelbeek et al., 1994; Pace et al., 2002). The initial slip, which is generally located in the deeper part of the seismogenic layer can dynamically generate displacement even at locations where the resolved stresses were initially under the slip threshold. The location of induced slip can be kilometres or even tens of kilometres away from the initial slip (e.g., Camelbeek et al., 1994). As it was demonstrated by Houtgast et al. (2003) propagation of the induced displacement along an active fault may take considerable time (10^2 – 10^3 years) in the form of post-seismic creep.

Due to the aforementioned difficulties, it would be incorrect to think that the calculated slip tendency values at one location can be directly associated with the likelihood of fault reactivation at the same location. It is more reasonable to compare the calculated slip tendency pattern with a range of possible slip thresholds (frictional coefficients). With this approach the accuracy (“resolution”) of the reactivation pattern is decreased, but its reliability will be higher. For example, if the slip

tendency on one fault is lower than the lower limit of a reasonable range of slip thresholds then one could reliably say that the given fault is most likely locked in that particular stress field. Or if the slip tendency is higher than the higher limit of the slip threshold then that fault can be considered reactivation prone.

One should bear in mind that the value of slip tendency correlates with the likelihood rather than the “amount” of fault reactivation: higher slip tendency values suggest a higher probability of slip and not more displacement along a given fault. Numerical and field studies showed (e.g., Dirkwager et al., 2000; Dirkwager, 2002; Malservisi et al., 2003) that the amount of displacement on the surface reflected by the geological record depends primarily on the local rheology, the frictional coefficient and the geometrical parameters of the fault (e.g., length, maximum depth, connectivity). Considering identical orientation and stress field, more displacement is expected along faults that are long and interconnected with underlying deep crustal fractures than along shallow, secondary faults.

Chapter 3

3–D slip tendency analysis in the Roer Valley Rift System (SE Netherlands)

In the previous chapter a novel 3–D approach was presented, which aims to constrain the probability and style of fault reactivation. The method is based on significant simplifications, which have some consequences on the reliability of the results. In order to appreciate the capabilities, limitations and reliability of the method it needs to be tested and justified, which can be achieved in two possible ways. The first method is to compare the slip direction and slip tendency values of a detailed 3–D fault pattern obtained by the approach presented in *Chapter 2* with those calculated from a method, in which the physical problem (i.e., elastic or plastic deformation) is not simplified. This method could be the 3–D finite element geomechanical modelling technique. The other option is the classical way of justification of any novel approach: applying the method on a case study area, which is well-explored, seismically active, and where relatively much is known about the behaviour of the faults. Comparison of the modelled and observed fault behaviour provides important information about the capabilities and limitations of the method.

In this chapter this second route is followed: a detailed 3–D slip tendency analysis is performed in the Roer Valley Rift System (SE Netherlands). The scope of this study is two-fold: (1) justifying the method presented in the previous chapter by comparing the modelling results to observations regarding fault activity in the region; (2) by doing so obtaining important knowledge about the detailed reactivation pattern, about the faulting mechanism and about the regional stress field in the study area.

This chapter is partly based on: Worum, G., Van Wees, J.D., Bada, G., Van Balen, R.T., Cloetingh, S. and Pagnier, H. 2004 Slip tendency analysis as a tool to constrain fault reactivation: A numerical approach applied to 3D fault models in the Roer Valley Rift System (southeast Netherlands). *Journal of Geophysical Research* (109), B02401, doi:10.1029/2003JB002586

3.1 Introduction

The study area forms part of the Roer Valley Rift System (RVRS), which is located in the SE part of the Netherlands and adjacent parts of Belgium and Germany (Fig. 3.1). The RVRS is the most tectonically active part of the Cenozoic NW European Rift System (e.g., Ziegler, 1994), which is one of the major tectonic features of Western Europe.

The RVRS consists of three major tectonic units: the tectonically uplifted Campine and Peel Blocks, which bound the central Roer Valley Graben unit from the south and north respectively (Fig. 3.1a). Following the Mesozoic–Early Cenozoic multiphase rifting and inversion periods (Ziegler, 1990; Zijerveld et al., 1992; Geluk et al., 1994) the RVRS experienced a renewed rifting, which started in the Oligocene and it is still going on today (Zijerveld et al., 1992; Michon et al., 2003). Recently, the relative tectonic subsidence map inferred from levelling data (Kooi et al., 1998) and the study of the Quaternary deposits and river terraces in the RVRS (Van den Berg, 1994; Houtgast and van Balen, 2000) have indicated that differential tectonic movements are taking place between the Roer Valley Graben and its flanks. This differential subsidence is strongly fault controlled (Geluk et al., 1994; Van den Berg, 1994; Van den Berg et al., 1994; Houtgast and van Balen, 2000; Houtgast et al., 2002) and has manifested itself in several significant earthquakes in the last century (Fig. 3.1a). Most of these earthquakes are related to slip along the two most important fault zones: the Peel Boundary Fault Zone (PBFZ) and the Feldbiss Fault Zone (FFZ), which separate the central Roer Valley Graben from the Peel and Campine Blocks respectively.

It is generally accepted that far field stresses driven by the Alpine collision as well as the opening of the North Atlantic (*ridge-push*) control the present day dynamics of the RVRS (e.g., Ziegler, 1990; Gölke and Coblenz, 1996). In light of this the Cenozoic Roer Valley Graben has been interpreted as a transtensional basin (Kooi et al., 1991; Van den Berg, 1994). However, Digital Elevation Model (Michon and Van Balen, 2004) and earthquake focal mechanism studies (Camelbeeck et al., 1994; Plenefisch and Bonjer, 1997) have indicated recently that the two border fault zones (PBFZ and FFZ) have experienced displacement with no or minor strike-slip components.

In order to investigate the fault behaviour in the RVRS, analysis of the resolved stresses induced by the present day stress field was carried out. 47 3–D fault models, which were built using the techniques presented in *Appendix A* have been analysed during the analysis (Fig. 3.1b). These fault models represent the most important faults in the area but not all of them, since the 3–D fault database is being continuously updated. There is evidence that the faults in the area are not new faults: they have existed since Palaeozoic times (see *Chapter 4*). This makes the Roer Valley Rift System a suitable area to study the reactivation of pre-existing faults in the present day tectonic stress field.

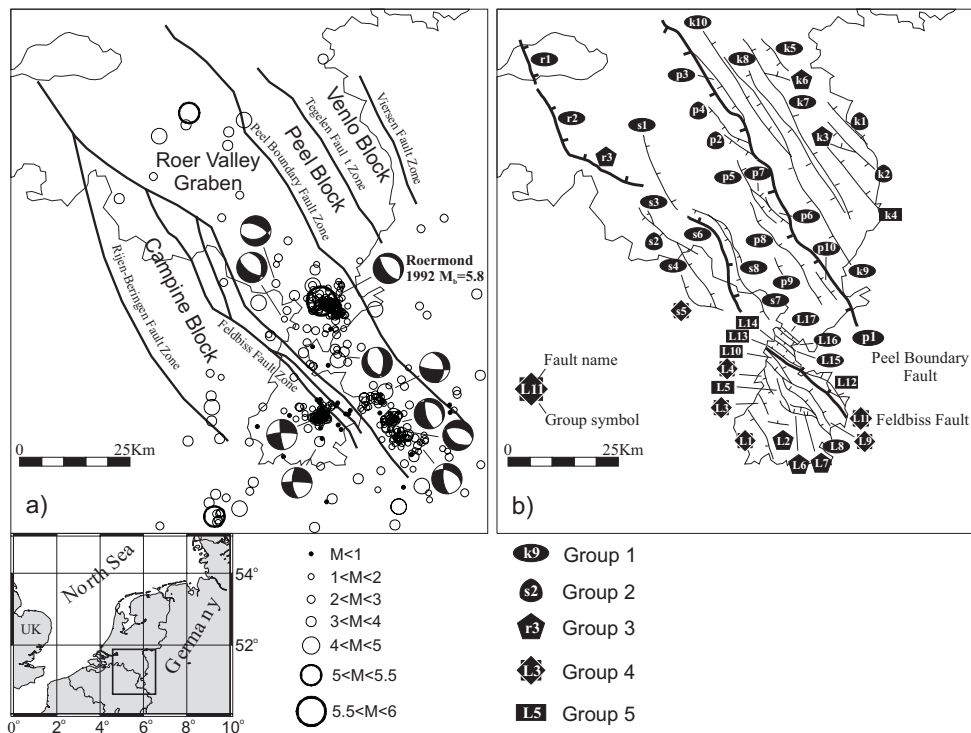


Figure 3.1: a) Main structural elements of the Roer Valley Rift System. Earthquakes that have occurred during the last century are shown by circles. The size of the circle reflect the magnitude of the event. Focal mechanisms are after Camelbeeck and van Eck (1994). b) Map view of the 3D fault models contributing to the analysis. The faults are clustered into five groups, all of which have a specific symbol. For group definition see text.

3.2 Modelling assumptions

3.2.1 Stress field

Regarding the stress field the modelling has to rely upon regional stress indicators, since local data with high spatial density are not available. By inverting the focal mechanism data of the 1992 Roermond earthquake and its aftershocks Camelbeeck et al. (1994) and Camelbeeck and van Eck (1994) found that the direction of the maximum horizontal (σ_H) principal stress was N139°. The confidence interval of the stress inversion on the other hand suggests that N135–165° directions are also possible. Borehole breakout analysis carried out in the NE Netherlands indicated a N160° ± 5 σ_H orientation (Rondeel and Everaars, 1993). These observations are in agreement with intra-plate stress orientations found in Western Europe (e.g., Ahorner, 1975; Klein and Barr, 1987; Müller et al., 1992; Plenefisch and Bonjer, 1997).

The published stress inversion data constrain also the principal stress magnitudes in the area. The R -value range (equation (2.1), p. 14) of 0.25–0.45 found by Camelbeeck et al. (1994) using the 1992 Roermond earthquake sequence, is in agreement with that of Plenefisch and Bonjer (1997) ($R = 0.4$), who used focal mechanism data from a much larger area (Upper Rhine Graben–Roer Valley Rift System). Both of these authors emphasised that the confidence regions of the stress inversion do not make possible to make an unequivocal distinction between normal faulting and strike-slip faulting stress regimes.

Based on the aforementioned observations, the following assumptions were made regarding the recent stress field in the study area: (1) due to the lack of available stress indicators with high spatial density the stress field is assumed to be laterally homogeneous within the study area; (2) σ_H direction is between N145° and N160°; (3) the R -value of the stress tensor is between 0.25 and 0.45; (4) the maximum principal stress is either vertical (normal faulting regime) or horizontal (strike-slip faulting regime).

As input, depth dependent stress fields described by equation (2.4) (p. 16) were applied. The orientation and magnitude of the input stress tensors were in agreement with the observed end members of the σ_H direction and the R -value range. Thus, slip tendencies and slip directions were calculated for stress tensors having 0.25 and 0.45 R -value as well as N145° and N160° σ_H direction. All the four R -value— σ_H orientation combinations were modelled both in normal faulting and in strike-slip faulting stress regimes. Since stress tensors with different principal stress ratios can have the same R -value, the σ_h/σ_H ratio for both R -value end members was modelled between 0.2 and 0.9 with 0.1 steps. Although there are published data sets available constraining the σ_h/σ_H ratio ($\sigma_h/\sigma_H = 0.6$; Grünthal and Stromeyer, 1994) I wanted to study the resolved stresses caused by stress fields having also lower σ_h/σ_H ratios. This altogether resulted in 64 different input stress tensors (Table 3.1).

3.2.2 Mechanical parameters

To constrain the likelihood of possible fault reactivation in the different input stress fields, mechanical parameters for the faults as well as pore pressure values should be considered. Despite the rapid late Cenozoic sediment loading, however, pore fluid overpressure is not observed in the area, therefore it has been neglected. There are no direct or indirect measurements available regarding the cohesion and frictional coefficients of the faults in the area. In this regard therefore, one has to rely upon published data sets. Following other authors (e.g., Brace and Kohlstedt, 1980; Reches, 1987; Twiss and Moores, 1992; Zoback, 1992; Plenefisch and Bonjer, 1997) the faults are considered being cohesionless. As it was discussed in *Chapter 2*, frictional coefficients ranging from 0.3–0.6 were determined for large faults in normal pore pressure conditions. For every modelled fault this range of frictional coefficients was adopted as the threshold for possible slip.

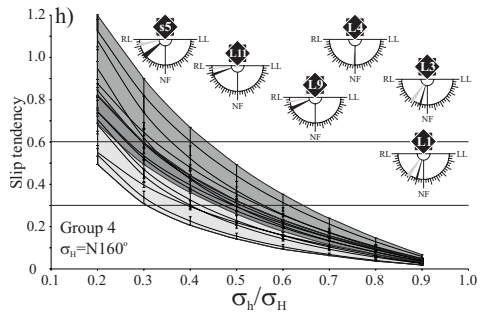
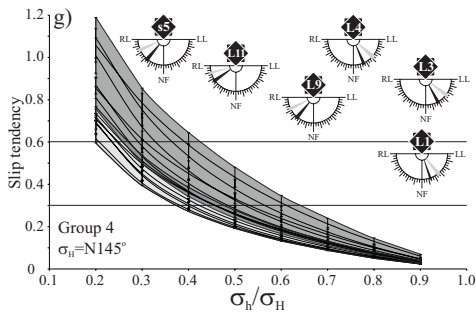
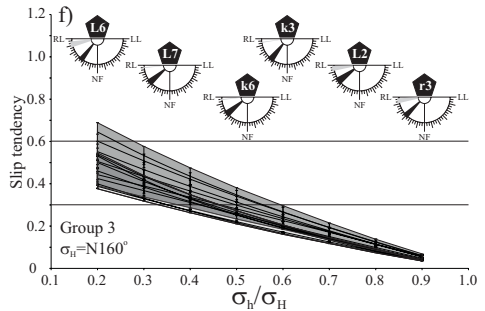
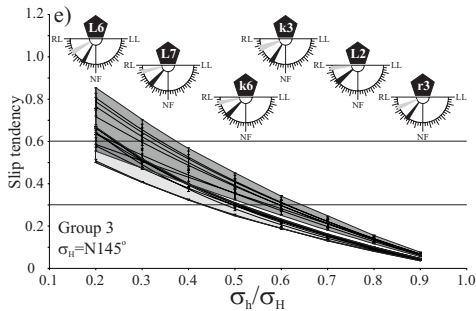
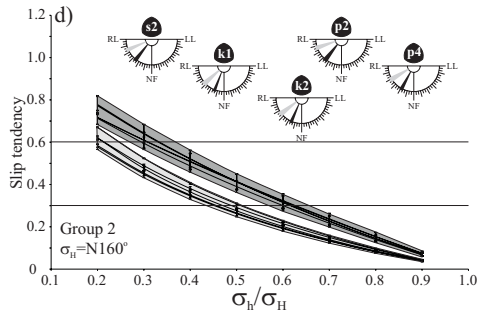
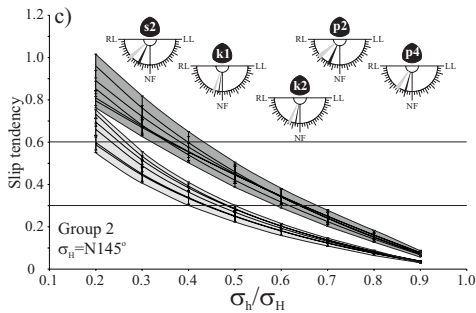
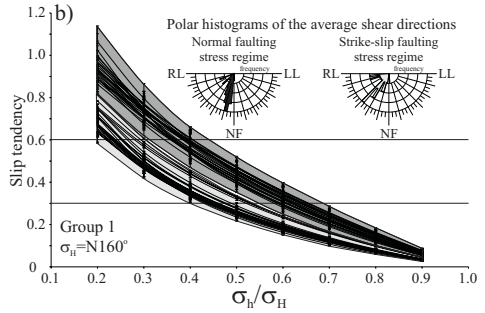
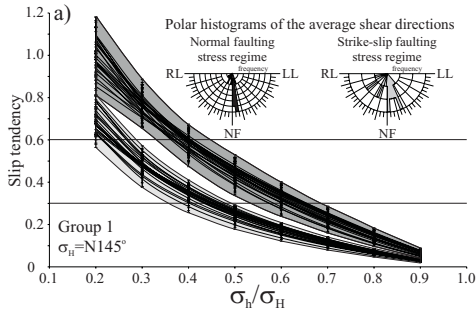
Table 3.1: Principal stress ratios of the stress tensors applied as inputs during the analysis. Stress tensors in the left- and right-hand side describe respectively normal faulting and strike-slip faulting regimes. The stress tensors are characterised by R-values (equation (2.1), p. 14) of 0.25 and 0.45, respectively. Stress tensors where any of the principal stress ratios is lower than 0.33 is marked by grey. Note that these stress tensors could generate failure in the intact rock depending on its internal cohesion, since the average internal friction angle of rocks was found to be 30° (Twiss and Moores, 1992).

R=0.25			R=0.45			R=0.25			R=0.45		
σ_h/σ_H	σ_v/σ_H	σ_h/σ_v									
0.2	1.267	0.158	0.2	1.655	0.121	0.2	0.800	0.250	0.2	0.640	0.313
0.3	1.233	0.243	0.3	1.573	0.191	0.3	0.825	0.364	0.3	0.685	0.438
0.4	1.200	0.333	0.4	1.491	0.268	0.4	0.850	0.471	0.4	0.730	0.548
0.5	1.167	0.429	0.5	1.409	0.355	0.5	0.875	0.571	0.5	0.775	0.645
0.6	1.133	0.529	0.6	1.327	0.452	0.6	0.900	0.667	0.6	0.820	0.732
0.7	1.100	0.636	0.7	1.245	0.562	0.7	0.925	0.757	0.7	0.865	0.809
0.8	1.067	0.750	0.8	1.164	0.688	0.8	0.950	0.842	0.8	0.910	0.879
0.9	1.033	0.871	0.9	1.082	0.832	0.9	0.975	0.923	0.9	0.955	0.942

3.3 Modelling results

Due to the large number of input stress tensors, not all of the results are presented in the form of a 3-D perspective view. Instead, for every fault the minimum and maximum of the average slip tendency and slip direction values were calculated. The minimum and maximum values correspond to the two end-members of the modelled R -value range (0.25 and 0.45). The range of average slip tendencies is displayed as the function of the σ_h/σ_H ratio (Fig. 3.2). For a given R -value the average shear direction does not change with the σ_h/σ_H ratio, therefore for the shear directions no such graph was created. It should be noted that on figures 3.3 and 3.4, where the 3-D pattern of slip tendencies and slip directions are shown, only a ~ 1500 m high strip in the centre of the faults is visualised. I did this in order to prevent the view of the faults from being obstructed by other faults. In reality the depth range of the faults is much larger.

For the sake of clarity the faults were clustered into five groups based on the characteristics of the $ST-\sigma_h/\sigma_H$ curves (Fig. 3.2). In the case of group 1-3, the faults belonging to the same group have similar orientations. Group 1 is the most packed group (25 faults) containing faults having $\sim N145-150^\circ$ orientation (see Fig. 3.1b). Group 2 and 3 contain faults with $\sim N130-140^\circ$ and $\sim N120^\circ$ orientations respectively. Group 4 contains faults mainly from the southernmost Limburg province having less consistent orientations and therefore less consistent $ST-\sigma_h/\sigma_H$ curve shapes than faults in the previous groups. Group 5 (not represented on figure 3.2) is the “group of outliers” (6 faults also mainly from Limburg), which contain faults with $ST-\sigma_h/\sigma_H$ curve characteristics not fitting into any of the previous groups.



3.3.1 Slip tendencies

Both the average values (Fig. 3.2) and the 3-D patterns (Fig. 3.3) indicate that the slip tendency is a decreasing function of the σ_h/σ_H ratio both for normal faulting and for strike-slip faulting stress regimes. It is also clear that the slip tendency of the modelled faults is always lower for strike-slip faulting stress tensors than for normal faulting ones, indicating that reactivation would be more difficult if the σ_2 were vertical. None of the faults is likely to reactivate if the σ_h/σ_H ratio is larger than 0.65 for normal faulting and 0.5 for strike-slip faulting regimes, since then the calculated slip tendency is lower than the lower limit of the adopted frictional coefficient (i.e., 0.3).

In all the modelled stress tensor cases, there is an observable difference in slip tendency between faults belonging to group 1, 2 and 3. When the stress tensor describes a normal faulting regime, groups 1 and 3 have the highest and the lowest average slip tendency, respectively. This indicates that faults in group 1 are more suitably oriented to these stress tensors than faults in group 3. This is expected considering the orientations of the faults within these groups. The σ_h/σ_H ratio where the slip tendency overcomes the upper limit of the reasonable frictional coefficient (0.6) is different for every group. For normal faulting stress regimes it is between 0.4 (group 1) and 0.3 (group 3), for strike slip faulting regimes it is lower than ~ 0.25 . This means in other words, that either a reduced slip threshold or stress tensors with very low σ_h/σ_H ratio are needed to reliably indicate that the faults are active in the study area. To provide more accurate predictions, better constraints regarding the stress magnitudes and the frictional parameters of the faults would be required.

The slip tendency difference observed for stress tensors having identical magnitudes but different orientations can be characterised by a constant value, therefore the 3-D slip tendency patterns are only provided for the N145° case (Fig. 3.3). In cases where the stress field describes a normal faulting regime, all of the faults experience a slip tendency drop if the stress field is rotated to N160° (Fig. 3.2). This drop is the largest for group 3 ($\sim 1-1.5$). An opposite effect (slightly higher *ST* values) can be observed in examples, where the stress field is within the strike-slip-faulting regime.

Figure 3.2: Average calculated slip tendency of the faults as the function of the σ_h/σ_H ratio. The shaded areas indicate the total range of possible slip tendencies within the given group of faults. Light grey is for strike-slip-faulting stress tensors, dark grey is for stress tensors describing a normal faulting stress regime. Insets for panel “a” and “b” show the polar histograms of the average shear directions for group 1 (for group definition see text and figure 3.1b). Other insets (panel “c”–“h”) show the average shear direction range for the given fault representing the two end-members of the *R*-value range (0.25–0.45). Black colour is to indicate normal-faulting stress tensors light grey is for strike slip faulting stress tensors. The left and right panels correspond to stress tensors with σ_H orientation being N145° and N160°.

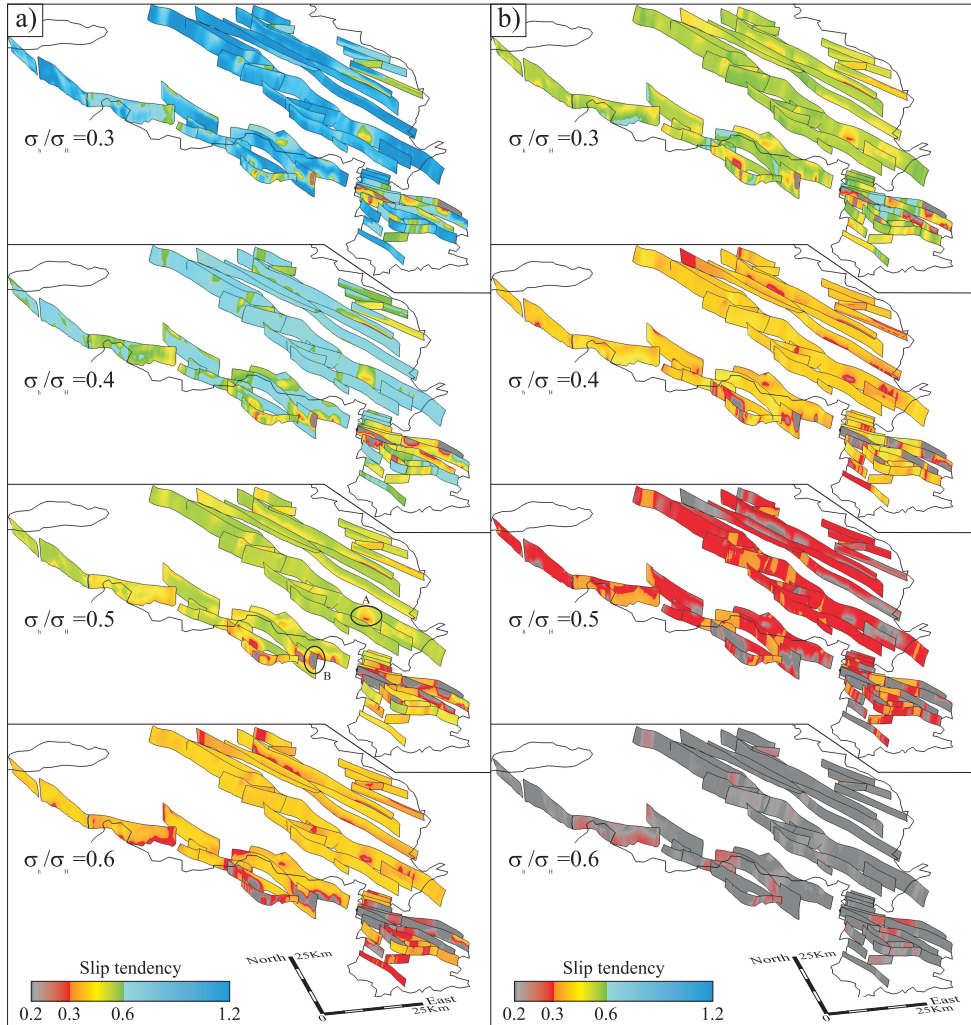


Figure 3.3: Perspective view of the 3-D faults with slip tendency patterns calculated for stress tensors having different σ_v/σ_H ratios and σ_H directions of N145°. Vertical scale is 4x exaggerated. Panel “a” is for stress tensors describing a normal faulting regime, panel “b” is for strike-slip-faulting stress tensors. The R -value of the stress tensor was modelled as 0.45 for panel “a” and as 0.25 for panel “a” representing the maximum slip tendencies within the modelled R -value range. *Colour plate in Appendix B (p. 140).*

3.3.2 Slip directions

Due to the relatively low R -value of the input stress tensors, there is a moderate to significant strike-slip component in the shear vectors even when the stress tensor describes a normal faulting regime and the angle between the fault strike and the orientation of σ_H is small (see Fig. 3.2 and the greenish and reddish cast on figure 3.4a). Shear directions with minor (0 – 15°) lateral components were found only along the Peel Boundary Fault (p1 fault) and along other faults within group 1. This is expected since σ_H of the modelled stress tensors is quasi parallel to these faults. Since the Peel Boundary Fault consists of differently oriented segments, along its length there is a slight alternating left- and right-lateral shear component (greenish and reddish cast respectively) superimposed onto the pure dip-slip (yellow) component (Fig. 3.4).

If the stress tensor describes a strike-slip-faulting regime, the lateral component of the shear direction is more important even if the σ_H is oriented as $N145^\circ$. If σ_H has a $N160^\circ$ direction even the faults in group 1 are predicted to have oblique shear directions, while other faults, especially in the southernmost Limburg area (L-faults) show pure right-lateral shear directions (red colours on Fig. 3.4).

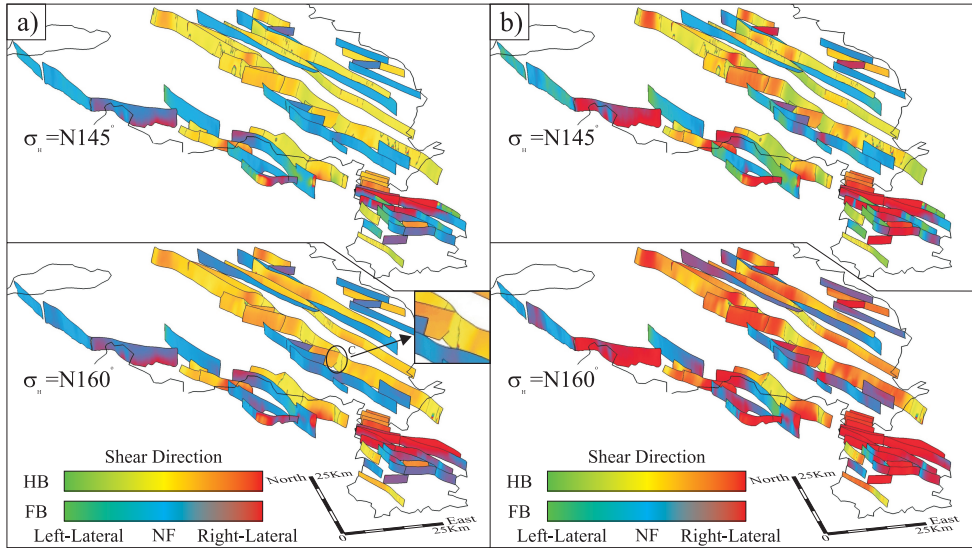


Figure 3.4: Perspective view of the 3-D faults with shear direction patterns calculated for stress tensors having different σ_H directions of $N145^\circ$ and $N160^\circ$. Vertical scale is 4x exaggerated. Panel “a” is for stress tensors describing normal faulting regime, panel “b” is for strike-slip-faulting stress tensors. The R -value of the stress tensor was modelled as on figure 3.3. HB: hangingwall-block; FB: footwall-block; NF: normal faulting (dip slip shear direction). *Colour plate in Appendix B (p. 141).*

3.3.3 Synthesis of the results

From the results presented above it is concluded that the maximum principal stress of the stress field in the area is more likely to be vertical (normal faulting regime) than horizontal. This conclusion is built upon the following: (1) if the stress tensor describes a strike-slip faulting regime then a much lower σ_h/σ_H ratio is required to overcome a given slip threshold; (2) very low σ_h/σ_H ratios would be in disagreement with σ_h/σ_H predictions based on finite element modelling (Grünthal and Stromeier, 1994); (3) in case of a stress tensor with σ_2 being vertical, a very low slip threshold (0.1–0.2) would be required to reactivate the faults within a reasonable range of σ_h/σ_H ratios, which would suggest very low frictional coefficients or high pore fluid pressures, which are not observed in the area.

3.4 Discussion

3.4.1 Reliability of the results

In this chapter slip tendency and slip direction patterns were calculated for 3-D fault models in different tectonic stress fields. The results were presented as detailed 3-D patterns along the faults as well as average values. The reliability of the results depends on the reliability of the fault models and the validity of the input stress field. The fault models in the area are based on regional mapping data and were created in GOCAD from fault trace lines. Due to inconsistencies within these data, some fault models contain unreal features, which are also reflected in the slip tendency and slip direction patterns. Locations A and B on figure 3.3 are two typical examples of this, where a small area with a low slip tendency value is surrounded by slip tendencies with twice the value. These are artefacts, since it would be unrealistic to think that a small patch in the middle of the fault could be locked while the surroundings are active. The average of the calculated parameters (ST and α) along the faults was also taken, since it sometimes provides a more reliable representation of slip tendencies and slip directions than the detailed 3-D pattern.

This study revealed that all shear directions calculated for some fault models in the Limburg area (L9, L10, L11, L12, L13, L14) contain significant lateral components even if the input stress tensor describes a normal faulting regime. The analysis of river terraces displaced by the Feldbiss Fault Zone (L9, L10, L11, L12), however, revealed that dip slip reactivation of these faults has taken place in the Quaternary (Houtgast et al., 2002). The observed difference could be explained by the fact that the 3-D models of the relevant faults are very steep (L12 is almost vertical). It is suggested that these geometrical fault models (and the results) are not reliable and should be reviewed.

The validity of the input stress field (and therefore the reliability of the results) depends on the general style of deformation within the study area. In those cases where the stress tensor described a strike-slip-faulting regime, the lateral component of the calculated shear directions was found to be significant. As discussed in the previous chapter, in a scenario like this the curvature of the fault bends and the spacing between faults are very important parameters, which could deviate the local stress pattern from the stress pattern calculated using the Wallace–Bott hypothesis. Since as input the regional stress field was used, and since this approach does not take into account distorting factors such as fault interaction, a higher uncertainty should be considered in cases of strike slip faulting stress regimes. Precise evaluation of the amount of uncertainty, however, was not performed, since a more sophisticated method would be required to do so.

Kinematic interaction between intersecting faults could be significant in some cases in the study area even if the stress field describes normal faulting. Location C in figure 3.4 is an example, where besides the dominant dip-slip component a slight left- and right-lateral component is present in the shear direction along two intersecting faults. Along this and similar intersection lines there is a discrepancy in the shear directions between the two faults. The calculated slip tendency therefore is also expected to be less reliable.

3.4.2 Comparison of the results with observations

In figure 3.5 the depth of the base Quaternary horizon as well as its gradient map is shown. This map as well as some published earthquake focal mechanism data are used to compare the modelling results with observations. Only those results, where the stress fields described normal faulting regimes, are considered.

Quaternary fault activity

The calculated slip tendencies are compared with the gradient map of the base Quaternary horizon as a recorder of the Quaternary fault activity. The first important observation is that the largest offsets are found along the Peel Boundary Fault (p1) and the Feldbiss Fault Zone (L11, L9, s6, r3, r2, and r1 faults). These faults were reported to be the neotectonically most active faults in the area (e.g., Houtgast et al., 2002; Michon and van Balen, 2004). As it was discussed in *Chapter 2*, this may imply that these faults are primary faults interconnected with deeper fractures rather than that the slip tendency along them is higher than along other faults in the area. This further suggests that the small secondary faults related to these boundary faults (almost all of the p faults for example) cannot be considered as being independent from the boundary faults: their reactivation has been strongly affected by the behaviour of the main fault (e.g., Pace et al., 2002; Martinez-Diaz, 2002). Location A in figure 3.5 shows a good example of this, where the amount of vertical displacement along the Peel Boundary Fault drops by a factor of two. The

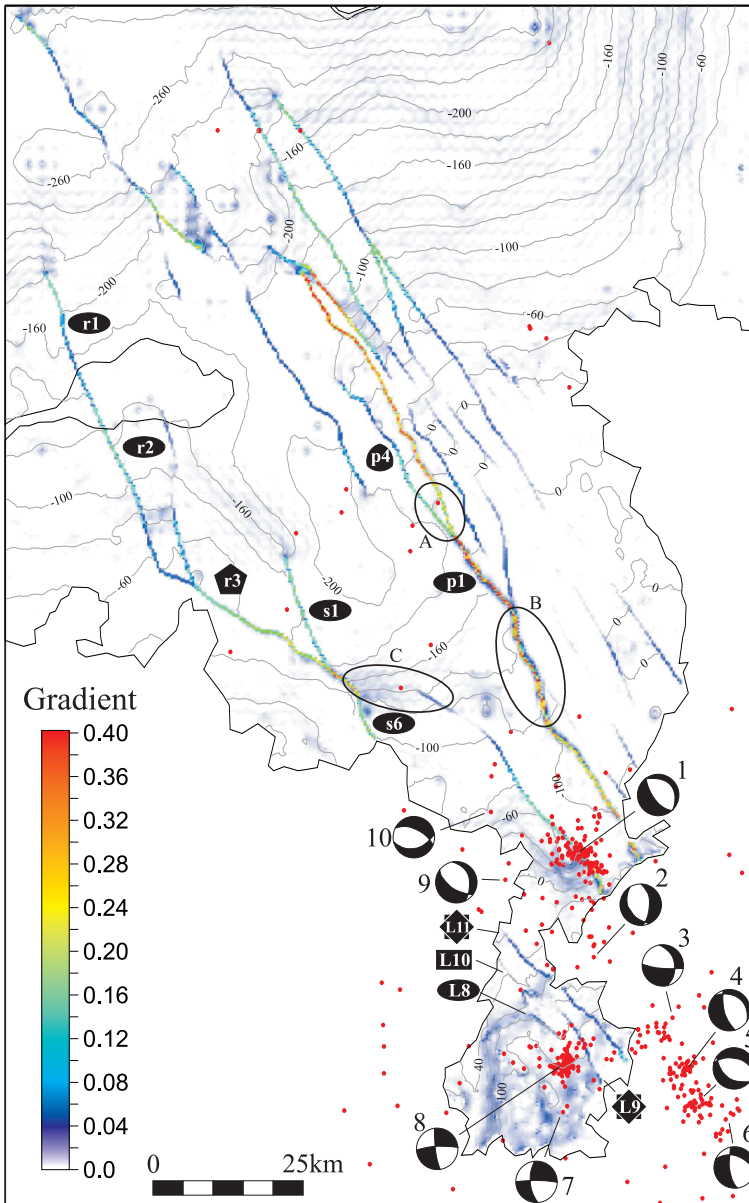


Figure 3.5: Depth map of the base Quaternary horizon (contours; after De Mulder et al., 2003) and its gradient map. Higher gradients imply larger offsets. Earthquakes of the last century are shown in red. Focal mechanisms are from Camelbeeck and van Eck (1994). *Colour plate in Appendix B (p. 144).*

“missing” displacement is taken up by the fault p4, which branches from the PBF. As the figure shows however, this interaction decays rapidly away from the intersection point. Therefore, although the main assumptions of the modelling technique include independent faults, it is proposed that the slip tendency and slip direction patterns along faults should always be evaluated in a regional tectonic context.

The second interesting observation is that the majority of the faults which have expression in the Quaternary record are directed as $\sim N145^\circ$, that is parallel to the orientation of the stress field. In other words, the high calculated slip tendency for these faults (group 1) in normal faulting stress regimes is in agreement with their Quaternary activity. Faults k3 and k6 (see Fig. 3.1) which are differently oriented than the faults in group 1 always experience lower slip tendency values during the analysis and do not show any activity in the Quaternary. Unfortunately there is no direct correlation between slip tendency and the activity of a given fault: fault r3 is one of the most active faults in the area despite the fact that it is similarly oriented and has similar slip tendency values as faults k3 and k6. This again emphasises that the tectonic context of a fault and its position in the fault hierarchy is equally if not more important with respect to fault reactivation than its orientation: k3 and k6 are short secondary faults, while r3 forms part of the southern boundary fault zone (FFZ). Displacement along this segment, which was predicted to have $\sim 30^\circ$ of lateral component, is suggested to be dependent on the displacement along adjacent segments (s6 and r2), which are optimally oriented to the stress field.

Earthquake focal mechanisms

Camelbeek et al. (1994) suggested that a simple plane extrapolation of faults known from the uppermost crust to the lower crust is unsatisfactory in the case of the Roer Valley Rift System. I used 10 published earthquake focal mechanisms presented on figure 3.5 to compare displacements in the deeper part of the seismogenic layer with calculated shear directions believed to be valid in the upper few kilometres of the crust. With the exception of events 7 and 8 these earthquakes occurred along the SW dipping PBFZ and the NE dipping FFZ and therefore their epicentres are located in the middle of the graben. The nodal planes of events 1, 4, 6 and 9 correlate well with the general strike of the Peel Boundary and Feldbiss faults. Other events (events 2, 3, 5 and 10) are postulated either to occur along differently oriented segments (similar to the segment marked by B on Fig. 3.5) or along branching faults of the main boundary faults. Faults with directions parallel to the nodal planes of events 3, 5, and 10 are present in the basement, and the Quaternary geological record reflects displacement along them (fault r3 and its continuation (Location C on Fig. 3.5)). The joint presence of earthquakes along the PBF/FFZ and along branching faults suggests that the influence of the boundary faults on closely related secondary faults is important in the area.

The focal mechanisms of events 7 and 8 suggest pure lateral displacement along very steep planes. The orientations found for these nodal planes (\sim E-W or N-S) are also present in the subsurface fault pattern: L2, L6, and L7 for example. However, there is some discrepancy between the predicted slip direction for these faults and the focal mechanisms of events 7 and 8 (oblique slip vs. pure strike-slip), which could be attributed to the different dip angle. This on one hand may suggest that fault dip is different in the deeper than in the uppermost part of the crust in this area. On the other hand it may also be attributed to the fact, that due to the morphology and the lack of high quality seismic surveys the fault models in this southernmost area are not so reliable.

The focal mechanisms of events 1–6 and 9–10 describe dip-slip movements with no or minor strike-slip component, which is in agreement with the modelling results. On one hand this is not surprising since the input stress tensors used in the analysis were constrained by the results of stress inversion methods, which are based on the same principles as the forward method used during the modelling. On the other hand, however, it is interesting to see that the slip directions observed in the deeper part of the seismogenic layer correlate reasonably well with the calculated shear directions using fault data from the uppermost crust. This suggests that as a first order approximation both the principal stress ratios and the fault orientations can be considered invariable throughout the whole seismogenic layer in the Roer Valley Rift System. Quasi depth independent principal stress ratios were found to be reasonable in intra-plate conditions (e.g Jaeger and Cook, 1976; Brudy et al., 1997; Plenefisch and Bonjer, 1997; Ito and Zoback, 2000).

3.4.3 Comparison with other studies

Based on the finite element method Grünthal and Stromeier (1994) modelled the present day state of stress in Central and Western Europe induced by far field processes such as the push of Africa and the opening of the Atlantic. They determined that the ratio of the minimum and maximum horizontal principal stresses are nowhere lower than 0.6. The results presented in this chapter reveal that the calculated slip tendencies at $\sigma_h/\sigma_H = 0.6$ are below or just above 0.3. Below the slip tendency of 0.3 the faults are likely to be locked, which is in disagreement with the Quaternary record. This discrepancy could be resolved by assuming that the slip threshold of the faults is lower (0.2–0.3) than was assumed. On the other hand Grünthal and Stromeier (1994) used regional data to determine the $\sigma_h/\sigma_H > 0.6$ relation: local effects were not taken into account. For example, deep seismic profiles across the Netherlands suggest that a thicker crust with different rheology exists in the London–Brabant Massif than in the Roer Valley Graben (Rijkers and Duin, 1994). Other studies (Illies and Fuchs, 1983) suggest that oppositely rotating crustal blocks present in the Rhenish Massif could explain the opening of the Lower Rhine Embayment. This process, together with a heterogeneous rheology, could generate concentrated excess stresses in the SE Netherlands. This could result in a somewhat

lower σ_h/σ_H ratio in the crust being more favourable for fault reactivation. However, significant lowering of the σ_h/σ_H ratio by these local effects is not expected. This suggests that in order to explain the observed fault activity slip thresholds in the lower section of the adopted range (between slip tendency of 0.3 and 0.4) have to be assumed.

3.5 Conclusions

3-D geometrical fault models give an excellent opportunity to study the 3-D pattern of forces acting along faults in a certain tectonic stress field. Using these models in combination with assumptions of the regional tectonic stress field around the faults, the shear and normal stresses at every location of the faults can be quickly calculated. Although the shear and normal stresses calculated using the method that was presented in the previous chapter represent only a first order approximation of the real stresses around the faults, the patterns of slip tendency and shear direction provide useful, three-dimensional constraints on the likelihood and style of fault reactivation.

In the Roer Valley Rift System earthquake focal mechanism studies are inconclusive as to whether the stress regime is normal- or strike-slip faulting. Analysis of the slip tendency and shear direction patterns in the Roer Valley Rift System demonstrates that the faults are more likely to reactivate in a normal faulting stress regime. In a strike-slip faulting regime a very low σ_h/σ_H ratio would be required to reactivate the faults, which is not in accordance with continent-scale modelling studies. Even in case of normal faulting stress regimes high probabilities of fault reactivation (i.e., $ST > 0.6$) were obtained only at σ_h/σ_H ratios lower than ~ 0.4 . This is still lower than that determined by these European-scale studies ($\sigma_h/\sigma_H \sim 0.6$). In order to explain the observed fault activity within a reasonable range of tectonic stress magnitudes a slip threshold (frictional coefficient) of 0.3–0.4 and a stress tensor with a σ_h/σ_H ratio of 0.5–0.6 would be required. Slight discrepancies between the σ_h/σ_H ratios suggested by this study and those inferred from continent-scale modelling could be attributed to local effects.

In the case of normal faulting stress regimes the case study demonstrates that the faults that were active in the Quaternary also have the highest slip tendency values. In addition there is a reasonably good correlation between the calculated and observed slip directions represented by earthquake focal mechanisms. These results suggest that in the Roer Valley Rift System the fault models mapped in the uppermost part of the crust are suitable to constrain fault behaviour even in the deeper parts of the seismogenic layer. On the other hand model results also show that knowledge of the hierarchy and the regional tectonic context of the faults are required to explain the slip tendency and shear direction patterns. For example, secondary faults in the close vicinity of the Peel Boundary and Feldbiss Faults interconnected with deep crustal fractures should not be considered as being independent.

Chapter 4

Pre-Neogene controls on present-day fault activity in the southern Netherlands: role of variations in fault orientation in a uniform low-stress regime

The West Netherlands Basin (WNB) and the neighbouring Roer Valley Rift System (RVRS) form two of the most prominent geological features of the onshore Netherlands (Fig. 4.1). The basins are part of a 250 km long and 50 km wide Mesozoic basin system stretching in a NW–SE direction, which has been extensively studied in the past and is one of the geologically most explored areas of the Netherlands (e.g., Van Balen et al., 2000; Michon et al., 2003).

The present-day tectonic activity of the RVRS and WNB is markedly different despite their common tectonic origin and Mesozoic evolution. The seismic record of the last 100 years and numerous geological, morphological and geophysical studies indicate that the RVRS is currently characterised by ongoing, fault controlled intraplate deformation (e.g., Groenewoud et al., 1991; Camelbeeck et al., 1994; Van den Berg, 1994; Ziegler, 1994; Kooi et al., 1998; Houtgast and Van Balen, 2000; Michon et al., 2003; Michon and Van Balen, 2004; Van Balen et al., 2004). Faults and tectonic basement blocks of Mesozoic and Palaeozoic origin play a major role in the neotectonic activity of this region. In contrast, the WNB area has been in the Neogene–Quaternary characterised by a uniformly distributed, low amount of regional subsidence without abrupt changes in sediment thickness (Zagwijn, 1989; Kooi et al., 1998; De Mulder et al., 2003). In addition, there are no geomorphic indications for fault activity and the area is seismically quiet.

This chapter is based on: Worum, G., Michon, L., Van Balen, R.T. Van Wees, J.D., Cloetingh, S. and Pagnier, H. 2004 Pre-Neogene controls on present-day fault activity in the West Netherlands Basin and Roer Valley Rift System (southern Netherlands): role of variations in fault orientation in a uniform low-stress regime. *Quaternary Science Reviews*, in press

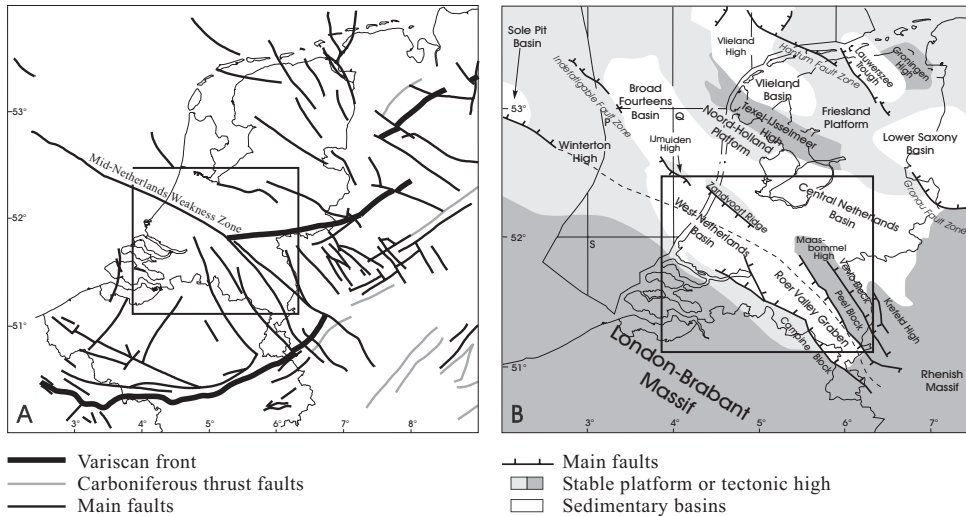


Figure 4.1: a) Main tectonic features of the Netherlands and its surroundings after the Variscan orogeny (modified after Lokhorst, 1998). b) Main Mesozoic tectonic features (modified after TNO–NITG, 2002). The Mid Netherlands Weakness Zone is indicated by a dashed line. Box indicates the study area.

In this chapter the present-day tectonics and fault behaviour of the WNB and the RVRs are compared and modelled using the three-dimensional pre-Tertiary fault pattern of the two basins. Structural analysis of the two basins reveals slightly different fault orientations. Using the technique presented in the previous chapters (3-D slip tendency analysis, Worum et al., 2004) it is to be determined whether — assuming a uniform regional stress field — these differences in fault orientation are substantial enough to produce significantly different resolved stresses along the faults, and to explain the difference in style of deformation.

In order to better understand and explain the modelling results and the observed differences in neotectonic behaviour it is essential to review the pre-Quaternary basin evolution prior to modelling. This is done in the first part of this chapter, and delivers important constraints regarding the origin of the present-day tectonic movements in the RVRs. Then a detailed fault orientation analysis is performed comparing the Mesozoic, Tertiary and present-day fault patterns in the basin system. This analysis reveals that the Mesozoic fault orientations in the two basins are slightly different, and also that ancient tectonic orientations exert a great influence on the Tertiary and present-day deformation in the basins. Finally, a slip tendency analysis is performed using the 3-D geometry of the fault systems. The results are discussed in light of the pre-Quaternary evolution of the basin system. Possible processes and tectonic models that could explain the observed neotectonic differences, are also discussed.

4.1 Tectonic setting and evolution of the WNB–RVRS basin system

Due to differences in the sedimentary record and in neotectonic activity, the two basins have always been treated as separate tectonic units, despite the fact that they have a common tectonic origin and Mesozoic evolution. It is generally accepted that the WNB and the central trough of the RVRS (Roer Valley Graben (RVG)) are superimposed on an ancient tectonic lineament, which was formed due to wrench movements after the Late Carboniferous–Early Permian Variscan orogeny (e.g., Ziegler, 1990; Michon et al., 2003; Fig. 4.1a). In addition, study of the Campine Basin (part of the Carboniferous Variscan foredeep (see Fig. 1.3; p. 5) and “ancestor” of the Mesozoic WNB–RVG system) indicates an even older origin (Langanaeker, 1998; TNO–NITG, 2002). From now on I refer to this deep crustal lineament as the Mid Netherlands Weakness Zone, which is located in the centre of the basin system, as indicated by earthquake epicentres (see Fig. 3.1a; p. 33). The Mid Netherlands Weakness Zone is not to be confused with the Mid Netherlands Fault Zone (e.g., TNO–NITG, 2002), which is the subsurface manifestation of the former. The Mid Netherlands Fault Zone came into existence during the Mesozoic and forms the north-eastern boundary of the basin system. Several uplifted tectonic blocks are associated with this fault zone such as the IJmuiden High, the Zandvoort Ridge, the Maasbommel High and the Peel Block (Fig. 4.1b). To the SW, the basin system is bounded by the tectonically stable London–Brabant Massif of Variscan origin.

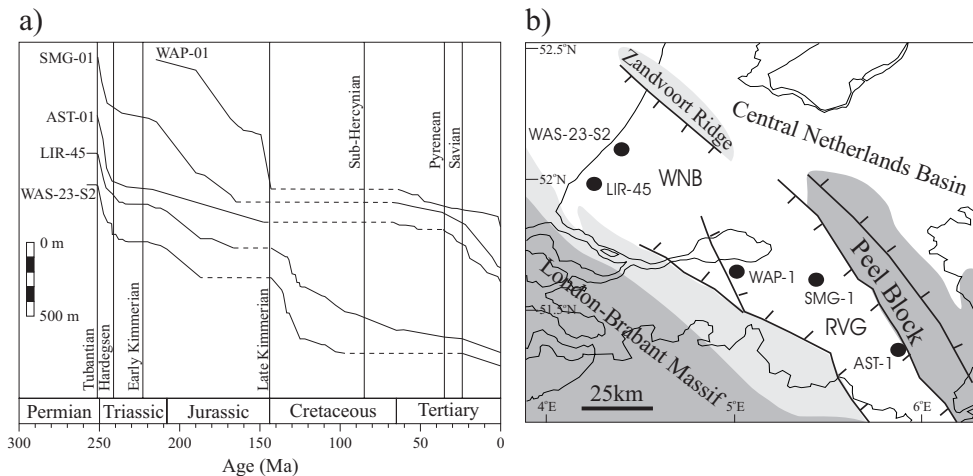


Figure 4.2: Tectonic subsidence curves of five representative wells located in the WNB–RVRS system. Horizontal dashed lines indicate unconformities. b) Location of the wells (after Zijerveld et al., 1992 and Van Balen et al., 2000).

The Late Palaeozoic–present day evolution of the WNB–RVRS basin system is illustrated by tectonic subsidence curves of five representative wells (Fig. 4.2). The curves provide the tectonic component of the total observed subsidence after removing the effect of compaction of the sedimentary column and the isostatic response of the lithosphere due to the sediment load. The backstripping analysis was carried out by Van Balen et al. (2000) (LIR–45 and WAS–23–S2 wells) and by Zijerveld et al. (1992) (WAP–1, SMG–1 and AST–1 wells).

4.1.1 Late Palaeozoic–Mesozoic

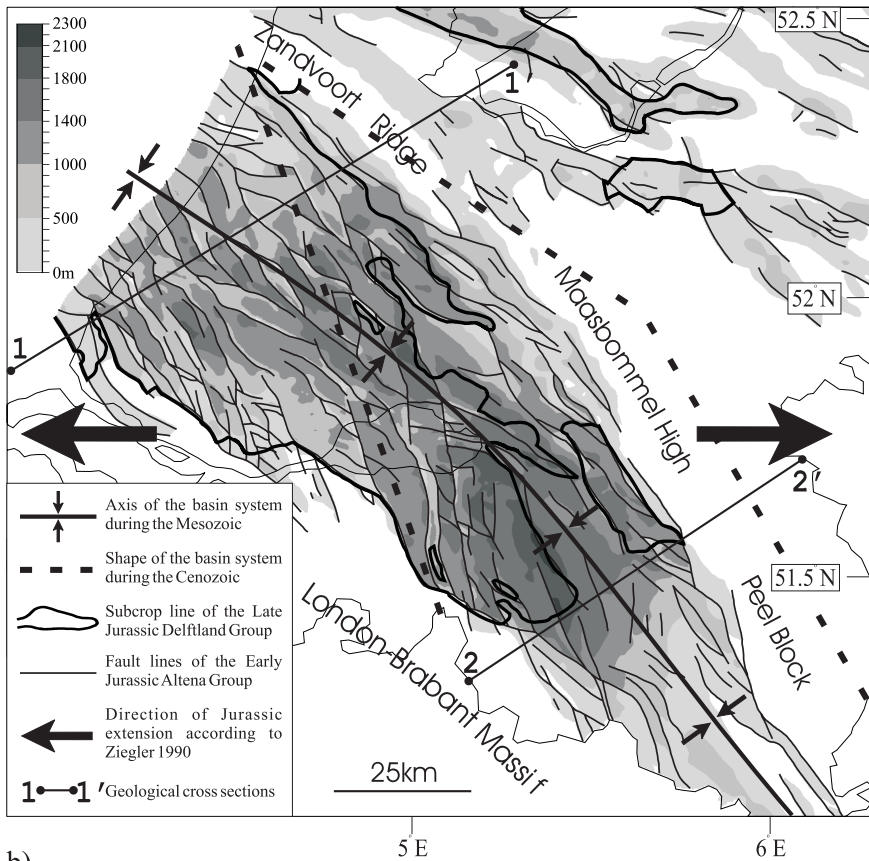
The late Palaeozoic–Mesozoic evolution of the WNB–RVRS system is characterised by multiple rifting phases induced mainly by the opening of the Tethys and the North Atlantic oceans (e.g., Ziegler, 1990). Of these the late Permian, Late Triassic and Late Jurassic–Early Cretaceous rifting phases are the most important (Fig. 4.2a). The last phase is not always recognisable in the RVG due to the Late Cretaceous inversion, which resulted in a significant hiatus in the sedimentary record (dashed lines in Fig. 4.2a). The deformation phases during these periods induced differential subsidence and created several sub-basins in the area. The margins of this system were significantly uplifted (Van Wijhe, 1987; Ziegler, 1990; Geluk et al., 1994).

The Mesozoic evolution is well illustrated by the thickness map of the Lower Jurassic Altena Group (Fig. 4.3 and Fig. 1.2 (p. 3)). Analysis of the structural cross-sections and the thickness pattern reveals that in the RVRS one sub-basin was formed, which is narrow, relatively deep and apparently controlled by NNW directed faults. Considering an E–W oriented extension during this period (Ziegler, 1990), the nearly N–S orientation of the faults favoured (1) important vertical displacement along the fault planes and (2) large subsidence in a narrow area. Contrary to the RVRS, in the WNB several small-scale elongated Jurassic depocentres can be recognised, which are located along WNW–NW oriented faults. In addition, the overall width of the basin is larger than that of the RVG. The narrow, elongated shape of the depocentres together with the significant thickness difference between adjacent fault blocks (“horst–trough–horst” geometry, Fig. 4.3b) suggests that the WNB is a basin of transtensional origin.

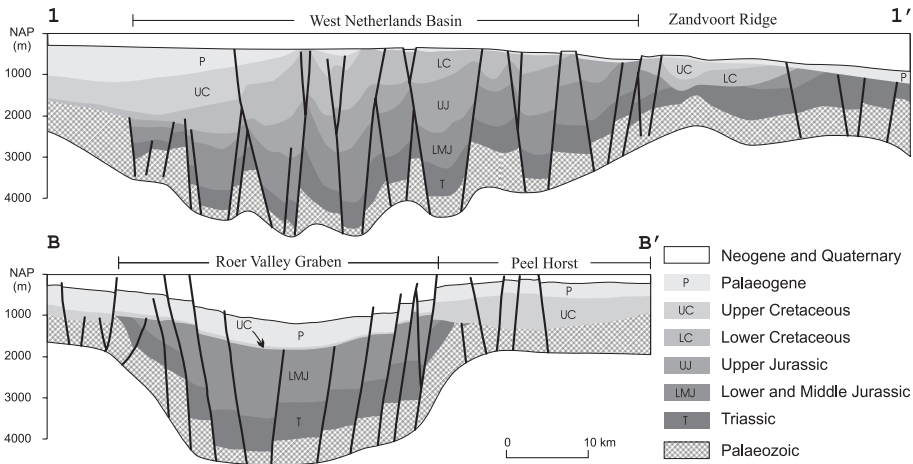
In addition to these observations it is important to note that the shape of the axis of the Mesozoic WNB–RVRS basin system (slightly curved) coincides with the shape of the Mid Netherlands Weakness Zone (see Fig. 4.1a). This suggests that the tectonic fabric underlying the basin system directly controlled its shape and location during the Mesozoic.

Figure 4.3: a) Thickness map of the lower Jurassic Altena Group. Note that the group is partly or totally eroded outside the subcrop line of the Delftland Group. b) Geological cross-sections of the WNB and the RVG (after TNO–NITG, 1999; 2001; 2002; 2003 and De Mulder et al., 2003). NAP: National Ordnance Datum.

a) Thickness of the Altena Group



b)



In summary, based on the characteristics of the subsidence curves (Fig. 4.2a) and the Jurassic subsidence pattern (Fig. 4.3a), it is concluded that the WNB–RVRS basin system formed a single tectonic unit during the Mesozoic. These figures reveal that (1) the main tectonic phases were coeval in both basins, and (2) the resulting deformation is in agreement with the deformation expected from the proposed E–W extension during the Mesozoic (Ziegler, 1990). Considering the regional-scale orientation of the Mid–Netherlands Weakness Zone and the overlying basin system, in the RVG, where the weakened zone is more perpendicular to E–W extension, the tectonic forces have resulted in a narrow, concentrated zone of deformation controlled by ~NNW oriented faults. The orientation of these normal faults is consistent with the E–W extension. In the WNB, where the orientation of the Mid Netherlands Weakness Zone is more oblique to the direction of extension, transtensional deformation occurred. The distribution of deep, elongated sub-basins concentrated along WNW oriented faults reflects this.

The subsiding period of the Mesozoic evolution ended in the Late Cretaceous–Early Paleocene when compressive forces originating from the Euro–African collision inverted both the WNB and the RVG (Sub-Hercynian and Laramide phases). Sedimentation continued during the Late Cretaceous–Early Paleocene inversion phases on the former tectonic highs north and south of the basin system, while the former depocentres were deeply eroded (dashed lines in Fig. 4.2; see also *Chapter 5*, Van Wijhe, 1987; Ziegler, 1990; Geluk et al., 1994; Gras and Geluk, 1999).

4.1.2 Tertiary

After the Early Paleocene Laramide inversion phase the subsequent tectonic evolution of the WNB and the RVRS were very different. The WNB was characterised by continuous uplift during the Eocene and became a stable tectonic high (Letsch and Sissingh, 1983; Zagwijn, 1989; Worum and Michon, 2004; *Chapter 6*), in the RVRS gentle regional subsidence occurred (see Fig. 4.2, Michon et al., 2003). The Eocene subsidence in the RVRS was not fault-controlled and is probably related to thermal contraction of the lithosphere after the Early Cretaceous rifting, or to the elastic relaxation of the lithosphere following the Late Cretaceous inversion (Michon et al., 2003; De Lugt et al., 2003).

From the Late Oligocene onwards the differences between the two areas increased (Fig. 4.4). The WNB remained a tectonic high, as recorded by the Oligocene–Miocene sediment thickness not exceeding ~100 m. In contrast, the RVRS restarted to subside and, as part of the NW European rift system, became a major Neogene–Quaternary depocentre (Letsch and Sissingh, 1983; Zagwijn, 1989; Ziegler, 1990; 1994; Geluk et al., 1994; Michon et al., 2003). Comparison of the Neogene and Jurassic thickness maps reveals that the main Neogene depocentre in the RVRS is superimposed on top of the Jurassic depocentre. This indicates the strong influence of older structures in the Cenozoic structural development.

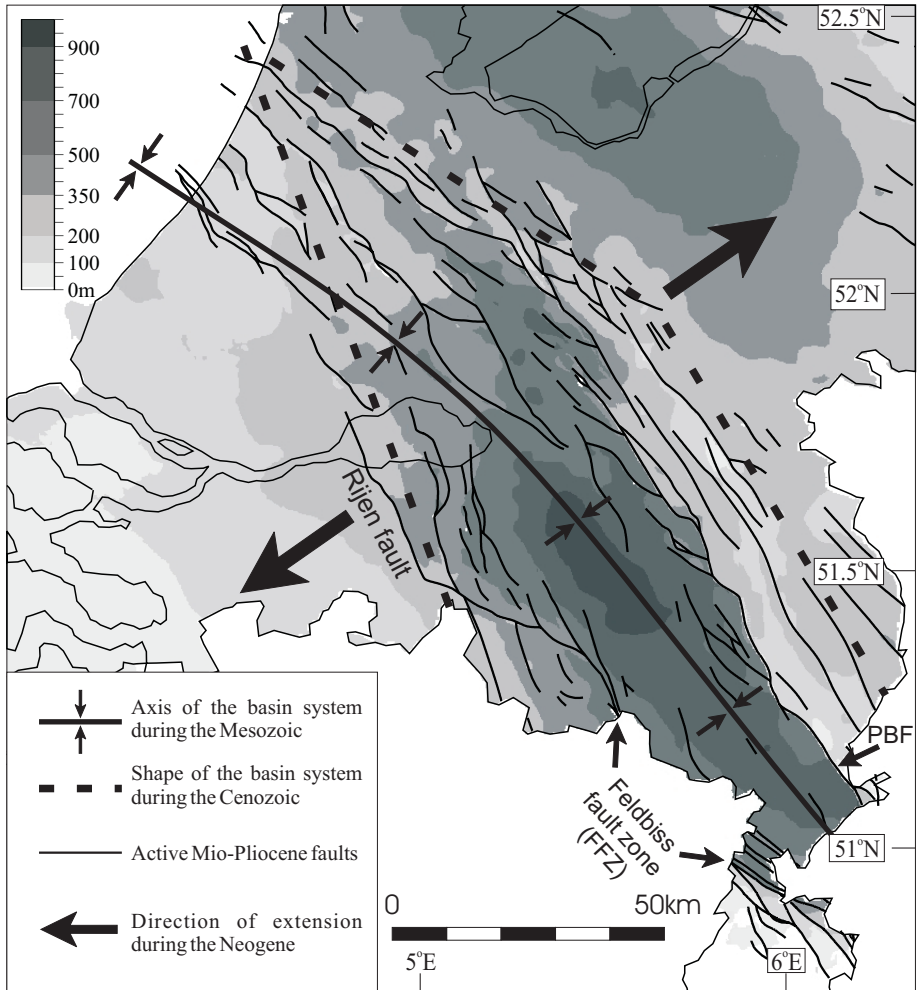


Figure 4.4: Thickness and active fault map of the Neogene (PBF: Peel Boundary fault).

It is important to note that the curved shape of the basin system in the Mesozoic significantly changed in the Tertiary. The dashed lines in figure 4.4 mark the area within the basin system, where differential subsidence can be observed during the Neogene. The shape of this zone is lensoid and is strongly controlled by the south-western (i.e., Rijen fault and Feldbiss fault) and north-eastern (Peel Boundary fault) border faults of the RVG. This deformation zone is from now on referred to as the “extended” Roer Valley Rift System. In the WNB area no significant fault activity can be observed.

4.1.3 Quaternary

The tectonic style of the two areas remained different in the Quaternary. The few hundred meters of Quaternary subsidence in the WNB seems to be part of the general WNW directional tilting of the Netherlands caused by the flexural downwarping of the southern North Sea basin in response to the Plio–Quaternary sediment load and/or to the present-day stress field (Zagwijn, 1989; Kooi et al., 1991). As indicated by the Quaternary sediment thickness distribution (Fig. 4.5, De Mulder et al., 2003) and the seismic quietness of the WNB, this subsidence was not accompanied by faulting.

Contrary to the WNB, in the RVRS Quaternary subsidence continued to be strongly fault controlled (Geluk et al., 1994; Van den Berg, 1994; Van den Berg et al., 1994; Houtgast and Van Balen, 2000; Houtgast et al., 2002; Worum et al., 2004) and has manifested itself in several significant earthquakes in the last century. In addition, in the RVRS the main Quaternary depocentre is superimposed on the Neogene depocentre suggesting that the locus of ongoing sedimentation in the Quaternary is inherited from the Tertiary. Michon et al. (2003) showed however, that besides tectonics, compaction of the Tertiary sediments also significantly contributed to the Quaternary subsidence.

4.2 Comparison of fault patterns

Comparison of the Mesozoic, Tertiary and present-day fault patterns of the study area provides important constraints regarding the influence of older structures on the Cenozoic and present-day tectonic activity in the region. In addition, it might provide an explanation for the markedly different neotectonic behaviour of the two basins.

4.2.1 Mesozoic fault pattern

Fault lineaments incorporated in the analysis represent the active fault pattern during the Early–Middle Mesozoic. The input fault pattern was compiled from fault maps corresponding to various Mesozoic sedimentary units provided by the project “Geological atlas of the deep subsurface of the Netherlands” carried out at TNO–NITG Dutch Geological Survey (dinoloket.nitg.tno.nl). In the Belgian part of the study area, geological cross sections and maps published by Langanaecker (1998) were used.

Active faults were identified using thickness differences across fault lines. Due to later erosion, the distribution of the Mesozoic formations is non-uniform in the area (e.g., Fig. 4.3). Therefore different sedimentary packages were used in various parts of the study area. Determination of the active fault pattern in the WNB and in the western part of the RVG was based on the thickness map of the Lower Jurassic Altena Group. In the eastern part of the RVG and north of the basin

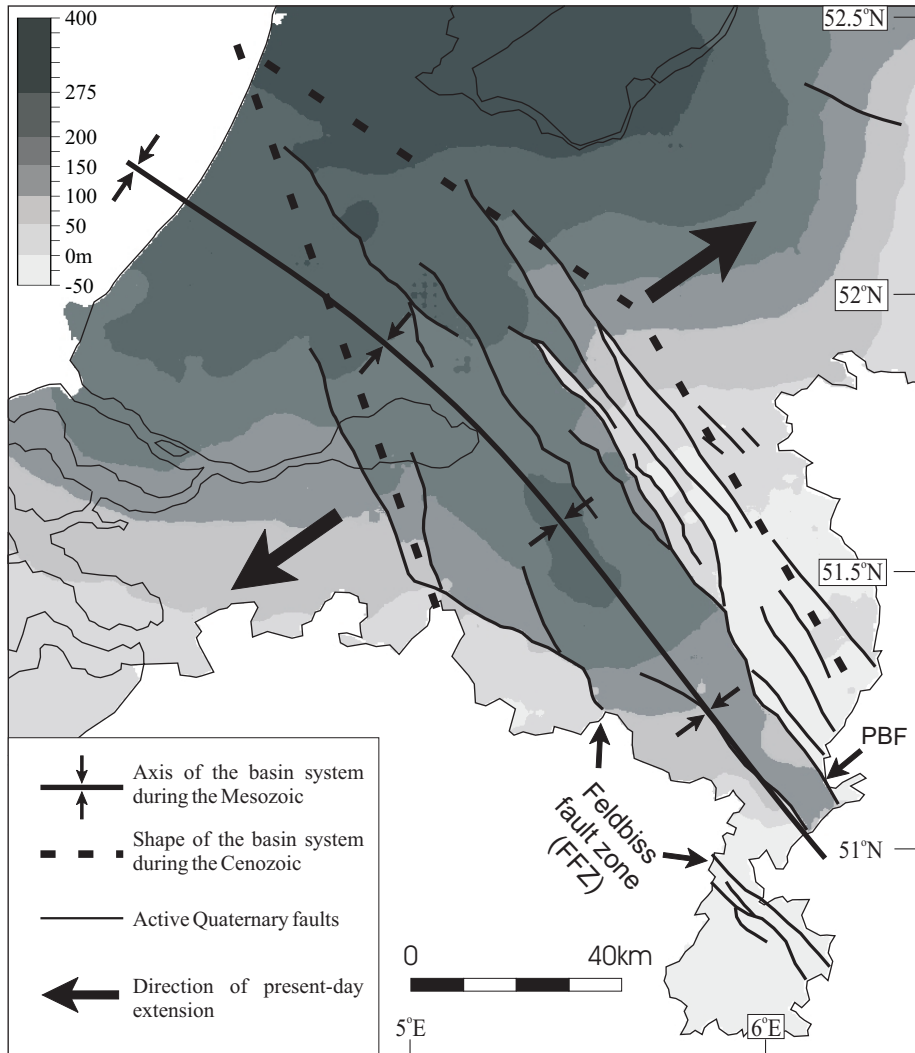


Figure 4.5: Depth map of the base Quaternary. Active Quaternary faults are indicated (PBF: Peel Boundary fault).

system the thickness map of the Triassic was used. In locations where both the Triassic and Jurassic are absent or deeply eroded (Zandvoort Ridge, Peel Block, SE corner of the Netherlands, Fig. 4.1) the Lower Cretaceous Rijnland Group or the Upper Cretaceous Chalk Group was used to identify the active faults.

During the analysis each fault line was divided into 250 *m* long segments and their orientation with respect to North was calculated using a Java2 computer software developed during this Ph.D. research. The subdivision makes it possible to take into account the fact that some faults consist of sections with different orientations. The results are presented in rose diagrams, where a bin size of 4° is used.

The rose diagrams were calculated in 6 different regional domains (Fig. 4.6). Although the selected domains correspond to areas with different tectonic (fault) style, their boundaries are not clearly delimited by particular tectonic lines. The choice of the domains is based on clearly visible changes in the fault pattern.

Since domains C–F cover the area of interest these will be presented and discussed. Detailed discussion about domains A and B is beyond the scope of this chapter, although, it is worthwhile to note that the fault pattern in domain B is significantly different from that of the other domains.

Domains C and D are located in the eastern part of the study area (i.e., RVRS). Domain C represents the northern part of the RVRS including the tectonic highs north of the main graben (Peel Block, Maasbommel High). The fault pattern in this domain is unidirectional with fault orientation of N148°. Domain D is located south of domain C and it covers the southern part of the RVRS. In this domain 3 main fault orientations are observed: (1) N148°, which coincides with the main orientation of domain C; (2) N162° and (3) N128°.

Domains E and F cover the western part of the study area (i.e., WNB and surrounding areas). Domain E represents the southern areas of the WNB and also has three main fault orientations: N154°, N132° and N112°. Domain F covers the northern areas of the WNB including the tectonically elevated Zandvoort Ridge. In this domain the dominating fault orientation is N130°. There are two other fault orientations present (N108° and N154°), but these are of secondary importance.

Below, fault orientation differences observed between the eastern (C and D) and western (E and F) domains are discussed. As demonstrated by the rose diagrams domains C and F have unidirectional fault distributions (Fig. 4.6). Thus, a ~20° of counter-clockwise rotation of the fault direction can be observed from domains C to F (i.e., from east to west). Similar rotation of the main fault direction from east to west — although with less magnitude — can also be observed between domain D and E (N162° and N154° respectively). It has to be emphasised that the fault patterns in domains C and F are unidirectional. That is, in contrast to other domains, in domains C and F the Mesozoic deformational phases always created/reactivated N148° and N130° oriented faults, respectively. Faults with other orientations were not developed. This implies that the N148° direction in domain C and the N130° direction in domain F represent fundamental pre-existing lineaments, which were so weak that during the Mesozoic they were always reactivated before faults with other directions could be created/reactivated.

Domains D and E correspond to the southern part of the WNB–RVRS basin system. The slight rotation of the main fault orientation from domain D to E was already mentioned. In addition to this it is also important to note that the N146–

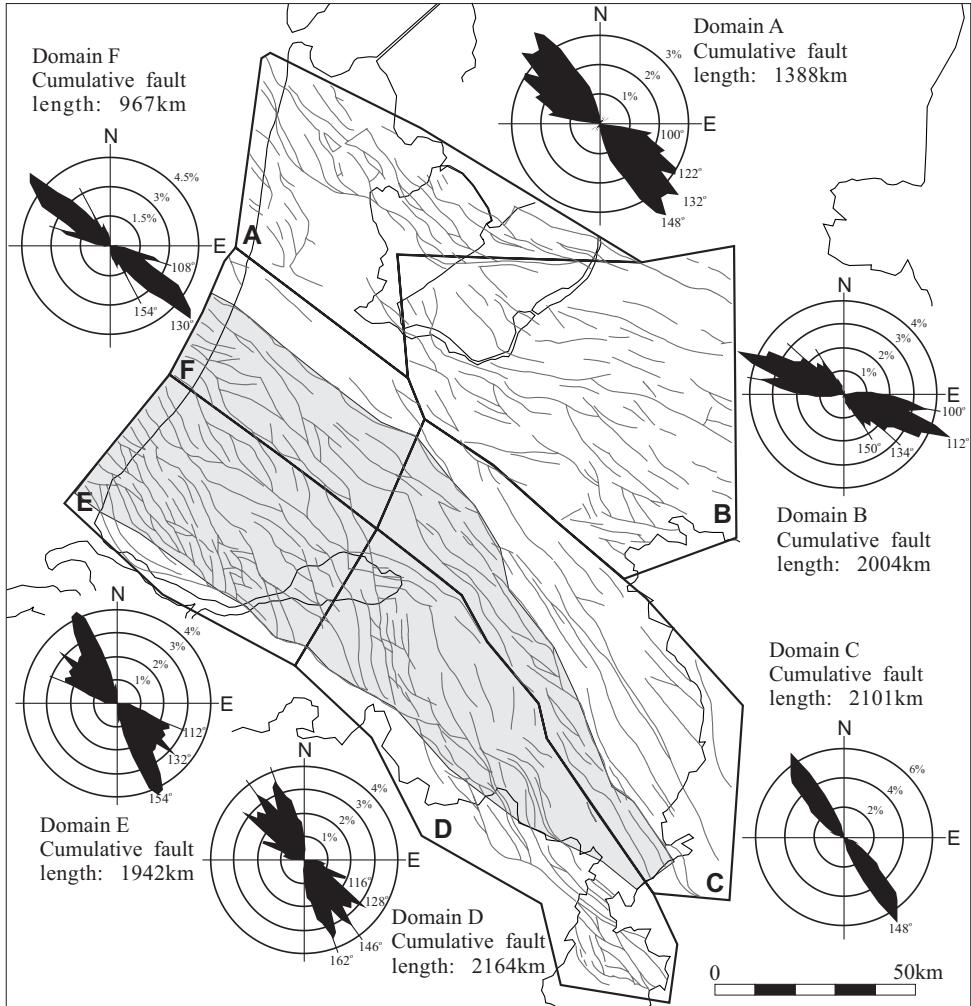


Figure 4.6: Compiled map of the active Early–Middle Mesozoic faults (after TNO–NITG, 1999; 2001; 2002; 2003). Background shading represents the outline of the WNB–RVG basin system (as on Fig. 4.3). Rose diagrams (% of cumulative fault length/orientation) were calculated for different regional domains. The boundaries between domains E and F as well as between domains C and D represent approximately the location of the Mid Netherlands Weakness Zone.

148° peak, which characterises domain C is also present south of it (i.e., in domain D), but it is completely absent in the western domains (i.e., in domains E and F). In domain C the N148° orientation was attributed to pre-existing weak lineaments.

Therefore it is proposed that the presence of the N148° direction in domain D and its absence in domains E and F is related to the fact that the N148° direction is indeed an inherited direction, specific only to the eastern part of the study area (RVRS).

The above fault patterns suggest that the southern (domains D and E) and northern (domains C and F) part of the study area represent different crustal domains (see also Michon et al., 2003). In the deeper parts of the crust the lineament separating these fundamental crustal domains, the Mid Netherlands Weakness Zone, is located in the middle of the RVG and slightly north of the centre of the WNB. In the subsurface it manifested itself in a zone having a unidirectional fault pattern (i.e., Mid Netherlands Fault Zone; domains C and F). This indicates the weak nature of these crustal segments compared to the other domains in the study area. The direction of the weakness zone changes between the RVRS and the WNB (~20° of counter-clockwise rotation). As explained earlier and indicated by figure 4.3, the curved shape of the weakened zone directly controlled the shape of the developing basin system and the style of deformation in it during the Mesozoic.

4.2.2 Neogene–Quaternary

Active Neogene and Quaternary faults have similar orientations, and therefore they are discussed in the same section (Fig. 4.7). The overall Neogene fault pattern is dominated by NW oriented faults as indicated by the rose diagram in figure 4.7. Comparison of the orientation of the Neogene and Mesozoic faults reveals that the Neogene fault pattern is the result of the reactivation of faults already active during the Mesozoic. This indicates that Mesozoic structures strongly influenced the Cenozoic structural development. The primary fault direction in the Neogene is N148° reflecting the particular importance of this direction and/or a stable Neogene stress pattern in the long term. Another peak at N138°, which was not present in the Mesozoic fault pattern (Fig. 4.6) is observed. The development of this fault direction can be explained by upward rotation of the fault planes of the reactivated N132° and/or N148° Mesozoic faults in the thick Tertiary cover as an accommodation to the new stress field. The ancient N132° and N155–160° directions are also present in the “extended RVRS”, but not in the rose diagram as main peaks. Despite this they play a major role at a regional scale as they correspond to the south-western and north-western limit of the “extended RVRS”.

As figure 4.7 shows, in the area of the former WNB the Quaternary fault activity was limited to one fault in the northern part of the former basin. Other than that, there is no fault activity observed. In contrast, in the RVRS the Quaternary has been characterised by significant faulting. The Quaternary fault pattern correlates well with the fault patterns of the Neogene or Mesozoic deposits (Fig. 4.6, see also Houtgast and Van Balen, 2000). This implies that the Quaternary and present day tectonics of the RVRS has to a great extent determined and still is being determined by older structures of Palaeozoic–Mesozoic origin.

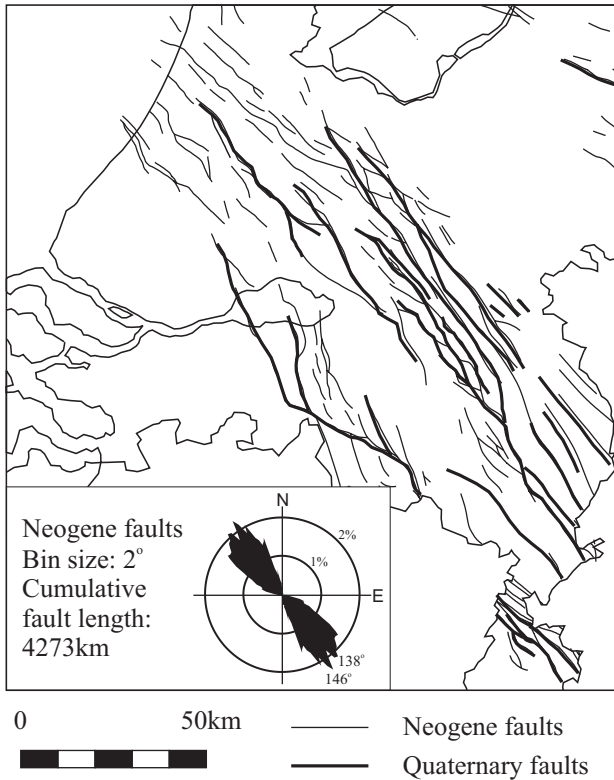


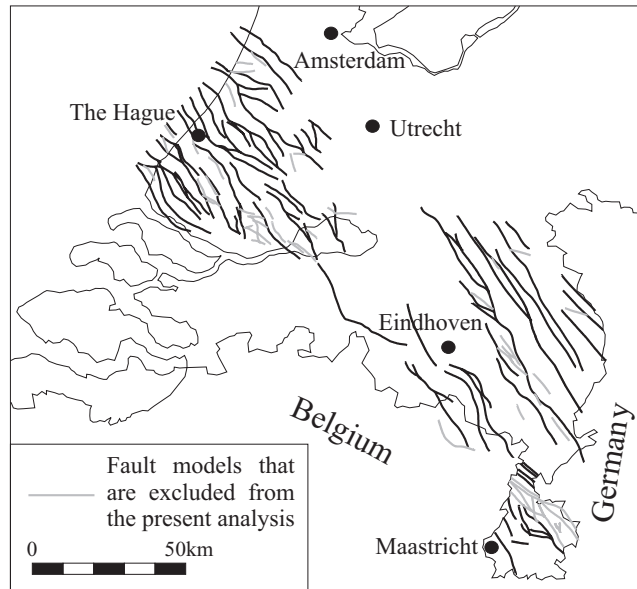
Figure 4.7: Map of the active Neogene and Quaternary faults of the study area (after TNO–NITG, 1999; 2001; 2002; 2003; and De Mulder et al., 2003). Inset: rose diagram of the Neogene fault pattern.

4.3 Neotectonic implications: slip tendency analysis

As shown above, there are orientation differences in the Mesozoic fault pattern between the RVRB and the WNB. Due to these differences the faults in the two basins can be expected to behave differently under conditions of a uniform regional stress, which could explain the markedly different Quaternary tectonic activity. In this section the newly developed modelling technique (3-D slip tendency analysis; Worum et al. (2004)) presented in *Chapter 2* is used to investigate whether the observed fault orientation differences are substantial enough for the present-day tectonic stress field to produce significantly “weaker” resolved stresses along the faults in the WNB.

The principles of the method were discussed in the previous chapters, therefore they are not repeated here. It is important to note however, that in order to adequately estimate fault reactivation with this method the frictional parameters along the faults have to be known. Due to lack of data the exact slip threshold is difficult to determine, and in addition, it can change from fault to fault and even along one

Figure 4.8: Available 3-D fault models in the study area. Fault models, which were excluded from the slip tendency analysis are indicated.



particular fault. Fortunately, in the present study the exact value of a slip threshold is not needed, since the aim is to determine whether slight differences in fault orientation between the WNB and the RVRS can cause significantly different slip tendencies in the same regional stress field. The slip tendency values of the faults of one basin, therefore, are simply compared to those of the other in order to determine which fault system is better aligned to the present-day stress field.

4.3.1 Input data

Input data of the method consists of the 3-D geometrical fault models and parameters describing the regional stress field. In the present analysis fault models available from the database of TNO-NITG were used. Some of these models were also used in *Chapter 3*. Those fault models, quality of which was questioned in the previous chapter (SE corner of the Netherlands, Limburg province) were not considered in the present analysis. In the discussion of *Chapter 3* it was also suggested that secondary faults located close to primary faults that have connections with deeper fractures, cannot be considered as being independent regarding fault reactivation. By analysing the 3-D geometrical fault database and seismic sections, such dependent minor faults can be identified. These faults are excluded from the present study. The remaining faults represent the first order fault pattern, which plays a key role in the brittle deformation of the area (Fig. 4.8; black lines).

As stress indicators with high spatial density are not available in the study area stress tensors constrained by regional data have been used. The stress field is therefore assumed to be laterally homogeneous and linearly depth-dependent. It is also assumed, that the stress field is Andersonian, that is, the observed maximum horizontal (σ_H), minimum horizontal (σ_h) and vertical (σ_v) stresses represent the principal stresses. As discussed in detail in *Chapter 2*, with respect to fault reactivation, the above stress field can be represented by a tensor having three independent parameters. These are the direction of σ_H as well as the σ_h/σ_H and σ_v/σ_H ratios.

The orientation and the principal stress ratios of the stress field were constrained by regional observations. σ_H directions were modelled as the two extremities of the range of various observations (i.e., N145E and N160E degrees, e.g., Bergerat, 1987; Müller et al., 1992; Rondeel and Everaars, 1993; Camelbeeck et al., 1994; Plenefisch and Bonjer, 1997; Michon et al., 2003). It is worthwhile to emphasise that both slip tendency and slip direction are continuous functions of the stress orientation. Therefore, it is sufficient to investigate the two extremities of the modelled σ_H direction interval, since intermediate orientations would not provide slip tendency and slip direction values out of the range represented by the two extremities.

The shape ratio of the input stress fields (equation (2.1), p. 14) was kept $R = 0.4$ in agreement with stress inversion results (Camelbeeck et al., 1994; Plenefisch and Bonjer, 1997). These studies have emphasised that an unequivocal distinction between a normal faulting and a strike-slip faulting stress regime was not possible. As demonstrated in the previous chapter, however, the present-day observed fault activity in the RVRS, using a reasonable range of stress ratios and slip thresholds can be explained only by normal faulting stress regimes ($\sigma_v/\sigma_H > 1 > \sigma_h/\sigma_H$). In addition, recent morphological and geological studies also suggest that a normal faulting stress regime is more likely (Houtgast et al., 2002; Michon and Van Balen, 2004). In the present modelling therefore only this stress regime is considered. As the faults are approximately parallel to the orientation of σ_H , it is expected that the calculated slip tendencies are very sensitive to the σ_h/σ_v ratio (S). Therefore, a wide range of S ratios have been evaluated in the modelled stress scenarios. This range was adopted for both stress orientations ($\sigma_H = \text{N}145^\circ$ and $\text{N}160^\circ$), resulting altogether in 16 different stress scenarios (Table 4.1).

Table 4.1: Stress ratio triplets of the stress tensors applied as inputs for the slip tendency analysis.

σ_h/σ_v	0.2	0.3	0.4	0.5	0.6	0.7	0.8	0.9
σ_v/σ_H	1.471	1.389	1.316	1.250	1.190	1.136	1.087	1.042
σ_h/σ_H	0.294	0.417	0.526	0.625	0.714	0.795	0.870	0.938

4.3.2 Analysis of the calculated slip tendency patterns

Due to the large number of input stress tensors, only a selection of the most instructive results is presented in the form of a 3-D perspective view (Fig. 4.9). It should be noted that on this figure only a ~ 1500 m high strip in the centre of the faults is visualised. This was necessary in order to prevent the view of the faults from being obstructed by other faults. In reality the depth range of the faults is much larger. Regarding the modelled shear directions, first the averages of the shear direction pattern were calculated for every fault, and these were later displayed as polar histograms. These histograms provide information about shear directions regarding the whole fault population and not the individual faults. As the R -value of the input stress tensors was kept constant, the calculated patterns of shear directions are identical for every stress field of the same orientation (Fig. 4.9).

Influence of S

The results reveal that the calculated slip tendencies are very low for cases with $S = 0.6$. Although it is not an objective here to compare the ST values with a particular slip threshold, based on the experience in *Chapter 3* it is suggested that all the faults would be likely locked in a stress field with an S ratio higher than 0.6. As expected, with decreasing S ratio the slip tendency increases, suggesting higher probability of slip (Fig. 4.9). One may note that there is no observable difference in fault behaviour in terms of average slip tendency between the WNB and the RVRS in any of the cases. This implies that the fault pattern differences between them are not large enough to result in markedly different slip tendencies. Figure 4.9 shows on the other hand, that a rise of S by 0.1 decreases the slip tendency by 0.1–0.15. This will be discussed below.

Influence of σ_H direction

Comparing slip tendency patterns related to stress fields having the same magnitude but different orientation reveals that the calculated slip tendencies are slightly lower when the direction of σ_H is N160° than when it is N145°. The reason is that in case of a N145° orientation of σ_H , the plane of the maximum and minimum principal stress ($\sigma_h - \sigma_v$ plane) is perpendicular to most of the faults. This results in an optimal orientation and therefore higher in a slip tendency (see “2.5-D” experiment in *Chapter 2*; Fig. 2.6, p. 26). The ST drop due to the rotation of the stress field however, is significantly less than that observed by changing the S ratio.

The polar histograms of the average shear directions imply shear forces with a large dip-slip component along the faults. In case of a N145° direction of σ_H there is a small ($< 10^\circ$) oblique component in the shear direction. The oblique component increases to 10–20° in cases where the orientation of σ_H equals N160°. Observations regarding the direction of slip along the main borderfaults of the RVRS indicate predominantly normal faulting behaviour, which does not disagree with the results

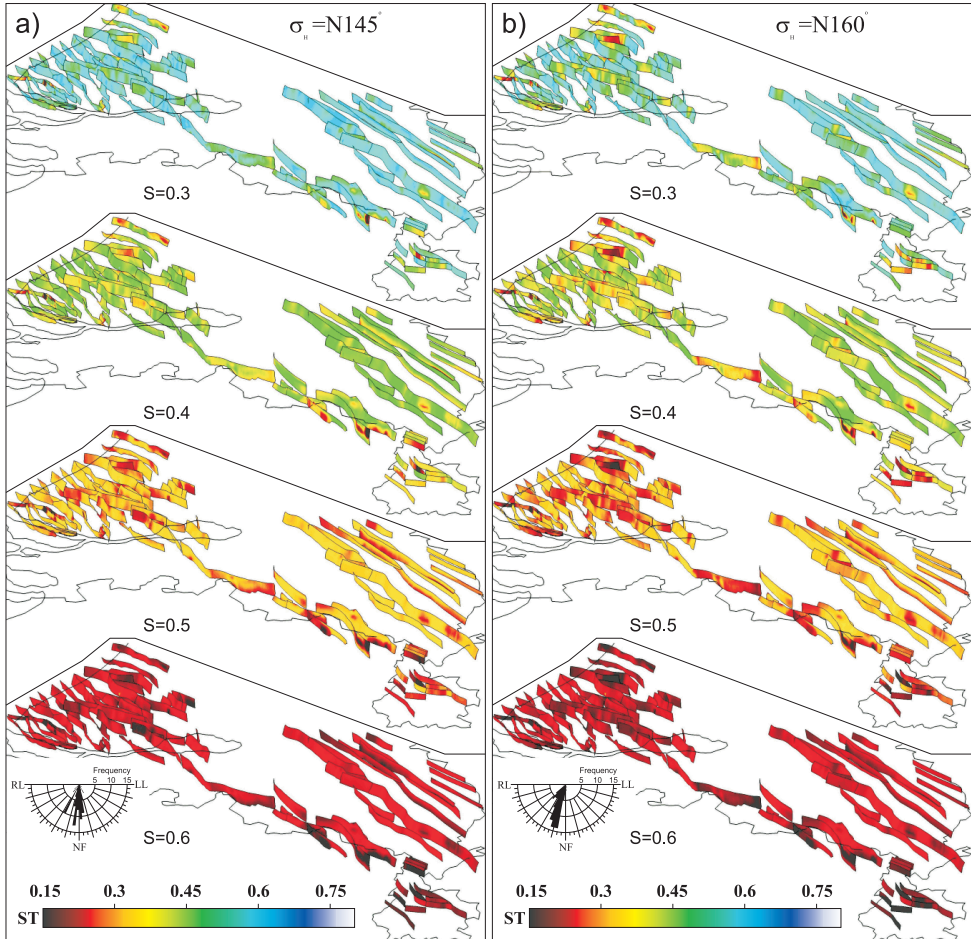


Figure 4.9: Calculated 3-D slip tendency (ST) patterns of the modelled faults for different stress tensors having σ_H direction of a) $N145^\circ$ and b) $N160^\circ$. The polar histograms display the number of faults along which the average of the shear vectors point into the given direction. (NF: normal faulting (dip slip); LL: left lateral slip; RL: right lateral slip; $S = \sigma_h/\sigma_v$). Colour plate in Appendix B (p. 145).

of this study. Using earthquake focal mechanism data Camelbeeck et al. (1994) and Camelbeeck and Van Eck (1994) determined shear directions with only a minor oblique component. The morphological study of Michon and Van Balen (2004) on the other hand determined pure dip slip motions. In light of these observations a stress tensor with $\sigma_H = N145^\circ$ orientation is most likely.

Synthesis of the slip tendency analysis

The results of the slip tendency analysis reveal that due to the small difference in fault orientations the faults of the WNB and RVRS should behave almost identically in a uniform stress field. Among the different input stress tensors none could explain the observed neotectonic quietness in the WNB and the strong fault activity in the RVRS. On the other hand, the analysis has revealed that a relatively small rise in the ratio of the minimum horizontal and the vertical principal stresses (S) is enough to significantly decrease the calculated slip tendency. This drop may be high enough to bring the slip tendency in the WNB below a given slip threshold. The analysis indicates therefore, that the observed fault activity in the RVRS and the coeval inactivity in the WNB can only be achieved if different stress fields and/or slip thresholds are assumed for the two areas.

4.4 Discussion and conclusions

Modelling the present-day reactivation of Mesozoic faults in the WNB and the RVRS under simple, laterally homogeneous stress fields predicts similar fault behaviour throughout the basin system. This is in disagreement with the observations. The explanation for this could be possible differences in the state of stress and/or in the slip thresholds between the two areas. That is, there is either more extension in the RVRS in terms of lower S ratio (σ_h/σ_v), or/and the slip thresholds are lower in the RVRS than in the WNB. These possible differences are assumed to be responsible for the lack of Quaternary fault activity and the present-day seismic quietness in the WNB.

This study emphasised that differentiation in the tectonic evolution already started in the Tertiary. Therefore, it is suggested that the different tectonic stress fields and/or slip thresholds between the two areas are directly related to the origin of the Cenozoic rifting in the RVRS. Several hypothesis are presented below, however, none is conclusive. Additional research is needed to better understand the origin of the RVRS and to put the southern Netherlands into a broader tectonic context. This research might also help future studies to find the reason why the neotectonics of the RVRS and the neighbouring WNB are so different from each other.

4.4.1 Possible causes of different stress fields

As the RVRS is part of the NW European Cenozoic Rift System, for an explanation of a possibly stronger present-day extension in this area relative to the WNB, the RVRS has to be put in a broader, NW European tectonic context. At a European scale there is a general consensus that the Late Eocene rifting in the southern Rhine Graben propagated northward and breached the Rhenish Shield in a NW–SE direction during the Early Oligocene. The rift then propagated further to the NW and reached the RVRS area in the Middle–Late Oligocene (e.g., Ziegler, 1994). Mechanisms proposed

so far to explain the formation of the NW European Rift System focus primarily on the development of the regional tectonic stress pattern in NW Europe (for a summary of these models see the discussion of Michon et al., 2003). These models do not explain why the rift did not propagate further to the WNB.

In search for an explanation of the possibly different stress fields, the deeper crustal and lithospheric configuration of the southern Netherlands has to be taken into account. Unfortunately, there are no observations regarding the lithospheric structure in this area. However, crustal seismic surveys show that both areas are characterised by a thinned crust, which is more pronounced in the RVRS (i.e., crustal thickness of around 28 km) than in the WNB (~30 km, Rijkers and Duin, 1994). A thinner and consequently weaker crust could result in higher stress magnitudes in the crust of the RVRS compared to that of the WNB. However, it still remains unclear why the Oligocene rifting, as the most probable cause of the additional thinning of the crust in the RVRS, did not propagate further into the WNB.

South of the RVRS, the Variscan Rhenish Massif (Fig. 4.10) is a neotectonically uplifted area. The uplift is coeval with the subsidence in the RVRS. In addition, paleomagnetic data presented by Schreiber and Rotsch (1998) indicate that a 10–16° clockwise rotation of the Eastern Rhenish Massif has taken place since the Late Oligocene, coeval with the rifting in the Lower Rhine Graben (and in the RVRS). Thus, unravelling the tectonic relations between the Rhenish Massif and the RVRS may also explain the neotectonic differences between the RVRS and the WNB. Although the exact driving force of the rotation of the NE Rhenish Massif is still unknown (probably the NE–SW extension itself), it was proposed that it is directly responsible for the V-shaped opening of the Lower Rhine Graben and for the rifting in the RVRS (Illies and Fuchs, 1983; Schreiber and Rotsch, 1998). Considering the hypothesis that the rotation of the NE Rhenish Massif generated additional extension in the Lower Rhine Graben, it is necessary to postulate that a transfer zone existed in the NW part of the rotating block in order to explain why the rifting did not step into the WNB. As illustrated by figure 4.10, in such a scenario ~NE oriented faults of Variscan origin could have played the role of a transfer zone. However, these faults have not yet been identified as acting as transfer faults during the Neogene.

Geophysical surveys as well as teleseismic tomography results show that a pronounced column-like mantle structure lies below the Rhenish Massif, extending to at least 400 km depth (Fig. 4.10, e.g., Prodehl et al., 1992; Ritter et al., 2001). Various field and modelling studies have indicated that this mantle feature is very young (~1 Ma, e.g., Lippolt, 1983; Garcia-Castellanos et al., 2000) and that it has not (yet) produced a corresponding surface heat flow signal (Haenel, 1983). The plume is not wide enough (~100 km) to affect the mantle part of the lithosphere below the RVRS and in addition, its emplacement post-dates the initiation of the main rifting.

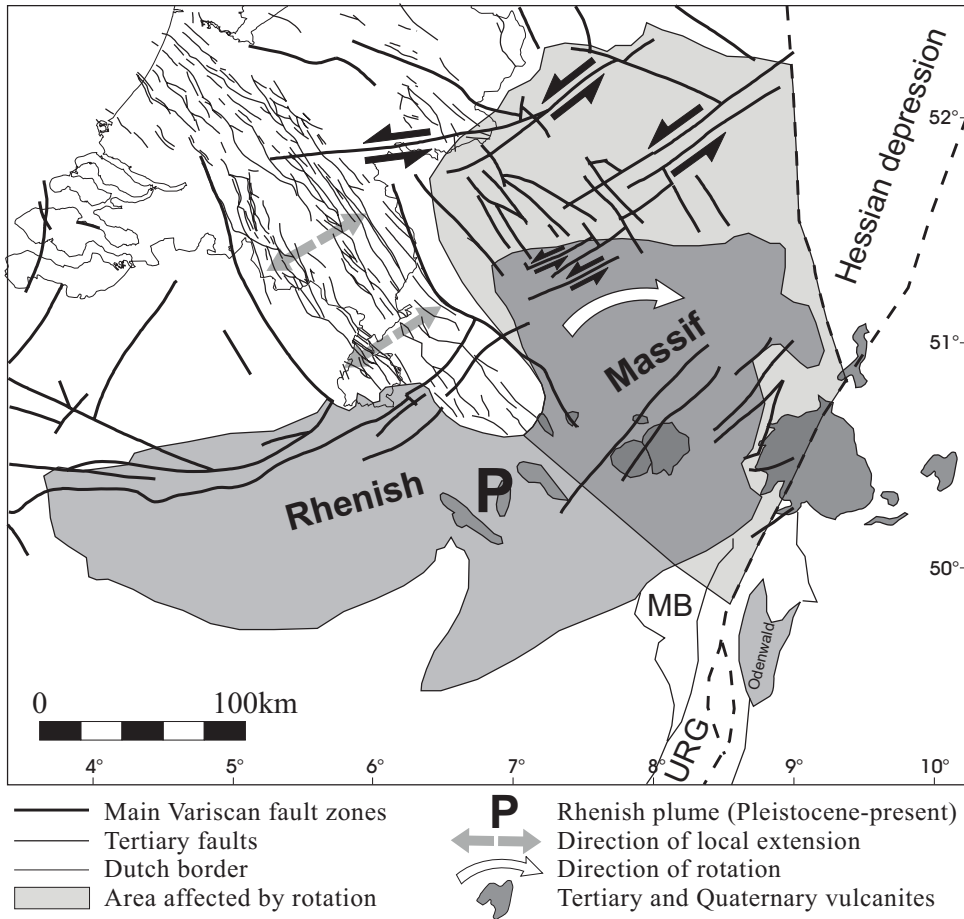


Figure 4.10: Tectonic features of the Rhenish Massif area since the Late Oligocene. (URG: Upper Rhine Graben, MB: Mainz Basin). Modified after Schreiber and Rotsch (1998). Variscan fault pattern is from Lokhorst (1998).

The geological record on the other hand shows that there was also an earlier volcanic activity at the same location well before the development of the plume (e.g., Huckenholz, 1983; Lippolt, 1983). This volcanism is coeval with or slightly pre-dates the rifting episode. These older volcanites reached the surface along pre-existing fractures, whose orientation seems to coincide with that of the Lower Rhine Graben and the RVRs (e.g., Schreiber and Rotsch, 1998). The cause of this volcanism is still unclear. However, it is speculated that it might be related to a mantle anomaly (see also Huckenholz, 1983), from which the later plume developed. This swell must have been much more gentle and wider than the present-day plume and

might have existed already during the onset of rifting. A thermal anomaly in the lithosphere due to elevated heat flow was determined as being one of the possible explanations for high seismicity in intra-plate conditions (New Madrid seismic zone, Central USA, Liu and Zoback, 1997). Due to the higher temperature the bulk strength of the upper mantle in thermally perturbed areas is significantly reduced, resulting in concentrated and higher tectonic stresses in the upper crust compared to those areas that are thermally not perturbed. Unfortunately this model cannot be confirmed in the study area, since available subsurface temperature and heat flow data are sparse in the southern Netherlands. In addition these heat flow calculations are based on significant simplifications. This presents an obstacle to reliable and detailed thermal comparisons between the RVRs and WNB (Ramaekers, 1991; Van Balen et al., 2002).

4.4.2 Possible causes of different slip thresholds

It has been shown by analogue experiments that repeated reactivation reduces the frictional parameters of faults, most probably by the development of a gradually thicker gauge layer (e.g., Krantz, 1991). It can be proposed therefore, that the Oligocene rifting in the RVRs decreased the slip threshold in the RVRs along the primary faults. In contrast, in the WNB, where Oligocene rifting did not take place, the slip threshold did not decrease. However, significant differences are not likely since, as has shown earlier, the faults in both basins were already subjected to considerable amount of deformation during the Mesozoic: This should have led to a significant weakening of the faults in both the RVRs and the WNB. On the other hand as demonstrated by Tenthorey et al. (2003) faults can also heal due to mineralization. Thus, during the Oligocene–Miocene tectonic quietness in the area of the WNB, the faults might have become stronger relative to those in the RVRs, where during the same period the primary faults were active. In reality both of the above mentioned processes might have played a role: in the WNB the faults became slightly stronger due to healing, while in the RVRs they became slightly weaker due to the renewed fault activity.

Chapter 5

Quantitative reconstruction of Late Cretaceous–Tertiary erosion in the West Netherlands Basin

The amount of erosion in a sedimentary basin is a vital parameter in basin analysis and in hydrocarbon geological studies. For example, the detailed burial-, porosity- and diagenetic history of the reservoir rocks in an inverted basin cannot be estimated without quantifying the amount of erosion. Also, the maximum burial-depth of the source rock, which has important impact on the thermal maturation of organic material and timing of hydrocarbon expulsion, can be estimated only if the amount of post-depositional erosion is known. In certain tectonic and hydrogeological studies it is crucial to know not only the amount, but also the pattern of erosion, since in inverted basins it provides important constraints on the style of inversion tectonics and on the fluid-flow system during inversion (e.g., Nalpas et al., 1995; Verweij, 2003; Bouw and Oude Essink, 2003).

There are several methods that aim to quantify the amount of removed sediments. In combination, these provide fairly accurate estimates on the erosion magnitudes (Skagen, 1992; Nyland et al., 1992; Japsen and Chalmers, 2000). Of these methods the shale compaction trend-, the vitrinite reflectance profile- and the drilling exponent-based drilling parameter analysis have been found to have a potential accuracy of ± 200 m (Skagen, 1992). The shale compaction and drilling parameter methods have the additional advantage of utilizing data that are directly available from exploration wells. They do not require additional laboratory analysis. Time—temperature index-based (TTI) maturity modeling of organic material can also provide constraints on the magnitude of erosion. However, since the maturity of organic material at a given depth beside the post-depositional erosion depends also on many other factors (e.g., thermal parameters of the sediments, paleo-heat flow, fluid flow system, sedimentation rates etc.) a wide range of input parameter combinations can provide the same “best fit” to the measured maturity indicators. This makes maturity modeling a less reliable method to quantify erosion. As with maturity modelling, the temperature history of a sample revealed by fission track

modelling is also affected by both the burial/exhumation of the sample and by the heat flow history (e.g., Green et al., 1989; Andriessen, 1995). Although the accuracy of the estimated exhumation is less than that of the shale compaction analysis ($\sim 500\text{--}1000\text{ m}$; Skagen, 1992), fission track modelling is an extensively used method for erosion estimation, since it is the only method that gives constraints also on the timing of the event (e.g., Rohrman et al., 1995; Mathiesen et al., 2000).

Shale compaction trends have been widely used to determine erosion magnitudes in uplifted basins (e.g., Nyland et al., 1992; Richardsen et al., 1993; Hansen, 1996; Van Balen and Simmelink, 1999 NITG 02-37A internal report). Shales are ideal for this purpose because their porosity and other porosity related physical properties (i.e., sonic velocity, bulk density) show a clearly depth-controlled trend, provided that during and/or after deposition overpressure did not developed in the succession. Other studies have demonstrated however, that beside shales, sandstones, mixed sediments and carbonates could also be used for this purpose (e.g., Bulat and Stoker, 1987; Hillis, 1991; 1993; Hillis et al., 1994; Japsen, 1998; 2000).

In this chapter interval velocity analysis of various stratigraphic units in the West Netherlands Basin (WNB) has been used to quantify the amount of eroded sediments. As discussed in *Chapter 4* the WNB is one of the major tectonic features of the onshore Netherlands, which, together with other sedimentary basins, came into existence during the Mesozoic (e.g., Van Wijhe, 1987; Ziegler, 1990; Dronkers and Mrozek, 1991; Racero-Baena and Drake, 1996; De Jager et al., 1996; Worum et al., 2004). In the Late Cretaceous–Eocene period compressional stresses originating from the Alpine orogen inverted the basin in multiple stages, which resulted in the deformation and deep erosion of the basin fill. The erosion, which is marked by a significant hiatus across the basin, affected sediments from Eocene–Oligocene to Cretaceous, or even down to mid-Jurassic levels (Fig. 5.1). The deep erosion has also manifested itself in the destruction and/or biodegradation of hydrocarbon accumulations that were charged prior to inversion (Bodenhausen and Ott, 1981; De Jager et al., 1996). Concerning the amount of removed sediments only few published data are available. Bodenhausen and Ott (1981) assumed $\sim 800\text{ m}$ of uplift in the north-western part of the basin, while Van Bergen (1998 NITG 98-148B internal report) considered that erosion of $1300\text{--}1900\text{ m}$ must have taken place to account for maturity models of hydrocarbon source rocks. It has to be emphasized, however, that the amount of erosion is expected to be laterally highly variable, since reverse reactivation of pre-existing faults played a major role during inversion (e.g., Racero-Baena and Drake, 1996).

In this chapter a contribution is made to the quantification of the amount of eroded sediments and to the understanding of inversion tectonics in the WNB by presenting the interval velocity analysis of nine lithostratigraphic units from six Jurassic–Cretaceous formations. Quantitative reconstruction of the erosion has not been performed in the WNB before. For the analysis publicly available sonic- and density well logs were used provided by TNO–NITG National Geological Survey (Fig. 5.1). Furthermore, high quality 3–D seismic surveys were also analyzed in

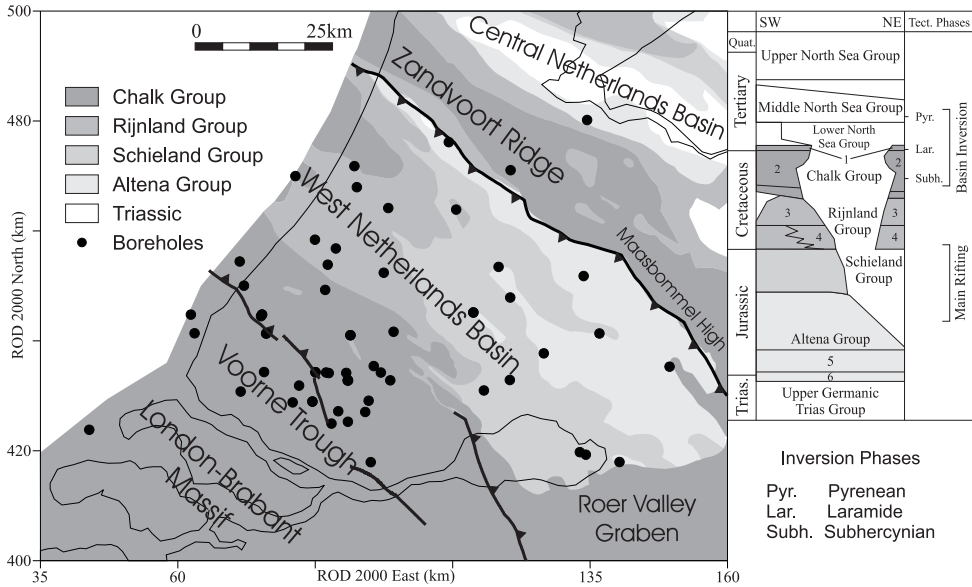


Figure 5.1: Pre-Tertiary geological map and simplified litho-chronostratigraphical chart of the onshore West Netherlands Basin and surrounding areas. Boreholes used in the present study and the investigated formations are indicated. 1: Houthem Fm., 2: Ommelanden Fm., 3: Holland Fm., 4: Vlieland Claystone Fm., 5: Aalburg Fm., 6: Sleen Fm.

order to geometrically determine the pattern of erosion in the western part of the basin. The results provide important constraints on the Late Cretaceous–Eocene tectonic evolution of the basin.

5.1 Methodology

The principle behind the analysis presented in this chapter is the observation that average seismic velocity of a stratigraphic interval follows an increasing trend with depth. The seismic interval velocity is generally measured either from seismic lines (e.g., Richardsen et al., 1993) or from sonic logs (e.g., Bulat and Stoker, 1987; Hillis, 1991; 1993; Hillis et al., 1994; Japsen, 1998; 2000). The velocity-increase is caused by compaction and is assumed to be irreversible. Consequently, horizons that were uplifted and are closer to the surface due to later erosion have higher sonic velocities than those that followed an uninterrupted subsidence path (Fig. 5.2). Comparison of the measured interval velocity with the normal depth-trend (i.e., the trend one would get if no erosion had taken place; also called “baseline”) enables one to estimate the amount of erosion. The displacement, along the depth axis, of the measured interval velocity from the normal-depth trend is called the

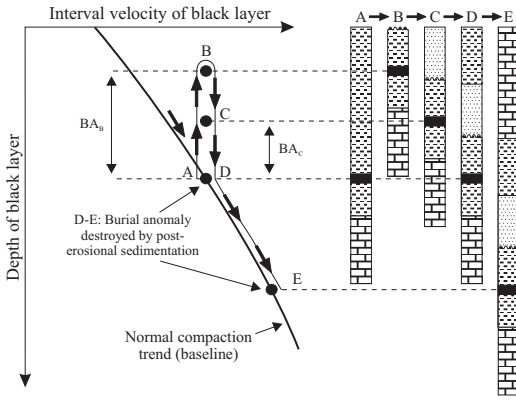


Figure 5.2: Evolution of interval velocity with burial/erosion. The interval velocity of a layer in an eroded sequence remains anomalous until the amount of post-erosional sedimentation reaches and exceeds the amount of erosion.

burial anomaly (BA) or apparent erosion (Fig. 5.2; Hillis, 1993; Japsen, 1998). It is zero for normally compacted sediments. Using the present-day depth of the studied interval (D_p) and the amount of post-erosional sediment thickness (T_{pe}) the amount of erosion (E) and the maximum depth of burial (D_{max}) can be calculated (e.g., Hillis, 1993):

$$D_{max} = BA + D_p \quad (5.1)$$

$$E = BA + T_{pe}$$

Note that erosion estimation with this method is not possible if $T_{pe} > E$, since in this case the burial anomaly is destroyed (Fig. 5.2).

The reliability of the method can be increased if more than one stratigraphic unit is investigated at the same location. If no significant erosion occurred between the deposition of the units (i.e., they reached their maximum depth of burial at the same time) burial anomalies resulting from a young erosional episode should be equal (Japsen, 2000). Should this be the case the estimation of erosion at the given location is more reliable.

The accuracy of the erosion estimates using burial anomalies depends on three factors: (1) the validity of the basic assumption (i.e., lithology and porosity are the primary controlling factors of the sonic velocity); (2) the type of stratigraphic interval chosen for the analysis and (3) the way the baseline is defined.

Although the sonic velocity of a given stratigraphic unit depends primarily on the lithological composition and the porosity of the sample (e.g., Vernik and Nur, 1992; Japsen, 1993; Kenter et al., 1997), other internal and external factors may be also important. For example, diagenetic differences between two samples having the same porosity and lithology often result in different sonic velocities, especially in carbonate rocks (Anselmetti and Eberli, 1993; Kenter et al., 1997; Mallon and Swarbrick, 2002; Fabricius, 2003). Effective stress variations caused by pore fluid pressure fluctuations also have impact on the sonic velocity (Anselmetti and Eberli, 1993; Japsen, 1994; 1999; 2000; Kenter et al., 1997; Poix, 1998). Furthermore, Moos and Zoback (1983) and Monsen (2001) demonstrated that the presence of microfractures can also significantly influence (reduce) sonic velocity. In light of these results it is crucial to take into account local geological and sedimentological considerations during interpretation of velocity fluctuations around the baseline.

The second factor controlling the accuracy of the estimated erosion is the type and characteristic of the investigated stratigraphic interval. Since sonic velocity

greatly depends on lithology and since the analysis is performed on a regional scale, laterally uniform lithological units (openwater shales for example) are preferred for the analysis. Sediments deposited in a continental or near-shore environments are not ideal for the analysis, since they are often characterized by rapid lateral facies and lithological changes, which could result in a misleading interpretation of the burial anomalies. It is also preferable that the investigated stratigraphic unit can be easily recognized and correlated over large distances, so average interval velocities are generally calculated for lithostratigraphic groups or formations (e.g., Bulat and Stoker, 1987; Hillis, 1991; 1993; Hillis et al., 1994; Japsen, 1998; 2000). However, lithological and sedimentological circumstances are rarely uniform vertically through a thick stratigraphic unit. This is one of the main reasons why interval velocity values of normally compacted samples corresponding to the same depth may demonstrate a wide range in some studies (“noise”). Another example of the potential disadvantages of using thick intervals may be a situation, where only the lower, high-velocity part of the given formation was deposited. In this case a higher average velocity would be observed in a well section compared to other wells where the formation is complete. The higher velocity and the consequent observed burial anomaly is clearly not the result of a post-depositional erosion. In studies where wireline suites are available an effort can be made to define, based on the log patterns, a thinner interval, which is lithologically and sedimentologically uniform. The log pattern would also make it possible to reliably correlate this interval over the study area. It is assumed that with this approach the influence of lateral and vertical lithological/sedimentological variations on the burial anomalies and erosion estimates is minimal.

The third crucial factor of the burial anomaly analysis is the definition of the baseline (normal compaction trend) since it has great impact on the amount of estimated erosion. In case of a lithologically clean formation (e.g., shale, chalk) published baselines can be used, which have been determined for the given lithology (e.g., Nyland et al., 1992; Japsen, 1998; 1999). These baselines are often based on data from different basins and are represented by one or more analytical formulas (e.g., Magara, 1976; Heasler and Kharitonova, 1996; Japsen, 1998). Other authors (Bulat and Stoker, 1987; Hillis, 1993; Hillis et al., 1994) used baselines fitting to the lowest interval velocity values observed in the given region. Such baselines overestimate the erosion and provide only rough estimates. When regional geology and available data allows it baselines should be determined from wells where no erosion is expected, or where the effect of erosion is overprinted by the post-erosional sedimentation. This way of baseline definition provides the most accurate erosion estimates, since local sedimentological and lithological circumstances affecting the sonic velocities are incorporated into baseline and taken into account.

The shape of the baseline is also an important factor. At greater depth where the gradient of interval velocity increase is smaller, the baseline is steep (and ultimately becomes vertical). In case of a steep baseline small variations in sonic velocity are manifested in significant fluctuations of the burial anomaly, and consequently of the estimated erosion.

5.2 Burial anomaly analysis in the West Netherlands Basin

Below, the interval velocity analysis of nine stratigraphic units from six Jurassic–Cretaceous formations are presented. The analyzed formations belong to the Late Cretaceous Chalk Group (Houthem and Ommelanden Fm.), the Early Cretaceous Rijnland Group (Holland and Vlieland Claystone Fm.) and the Early Jurassic Altena Group (Aalburg and Sleen Fm.) (Fig. 5.1). Based on the unique gamma-ray-, sonic- and resistivity log response of these formations several 50–100 *m* thick intervals having uniform log characteristics were defined within these formations. From the invariable log pattern it is assumed that the selected intervals are lithologically/sedimentologically uniform, which is ideal for the burial anomaly analysis. In some cases the log pattern of the formations made it possible to reliably correlate the selected intervals across the basin.

The average sonic velocities of the selected intervals were calculated using the integrated travel time (ITT) and the thickness of the interval. In cases where the ITT peaks were not displayed along the sonic log, manually averaged slowness values were obtained, which later were converted into interval velocity. The true vertical depth of the midpoint of the interval represents the reference depth for every interval velocity measurement. The true vertical depth was calculated using the path of the borehole.

On the southern flank of the WNB only a small amount of Late Cretaceous erosion occurred, which was followed by significant Tertiary subsidence (Fig. 5.1; Voorne Trough). In this part of the basin Mesozoic sediments presently are at maximum depth of burial. Therefore, interval velocity data from wells located in this part of the basin (referred to as reference wells/points) are used to constrain the normal depth trends. It is to be emphasized that in an ideal case the reference point should align along a smooth, quasi linear trend. A “noisy” reference data set suggests that not uniform lithology/diagenesis, borehole conditions or post-depositional impacts such as overpressure or hydrocarbons rather than extent of erosion are affecting the signal. In these cases the general reliability of the estimated erosion should be considered being lower. As the reference points never perfectly align along a trend, only those deviations that are clearly separated from the cloud of reference points are considered to be true anomalies.

5.2.1 Chalk (Houthem and Ommelanden Formations)

As demonstrated by Anselmetti and Eberli (1993) sonic velocity of limestones depends on the porosity and diagenesis of the rock rather than on its depth. Sonic velocity inversions with depth are common, which makes limestones less ideal for the burial anomaly analysis. Chalks however, though chemically identical to limestones, usually show a clearly depth controlled compaction trend (e.g., Mallon and Swarbrick, 2002; Fabricius, 2003), which makes them suitable for this kind of analy-

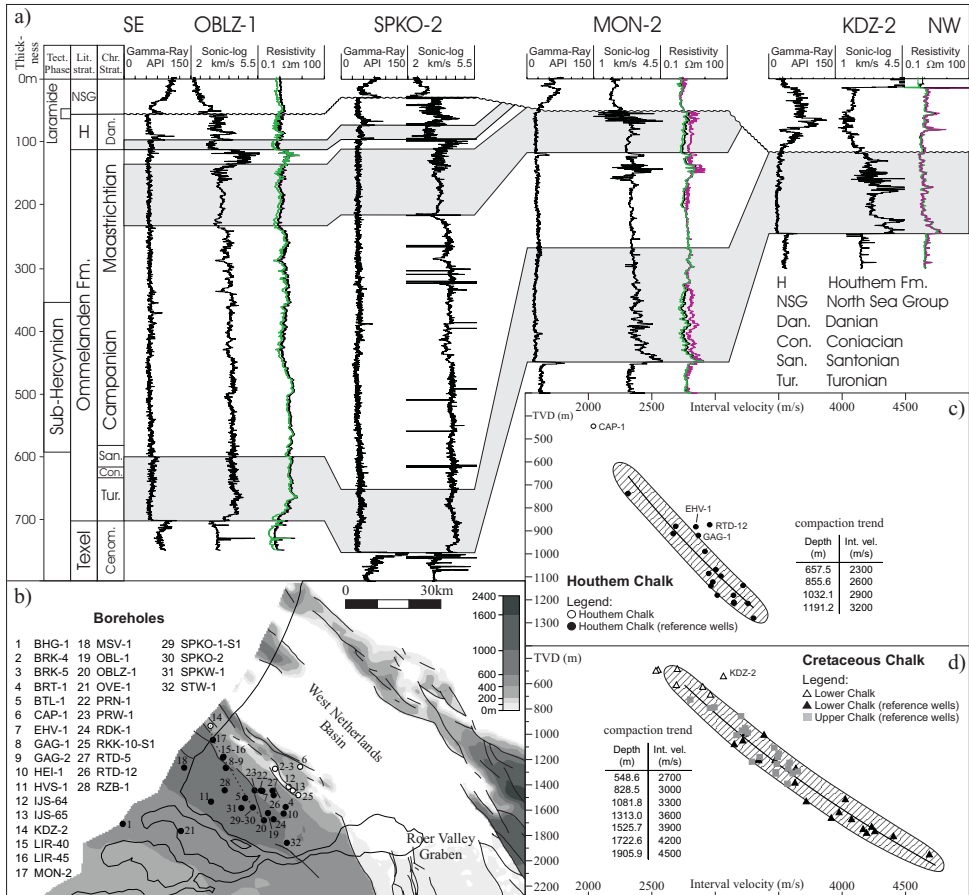


Figure 5.3: a) Litho-chronostratigraphy and characteristic log pattern of the Chalk Group. The investigated intervals (Lower-, Upper and Houthem Chalk) are indicated in grey. b) Preserved thickness of the Chalk Group. Boreholes indicated by black circles represent the reference wells that were used to constrain the baselines. c) Interval velocity—depth pairs for the Houthem Chalk interval. d) Interval velocity—depth pairs for the Lower and Upper Chalk intervals.

sis (Hillis, 1991; Japsen, 1998). It should be noted however, that syn-sedimentary features such as chalk slumps are often associated with zones with significant overpressure and consequently anomalous porosity and sonic velocity values, and form excellent reservoirs in the North Sea region. The early entry of hydrocarbons into the pore space can further enhance the porosity anomaly (e.g., Cornford, 1994).

Deposition of the Late Cretaceous–Early Paleocene chalk in the WNB is coeval with the early phases of basin inversion (Fig. 5.3a). Because of this, interval ve-

locity analysis of the chalk may provide important constraints not only on the mid Paleocene and Late Eocene, but also on any intra-chalk (Late Cretaceous) erosion, since the earliest deposits of the chalk pre-date the Late Cretaceous inversion phase. On the other hand, slumping might have occurred during the inversion (see lensoid features on the seismic section of figure 6.3a (p. 101) between 12000–14000 *m*), which makes those intervals not ideal for the interval velocity analysis. The chalk, which is preserved only on the flanks of the basin (Fig. 5.3b), is subdivided into the Late Cretaceous Ommelanden and the Early Paleocene Houthem Formations (Van Adrichem Boogaert and Kouwe, 1997). No further lithostratigraphic subdivision (members) are defined within the chalk. Three chalk intervals were investigated, which were defined and correlated using wireline log patterns in 32 wells (Fig. 5.3).

The lowermost unit, here referred to as Lower Chalk interval, is defined from the bottom of the Ommelanden Formation upto the maximum of a slightly increasing GR log (Fig. 5.3a). This interval, which is ~100–150 *m* thick, represents chalks of Turonian to Coniatian–Early Santonian age (TNO NITG, 2002). The second unit comprises the uppermost part of the Ommelanden Formation. This chalk interval (referred to as Upper Chalk interval) is of Maastrichtian age and can be easily identified and correlated using the resistivity- and sonic log response. The uppermost ~20 *m* of chalk with very high sonic velocity and resistivity is not included in this interval. The third investigated interval represents the lowerst part of the Houthem Formation (referred to as Houthem Chalk). This is represented by low resistivity and sonic velocity and slightly higher GR than the surrounding rock and is bounded both at the top bottom by two distinct spikes in the GR. The thickness of this interval is ~20 *m*. The succeeding upper part of the formation has a very “noisy” log response and is not included in the analysis (Fig. 5.3a). It is important to note that the lowest interval pre-dates, while the upper intervals post-date the Late Santonian–Mid Campanian inversion phase. Probably this is the reason why the syn-inversion chalk interval between them has a non-uniform sonic and resistivity response (syn-tectonic features?), which makes the correlation of this interval over large distances not possible.

The interval velocity—depth pairs for the three chalk intervals are shown in figure 5.3c–d. The log suites of 6 wells contain not only sonic- but also density logs, which made it possible to calculate average bulk densities for the Lower Chalk interval. Using the average density vs. sonic velocity plot a conversion formula was calculated, which was used to convert the measured average bulk density of wells RKK–10–S1 and IJS–65 into a sonic velocity. In these wells sonic velocity data are not available.

Houthem Chalk

The Houthem Chalk (Fig. 5.3c) has a slightly lower sonic velocity than the Lower and Upper Chalk intervals, which implies that the lithological composition and/or texture of the Paleocene and the Cretaceous chalk is different. Except for three data

points (EHV-1, GAG-1 and RTD-12) the velocity—depth pairs of the reference wells follow a quasi-linear trend. The observed anomalies are not erosion-related, since in these wells minor erosion is thought to have taken place and the post-chalk sedimentation is significant. It is important to note that well CAP-1 also fits into the trend, although has only 86 m of preserved chalk, suggesting that the burial anomaly signal is masked by the Cenozoic subsidence.

Lower and Upper Chalk

The interval velocity of the Lower and the Upper Chalk intervals for the reference wells behaves similarly with depth (Fig. 5.3d). The trends align along a clean line, which represents the baseline. Data points shallower than ~ 700 m belong to wells that are located along the axis of an uplifted/folded half-graben (only 50–100 m of preserved chalk; Fig. 5.3b). In these wells (CAP-1, BRK-4, BRK-5, IJS-64, IJS-65, RKK-10-S1) a certain amount of burial anomaly would be expected, but none was found, suggesting that presently the Cretaceous chalk in these wells is buried at its maximum. In case of well KDZ-2 ~ 250 m of burial anomaly is observed. Considering the similar tectonic position and preserved chalk thickness in this well compared to the wells mentioned above it is unlikely that this anomaly is erosion-related. A clear explanation for this anomaly has not yet been found.

Comparison with published baselines

The uniform lithology of the chalk makes it possible to compare the results of this study with compaction trend lines obtained from other Cretaceous basins or from present day oceanic basins (Fig. 5.4; Scholle, 1977; Sclater and Christie, 1980; Japsen, 2000; Mallon and Swarbrick, 2002). In order to convert the porosity—depth baselines of Scholle (1977) and Sclater and Christie (1980) into sonic velocity—depth lines the conversion formula of Japsen (1998) and of Mallon and Swarbrick (2002) were used. The baselines of Bulat and Stoker (1987) and Hillis et al. (1994) are not considered in the present discussion since they are based on data measured in significantly uplifted basins.

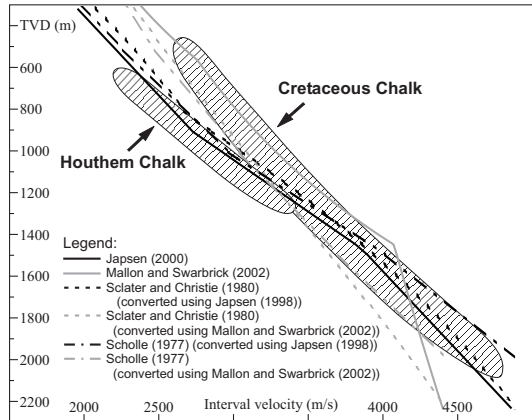


Figure 5.4: Comparison of the observed compaction trend of the Ommelanden and Houthem Chalk with those from published studies.

Comparison of the various baselines reveals that the impact of the porosity—sonic velocity conversion formulas on the resulting baselines is significant. The baseline of Mallon and Swarbrick (2002) is based on interval velocity measurements of non-reservoir North Sea chalk as well as carefully selected DSDP wells, in which the composition of the sediments is comparable with that of the North Sea chalk. Above 1000 *m* this curve as wells as the porosity—depth curves converted by Mallon and Swarbrick's (2002) formula fit particularly good with the data presented in this study. The curve of Japsen's (2000) and the porosity—depth curves converted by Japsen's (1998) formula seems to fit better to the Houthem Chalk at shallow depth. At greater depth, almost all of the curves fit reasonably well taking into account the estimated accuracy of the method (± 200 *m* Skagen, 1992).

To summarise, it is concluded that the baseline determined for the Cretaceous chalk in the WNB is consistent with published compaction trend curves. This implies that the Late Cretaceous–mid Paleocene chalks in the southern part of the WNB presently are all at maximum depth of burial.

5.2.2 Holland Formation

The Early Cretaceous Holland Formation (Upper Rijnland Group) was deposited in the thermally subsiding WNB following the Late Jurassic–Early Cretaceous rifting phase and is subdivided into five members: the Lower Holland Marl, the Holland Greensand, the Spijkenisse Greensand, the Middle Holland Claystone and the Upper Holland Marl Members (Fig. 5.5a). Except for the two Greensand Members, which correspond to a major regression period, the marl and claystone members were deposited in an open marine environment and have consistent lithology in the entire basin (Van Adrichem Boogaert and Kouwe, 1997). The upper part of the formation in a large part of the basin is missing due to erosion (Fig. 5.1).

Two intervals were selected for the analysis. The first interval consists of the lowermost ~ 80 – 100 *m* of the Lower Holland Marl Member (referred to as Lower Holland interval) and was defined in 26 wells (Fig. 5.5a). The base of this interval is characterised by a distinct gamma ray bulge (representing the maximum of transgression, Den Hartog Jager, 1996) followed by lower gamma ray values. A gentle drop in the gamma ray log marks the top of this interval. In the marginal part of the basin, where the Lower Holland Marl Member is thin, the entire sequence was used for the analysis. The other interval used in the analysis is represented by the uppermost part of the Middle Holland Claystone Member (~ 50 *m* thick), which is present in 18 wells (referred to as Middle Holland interval). Its lower boundary is marked by a gentle drop in the gamma ray log, while from above it is bounded either by the Upper Holland Marl or by a thin layer of very low sonic velocity (Fig. 5.5a).

To reliably define the baselines for the Lower- and Middle Holland intervals, reference data points with shallow depth are needed. The group of reference wells for the Holland Formation therefore was extended by wells where only a thin chalk layer is preserved, but no chalk anomaly was observed (see Fig. 5.5b).

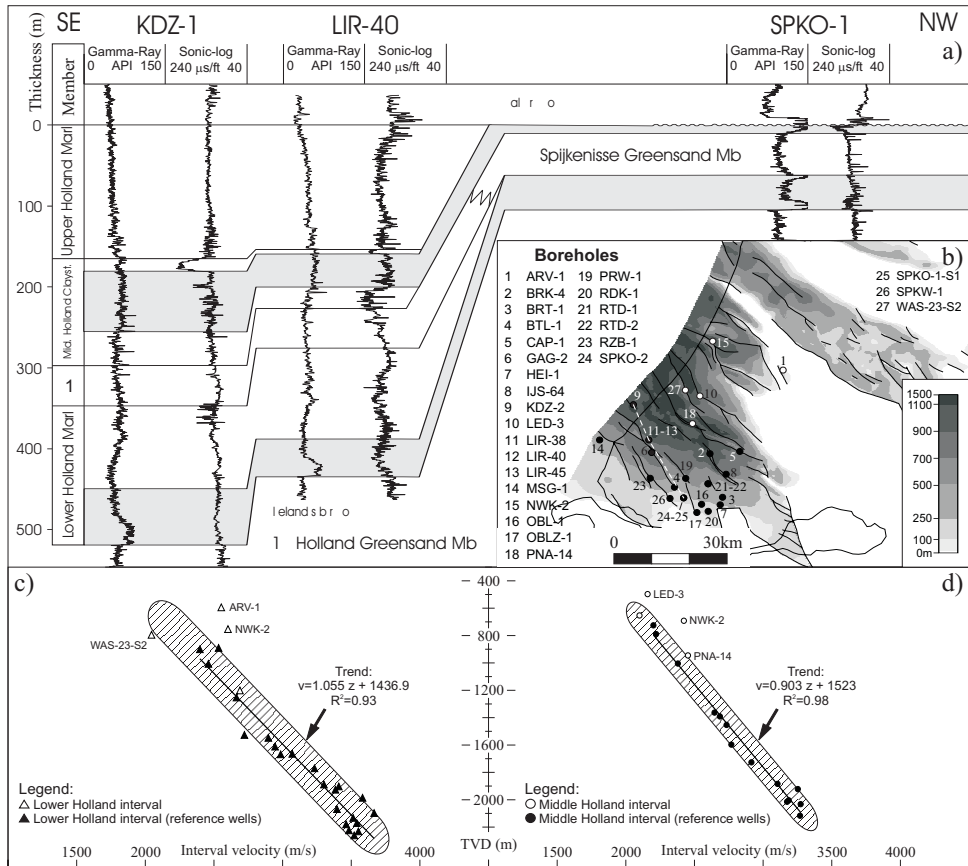


Figure 5.5: a) Lithostratigraphy and characteristic log pattern of the Holland Formation. The investigated Lower-, and Upper Holland intervals are indicated in grey. b) Preserved thickness of the Early Cretaceous Rijnland Group. Boreholes indicated by black circles represent the reference wells, which were used to constrain the baselines. c) Interval velocity—depth pairs for the Lower Holland interval. d) Interval velocity—depth pairs for the Upper Holland interval.

The cloud of reference data points for the Middle Holland interval shows little scatter and defines a very reliable baseline (Fig. 5.5d). For the Lower Holland interval the quality is also good, although there is some scatter between 1800–2100 m caused by wells located at the margin of the basin (Fig. 5.5c). Probably the thin preservation and/or a slightly different lithology cause this. It is important to note that for both intervals the increase of velocity with depth is smaller than for the chalk (the baseline is steeper). Consequently, smaller burial anomalies are more difficult to recognise in the case of the Holland Formation.

For the Lower Holland interval two anomalies clearly separated from the reference points are observed (NWK-2 and ARV-1; Table 5.1). For the Middle Holland interval also two positive anomalies were found (NWK-2 and LED-3). Considering the tectonic position of the NWK-2, LED-3 and ARV-1 wells in the basin it is possible that these anomalies are caused by exhumation.

5.2.3 Vlieland Claystone Formation

The Vlieland Claystone Formation of Early Cretaceous age belongs to the Vlieland Subgroup of the Rijnland Group. The group was deposited in a shallow marine, near-shore environment (e.g., Den Hartog Jager, 1996) and has a complex, laterally inhomogeneous structure with interfingering clay and sand bodies (Fig. 5.6a). Because of this it is difficult to identify and correlate a stratigraphic unit of uniform lithology that is ideal for the interval velocity analysis.

For the present analysis the thick sandy clay deposits succeeding the Berkel Member of the Vlieland Sandstone Formation were used (referred to as Upper Vlieland; Fig. 5.6a). This interval is characterised by a relatively “calm” sonic log response compared to the succession below the Berkel Member. The lack of characteristic log patterns, however, did not allow for further subdivision. For the analysis therefore, one or more ~50–100 *m* thick intervals were selected, whose sonic log indicated consistent seismic velocities. For wells located in a marginal position the Eemhaven member of the formation was used (Fig. 5.6a).

Below 1300 *m* the reference data points show some scatter, which is partly due to the thin Eemhaven member (Fig. 5.6c). The figure reveals on the other hand that the linear trend determined by the reference points coincides remarkably well with the shallow data points, where a burial anomaly would be expected. None of these wells shows a clear separation from the reference cloud.

5.2.4 Lower Jurassic clays (Sleen and Aalburg Formations)

In the Early Jurassic open marine environments dominated the area of the WNB, in which a thick clay succession with occasional limestone beds was deposited. The Sleen and the Aalburg Formations represent the lowermost part of this succession, which displays pronounced differences in thickness as a result of syn-sedimentary faulting (see *Chapter 4* (p. 51) or Fig. 5.7b). Both of these formations are widespread in the WNB, but they are missing, or significantly reduced in thickness outside the basin centre due either to the Late Cretaceous inversion, or to the mid Jurassic erosion resulting from the thermal uplift of the southern North Sea region. (e.g., Ziegler, 1990). It is suggested that within the boundaries of the WNB the mid Jurassic erosion was less than the subsequent Late Jurassic–Cretaceous sedimentation, that is, any burial anomaly resulting from the mid Jurassic erosion was destroyed prior to the inversion. Three intervals, defined in 41 wells, were selected for the analysis.

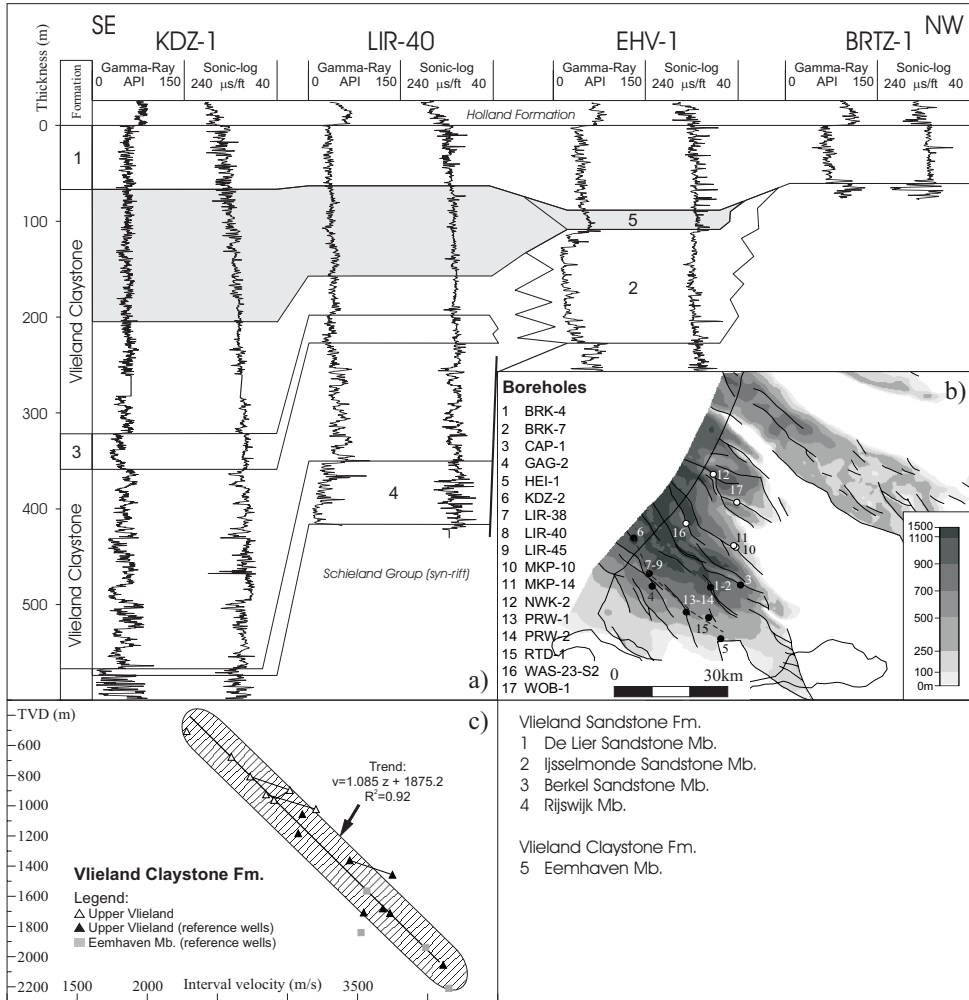


Figure 5.6: a) Lithostratigraphy and characteristic log pattern of the Vlieland Subgroup of the Rijnland Group. The investigated interval is indicated in grey. b) Preserved thickness of the Early Cretaceous Rijnland Group. Boreholes indicated by black circles represent the reference wells, which were used to constrain the baseline. c) Interval velocity—depth pairs for the Upper Vlieland interval.

The first interval is represented by the entire Sleen Formation, since it is only $\sim 30\text{--}50\text{ m}$ thick (Fig. 5.7a). Within the Aalburg formation two intervals were investigated. The lower interval (referred to as Lower Aalburg interval) is defined by the lowermost $80\text{--}100\text{ m}$ of the formation, which consists of an alternation of clay and

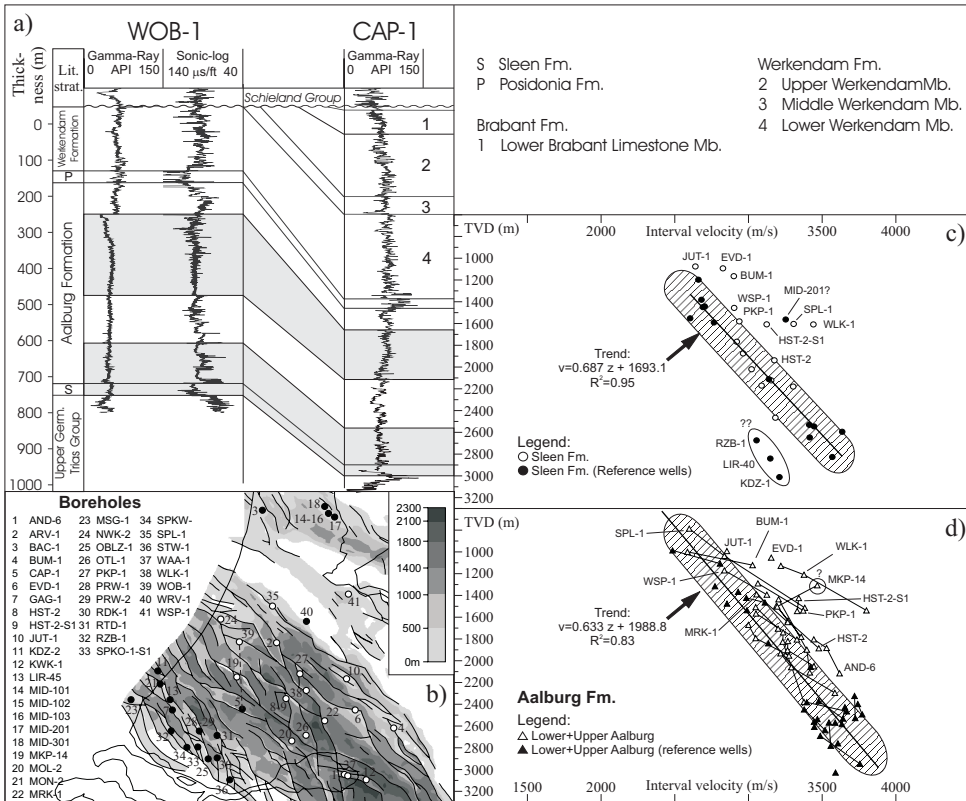


Figure 5.7: a) Lithostratigraphy and characteristic log pattern of the Early Jurassic Altena Group. The investigated intervals (Sleen, Lower- and Upper Aalburg) are indicated in grey. b) Preserved thickness of the Altena Group. Boreholes indicated by black circles represent the reference wells, which were used to constrain the baselines. c) Interval velocity—depth pairs for the Sleen Formation. d) Interval velocity—depth pairs for the Aalburg Formation.

limestone layers (TNO–NITG, 2002). On the logs this interval is characterised by alternating zones of low and high (and a bit “noisy”) gamma-ray and sonic values. A 100–150 m thick interval from the upper part of the Aalburg Formation defines the third studied interval (Fig. 5.7a, referred to as Upper Aalburg interval). Both the gamma-ray- and the sonic log response of this interval are more uniform than that of the Lower Aalburg interval. In wells where the formation is very thick, an additional 100–150 m thick interval from the upper part of the Aalburg Formation was also studied. The lack of characteristic log patterns however, did not allow correlating these intervals precisely between the wells.

Compared to the reference points of the younger formations discussed above, the reference points for the lower Jurassic intervals do not cover a large depth range.

This makes the definition of the baseline difficult. For this reason additional wells located north of the basin (Zandvoort Ridge (WRV-1 well) and in the NW part of the Central Netherlands Basin (BAC-1 and MID- wells)) were added to the reference wells (Fig. 5.7b). In these wells erosion is suggested to be either small and/or masked by the significant Cenozoic sedimentation.

Sleen Formation

For the Sleen Formation the RZB-1, the LIR-40 and the KDZ-2 wells show significantly lower interval velocity than the rest of the reference wells (Fig. 5.7c; see discussion at the Aalburg Formation below), while well MID-201 — despite being a reference well — shows anomalously high interval velocity. These four wells were excluded from the definition of the baseline, which is significantly steeper than that of the overlying formations. Consequently, for the Sleen Formation the same amount of velocity anomaly corresponds to a larger amount of burial anomaly. Outside the cloud of reference points 9 anomalies were found (Table 5.1), the locations of which coincide with a major hiatus in the sedimentary record. It is suggested therefore that these deviations represent true burial anomalies related to erosion. Four of the anomalies, however, are considered to be minor, since they are not separated clearly from the cloud of reference points.

Aalburg Formation

The reference points for the Lower and Upper Aalburg intervals define almost the same baseline, so it was decided to merge the two data sets (Fig. 5.7d). This has two major advantages: (1) the definition of the baseline is based on a larger, combined data set; (2) each well contains more (two or three) data points, consistency of which provides constraints on the quality and reliability of the burial anomaly. In an ideal case the line connecting the data points of a given well (intra-well compaction trend) should be parallel to the baseline defined by the reference wells (“global” compaction trend). This kind of consistency of the data points help to identify true burial anomalies even where there is no clear separation from the cloud of reference points.

As with the Sleen Formation the baseline for the Aalburg formation is also very steep. In addition, the cloud of reference points is wider than for the other studied intervals (i.e., the reference points are “noisier”). Inconsistencies are most significant below 2300 m, which is also manifested in the intra-well compaction trends in this depth being not parallel to the “global” baseline. Presently, the pressure of the pore fluid in the Aalburg formation, which contains several hydrocarbon-prone bituminous layers (Bodenhausen and Ott, 1981), is hydrostatic. In the past however, during for example the Late Jurassic–Early Cretaceous period of strong subsidence or during the expulsion of hydrocarbons, overpressure might have developed within the thick clayey succession. This could have caused abnormal compaction of the formation. In addition, Beekman et al. (2000) showed that mechanically weak clay layers tend to experience significant plastic deformation during inversion. Considering that

the formation is relatively uniform lithologically, it is suggested that external factors such as those mentioned above could play an important role in the scatter of the sonic velocities of the reference wells.

Clear burial anomalies are identified in 10 wells, which are located in the significantly eroded northern and north-eastern part of the basin (Fig. 5.1 and 5.7b). These anomalies are suggested to be erosion-related. The anomalies for wells MRK-1 and WSP-1 do not separate clearly from reference points. The position of these wells however suggests that these anomalies although being small ($\sim 200\text{--}300\text{ m}$) are related to erosion. When determining the burial anomaly in well MKP-14 the shallowest data point was not taken into account, since it is not consistent with the other two data points and with the baseline. For well NWK-2 the uppermost interval investigated within the Aalburg Formation is separated by a major thrust fault from the two other intervals. The interval velocity—depth points from the deeper intervals (footwall) are located within the cloud of reference points, while the third data point (hangingwall) shows a clear anomaly. This suggests that uplift and erosion in this well is related to a local phenomenon (uplift of the hanging-wall block of a reverse fault) rather than to the regional uplift of the area (see further discussion later).

5.3 Geometric reconstruction of the amount of erosion

Before discussing the results of the burial anomaly analysis a geometrical approach is presented, which aims to determine the pattern of erosion. This approach is complementary to the burial anomaly analysis and on a local scale should provide comparable results. The geometric restoration of the erosion was performed only in the western part of the basin where from a lithostratigraphic point of view only few units are missing (i.e., the Chalk Group and the upper part of the Rijnland Group; Fig. 5.1), and where excellent quality 3-D seismic surveys are present. The reconstruction is performed in four steps (Fig. 5.8a).

Step 1. The first step is to restore the base Chalk Group horizon in areas of the basin where it is not preserved (Fig. 5.8a). This restored horizon is referred to as fictional base Chalk Group horizon (FBCG). Where 3-D seismic surveys are available (central part of the basin) the FBCG horizon was interpreted on seismic sections using the geometrical characteristics of preserved reflectors within the Rijnland Group as guides (Fig. 5.8b). The principle behind this interpretation is the assumption that the pattern of the FBCG horizon is similar to the pattern of preserved reflectors within the Rijnland Group. In other words, the position of the FBCG horizon — and therefore also the thickness pattern of the Rijnland Group — is estimated using the thickness pattern of preserved subunits observed on the seismic sections. The applicability of this procedure is justified by the excellent correlation observed between the total thickness of the uneroded Rijnland Group

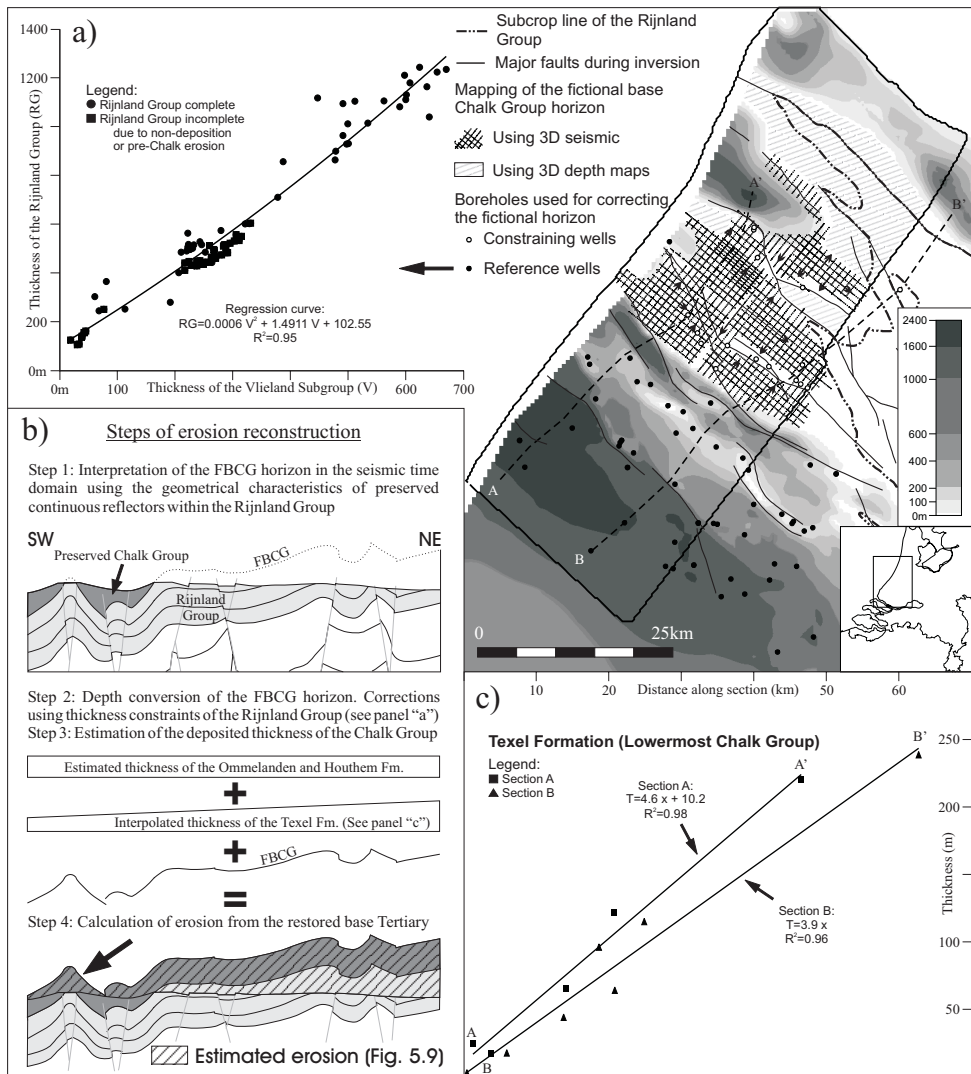


Figure 5.8: Geometric restoration of the amount of sediment eroded from the western part of the West Netherlands Basin. a) Cross-plot between the thickness of the Vlieland Subgroup and the Rijmland Group. The map on the right shows the outline of the restored area. The colour scale shows the preserved thickness of the Chalk Group. Black arrows show the "path" of the seismic interpretation commencing from preserved patches of the base chalk horizon. b) Main steps of the erosion reconstruction (see text for discussion). c) Deposited thickness of the Texel Formation along sections A and B.

and the thickness of the Vlieland subgroup within it (Fig. 5.8a). This correlation is also found to be valid in wells located at the SW margin of the basin, where due to non-deposition or small amounts of pre-chalk erosion the Rijnland Group is not complete. Interpretation of the FBCG horizon commenced from preserved patches of the Chalk Group, allowing for reliable interpretation across faults.

Step 2. The second step of the reconstruction was the depth conversion of the FBCG horizon. For this a linear velocity model (v_0 - K method) was used with v_0 and K parameters determined for the Rijnland Group (TNO-NITG, 2002). As reference the mid-depth of the preserved Rijnland Group was used. As a quality control the depth converted FBCG horizon was compared with values calculated using the estimated thickness of the Rijnland Group subtracted from the base Rijnland Group horizon. The thickness of the Rijnland group was estimated in the constraining wells (wells shown by open circles; Fig. 5.8a) using the Rijnland Group—Vlieland Subgroup cross-plot. The comparison revealed that the depth converted FBCG horizon systematically overestimated the depth obtained from the cross-plot method (~ 200 m in average). For this reason a depth correction map was constructed, which has a value of zero where the chalk is preserved and gradually increases towards the interior and eastern parts of the map. Correcting the depth converted FBCG horizon with this map does not change the general pattern (i.e., shape) of the FBCG horizon. The corrected horizon satisfies the well data within the error range of the cross-plot. In the northern part of the map where there is no 3-D seismic coverage the FBCG horizon was determined using digitally available 3-D depth models and cross sections. The procedure is similar to that used in the seismic interpretation. Note that because of the lack of data, in this area the FBCG horizon could not be constrained in the same way as in the central part of the map (i.e., cross-plot), therefore more uncertainty should be considered. At the end of the second step the base Chalk Group horizon was fully restored in the entire study area by merging the FBCG horizon and the preserved patches of the base Chalk Group horizon obtained using traditional mapping.

Step 3. The third and most critical step of the erosion reconstruction involves estimation of the pre-erosion thickness of the Chalk Group: this consists of the determination of the deposited thickness of the Houthem and Ommelanden Formations as well as the thickness of the Texel Formation (lowermost Chalk Group). For the latter this is not problematic, since borehole data indicate a gradually increasing thickness towards the N-NNE (Fig. 5.8c). This behaviour is expected from a formation that was deposited in a thermally subsiding shallow marine, near-shore environment (Van Adrichem Boogaert and Kouwe, 1997). Based on the observed thickening trend a map representing the thickness of the Texel Formation was constructed.

Estimation of the deposited thickness of the Ommelanden Formation is very difficult, since its deposition was coeval with the first phase of basin inversion (Late Santonian–Mid Campanian; Baldschuhn et al., 1991; Gras and Geluk, 1999). Indirect evidence from the WNB and neighbouring Roer Valley Graben (RVG) was used to constrain the thickness of the Ommelanden Formation. As demonstrated by

the sonic velocity data of the Ommelanden Formation (p. 74), the chalk presently is at maximum depth of burial in the southern flank of the WNB. This indirectly indicates that — taking into account the thickness of the preserved chalk and the amount of post-inversion sedimentation — the total deposited thickness of the Ommelanden Formation in the central part of the basin was definitely less than ~ 500 m (BRK- and CAP-1 wells). This thickness is less than the amount preserved in the marginal chalk depocentres north and south of the WNB and RVG (i.e., Voorne Trough, South Limburg, Peel Block, Maasbommel High). Gras and Geluk (1999) showed that the thickest Late Cretaceous succession on the Maasbommel High is coeval with the basin inversion and suggested that it originated from the uplifting and eroding RVG. In contrast to the Roer Valley area the syn-inversion sediments on the southern flanks of the WNB are not siliciclastic (TNO-NITG, 2002). This suggests that during the first phase of inversion, erosion (if it occurred) was not large enough to truncate down to the Early Cretaceous and older siliciclastic sediments. In fact, considering the continuously rising sea level during the first phase of basin inversion (Haq et al., 1987), it is speculated that in the WNB, the sea level rise and the thermal contraction of the lithosphere could keep up with the inversion-related tectonic uplift of the basin. In other words, it is possible that in the centre of the basin, non-deposition rather than erosion characterised the first phase of inversion. As Gras and Geluk (1999) demonstrated in the RVG, sediment deposition in the central, inverted part of the basin resumed only when the inversion movements abated at the end of the Cretaceous. This is assumed to be valid also in the WNB, which is supported by the well CAP-1, where the Houthem Formation overlies the lower part of the Ommelanden Formation (correlation based on log patterns).

Following from the above it is suggested that the main erosional phase in the WNB occurred during the second main phase of inversion (Mid Paleocene), which was accompanied by a major drop in global sea level (Haq et al., 1987). During the Late Cretaceous inversion phase non-deposition was more likely. Consequently, the amount of deposited chalk in the centre of the basin roughly can be estimated by summing the thickness of the pre-Campanian chalk and Maastrichtian–Danian chalk, which is $\sim 100 + 200 = 300$ m (based on Fig. 5.3a). Note that this amount (1) is only a rough estimate, since precise chronostratigraphic markers are not available and (2) is only valid in the centre of the basin. In the Voorne Trough and in inversion-related synclines where sedimentation was most probably continuous during the first phase of inversion the thickness of the deposited chalk is (much) larger (see Fig. 5.3a).

Step 4. During the last step of the erosion reconstruction the amount of eroded sediments are summed up. This is equal to the difference between the present-day base Tertiary horizon and a horizon calculated by adding the estimated thickness of the Chalk Group to the already restored base Chalk Group horizon (Fig. 5.8b). The thickness of the Chalk Group is estimated by the sum of the 2-D grid representing the Texel Formation and a uniform thickness of 300 m representing the Ommelanden and Houthem Formations.

5.4 Discussion

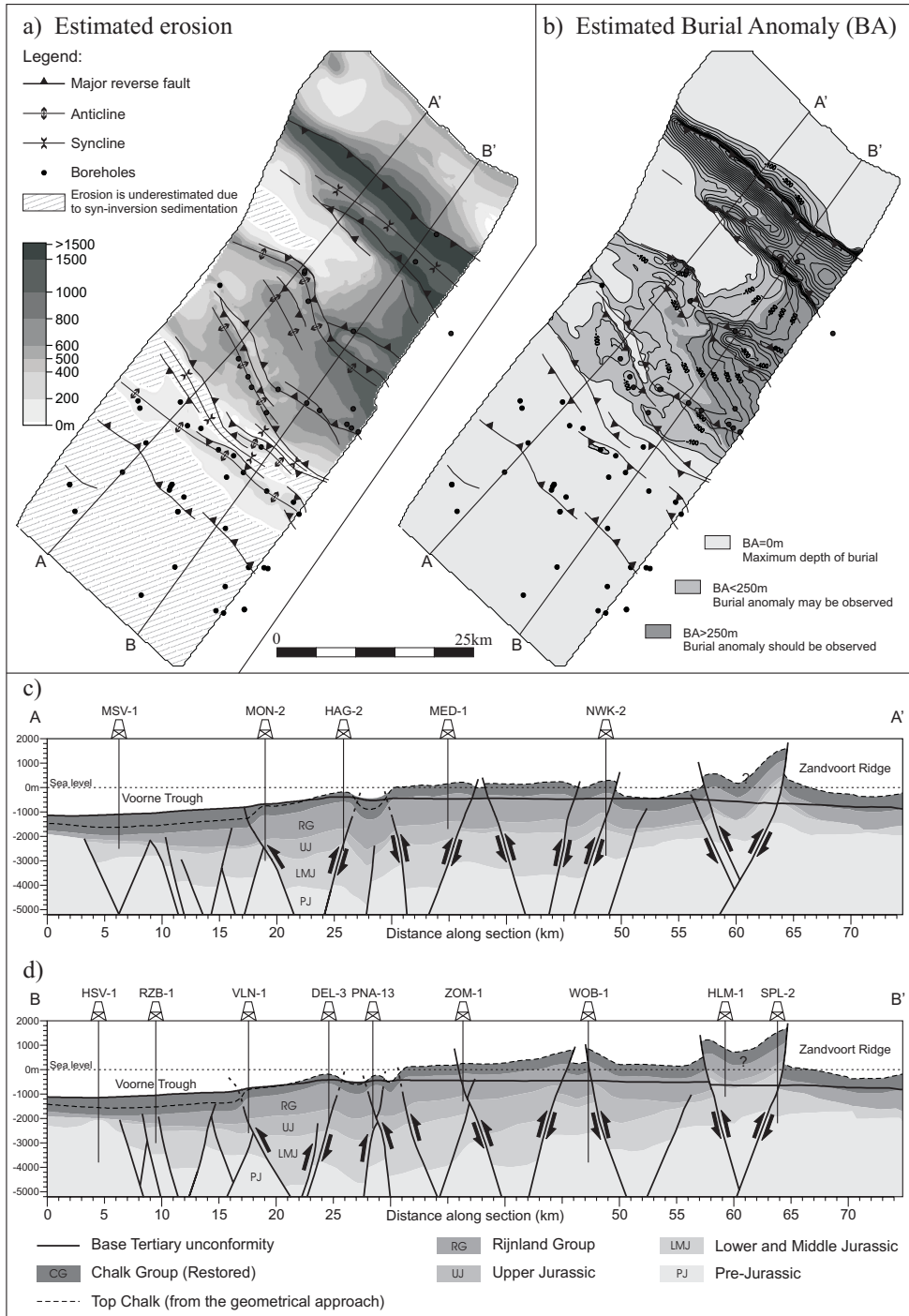
In the following the map of the geometrically restored erosion (Fig. 5.9) and the results of the burial anomaly analysis are discussed. First the pattern of erosion is studied, followed by a discussion on the erosion magnitudes.

5.4.1 Pattern of erosion

The most crucial (and least reliable) step of the geometric approach presented above is the estimation of the original thickness of the Ommelanden and Houthem Formations. Considering the transgressive nature of the Late Cretaceous sedimentation in NW Europe (e.g., Ziegler, 1990) it is reasonable to assume that in the centre of the WNB the thickness of the deposited chalk was relatively uniform. Therefore, in this part of the basin the pattern of removed sediments determined by the geometrical approach is valid even if the magnitude of the deposited Late Cretaceous chalk was estimated incorrectly. It should be emphasised however, that in the south-western part of figure 5.9a (Voorne Trough) the amount of originally deposited chalk and consequently the amount of erosion is underestimated.

Analysis of figure 5.9a reveals that the pattern of erosion varies significantly laterally and has a high frequency local and a low frequency regional component. The regional component shows a general increase of erosion towards the East. This is in agreement with the observed subcrop pattern below the base Tertiary horizon (Fig. 5.1). The eastward increasing erosion suggests a regional, dome-like uplift of the WNB, which reached its maximum in the eastern part of the basin. The local, high frequency pattern of erosion is superimposed onto the regional trend and is fault-related (Fig. 5.9). The maximum of local erosion is associated either with strongly tilted fault blocks (e.g., northern boundary fault of the WNB) or with the axis of fault-related anticlines (fault propagation folds and fault-drag folds), which contain the majority of the hydrocarbon fields in the WNB. The faults involved in the folding are steep normal faults, which were reactivated in a reverse manner (Fig. 5.9c–d). Low angle thrust faults are not observed, which suggests that the reactivation of the normal faults in the western part of the basin was transpressional. The local minima of erosion are generally associated with elongated “erosional shelters”, which are bounded on both sides by uplifted and/or folded areas (i.e., inverted half-grabens). These elongated zones of minimum erosion generally form synclines deformed to varying degrees (Fig. 5.9c–d), and likely to be locations of syn-inversion sedimentation during the Late Cretaceous.

Figure 5.9: a) Amount of erosion and b) burial anomaly estimated using the geometrical approach (Fig. 5.8). Note that erosion is underestimated in the south-western part of the map (see text for discussion) c–d) Geological cross sections across the restored area (location on panel “a” and “b”).



5.4.2 Magnitude of erosion

The results of the burial anomaly analysis and the geometrical approach are summarised in Table 5.1. The burial anomaly-based erosion was calculated from the post-erosion sediment thickness (equation (5.1)). Direct observations regarding the amount of uplift in five wells are also listed. These wells penetrate duplications of part of the sedimentary succession separated by major thrust faults. The depth difference between the same stratigraphic horizon below and above the thrust fault estimates the minimum uplift of the hangingwall block in the given well.

The table reveals that except for four wells the burial anomalies observed for the various intervals are consistent with each other (see the column “consistency”). This indicates that the estimated burial anomaly and consequently the calculated erosion are reliable. The results of the burial anomaly analysis show that in all wells where the Chalk Group is preserved, the measured sonic velocity of the studied intervals coincides with the normal compaction trends determined by the reference wells. As shown earlier the baseline determined for the Cretaceous chalk coincides also with published baselines. These results imply that the Late Cretaceous–Mid Paleocene chinks as well as underlying sediments in the south-western part of the WNB are presently at their maximum depth of burial. The amount of erosion therefore cannot be determined precisely. It is estimated that the line, south of which the formations presently are at their maximum depth of burial, coincides approximately with the northern limit of the preserved Chalk Group (Fig. 5.10). The results of the geometric approach approximate the same boundary (Fig. 5.9b).

Wells CAP-1, BRK-4, BRK-5, IJS-64, IJS-65, PNA-14 and RKK-10-S1, in which the Chalk Group is significantly eroded bring important constraints on the Late Cretaceous tectono-sedimentological setting of the WNB. On one hand in these wells — although they do not show burial anomalies — the amount of erosion can be better constrained, since the post-erosion sedimentation is smaller than in wells located in the Voorne Trough. The lack of burial anomaly in these wells indicates a relatively small amount of erosion (smaller than ~ 450 m) compared to other parts of the basin. On the other hand, since a certain amount of the Ommelanden chalk is still preserved in these wells, they imply that the maximum thickness of Late Cretaceous chalk deposited in the centre of the basin is much smaller than in the Voorne Trough.

Table 5.1: Results of the burial anomaly analysis and the geometrical approach (for map-view see Fig. 5.10). NWK-2* indicates the autochton part of the NWK-2 well below a major thrust fault. BA: amount of burial anomaly; HOUT: Houthem Chalk; OMM: Ommelanden Fm.; MH: Middle Holland interval; LH: Lower Holland interval; VL: Upper Vlieland interval; AAL: Aalburg Fm.; SL: Sleen Fm.; Cons.: consistency among the studied intervals regarding burial anomaly; Geom. Appr.: Geometrical Approach; Dir. Obs.: direct observation; WCRP: within cloud of reference points (i.e., no burial anomaly); REF: reference well used to constrain the baseline; MDB: maximum depth of burial (i.e., no burial anomaly). Values are in meters.

Reconstruction of erosion in the West Netherlands Basin

Well name	Burial anomaly analysis								Geom. Appr.		Dir. Obs.	Decision
	BA HOUT	BA OMM	BA MH	BA LH	BA VL	BA AAL	BA SL	Cons.	Erosion	BA Erosion	Uplift	Erosion
1 AND-6	—	—	—	—	—	100-450	<150/WCRP	NO	<1340	—	—	<900/MDB
2 ARV-1	—	—	—	325-475	—	150/WCRP	WCRP	NO	<1021	—	—	500-1100
3 BAC-1	—	—	—	—	—	WCRP/REF	WCRP/REF	YES	<948	—	—	MDB
4 BHG-1	—	WCRP/REF	—	—	—	—	—	YES	<896	—	—	<300/MDB
5 BRK-4	—	WCRP	—	WCRP/REF	WCRP/REF	—	—	YES	<460	MDB	—	<300/MDB
6 BRK-5	—	WCRP	—	—	—	—	—	—	—	—	—	—
7 BRT-1	WCRP/REF	WCRP/REF	WCRP/REF	WCRP/REF	—	—	—	YES	<940	—	—	<300/MDB
8 BTL-1	WCRP/REF	WCRP/REF	WCRP/REF	WCRP/REF	—	—	—	YES	<1083	MDB	—	<300/MDB
9 BUM-1	—	—	—	—	—	200-450	350-550	YES	1100-1400	—	—	1100-1400
10 CAP-1	WCRP	WCRP	WCRP/REF	WCRP/REF	WCRP/REF	—	—	YES	<426	—	—	<300/MDB
11 EHV-1	<100/REF	WCRP/REF	—	—	—	—	—	YES	<854	—	—	<300/MDB
12 EVD-1	—	—	—	—	—	450-700	325-525	YES	1200-1500	—	—	1200-1500
13 GAG-1	<80/REF	WCRP/REF	—	—	—	WCRP/REF	—	YES	<880	MDB	—	<300/MDB
14 GAG-2	WCRP/REF	WCRP/REF	WCRP/REF	WCRP/REF	WCRP/REF	—	—	—	—	—	—	—
15 HEI-1	WCRP/REF	WCRP/REF	WCRP/REF	WCRP/REF	WCRP/REF	-300/REF	—	YES	<1024	—	—	<300/MDB
16 HST-2	—	—	—	—	—	100-400	0-200	YES	800-1000	—	—	800-1000
17 HST-2-S1	—	—	—	—	—	300-600	250-450	—	—	—	—	—
18 HVS-1	WCRP/REF	WCRP/REF	—	—	—	—	—	YES	<1157	MDB	—	<300/MDB
19 IJS-64	—	WCRP	WCRP/REF	WCRP/REF	—	—	—	YES	<550	—	—	<300/MDB
20 IJS-65	—	WCRP	—	—	—	—	—	—	—	—	—	—
21 JUT-1	—	—	—	—	—	50-300	100-300	YES	1000-1200	—	>1510	1500-1600
22 KDZ-2	—	100-250/REF	WCRP/REF	WCRP/REF	<200/REF	WCRP/REF	-750/REF	NO	<645	MDB	152	<300/MDB
23 KWK-1	—	—	—	—	—	WCRP	WCRP	YES	<1146	—	—	MDB
24 LED-1/2	—	—	—	—	—	—	—	—	—	147	578	-600
25 LED-3	—	—	125-225	—	—	—	—	YES	575-675	220	667	-600
26 LIR-38	—	—	—	WCRP/REF	WCRP/REF	—	—	—	—	—	—	—
27 LIR-40	—	WCRP/REF	WCRP/REF	WCRP/REF	WCRP/REF	—	-700/REF	YES	<730	MDB	—	<300/MDB
28 LIR-45	WCRP/REF	WCRP/REF	WCRP/REF	WCRP/REF	WCRP/REF	WCRP/REF	WCRP/REF	—	—	—	—	—
29 MID-101	—	—	—	—	—	WCRP/REF	WCRP/REF	—	—	—	—	—
30 MID-102	—	—	—	—	—	WCRP/REF	WCRP/REF	—	—	—	—	—
31 MID-103	—	—	—	—	—	—	WCRP/REF	YES	<1150	—	—	MDB
32 MID-201	—	—	—	—	—	WCRP/REF	800/REF	—	—	—	—	—
33 MID-301	—	—	—	—	—	WCRP/REF	WCRP/REF	—	—	—	—	—
34 MKP-14	—	—	—	—	WCRP	75-375	—	NO	485-860	440	892	600-900
35 MOL-2	—	—	—	—	—	WCRP	—	YES	<671	—	—	MDB
36 MON-2	—	WCRP/REF	—	—	—	WCRP/REF	—	YES	<681	MDB	—	<300/MDB
37 MRK-1	—	—	—	—	—	0-300	—	YES	700-1000	—	—	700-1000
38 MSG-1	—	—	WCRP/REF	WCRP/REF	—	WCRP/REF	—	YES	<1095	MDB	>300	<300/MDB
39 MSV-1	WCRP/REF	WCRP/REF	—	—	—	—	—	YES	<1148	MDB	—	<300/MDB
40 NWK-2	—	—	200-350	225-375	0-150	175-475	—	YES	660-810	264	710	>580
41 NWK-2*	—	—	—	—	—	WCRP	WCRP	—	—	—	—	—
42 OBL-1	WCRP/REF	WCRP/REF	—	WCRP/REF	—	—	—	YES	<1054	—	—	<300/MDB
43 OBLZ-1	WCRP/REF	WCRP/REF	WCRP/REF	WCRP/REF	—	WCRP/REF	WCRP/REF	YES	<1122	—	—	<300/MDB
44 OEG-1	—	—	—	—	—	—	—	—	—	214	722	-700
45 OTL-1	—	—	—	—	—	WCRP	WCRP	YES	<628	—	—	MDB
46 PKP-1	—	—	—	—	—	200-450	0-225	YES	700-900	—	—	700-900
47 PNA-14	—	—	<150	WCRP	—	—	—	YES	<416	MDB	269	<300/MDB
48 PRN-1	WCRP/REF	WCRP/REF	—	—	—	—	—	YES	<845	MDB	—	<300/MDB
49 PRW-1	WCRP/REF	WCRP/REF	WCRP/REF	WCRP/REF	WCRP/REF	WCRP/REF	WCRP/REF	YES	<1000	MDB	—	<300/MDB
50 PRW-2	—	—	—	—	WCRP/REF	WCRP/REF	300/REF	—	—	—	—	—
51 RDK-1	WCRP/REF	WCRP/REF	—	WCRP/REF	—	WCRP/REF	WCRP/REF	YES	<1098	—	—	<300/MDB
52 RKK-10-S1	—	WCRP	—	—	—	—	—	YES	<622	—	—	<300/MDB
53 RTD-1	—	—	—	WCRP/REF	WCRP/REF	WCRP/REF	—	—	—	—	—	—
54 RTD-12	60-160/REF	WCRP/REF	—	—	—	—	—	YES	<840	—	—	<300/MDB
55 RTD-2	—	—	WCRP/REF	WCRP/REF	—	—	—	—	—	—	—	—
56 RTD-5	—	WCRP/REF	—	—	—	—	—	—	—	—	—	—
57 RZB-1	WCRP/REF	WCRP/REF	WCRP/REF	WCRP/REF	—	WCRP/REF	-700/REF	YES	<1064	MDB	—	<300/MDB
58 SPKO-1-S1	WCRP/REF	WCRP/REF	—	WCRP/REF	—	WCRP/REF	WCRP/REF	YES	<1150	MDB	—	<300/MDB
59 SPKO-2	WCRP/REF	WCRP/REF	—	WCRP/REF	—	—	—	—	—	—	—	—
60 SPKW-1	WCRP/REF	WCRP/REF	—	WCRP/REF	—	WCRP/REF	WCRP/REF	YES	<1222	MDB	—	<300/MDB
61 SPL-1	—	—	—	—	—	100-400	500-700	YES	800-1400	—	>140	800-1400
62 STW-1	—	—	—	—	—	WCRP/REF	—	YES	<1085	—	—	<300/MDB
63 WAA-1	—	—	—	—	—	WCRP	WCRP	YES	<910	—	—	MDB
64 WAS-23-S2	—	—	WCRP	-150	-150/WCRP	—	—	YES	490-640	150	603	-600
65 WAZ-1	—	—	—	—	—	—	—	—	—	MDB	441	>436
66 WLK-1	—	—	—	—	—	750-1050	700-900	YES	1400-1700	—	—	1400-1700
67 WOB-1	—	—	—	—	WCRP	~200/WCRP	WCRP	YES	430-630	~300	~730	~500-600
68 WRV-1	—	—	—	—	—	WCRP/REF	WCRP/REF	YES	<569	—	—	<300/MDB
69 WSP-1	—	—	—	—	—	0-250	75-275	YES	880-1130	—	—	900-1100

This suggests that continuous, syn-inversion sedimentation took place in the Voorne Trough while non-deposition or slight erosion characterised the central part of the WNB during the first phase of basin inversion in the Late Cretaceous. In the centre of the basin large amount of chalk deposition, which was later removed by erosion, is not supported by the results of this study.

The geometrical approach presented above is independent from the burial anomaly analysis. The two approaches therefore should provide consistent results. Comparison of the erosion estimates indicates reasonably good (WOB-1, MKP-14 and WAS-23-S2 wells) and excellent (LED-3, NWK-2 and PNA-14) agreement between the two approaches (Table 5.1). In case of NWK-2 and WAZ-1 wells the results of the geometrical approach are in very good agreement also with direct observations, which estimate the minimum amount of uplift due to thrust faulting. This excellent correlation between different methods indicates that assuming 300 *m* of sedimentary cover during the Late Cretaceous–Mid Paleocene in the central part of the basin was a reasonable assumption. A larger amount of burial would lead to disagreement with the observed burial anomalies. Note that the 300 *m* estimates the maximum sedimentary cover above the base Ommelanden horizon at any given moment during the Late Cretaceous rather than the total amount of deposited chalk. Namely, considering (1) 300 *m* of continuous sedimentation during the Late Cretaceous–Mid Paleocene followed by erosion is equally plausible regarding the burial anomaly analysis than the situation of (2) DEPOSITION(pre-Campanian) + EROSION(first inversion phase) + DEPOSITION(Maastrichtian–Danian) + EROSION(second inversion phase) < 300 *m* or (3) DEPOSITION + NON-DEPOSITION + DEPOSITION + EROSION < 300 *m*. The results of this study can not differentiate between these three possibilities. However, based on regional geological considerations it is suggested that the combination of case (2) and (3) is more likely than the case of continuous sedimentation.

It is worthwhile to note that in wells JUT-1, BUM-1 and SPL-1 the observed burial anomaly is smaller in the upper part than in the lower part of the succession (Aalburg and Sleen Fm.). In addition in case of JUT-1 the erosion estimated using the amount of observed burial anomaly is smaller than the uplift calculated from the duplicated sedimentary succession. All of these wells are located close to the northern boundary fault of the WNB (see Fig. 5.10), along which significant reverse faulting and block rotation occurred during the inversion of the basin (Fig. 5.9c–d). It is suggested that in these wells the observed differences between the burial anomaly of the lower and upper parts of the Jurassic succession are the result of the syn-inversion rotation/deformation of the hangingwall block. Namely, if the hangingwall block rotated during thrust faulting, then the uplift of the lower part of the succession is larger than in the upper part, which is closer to the pole of the rotation.

In the last column of Table 5.1 the results of the various approaches are compiled. In the final estimated erosion not only the results of the various approaches but also local geological considerations, structural trends and results from nearby

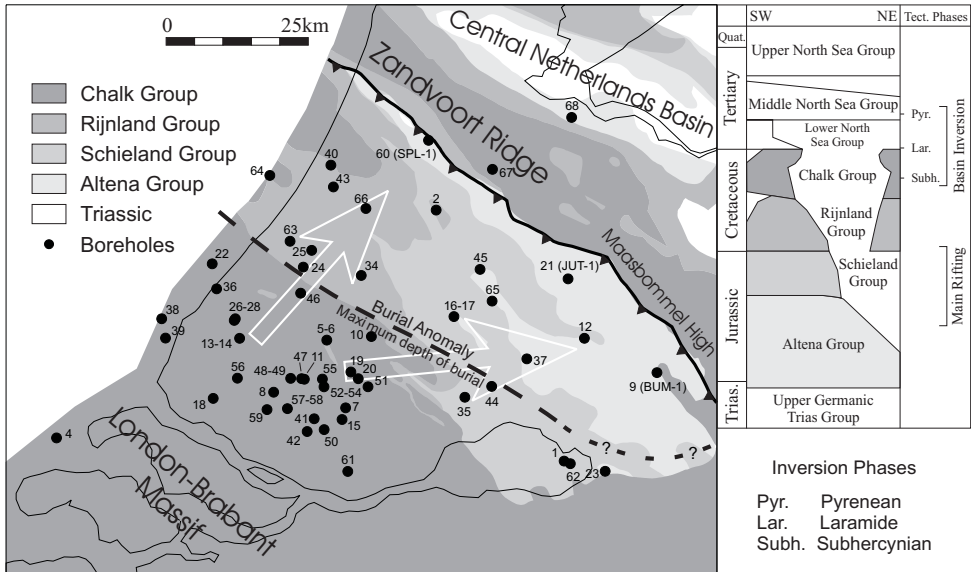


Figure 5.10: General pattern of erosion in the West Netherlands Basin (for data see Table 5.1). Well numbers are the same as in Table 5.1. Background map represents the pre-Tertiary outcrop pattern. White arrows indicate the direction of increasing erosion.

wells were taken into account. For example, in wells located in the Voorne Trough <math><300\text{ m}</math> erosion is estimated, since in these wells the erosion is probably equal to or smaller than the erosion estimated for well further to the NE (BRK-, CAP-1, IJS-, PNA-14). In case of BAC-1, MID-, OTL-1, MOL-2 and KWK-1 wells the burial anomalies were destroyed by the post-erosion sedimentation, and therefore the amount of erosion in these wells could not be estimated.

The compiled results indicate that the amount of erosion increases towards the east and northeast (Fig. 5.10). This can be seen also on the map of erosion constructed using the geometrical approach (Fig. 5.9a) and is in agreement with the subcrop pattern below the base Tertiary horizon. The erosion is highest in the eastern part of the basin especially along the main, north-eastern boundary fault (1100–1700 m ; EVD-1, JUT-1, WLK-1 and BUM-1 wells). In this sense the inversion of the WNB can be considered as being asymmetric. The amount of estimated maximum erosion is smaller than that determined for the neighbouring Broad Fourteens Basin, where 3000–3500 m of maximum erosion was suggested to have occurred along the central anticline of the basin (Nalpas et al., 1995). In the south-eastern part of the WNB (AND-6, WAA-1, KWK-1) also larger amount of erosion is expected than in the north-western part. This however, can not be confirmed, since the burial anomalies were destroyed by the large Oligocene–present day subsidence of the Roer Valley Graben.

5.5 Conclusions

Analysis of interval velocity anomalies is a good method of estimating the amount of exhumation in inverted sedimentary basins. Using the multi-formation approach, the observed burial anomalies and, consequently, the amount of erosion can be reliably estimated, provided consistency can be shown to exist between the results. By applying additional approaches, which are independent from the burial anomaly analysis the reliability of the estimated erosion can be further enhanced. In this chapter the multi-formation burial anomaly analysis in the West Netherlands Basin was combined with a geometrical approach using borehole data and high quality 3-D seismic surveys. The accuracy of the burial anomaly analysis was found to be 150–250 *m*. These results bear important information not only on the magnitudes, but also on the pattern of erosion, which ultimately provides useful constraints on the inversion tectonics of the basin.

The results of this study indicate that there are significant lateral variations in the pattern of erosion, which has a local, high frequency and a regional-, low frequency component. The regional component shows a general increase of erosion towards the east, which reaches its maximum along the north-eastern border fault of the basin. In a general sense this suggests asymmetric inversion of the WNB. Evidence from seismic sections and the high frequency component of the erosion suggest that reactivation of faults played a major role in the inversion and localised erosion of the basin fill. Across major faults several hundreds of meters of difference can be observed in the magnitude of erosion. The local maxima and minima of erosion are related respectively to fault-related anticlines and synclines.

Indirectly the results provide important constraints also on the tectono-sedimentological aspects of the intra-chalk inversion phase (Late Santonian–Mid Campanian). This study suggests that the maximum thickness of the Late Cretaceous chalk in the centre of the basin at any moment during the Late Cretaceous is ~ 300 *m*. This amount is much smaller than the total preserved thickness of the Chalk in the Vorne Trough, indicating that continuous syn-inversion sedimentation was taking place in the Vorne Trough, while non-deposition or slight erosion characterised the centre of the inverting basin.

Chapter 6

Implications of continuous structural inversion in the West Netherlands Basin for understanding controls on Palaeogene deformation in NW Europe

It has been long recognized that basin subsidence in many Mesozoic basins located in Central and NW Europe was terminated in the Late Cretaceous and was followed by basin inversion (see Ziegler, 1987 for summary). The timing of inversion in these basins seems to correlate well with the major Alpine orogenic phases, suggesting that compressional stresses generated by the Euro–African collision were transmitted deep into European Alpine foreland. Detailed analysis of the deformation as well as the main erosional events in these basins suggests that the inversion occurred in four major phases: the Late Cretaceous (~Santonian), the Mid Paleocene, the Late Eocene–Early Oligocene and the Late Oligocene–Early Miocene phases. However, there are indications from several inverted areas that (1) one particular inversion phase can take considerable time (several Myrs or more) and (2) the time interval between two subsequent inversion phases is not tectonically quiet, but is often characterised by ongoing, but calmer tectonic movements (e.g., Jones, 1980; Van Hoorn, 1987; Curry, 1992; Vågnes et al., 1998; Gras and Geluk, 1999). In this chapter a contribution is made to the characterization and understanding of the Late Eocene inversion process in the southern North Sea area by presenting a case study from the West Netherlands Basin (WNB).

The evolution of the WNB was discussed in details in *Chapters 4* and *5*. The most important episodes of this evolution consists of a series of rifting phases in the Late Palaeozoic–Mesozoic period and basin inversion during the Late Cretaceous–Tertiary (e.g., Heybroek, 1974; Van Wijhe, 1987; Ziegler, 1990; Dronkers and Mrozek, 1991).

This chapter is based on: Worum, G., Michon, L. 2004 Implications of continuous structural inversion in the West Netherlands Basin for understanding controls on Palaeogene deformation in NW Europe. *Journal of the Geological Society, London*, in press

All four aforementioned inversion phases are recognized in the WNB. As the cumulative result of these events large amount of sediments were removed from the basin, details of which were discussed in *Chapter 5*. Of these inversion phases the Late Cretaceous and Mid Paleocene events were the strongest, while the Late Oligocene phase was very gentle and is only represented by a regional unconformity.

The Late Paleocene–Eocene geological history of the WNB is markedly different from the Mesozoic evolution. Following the Middle Paleocene inversion phase the WNB ceased to exist as a major depocentre and became a tectonic high called the Early Tertiary High (ETH, also known the as Kijkduin high) (Fig. 6.1a). The sedimentary record indicates that depocentres (Voorne Trough, Zuiderzee Low) were located north and south of the WNB (e.g., Heybroek, 1974; Letsch and Sissingh, 1983; Zagwijn, 1989; Van Adrichem Boogaert and Kouwe, 1997; TNO–NITG, 2002). The Eocene evolution of the ETH is poorly known, since the Late Paleocene–Eocene sedimentary record was partly or totally removed during the Late Eocene tectonic movements. It is suggested, however, that on the ETH only a small amount of sediments was deposited during the Eocene.

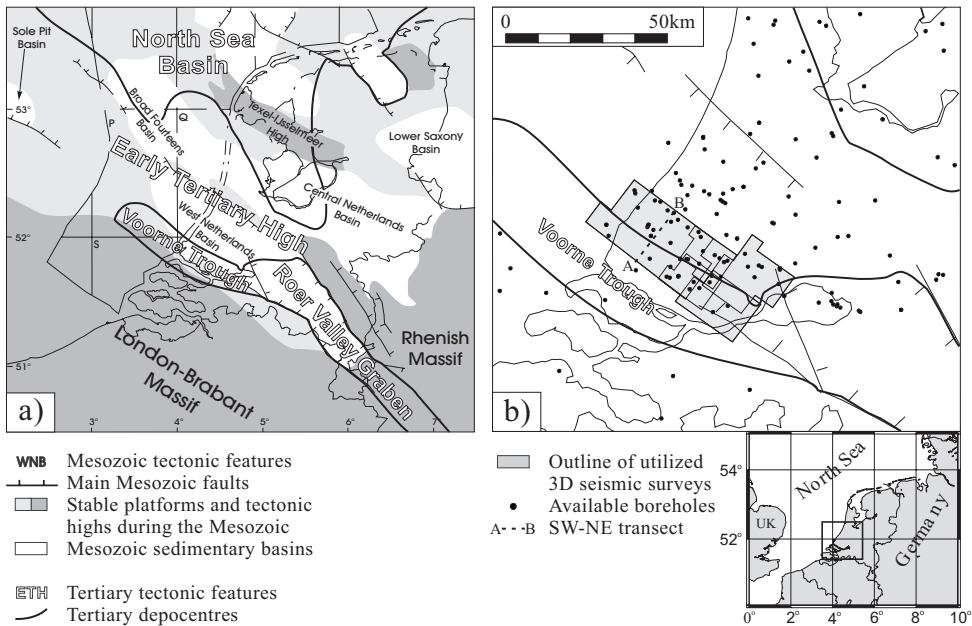


Figure 6.1: Main Mesozoic and Tertiary tectonic features of the Netherlands and its surroundings (after TNO–NITG (2002)). b) 3–D seismic surveys and location of all wells used in this study. The position of SW–NE transect A–B (Fig. 6.3) is indicated.

Considering the amount of deformation and erosion, the Late Eocene tectonic phase in the WNB and in other basins of the southern North Sea region is of secondary importance compared to the Late Cretaceous inversion (e.g., Van Hoorn, 1987; Ziegler, 1987; De Lugt et al., 2003). Because of this a detailed analysis of the preserved Palaeogene sediments is possible, which can help to characterise and better understand the Late Eocene tectonic movements in the southern North Sea region and can also provide useful constraints on syn-sedimentary inversion in general. Recently, in the area of the Broad Fourteens Basin (offshore Netherlands, NW of the WNB), De Lugt et al. (2003) addressed the issue of characterisation and quantification of the Late Eocene inversion phase. They pointed out that, although less intense, this phase affected a much wider area than that of the Late Cretaceous inversion. They explained this as resulting from differently oriented compressive stress fields during the Late Cretaceous and the Eocene. The corresponding uplift was quantified to be $\sim 200\text{--}250$ m.

Recently, good quality 3D seismic data became available in the area of the WNB and the Vorne Trough, the interpretation of which provides high-resolution insight into the lower Tertiary sediment structure. In this chapter this dataset, together with available borehole data is used to investigate the various tectono-sedimentological aspects of the Late Paleocene–Eocene geological history of the ETH and adjacent Vorne Trough. The aim is to quantify the Late Eocene inversion phase in terms of removed sediment thickness as well as to determine the temporal and spatial characteristics of the Eocene tectonic movements. The characteristics of the determined Palaeogene tectonic evolution are compared to those of the Broad Fourteens Basin and other basins in SE England and in Belgium. Differences between the Late Cretaceous–Mid Paleocene and the Late Eocene inversion phases are also discussed, taking into account the direction of Alpine intra-plate compression, the evolution of the Alps and the North Atlantic *ridge-push*.

6.1 Data and methodology

6.1.1 Stratigraphy

The Palaeogene stratigraphy in the study area shows a cyclic sequence of marine clays alternating with marginal marine-to-lagoonal sands and clays on top of the middle Paleocene erosional surface (e.g., Letsch and Sissingh, 1983; Zagwijn, 1989). In this study the litho-chronostratigraphic chart of Van Adrichem Boogaert and Kouwe (1997) is adopted (Fig. 6.2). The sedimentary succession starts with a thin basal sandy unit, the Heers Member of the Landen Formation, followed by the Landen Clay Member representing the climax of the first marine transgression. The Landen Formation is followed by the Dongen Formation, which is subdivided into four members: the thin basal Dongen Sand Member, the Ieper Member, the Brussel Sand Member and the Asse Member. The Ieper and Asse Members represent major transgressional periods, which are also observed elsewhere in the southern North Sea

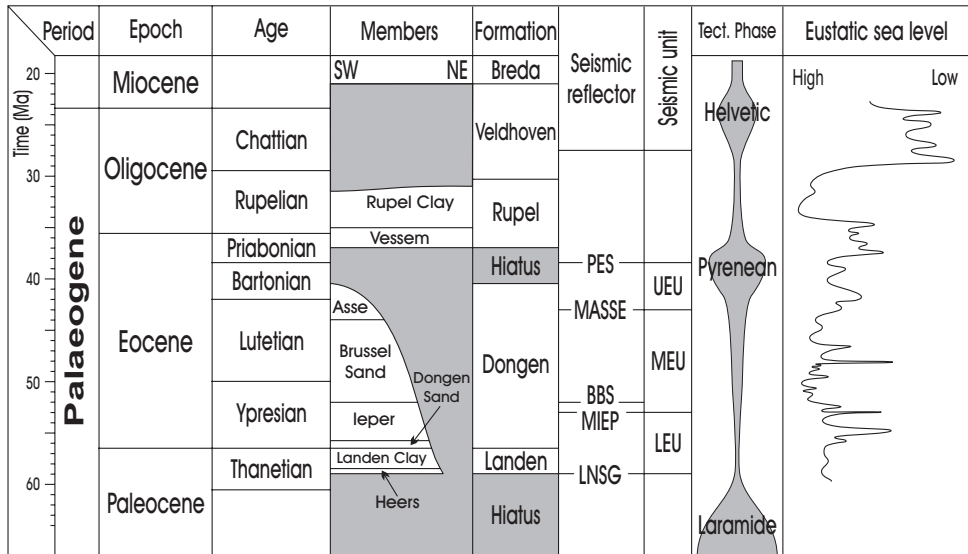


Figure 6.2: Palaeogene litho-chronostratigraphic chart for the West Netherlands Basin area (modified after Van Adrichem Boogaert and Kouwe (1997)). Sea level curve is from Haq et al. (1987). Seismic reflectors and seismic units analysed in this study are also indicated (LEU, MEU and UEU: Lower-, Middle- and Upper Eocene Unit, respectively).

region (e.g., Curry, 1992; Vandenberghe et al., 1998). In the centre of the former WNB these members are not present, probably due to the subsequent Late Eocene inversion phase, but they are preserved in the Voorne Trough.

The Rupel Formation, whose deposition coincides with another major transgression, represents the Oligocene succession preserved in the area. The succeeding Late Oligocene Veldhoven Formation is missing in the study area, but it is preserved elsewhere in the southern Netherlands. The regional unconformity separating the Rupel Formation from the overlying Breda Formation of Miocene age is partly the result of a major sea level drop at the Late Oligocene. Beside the sea level drop, however, a gentle tectonic uplift representing the latest inversion phase is also suggested to have played a role in this erosion (e.g., Ziegler, 1987).

6.1.2 Seismic data and mapping

This study is to a great extent based on public onshore 3-D seismic data (Fig. 6.1b) provided by TNO-NITG. For a detailed investigation of the various Eocene sedimentary units five easily detectable, regional reflectors were mapped and converted into 2-D grids. The time grids were depth-converted using a linear velocity model (v_0 - K method) with parameters representing the velocity—depth trend of the Cenozoic North Sea Supergroup ($v_0 = 1696$ (m/s) and $K = 0.465$ (1/s); TNO-NITG, 2002).

This velocity model was found to be valid also for other horizons within the clastic Cenozoic succession (see also De Lugt et al., 2003).

The seismic reflectors marked LNSG and PES represent respectively the base of the Lower North Sea Group and the Late Eocene Pyrenean erosional surface (Fig. 6.2 and 6.3). In the case of the LNSG horizon there is a 5% mismatch between depth values obtained from wells and from the depth-converted grid. Regarding the PES the discrepancy is higher and is very high in some wells. The reason for this is that in these wells the log-based lithostratigraphic subdivision of the Oligocene–Miocene interval is often uncertain and other stratigraphic markers, which could help the precise subdivision, are not available (Doornenbal pers. comm., 2003). To resolve this uncertainty, biostratigraphic dating of cuttings from three wells was carried out, which confirmed that the PES reflector represents the base of the Oligocene (Munsterman (2002) NITG 02–187–B internal report).

For a precise geometrical reconstruction of the eroded material (discussed below) the Eocene succession has to be subdivided into as many as possible, but not too thin sedimentary packages. In contrast with the work of De Lugt et al. (2003), it was found that some of the lithostratigraphic boundaries are not represented on the seismic sections by a continuous, well-detectable reflector. In addition, subdivision of the seismic sequence based on lithostratigraphy alone would result in an alternating series of sedimentary units that are too thick and too thin, which are not ideal for the thickness reconstruction. For this reason, two easily mappable reflectors were selected (reflectors in the middle–upper part of the Ieper Member (MIEP) and in the lower–middle part of the Asse Member (MASSE)), which divide the Eocene sequence into three units of approximately equal thickness.

The fifth mapped reflector (reflector BBS: Base Brussel Sand Member), was not used in the estimation of the amount of erosion. The purpose of the mapping of this reflector was to check the quality of the depth conversion by comparing the depth-converted grid with well data. The comparison confirmed that the parameters used for the depth conversion provide adequately matching depth maps.

6.1.3 Well data

Besides the seismic surveys, a large number of public borehole data are also available. For the investigated stratigraphic interval (Late Paleocene–Eocene), lithostratigraphic subdivision of the penetrated strata and various wireline logs are available in many of the boreholes. The wireline suites generally consist of gamma-ray and sonic logs, and in some cases density logs are also available.

The available sonic and density logs were used to estimate the amount of sediments eroded during the Late Eocene inversion phase. The principles behind the method and the procedure of erosion estimation are the same as those discussed in *Chapter 5*.

6.2 Results

6.2.1 Spatio-temporal reconstruction of the Eocene tectonic movements

Correlation of the seismic and well data reveals that the Early Palaeogene clastic sediments unconformably overlie the Middle Paleocene erosional surface (LNSG; Fig. 6.3). This horizon truncates the underlying sequence, as a result of the Late Cretaceous and Middle Paleocene inversion phases. It is important to note that onlap onto this basal surface is not observed (see also De Lugt et al., 2003). This implies that (1) the erosion following the Late Cretaceous–Middle Paleocene inversion phases levelled out any relief generated by the inversion, resulting in a flat morphology at the onset of the clastic sedimentation and (2) that the Late Paleocene marine transgression was relatively fast.

The Eocene sediments overlying the LNSG reflector are characterised by SW dipping sub-parallel reflectors truncated by a horizon representing the Late Eocene tectonic phase (PES). A closer inspection of these reflectors reveals that the Eocene units thin towards the NE (axis of the ETH). Considering that no onlap is observed onto the LNSG horizon this thinning indicates differential subsidence between the Voorne Trough and the ETH during the Eocene. This differential subsidence suggests differential compaction or/and the dome-like, syn-sedimentary uplift of the ETH relative to the Voorne Trough during the Eocene.

For a more detailed analysis two thickness maps were created from the depth-converted horizons. They represent the sedimentary units between the LNSG and MIEP horizons and the MIEP and MASSE horizons. For the sake of simplicity these sedimentary units are referred to as Lower Eocene Unit and Middle Eocene Unit, respectively. It is worth noting that these maps represent complete sedimentary sequences not affected by later erosion. In other words, the observed thickness variations are the results of tectonic (differential tectonic subsidence) and sedimentary (compaction effects) processes.

As the patterns of the two thickness-maps are similar, only the Lower Eocene Unit is presented (Fig. 6.4b). The map shows a definite thinning of the Lower Eocene Unit towards the NE. As mentioned already, this can be attributed either to the tectonic doming of the inverted WNB relative to the Voorne Trough during the Eocene, or to differential compaction between the north-eastern and the central parts of the Voorne Trough. This latter possibility can be a reasonable explanation of the thinning, since, as shown in figure 6.3, the amount of uplift and erosion resulting from the Late Cretaceous–Middle Paleocene inversion phases increases towards the NE. Consequently, at the onset of the Late Paleocene sedimentation the Mesozoic basement was overcompacted in the WNB, where significant erosion occurred and was normally compacted in the Voorne Trough, which was not affected by erosion. The Late Paleocene–Eocene sedimentary load caused further compaction of the Mesozoic basement resulting in an extra accommodation space, while this did not happen in

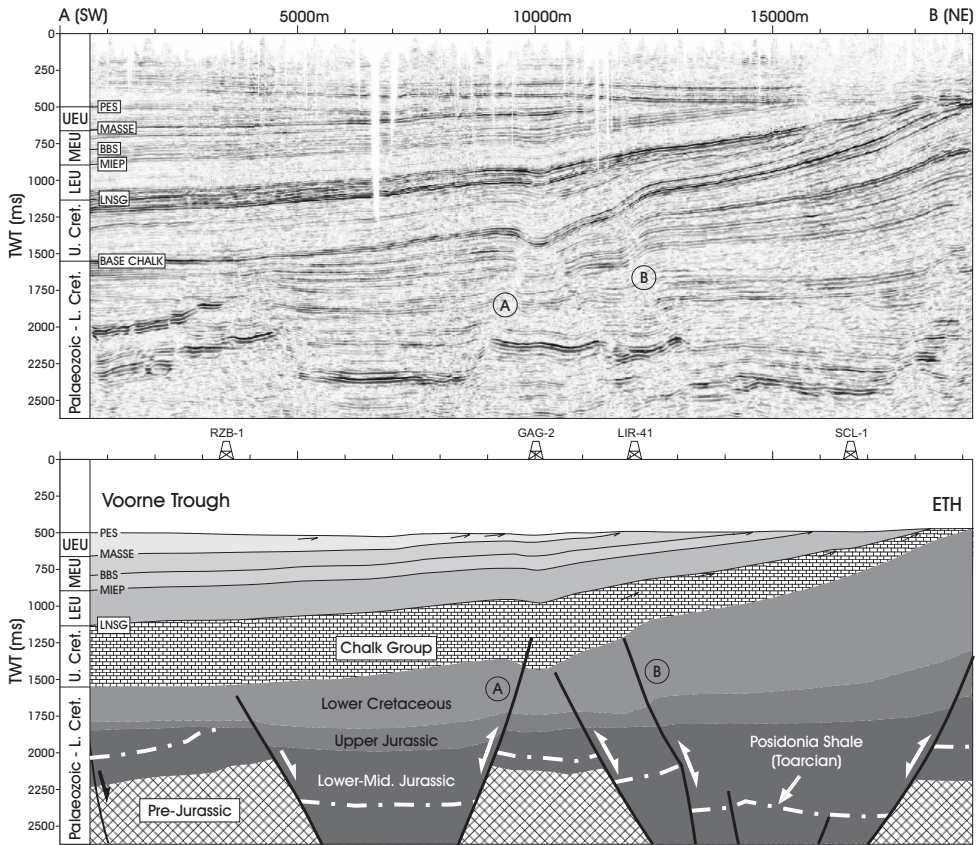


Figure 6.3: Characteristic seismic section through the northern flank of the Voorne Trough (southern part of the former West Netherlands Basin). Location of the section is shown in figure 6.1b. Stratigraphic positions of the mapped reflectors are shown in figure 6.2.

the internal parts of the WNB until the Mesozoic rocks reached their pre-inversion maximum depth of burial. 1-D backstripping analysis of four wells (discussed in details later) suggests that although differential compaction played an important role in the observed thinning, the existence of tectonically driven differential uplift cannot be excluded.

In the following section evidence is presented, which implies that syn-sedimentary tectonic movements took place during the Eocene. The first feature implying this is the abrupt thickness change across old Mesozoic faults (fault B on Fig. 6.3), which indicates fault reactivation during deposition (Fig. 6.4). The fault orientation implies reverse faulting, which is in agreement with the compressional tectonic setting proposed for the Eocene (e.g., Michon et al., 2003; De Lugt et al., 2003). A

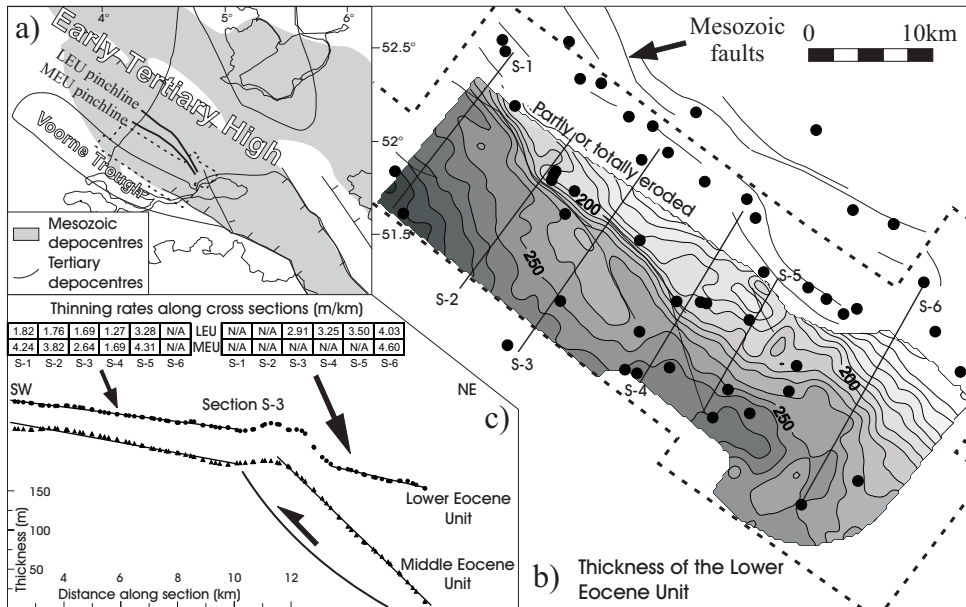


Figure 6.4: Thickness analysis of the mapped LEU and MEU stratigraphic units. a) Location of map shown in panel “b”. b) Thickness map of the Lower Eocene Unit. Boreholes and outline of the 3-D seismic surveys are indicated. c) Detailed analysis of six cross sections (S-1, S-2 . . . S-6). For sake of clarity only section S-3 is displayed. See text for discussion.

more detailed analysis of the thickness maps was carried out on six cross-sections (Fig. 6.4b,c). These cross sections reveal that the rate of thinning is higher on the hanging-wall side of the fault than on the foot-wall side. This suggests a syn-deposition deformation of the hanging-wall block and consequently syn-sedimentary reverse faulting during the Eocene.

Figure 6.4c shows that the thinning towards the NE can be represented by one or two linear trends, which are generally separated by a fault. Using regression analysis for every cross section and for both the Lower Eocene and the Middle Eocene thickness maps, the thinning rates and the location of the pinchline (where the thickness reduces to zero) could be determined (Fig. 6.4b,c). The pinchline geometrically approximates the northern depositional boundary of the given unit. These parameters show that the thinning rate of the Middle Eocene Unit is always higher than that of the Lower Eocene Unit and that the pinchline of the Middle Eocene Unit is closer to the centre of the Voorne Trough than that of the Lower Eocene Unit. These observations suggest that during the Eocene (1) the northern boundary of the sedimentation moved towards the south-west and (2) the Voorne Trough became narrower and its north-eastern flank became steeper. In addition, as the pinchlines are located on the southern flank of the ETH and not in its centre or on

its northern side, it is concluded that the ETH was probably a tectonic high during the Eocene, on which much less sediment was deposited than previously thought.

The lack of onlap onto the LNSG surface suggests that at the onset of the Late Paleocene clastic sedimentation the area was relatively flat with no significant topography. Currently, the LNSG horizon dips significantly towards the SW as a result of the Eocene and later tectonic movements. Assuming that the top of the sedimentary column was always horizontal during the Eocene, the shape of the LNSG horizon at any given time can be restored. Analysis of the dip of the restored LNSG horizon and the rate of dip change between two subsequent stages provides valuable information on the spatial and temporal characteristics of the deformation (i.e., doming) during the Eocene.

For the restoration of the LNSG horizon three stages, represented by the MIEP, MASSE and the PES horizons, were used. The restoration was achieved by subtracting the corresponding depth grid from the grid representing the present-day LNSG horizon (i.e., horizon flattening). Then the state of dip of the restored LNSG horizon was determined by calculating its first order directional derivative ($N45^\circ$). Finally, three dip-rate maps were calculated by dividing at every point in the grid the dip difference between two subsequent stages by the time difference.

As the age for the LNSG reflector the age of the lowermost Heers Member (59 *Ma*) was used, while the PES horizon was suggested to represent the middle of the Late Eocene–Oligocene hiatus (\sim base Priabonian 38 *Ma*, Van Adrichem Boogaert and Kouwe, 1997). As the MIEP and MASSE horizons do not represent particular stratigraphic boundaries, their ages were determined by linear interpolation between known age markers in the boreholes. As age markers the base Ieper Member, the base Brussel Sand Member and the base Asse Member were used. The final ages of the horizons (MIEP = 53 ± 0.27 *Ma*, MASSE = 43 ± 1 *Ma*) were determined by averaging the ages obtained from different wells.

Figure 6.5 shows the rate of tilting of the LNSG horizon for three consecutive time intervals. Due to the uncertainty of the age determination the actual dip-rates may be slightly different. Note that the tilting represented by figure 6.5 is the collective result of tectonics and the compaction of the sediments underlying the given unit. However, since mechanical compaction is time independent and since the thickness of the three mapped Eocene units is approximately equal, it is suggested that the effect of compaction of the underlying sediments in all three cases can be represented by a uniform or similar pattern. Consequently, although the real rate of tectonic tilting is not known, these patterns are suitable to qualitatively compare the tectonic activity between the stages: faster rate of tilting reflects stronger tectonic activity.

During the deposition of the Lower Eocene Unit (Fig. 6.5a), besides fault activity, a strong differential tilting can be observed between the eastern and western part of the map, which is attributed to tectonic activity. During the Middle Eocene (Fig. 6.5b) the tilting became smoother and more uniform compared to the Early Eocene. In addition its average magnitude also decreased slightly. Taking into

account the larger compaction of the Lower Eocene Unit compared to the Middle Eocene unit (sandy clay vs. sand) the difference in tilting rate between these two units is probably even larger. These may imply that tectonic activity during the deposition of the Middle Eocene Unit was reduced. In the third time interval tilting rates 2–3 times higher than in the previous periods can be observed, which can be attributed to the Late Eocene inversion phase (Fig. 6.5c). This inversion period led to the reactivation of several, previously inactive Mesozoic faults, clearly suggesting that the tectonic movements at the Late Eocene were stronger than that during the Early–Middle Eocene period.

The present analysis provides new constraints on the Eocene evolution of the WNB. As summary, it is concluded that the present day tilted and faulted state of the Eocene sediments is the collective result of differential compaction and a cumulative, continuous deformation throughout the Eocene rather than one separate tectonic pulse. The Late Eocene Pyrenean inversion phase was much stronger than the Early–Middle Eocene tectonic movements and is interpreted as a manifested climax of the compressional intra-plate stresses originating from the Alpine region at the end of the Eocene. As the seismic data demonstrate, the Eocene deformation, which is characterised by the continuous doming of the ETH relative to the Voorne Trough, was accompanied by reverse reactivation of

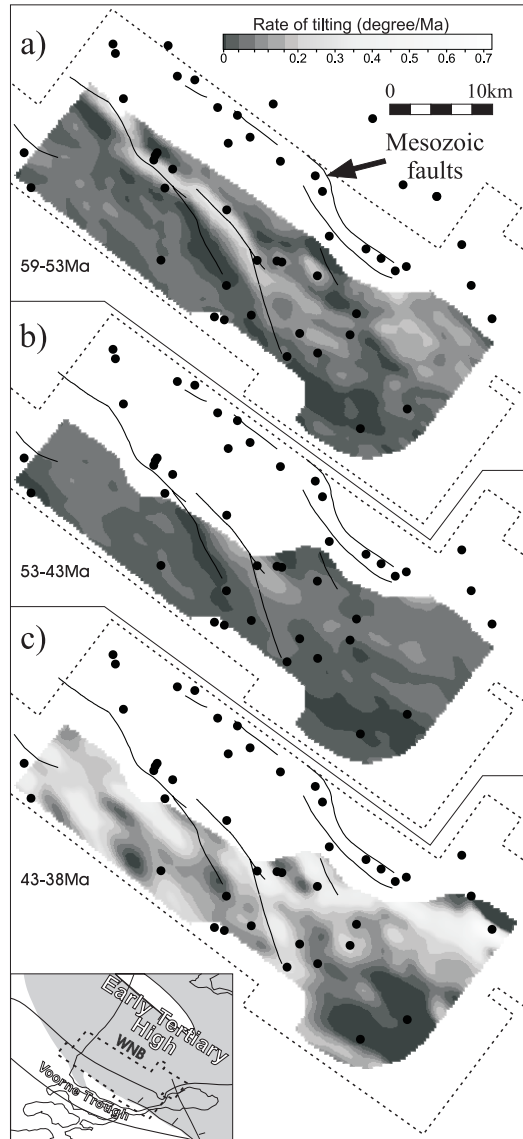


Figure 6.5: Reconstructed rate of tilting of the LNSG reflector for three time intervals. a) Lower Eocene Unit; b) Middle Eocene Unit; c) Upper Eocene Unit (Pyrenean inversion phase). Boreholes and outline of the seismic cover are indicated.

major Mesozoic faults. The doming at the end of the Eocene was complemented with the reactivation of additional faults and is characterised by a ~ 50 km wavelength (i.e., width of the ETH).

6.2.2 Quantitative reconstruction of the amount of erosion

Burial anomaly analysis

For the burial anomaly analysis, which was performed in 37 wells using sonic and density logs, it is essential to choose a stratigraphic interval in which lithology does not change significantly vertically and over large distances (see *Chapter 5* for discussion). By doing so apparent anomalies can be avoided. For this reason, the upper part of the Landen Clay Member was selected for the analysis (Fig. 6.6). The Landen Clay is a silty or sandy clay layer, which shows an upward increasing gamma-ray (GR) and an upward decreasing sonic velocity response. In the upper part of the layer selected for the analysis the GR and sonic log response do not change significantly (or are stationary) and reach respectively their local maximum and minimum (Fig. 6.6). The characteristic log response of the Landen Clay Member was very useful in identifying and correlating this interval in wells located far from each other or where detailed lithostratigraphic interpretation was not available.

Interval velocities 9 of the 37 wells where a sonic log was available are located north of the ETH. The rest of the wells are located south of this high, partly in the Voorne Trough (Fig. 6.6c). The average sonic velocity of the selected interval was calculated using the principles discussed in detail in *Chapter 5*.

The resulting velocity—depth pairs are shown on figure 6.6b. BAC-1, IJM-1, MID-101, PRW-1 and ALE-1 wells are excluded from the analysis, as in these wells the Landen Formation is either very thin or the calculated interval velocities resulted in abnormally low values. The figure shows that in wells located north of the ETH the interval velocities are lower than those situated in the Voorne Trough. Such a characteristic suggests that lithological and/or textural differences exist within the Landen Clay Member between the two areas (i.e., less sand north of the ETH). These lithological differences can be related to the near shore position of Voorne Trough and the more distal position of the area north of the ETH (e.g., Letsch and Sissingh, 1983). An alternative explanation of the lithological differences can be given by assuming that sedimentation took place in two detached sub-basins separated by a sediment barrier, namely the ETH.

To determine the normal depth trend, a linear regression line was fitted to specific datapoints corresponding to wells where no erosion is expected (i.e., deeper parts of the Voorne Trough), and where the quality of the log response is the best. The majority of the wells, including wells on the strongly truncated northern flank of the Voorne Trough, show interval velocities in agreement with the depth trend. This suggests that in these wells the Late Eocene erosion is masked by the post-inversion sedimentation. In consequence, this observation indicates that the erosion did not

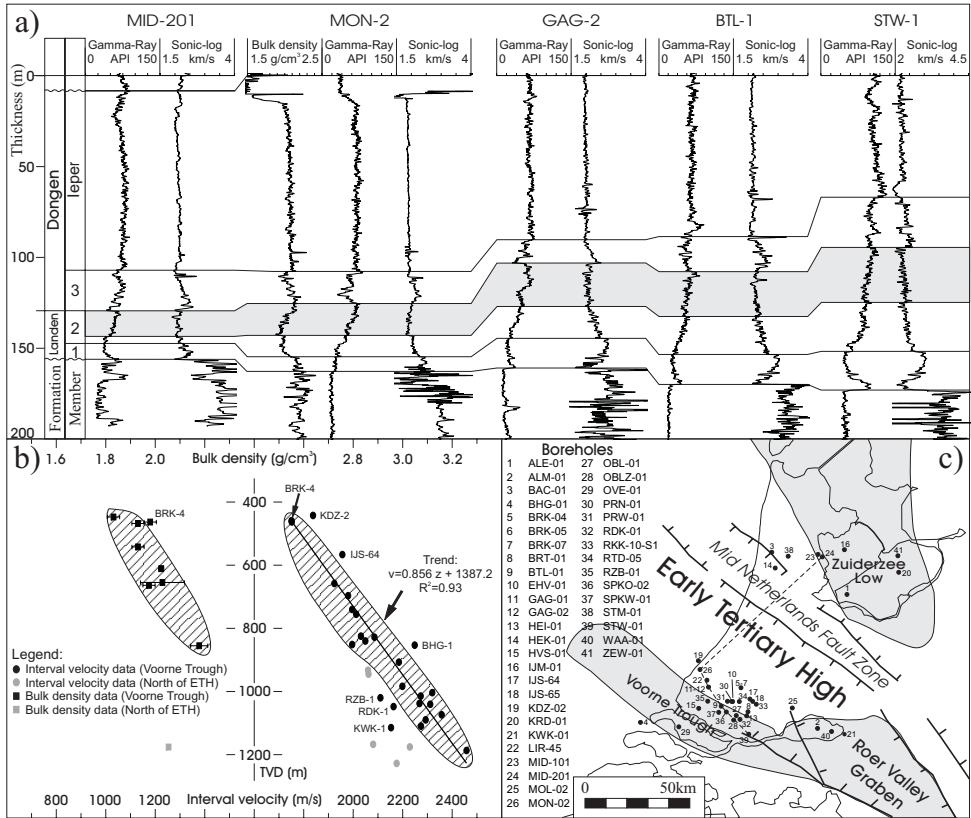


Figure 6.6: Burial anomaly analysis. a) Characteristic sonic-, gamma- and density log responses of the Landen and the lower part of the Dongen Formation in five representative wells located in the Voorne Trough and Zuiderzee Low (for location see panel “c”). The investigated stratigraphic interval is shown in grey. 1: Heers Member; 2: Landen Clay Member; 3: Basal Dongen Sand Member. b) Interval velocity and bulk density of the “grey layer” in different wells. Vertical axis represents true vertical depth. c) List and location of the boreholes used in the analysis. The dashed line indicates the cross section shown in panel “a”. See text for discussion.

exceed the thickness of the post-inversion sediments (~450–550 m).

Wells KDZ-2, IJS-64 and BHG-1 show positive burial anomalies relative to the trend, but none of them is concluded to be a true burial anomaly related to uplift. Well BHG-1 is located on the southernmost flank of the Voorne Trough, close to the fringe of the basin. Therefore, the investigated interval in this well has probably a sandier lithology, which could explain the 100 m/s higher sonic velocity. In case of the KDZ-2 and IJS-64 wells, the observed 120 m burial anomaly — considering

respectively the 500 *m* and 589 *m* of post-Pyrenean sedimentation — would yield 620 *m* and 709 *m* of erosion. This is unlikely since interval velocities of wells in similar tectonic positions are in agreement with the depth trend. In case of KDZ-2 it is more probable that the observed higher sonic velocity is also the result of lithological differences, since in this well due to the Late Eocene truncation only the sandier lower part of the Landen Clay is preserved and could be measured.

In wells RZB-1, RDK-1 and KWK-1 significant negative anomalies were found. Taking into account their location in the Voorne Trough and values from surrounding wells, no clear explanation is yet found for these anomalies.

Bulk densities Density logs were available for 10 wells. All the wells except KRD-1 are located south of the ETH. As the logs were available only on paper prints the average bulk density within the interval was obtained by manual averaging.

The bulk density—depth pairs are in agreement with the interval velocity analysis (Fig. 6.6b). They follow a quasi-linear trend and only three minor fluctuations (2 positive: BRK-4 and BRK-7; 1 negative: MOL-2) are observed. Lithological or borehole conditions could not explain these fluctuations. Considering the position of the wells, however, it is unlikely that they are caused by erosion. Well KRD-1, which is located north of the ETH is represented by a lower bulk density value than that expected from the trend south of the ETH. This difference between the two flanks of the ETH was also observed among the interval velocities.

The analysis of sonic and density logs demonstrated that both the interval velocity and the bulk density of the investigated lithological unit (upper part of the Landen Clay Member) show linear trends with depth. In the area covered by the selected wells (i.e., on the northern and southern rims of the ETH) the upper Palaeocene Landen Formation presently is at maximum depth of burial. Consequently, it can be deduced that on the rims of the ETH the thickness of the eroded Palaeogene sediments is smaller than the thickness of the post-inversion sediments, that is 450–550 *m*.

Geometrical approach

As the burial anomaly analysis only provides a maximum value of erosion (i.e., 450–550 *m*) a complementary approach (i.e., geometrical approach) was adopted to better constrain the amount of erosion during the Late Eocene. The basic assumption of the method is that the amount of deposited and later eroded Eocene material is equal to the difference between the present-day base Oligocene horizon (PES) and a fictional one, which could be observed if erosion had not occurred (Fig. 6.7). This fictional (or restored) base Oligocene horizon is calculated by adding the restored thickness of the Eocene sediments to the LNSG horizon. To estimate the thickness of the deposited Lower and Middle Eocene Units their observed thickness is linearly extrapolated using the thinning rates and pinchlines obtained during the analysis of the thickness maps. In locations, where they are preserved, the observed values are used. To estimate the uppermost Eocene, erosion-affected unit (~Asse Member), a

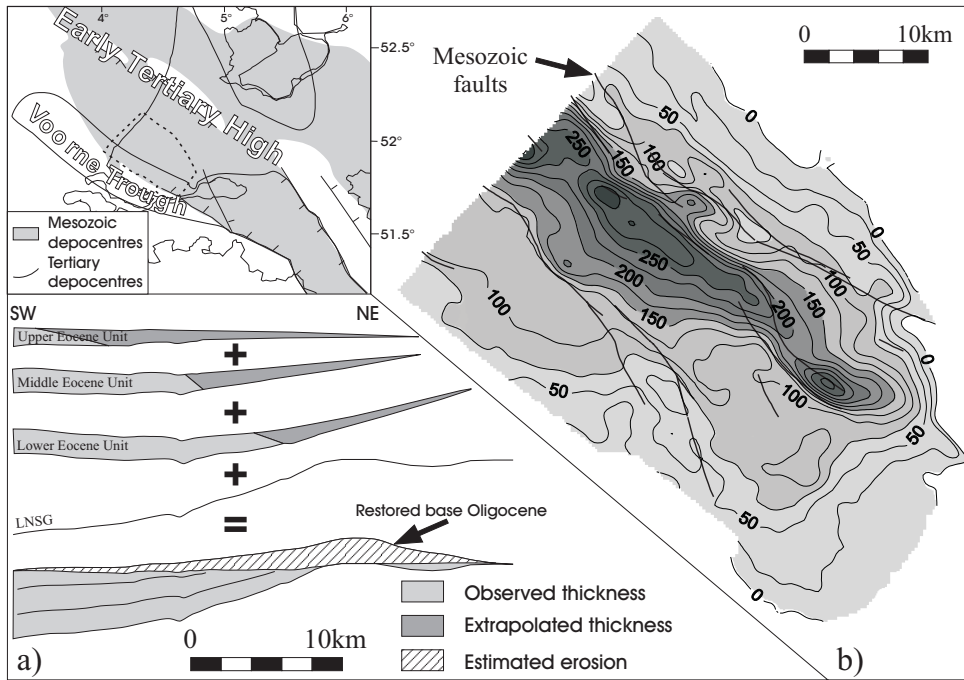


Figure 6.7: Geometric reconstruction of the amount of Upper Paleocene–Eocene sediments removed by the Late Eocene Pyrenean inversion phase. a) Principles of the reconstruction. b) Map of estimated erosion. Outline of the map is indicated in the inset. Note that the estimated erosion is relative: the reference point is located in the centre of the Vooorne Trough. See text for further discussion.

wedge-shaped body is used. Its maximum thickness corresponds to the maximum thickness of this unit observed in wells located in the centre of the Vooorne Trough, while its pinchline coincides with the pinchline determined for the Middle Eocene Unit. Note that because of this approach the estimated erosion is relative and is zero in the central part of the Vooorne Trough. To determine the absolute erosion, one should estimate the thickness of the nowhere preserved uppermost Eocene sediments. Also note that the erosion determined in this way estimates only the amount of deposited and later removed Eocene sediments: the amount of Mesozoic sediment removed from locations where none of the Palaeogene sediments are preserved (e.g., central part of the ETH) is not and cannot be taken into account with this method.

The map of removed Eocene sediments shows increasing erosion towards the NE (Fig. 6.7b), and reaches its maximum (~ 250 m) in a NW–SE trending zone above pop-up structures related to reactivated Mesozoic faults. From the axis of this zone the Late Paleocene–Eocene sediments were completely removed, and therefore the true erosion is underestimated. Since the thickness of the deposited Eocene

sediments was extrapolated, the amount of determined erosion becomes less and less reliable towards the NE.

The above results are not in disagreement with the results of the burial anomaly analysis. Compiling the results of the two approaches it is estimated that the Late Eocene Pyrenean inversion phase removed $\sim 250\text{--}450$ m of Eocene sediments from a NW–SE trending zone located in the southern part of the WNB. Towards the NE, in the central part of the basin, the amount of deposited sediments that were later removed by the Late Eocene inversion cannot be reliably estimated due to the lack of preserved Eocene layers. Although interval velocity analysis of older rocks presented in *Chapter 5* provides constraints on the amount of erosion, that amount is the cumulative result of three separate erosional phases. Using the methodology of *Chapter 5* the effect of the Late Cretaceous, the Middle Paleocene and the Late Eocene inversion phases cannot be separated.

6.3 Discussion

6.3.1 Differential subsidence vs. compaction

The NE thinning of the Eocene sediments in the Vorne Trough, could be explained by differential compaction of the Mesozoic basement resulting from the Late Cretaceous–Mid Paleocene erosion or by tectonic doming. The backstripping method (e.g., Sclater and Christie, 1980) separates isostatic and compaction effects of sediments from those of tectonic subsidence. The aim of the analysis presented in this section is to qualitatively compare the tectonic subsidence between the Vorne Trough and the ETH during the Eocene. Stratigraphic time—depth information and the amount of erosion of four analysed wells are shown in figure 6.8. The amount of erosion was constrained by the results of this and the previous chapter. The porosity—depth relations were calculated by software (Genex) using world-average porosity—depth relations for lithologically pure formations and the lithological composition of the various sedimentary units (“mixing rule”). Early Paleocene erosion and subsequent overcompaction of the Mesozoic sediments were taken into account during the calculation. Sea level changes and water depth were neglected, since they have the same effect on all four wells.

Comparison of the tectonic subsidence curves for the Vorne Trough and the ETH reveals that using the simple assumption of mechanical compaction and Airy isostasy the Eocene sedimentation can be explained without the presence of differential tectonics. In fact, tectonic subsidence was calculated to be slightly higher in the ETH than in the Vorne Trough. This would be in total disagreement with the observations presented in this paper. Note, however, that several important factors are not taken into account during the calculation. For example, a 1-D Airy isostatic model was used instead of the more satisfactory 2-D flexural isostatic approach. In reality, the load of the thick Eocene sediments in the Vorne Trough also contributed to the subsidence of the ETH, which, if taken into account, would result in smaller

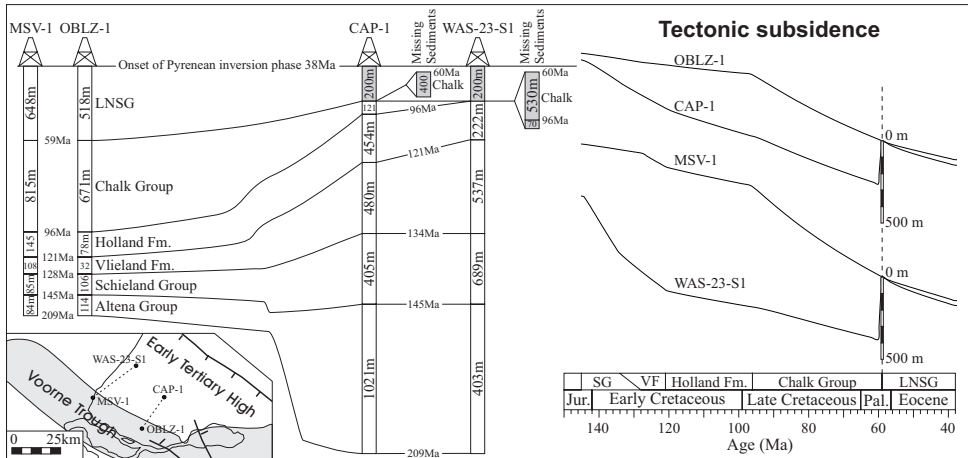


Figure 6.8: Jurassic–Eocene tectonic subsidence of four synthetic wells located in the WNB. The thickness of the grey-shaded sedimentary units (those removed by erosion) is an estimate, the others are taken from real wells. The thickness bars are not scaled. The origins of the curves were set to the base of the LNSG unit. Overcompaction of the Mesozoic sediments in the CAP-1 and WAS-23-S1 wells due to the Mid Paleocene uplift/erosion has been taken into account. LNSG: Lower North Sea Group; SG: Schieland Group; VF: Vlieland Formation. See text for discussion.

calculated tectonic subsidence in the ETH. In addition, it is reasonable to assume that some amount of erosion and consequently overcompaction of the Mesozoic sediments took place in the Voorne Trough prior to the Eocene sedimentation. In this case somewhat higher tectonic subsidence would be required in the Voorne Trough to explain the total subsidence. The most important factor affecting the calculated tectonic subsidence is the compaction of the Chalk Group, as it is the thickest pre-Eocene sedimentary unit in the Voorne Trough. Diagenetic studies of chalks have pointed out that, although mechanical compaction down to porosity of 40% can occur (Jones et al., 1984), limy chalk sediments tend to compact mechanically only up to ~250 m of depth and only slightly or not at all below that (e.g., Pettijohn, 1984; Grützner and Mienert, 1999; Mallon and Swarbrick, 2002). One of the reasons for this is the occurrence of contact cementation between grains, which gives a firm skeleton to the sediment and consequently arrests further mechanical compaction (Fabricius, 2003). Pore filling cementation is also common during the diagenesis of chalks resulting in rapid porosity loss. In other words, the observed porosity loss in chalks (e.g., Mallon and Swarbrick, 2002) can be rather the result of chemical processes than of grain reorganisation and bulk volume loss.

The aforementioned factors could result in a larger calculated tectonic subsidence in the Voorne Trough than in the ETH during the Eocene, which would be in accordance with the syn-sedimentary features presented in this chapter. However, quantitative demonstration cannot be provided here, since the utilised software cannot handle such complex models. As summary, it is concluded that although compaction of the pre-Eocene sediments must have significantly contributed to the thinning and tilted state of the Eocene sediments, differential tectonic movements between the Voorne Trough and the ETH also operated during the Eocene.

6.3.2 Characteristics and timing of inversion

Southern North Sea region

This study allows quantification of the uplift of the WNB consequent on the Late Eocene inversion phase. At a regional scale, a similar deformation was recognised for the Broad Fourteens Basin (BFB) (Nalpas et al., 1995; De Lugt et al., 2003), the Roer Valley Graben (RVG) (e.g., Michon et al., 2003) and the Sole Pit Basin (SPB) (e.g., Van Hoorn, 1987) (Fig. 6.1). The average amount of uplift is of the same order of magnitude in these four provinces (i.e., 200–400 *m* in the SPB (Cameron et al., 1992), 200–500 *m* in the BFB, 250–450 *m* in the WNB and around 300 *m* in the RVG). The style of inversion and consequently the amount of uplift/erosion primarily depend on (1) the tectonic stress field; (2) the geometry of the basin and its main faults; (3) the mechanical parameters of the lithosphere and the basin fill; (4) the duration and amount of lithospheric stretching prior to inversion, and (5) the elapsed time between basin formation and inversion (e.g., Gillcrist et al., 1987; Chadwick, 1993). From this it follows that the compressive intra-plate stresses inducing the inversion must not have been very different in the above mentioned basins during the Late Eocene, since their Mesozoic basin geometry, basin fill and structural evolution are very similar.

Seismic data analysis shows that the Eocene uplift affected both the WNB and its adjacent areas, forming a 50 *km* wide NW–SE trending dome (i.e., the ETH). This geometry differs from the deformation pattern that resulted from the Late Cretaceous and Middle Paleocene inversions. Indeed, during these earlier inversion periods, deformation was restricted to the Mesozoic graben and was controlled by the reactivation of major faults in reverse mode (see *Chapter 5*), whereas during the Eocene the affected area was much wider and fault reactivation was mild. A similar characteristic was determined for the neighbouring BFB and the RVG (De Lugt et al., 2003; Michon et al., 2003).

The second main difference between the Late Cretaceous–Middle Paleocene and Late Eocene inversion phases is the amount of uplift and eroded sediments. As mentioned, during the Late Eocene inversion a few hundred meters of sediments were removed. During the Late Cretaceous–Mid Paleocene inversion periods the amount of erosion was much greater. For the central part of the BFB ~2000–3000

m of erosion was determined (Nalpas et al., 1995), while in the RVG, the amount of uplift is less constrained but it definitely exceeds 600 *m* (Fig. 7a of Michon et al., 2003). As demonstrated in the previous chapter, in the WNB 600–1500 *m* of Late Cretaceous–Middle Paleocene erosion occurred.

This study reveals that the Late Eocene inversion of the WNB was not a sudden pulse at the end of the Eocene, but rather a continuous process throughout the Early Palaeogene, which culminated in the latest Eocene. Continuous, syn-sedimentary inversion in the Alpine foreland during the Cretaceous–Tertiary period is not a unique feature restricted only to the WNB. A similar, long-lasting, syn-sedimentary inversion phase has been reported from the RVG (Gras and Geluk, 1999), from the SPB (Van Hoorn, 1987) and from the Norwegian continental shelf (Våagnes et al., 1998).

Inspection of seismic lines in the neighbouring BFB reveals similar thinning of the Eocene sediments towards the centre of the former basin (see internal reflectors of Unit 2 in Fig. 10 of De Lugt et al., 2003). In addition, a drastic decrease in subsidence rates before the onset of the Late Eocene Pyrenean inversion was determined. This evolution is comparable to the Palaeogene evolution of the WNB, and therefore it is suggested that an inversion characterised by continuous Eocene tectonic movements/uplift followed by a stronger compressional climax probably occurred in other inverted basins in the southern North Sea region.

English Channel area

Two other inversion examples are discussed briefly below. These areas are located in a different tectonic domain compared to the WNB, and experienced a different timing of inversion (Fig. 6.9). Still, highlighting and comparing some important aspects of their inversion could contribute to a better understanding of the inversion process in the Alpine foreland.

The first example is the Tertiary deformation of the Mesozoic Weald and Channel basins, SE onshore and offshore England (e.g., Chadwick, 1985; Lake and Karner, 1987; Underhill and Paterson, 1998; Blundell, 2002). The Palaeogene tectonic and sedimentary scenario of this basin system is very similar to that of the WNB. In both areas subsiding Palaeogene basins developed on formerly stable tectonic highs and are separated from each other by newly developed tectonic highs inverted from Mesozoic depocentres. The concept of a single, post Oligocene deformation phase responsible for the inversion (e.g., Wooldridge and Linton, 1955), has now been replaced by one involving a longer, more complex history of uplift and deformation continuing from the latest Cretaceous onwards (e.g., Jones, 1980; Small, 1980; Chadwick, 1985; Lake and Karner, 1987). Indeed, numerous stratigraphical studies indicate that uplift-related erosion, faulting and warping occurred in SE England from late Early Eocene times onward; that is preceding the main deformation phase (e.g., Daley and Edwards, 1971; Plint, 1982; Isaac and Plint, 1983; Curry, 1992; Gale et al., 1999). Although the timing is different, this feature of basin inversion is very similar to the inversion of the WNB.

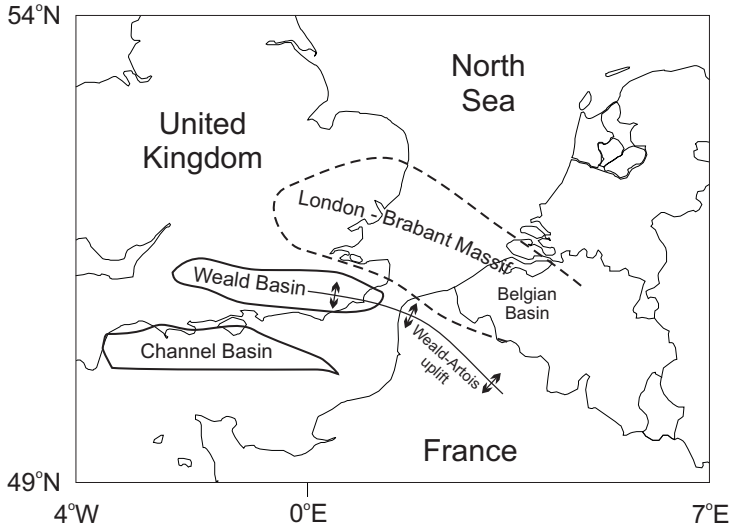


Figure 6.9: Location and main tectonic features of the Wessex- and Belgian basins.

In the area of the Belgian Basin, which developed during the Palaeogene on the tectonically stable Brabant Massif, the sediments were truncated and eroded in response to eustatic and tectonic causes (e.g., Vandenberghe et al., 1998). The timing of truncation was coeval with the main inversion phase of the Channel area (i.e., Late Oligocene–Miocene) and is related to the uplift of the Weald–Artois axes and the NE tilting of the Brabant Massif. On the other hand, detailed stratigraphic and seismic studies have revealed that tectonic-related unconformities occur throughout the whole Palaeogene succession, suggestive of continuous tectonic activity and uplift of the Brabant Massif from Middle Eocene onward — that is preceding the main deformation phase (e.g., Cameron et al., 1992; De Batist and Henriët, 1995; Vandenberghe et al., 1998; De Batist and Versteeg, 1999). Continuous tilting is also indicated by the southward thinning of seismic horizons in the Eocene (e.g., PA₃ layer in Fig. 9 of De Batist and Versteeg, 1999). Continuous Palaeogene deformation is comparable with the tectonic history of SE England and of the WNB revealed by this study.

The above examples demonstrate that in the NW European foreland of the Alps the inversion process often continues between two subsequent phases. The identified inversion phases therefore are considered to be subsequent, multiple culminations of a continuous inversion process. In light of the Euro–African collision being the primary cause of the compressive stresses in the Alpine foreland it is more natural and reasonable to imagine a continuous inversion process than one with distinct pulses. However, the exact causes of inversion culmination and the timing of inversion still require explanation.

6.3.3 Origin of the inversion

It has been proposed for a long time that the Late Cretaceous–Tertiary inversion phases in the southern North Sea region resulted from compressional stresses originating from the Alpine collision (e.g., Ziegler, 1990; Blundell, 2002). The other source of compressive stress that may have contributed to the inversion, is the ridge push force originating from the North Atlantic mid-oceanic ridge. These two stresses presently are constructively interacting in NW Europe (e.g., Gölke and Coblenz, 1996).

The Late Cretaceous–Mid Paleocene inversions are likely to be related to Alpine events, since they pre-date the Early Eocene break-up of the North Atlantic (e.g., Talwani and Eldholm, 1977). Ziegler et al. (1998) envisaged that they are caused by increasing compressional stresses related to the collision of the Alpine orogenic wedge with a subduction pediment (i.e., Briançonnais terrain/microcontinent) after the closure of the Piemont–South Penninic ocean. In contrast to the Late Cretaceous events, the Eocene deformation observed in the WNB and other areas in the southern North Sea region is coeval with the North Atlantic sea floor spreading. However, considering that the magnitude of *ridge-push* is proportional to the age of the produced oceanic lithosphere, it is unlikely that during the Eocene the contribution of the North Atlantic *ridge-push* to the compressional stresses originating from the Alpine region was significant. This assumption is supported by the detailed analysis of Eocene–present day contractional structures at the Norwegian continental shelf, which suggest that the contribution of the *ridge-push* became significant only during the Neogene (Våagnes et al., 1998). In light of these observations it is reasonable to think an Alpine origin for the Palaeogene deformation in the southern North Sea region.

In the Alps geochronological data from high pressure metamorphic rocks show that the Eocene period corresponded to a phase of intense deformation, with the formation of a deep crustal root (e.g., Monié and Philippot, 1989; Tilton et al., 1991). Consequently it is paradoxical that continuous deformation in the Alps during the Eocene resulted in a sudden inversion phase only in the latest Eocene. However, the results of this chapter clearly suggest that the continuous compression in the Alpine chain led to a continuous inversion in the southern North Sea during the Eocene. In addition, there is a good correlation between the timing of the Eocene inversion in NW Europe and tectonic movements observed in the North Alpine foreland basin (Blundell, 2002). Although the origin of the inversion climax is poorly constrained, it is considered that it could have resulted from an increase of the horizontal principal stress in the Alpine foreland related to the closure of the Valais rifted area in the Alps at this period (Ziegler et al., 1996). This period coincides also with a fast (15 mm/year) migration of a low-angle external orogenic wedge front in the Alpine region (Ford et al., 1999).

Comparison of the Late Mesozoic–Tertiary tectonic evolution of the various inverted areas in Central and Western Europe reveals that the occurrence of various inversion phases are not uniform. For example, Tertiary deformations are present in the Southern North Sea, the Channel region and further to the west, but they are completely missing from Central and Eastern Europe (see Fig. 3–6 of Ziegler, 1987). In addition, there seems to be an apparent westward shift of the strongest inversion phase through time, the latest, Oligo–Miocene inversion phase being strongest in the Channel area. These spatial fluctuations in inversion characteristics suggest that the interaction between the orogen, the foreland and other factors such as stresses originating from the opening of the North Atlantic is very complex (e.g., Ziegler et al., 1998) and that the inversion in the Alpine foreland cannot be explained by a single and simple model. It has been proposed that factors such as local and regional lithospheric structure, basin fill, basin geometry and geological history (amount, style and timing of basin formation etc.) of the inverted basins should also be taken into account (e.g., Gillcrist et al., 1987; Huyghe and Mugnier, 1995).

The magnitude and other characteristics of inversions can change not only spatially but also temporally as demonstrated by the Late Cretaceous–Middle Paleocene and Late Eocene inversion phases in the WNB and BFB. One possible explanation could be that the mechanical stabilisation of the previously weakened crust during and after the first inversion phase created a stronger lithosphere for the subsequent inversion periods (“locked system”, Ziegler, 1987). De Lugt et al. (2003) proposed that a different direction of compression during the Latest Cretaceous and the Eocene could be the explanation, but this is not supported by data regarding the relative motion between Africa and Europe (e.g., Lake and Karner, 1987). Therefore the alternative model is that the lithospheric strength profiles and/or the coupling between the orogen and the European foreland changed during and between these periods of inversion, leading to different stress magnitudes and different response of the lithosphere under compression (Cloetingh et al., 1999). The exact mechanism and cause of such fluctuations in the mechanical coupling between orogen and continent as well as the development, presence or absence of major intra-plate discontinuities during the Cretaceous–Tertiary period is not yet understood and should form the scope of future studies.

6.4 Conclusions

The Eocene inversion of the West Netherlands Basin was the result of a continuous inversion process throughout the Late Paleocene–Eocene rather than a distinct pulse at the end of the Eocene. The inversion was characterised by the continuous doming of the Early Tertiary High and was accompanied by the reactivation of pre-existing faults in a reverse mode. Beside tectonics, differential compaction significantly contributed to the present-day thinning and tilted state of the Eocene sediments. The intensity of the tectonic movements was not uniform throughout the Eocene: they

were much stronger during the Latest Eocene (Pyrenean inversion phase) than during the Early and Middle Eocene. A good correlation was found between Alpine tectonic events and the Eocene inversion of the West Netherlands Basin. In light of this and the inversion characteristics revealed by this study, the Latest Eocene inversion pulse in the West Netherlands Basin can be considered as the culmination of a continuous inversion process originated from the Alpine collision. This feature of continuous tectonic movements culminating in a stronger inversion phase seems to be a general characteristic of the Palaeogene inversion in NW Europe, since the same feature was also found in other southern North Sea basins (e.g., Broad Fourteens Basin) and, though with different timing, in the English Channel area as well as in Central Belgium.

Based on a geometrical approach and on the interval velocity and bulk density analysis of Lower Palaeogene sediments, it is estimated that $\sim 250\text{--}450\text{ m}$ of Palaeogene sediments were removed from the rim of the ETH during the inversion. This amount of erosion is of the same order of magnitude as in other basins in the southern North Sea region.

Chapter 7

Synthesis and additional remarks

This thesis targeted two main objectives: (1) modelling of 3-D fault reactivation potential using 3-D geometrical fault models constructed from exploration data and (2) reconstruction of the Late Cretaceous–Tertiary erosion/inversion history of the southern Netherlands.

7.1 Fault modelling

During interpretation of seismic data, horizon-based mapping techniques often dominate the strategy of the interpreter. However, in certain fields of modern geoscience, a detailed insight into fault geometry and the understanding of fault behaviour is very important. In the petroleum industry, a detailed knowledge of the geometry of faults and their structural relationship gives insight not only into the structure and volumetric constraints of the reservoir, but also into the sealing potential of a structural trap. In addition, dilatation pumping mechanisms (e.g., Sibson, 1994) related to cyclic reactivation of faults in sedimentary basins has been found to be an effective way to transport large volumes of fluids along major faults, which has an important impact on hydrocarbon migration pathways. In modern seismology using 3-D geometrical models of fault systems the detailed mechanism of stress release and faulting related to major earthquakes can be simulated (e.g., Aochi et al., 2003), which bears not only scientific but also societal importance.

Within the framework of this Ph.D. research two fault modelling methods were developed (see *Appendix A*), which aim to deliver high quality 3-D fault surfaces suitable for further studies. The **midline method**, which as input utilises the products of conventional mapping, required a development of software to make the link between the raw data and the fault modelling software. Using the **direct method** the fault models are constrained better, since they are based directly on raw exploration data. During fault modelling it was experienced that, even using the direct method, a better link should be made between the raw data and the final 3-D fault models. Interpretation and modelling of faults using the procedures discussed in *Appendix A* are performed with two or more different software packages, which hampers

the easy quality control of the models. Fortunately, software developers have also recognised the need for an integrated approach. Nowadays several software packages are available, where seismic interpretation and fault modelling can be performed within the same module (e.g., PETREL; www.sis.slb.com).

3-D geometrical fault models give an excellent opportunity to study the 3-D pattern of forces acting along faults in a certain tectonic stress field. Although the contact stresses calculated using the method presented in *Chapter 2* can represent only a first order approximation of the real stresses, the patterns of slip tendency and shear direction provide useful, three-dimensional constraints on the likelihood and style of fault reactivation. In addition, since the seal capacity of a fault zone greatly depends on the actual stresses on the faults, this method indirectly can constrain the sealing potential of faults on geological timescales.

In *Chapter 3* it was demonstrated that the 3-D fault modelling technique presented in *Chapter 2* could accurately reproduce the observed fault activity in the Roer Valley Rift System. The results suggest that, at least in continental intra-plate conditions, faults mapped in the uppermost part of the crust are suitable for constraining fault behaviour even in the deeper parts of the seismogenic layer. On the other hand, the modelling results also show that knowledge of the hierarchy and the regional tectonic context of the faults are required to explain the slip tendency and shear direction patterns.

Analysis of the slip tendency and shear direction patterns in the Roer Valley Rift System demonstrate that the faults are most likely to reactivate in a normal faulting stress regime. Even in such a stress regime, however, high probabilities of fault reactivation (i.e., $ST > 0.6$) were obtained only at σ_h/σ_H ratios lower than ~ 0.4 . This ratio is lower than that determined by European-scale modelling studies ($\sigma_h/\sigma_H \sim 0.6$). In order to explain the observed fault activity within a reasonable range of tectonic stress magnitudes a slip threshold (frictional coefficient) of 0.3–0.4 and stress tensors with a 0.5–0.6 σ_h/σ_H ratio would be required. Slight discrepancies between the σ_h/σ_H ratios suggested by this study and those inferred from continent-scale modelling could be attributed to local effects.

Modelling the present-day reactivation of Mesozoic faults in the WNB and the RVRS under simple, laterally homogeneous stress fields predicts similar fault behaviour throughout the basin system (*Chapter 4*). This is in disagreement with the observations, the explanation for which could be the possible differences in the state of stress and/or in the slip thresholds between the two areas. That is, there is either more extension in the RVRS in terms of lower σ_h/σ_v ratio, or/and the faults are easier to reactivate in the RVRS than in the WNB. These possible differences are assumed to be responsible for the lack of Quaternary fault activity and the present-day seismic quiescence in the WNB.

Chapter 4 emphasised the importance of structural inheritance on the Mesozoic–Cenozoic deformation of the WNB–RVG basin system. Although the patterns of deformation are slightly different in the two basins, they were found to be consistent with general structural patterns and with the regional tectonic movements. The study further emphasised that differentiation in the tectonic evolution started in the Tertiary. Therefore, it is suggested that the different tectonic stress fields and/or slip thresholds between the two areas are directly related to the origin of the Cenozoic rifting in the RVRS. Several hypothesis were presented in *Chapter 4*, however, none was conclusive. Additional research is needed to better understand the origin of the RVRS and to put the southern Netherlands into a broader tectonic context. This research might also help in the future to find the reason why the neotectonics of the RVRS and the neighbouring WNB are so different from each other.

7.2 Quantification of inversion tectonics

The Late Cretaceous–Tertiary period of basin inversion is an interesting and important episode in the evolution of NW European basins, including the basin system in the southern Netherlands (e.g., Ziegler, 1987). This is economically important, since the hydrocarbon accumulations found in the WNB are largely trapped in inversion-related structures. Quantification of the inversion tectonics provides not only insight into the tectono-sedimentological aspects of basin inversion, but also provides possibilities to sharpen the maturation and expulsion history of hydrocarbons in the WNB. In *Chapters 5* and *6* a multi-disciplinary approach was performed in order to provide a detailed, quantitative picture about the compressive tectonic movements in the WNB.

In *Chapter 5* the magnitude and pattern of erosion was reconstructed using bore-hole and seismic data, while *Chapter 6* focused on the Palaeogene tectonic movements in the WNB and on the characteristics and origin of basin inversion in NW Europe. The results of *Chapter 5* indicate that there are significant lateral variations in the pattern of erosion, which have a local, high frequency and a regional-, low frequency component. The regional component shows a general increase of erosion towards the east reaching its maximum along the transition zone between the WNB and the RVG (hinge-zone of the Mid Netherlands Weakness Zone). Considering that some amount of Early Tertiary Chalk (Houthem Fm.) is preserved in the RVG it is possible that the amount of removed sediments decreases further to the east. Analogue modelling results show that the amount of subsidence along a fault zone having two slightly differently oriented segments is the largest in the hinge-zone (L. Michon pers. comm., 2003; Michon and Sokoutis in prep.). The opposite behaviour (i.e., largest uplift in the hinge-zone) can be expected in a compressional setting. Should the amount of erosion indeed be smaller in the RVG than in the transition zone between the two basins, then it would be in agreement with these analogue modelling studies. This, however, cannot be confirmed with the method presented

in *Chapter 5*, since the large amount of Neogene sedimentation in the RVG has likely destroyed the burial anomaly signals.

Seismic sections and the high frequency component of the erosion in the WNB imply that reactivation of faults played a major role in the inversion and localised erosion of the basin fill. Across major faults several hundreds of meters of difference can be observed in the magnitude of erosion. The local maxima and minima of erosion are related to fault-related anticlines and synclines, respectively.

Backstripping analysis of virtual wells taking into account the amount of Late Cretaceous erosion (Fig. 6.8, p. 110) provides important constraints on the origin of Cretaceous subsidence in the Voorne Trough. These curves show that, in contrast to the basin centre, on the flank of the WNB (in the later Voorne Trough) the rate of tectonic subsidence increased in the Late Cretaceous, that is during inversion movements. This implies that the difference between the observed thickness of Chalk in the Voorne Trough and the restored thickness of Chalk in the WNB (*Chapter 5*) is not the result of reduced subsidence in the basin centre, but rather of an increased subsidence in the Voorne Trough. Based on these observations it is suggested that the increased subsidence on the flanks of the inverting basin was directly related to the basin inversion and consequently to compressional stresses. Therefore, this subsidence can be considered as being of a flexural type.

Differential tectonic movements — although with smaller magnitude — continued in the Palaeogene. The results of *Chapter 6* indicate that the Eocene inversion of the WNB is the result of a continuous inversion process throughout the Late Paleocene–Eocene rather than of a distinct pulse at the end of the Eocene. The inversion was characterised by the continuous doming of the former basin centre (Early Tertiary High) and is accompanied by the reactivation of pre-existing faults in a reverse mode. The intensity of the tectonic movements was not uniform throughout the Eocene: they were much stronger during the latest Eocene (Pyrenean inversion phase) than during the Early and Middle Eocene. Similar patterns of inversion tectonics were found also in other southern North Sea basins, on the Norwegian Continental Shelf, in the English Channel area and in Central Belgium. Furthermore, a good correlation was found to exist between Alpine tectonic events and the Late Cretaceous–Tertiary inversion of these areas. In light of these findings is suggested that not only the latest Eocene inversion pulse in the WNB Basin but also other Late Cretaceous–Tertiary inversion pulses in NW European basins are the peaks of a continuous inversion process originating from the Alpine collision.

The timing and intensity of inversion in NW European basins exhibit great temporal and spatial variations. This on one hand implies that temporal and spatial variations exist within the NW European lithospheric strength, which are controlled by the thermal regime, the crustal thickness, the pattern of pre-existing crustal and mantle discontinuities as well as by sedimentary loads and their thermal blanketing effect (e.g., Cloetingh and Burov, 1996; Ziegler et al, 1998). On the other hand, the mechanical coupling between the developing orogenic wedge and its foreland, which is responsible for the transmission of compressional stresses into the foreland,

might also be very variable. The process of collisional coupling of the orogen and the foreland, in which the rheology of the orogenic wedge, the lithospheric and crustal configuration of the passive margin, convergence rates and directions play an important role, is still poorly understood and requires further research. Ziegler et al. (1998) envisaged several scenarios, where the collisional coupling might be strong enough to give rise to inversion events in the foreland. In light of the results of *Chapter 6* it is clear however, that compressional stresses related to the collision can be high enough to cause deformation also between the stronger “inversion events” resulting in a long-lasting, continuous inversion process.

7.3 Future research perspectives

The 3-D fault models created during this Ph.D. research and the key geological horizons available digitally from TNO-NITG provide an ideal input data set for 3-D finite element geomechanical modelling. This data set offers a unique opportunity to study several exciting practical and theoretical questions such as: (1) Are the slip tendencies computed from the detailed pattern of “real” stresses (i.e., from FEM) along faults and those calculated using the method of *Chapter 2* comparable? (2) What are the conditions and degree of dynamic interaction between faults in a densely faulted sedimentary basin (WNB for example) in different stress scenarios? (3) What was the detailed 3-D geometry of the WNB prior to inversion? (4) What was the detailed pattern of deformation in the WNB and RVG during the Late Cretaceous–Tertiary inversion phase? (5) Under what conditions is this pattern comparable to the observed deformation pattern (e.g., the pattern of erosion reconstructed in *Chapter 5*)?

The erosion pattern determined in *Chapter 5* not only could give information about the pre-inversion geometry of the WNB, but also provides a more detailed picture about the subsidence history of the basin. Ultimately, this data set provides an excellent opportunity to revise the temperature and maturity history of the key hydrocarbon source rocks in the area.

Chapters 5 and *6* reveals accelerated Late Cretaceous–Palaeogene subsidence in the Voorne Trough. It is proposed that this subsidence is of a flexural type. However, the exact mechanism and cause of this subsidence is not clear, since it is unlikely that the vertical load of the elevated basin fill had very significant contribution. Crustal and lithospheric scale numerical or analogue modelling studies could provide solution to this dilemma.

Appendix A: Geometric modelling of faults

With the widespread use of computers in geosciences there is an ever-increasing demand for geological objects (such as sedimentary layers, stratigraphic horizons, faults etc.) to be available digitally. Digital three-dimensional databases are attractive to geoscientists, since the database immediately can be analyzed, modified according to the needs or be applied as input for various software packages. Time consuming digitization can be avoided. It is relatively easy to make a geological horizon digital even if it is available only as a paper map. In case of a fault, however, which is generally represented only by geological horizon-related fault-trace lines, a more complex procedure is needed, since the mere digitization of the fault lines does not produce a true 3-D surface adequately describing the geometry of the given fault. In turn, this is important since faults play an increasingly important role in modern geosciences. For example, the complex deformation patterns (e.g., Beekman et al., 2000; Cornu et al., 2003) and hydrogeological properties of faulted sedimentary basins (e.g., Foley et al., 1998; Alexander and Handschy, 1998; Verweij, 2003) or the 3-D reactivation potential of fault zones (e.g., Van Wees et al., 2003; Aochi et al., 2003) can now be evaluated using sophisticated software packages. This, however, is possible only if a detailed and reliable geometry of the fault system is digitally available as input for the user.

With this in mind a project has been initiated at TNO-NITG, which aimed to create the 3-D digital fault database of the Netherlands. As input, fault-trace lines and 2-D grids of key geological horizons (the products of the national mapping campaign of the Dutch subsurface) as well as raw exploration data such as 2-D and 3-D seismic surveys and borehole data are available. The fault models has been built using GOCAD (Mallet, 1992; www.t-surf.com), a commercially available, 3-D structural modelling software. As input for the fault modelling GOCAD, similarly to other structural modelling softwares available on the market (PETREL (www.sis.slb.com); VULCAN (<http://www.vulcan3d.com>); 3DMOVE (<http://www.mve.com>)) requires a data set — referred to as the 3-D “skeleton” —, which adequately represent the geometry of the 3-D fault surface. At the onset of the project it seemed that the data set, which was available at TNO-NITG and the modelling capabilities of GOCAD were sufficient to create high-quality 3-D fault surfaces even in complex tectonic situations (Fig. A.1). The created 3-D fault models are represented by triangulated

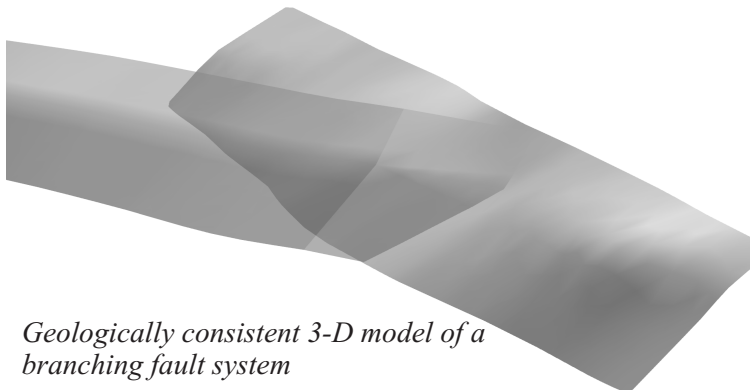
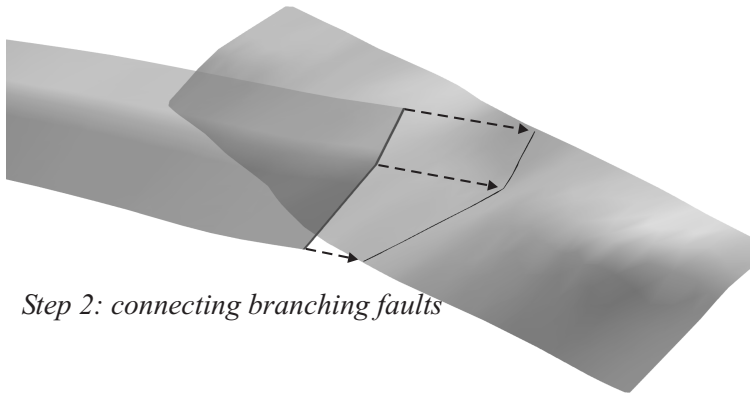
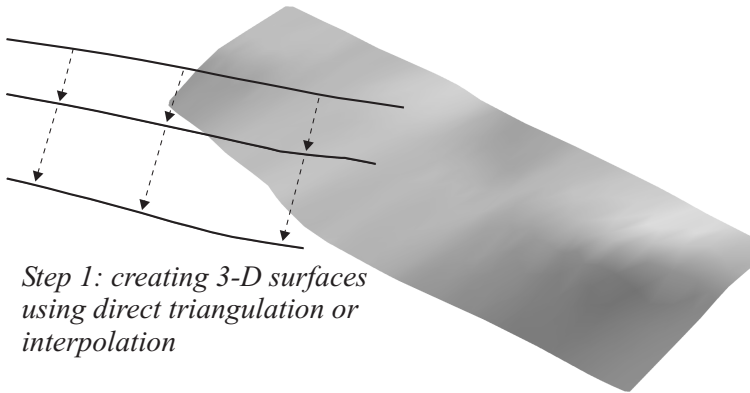


Figure A.1: The main steps of building the 3-D geometrical model of a branching fault system in GOCAD.

surfaces, and are adequate for being inputs not only of studies evaluating the fault reactivation potential (*Chapter 2-3*), but also of more sophisticated studies, such as reservoir modelling or geomechanical FEM. However, the early case studies have revealed that preparing an adequate, geologically consistent 3-D skeleton was very challenging. The procedure either was very time consuming or the 3-D skeletons created straightforward from the available geological data delivered fault models with insufficient quality (geological inconsistency within the input data). A solution was required, which helped to make the link between the input geological data and the structural modelling software.

As part of this Ph.D. research two methods have been developed, which aim to create adequate 3-D skeletons for GOCAD. The first procedure, which was named midline method, utilizes classical geological data as inputs (fault-trace lines and geological horizons). The other procedure is a direct method developed for modern and future mapping campaigns using fault data directly from 3-D seismic surveys. In this chapter the principles, advantages and disadvantages of these methods are discussed. The presently available 3-D faults models of the Netherlands, which are used in *Chapter 2-4* to evaluate fault reactivation potential in the southern Netherlands, are also presented.

A.1 The midline method

The midline method is a set of computer operations, which aims to prepare 3-D skeletons of the fault models from fault-trace lines associated with stratigraphic horizons. The input data set (depth maps and fault maps) is obtained using conventional mapping techniques and is insufficient to represent the 3-D skeleton of the fault models (because the fault-trace lines are two-dimensional). Development of this procedure was required because the vertical projection of the fault-trace lines onto the geological horizons did not deliver a 3-D skeleton of adequate quality (see below).

A.1.1 Principles of the midline method

The problem arises from the fact that the input geological horizons are represented by the discrete values of a *regular* grid, which cannot reproduce the path of the fault-trace line. Consequently, the representation of a fault-trace line in the grid is a zig-zag line (see in Fig. A.6 on the footwall). Furthermore, since 2-D mapping techniques assume that the faults are vertical, the geological horizon (i.e., grid) is not defined in the fault zone. As a consequence of these characteristics a direct projection of the 2-D fault-trace lines onto the grid to create a 3-D skeleton would result in “wavy” 3-D fault lines (see Fig. A.8; oscillating z values). This would have a significant impact on the quality of the fault models. To avoid this the midline procedure is proposed. The principle behind this approach is the observation, that outside the irregular zone on both the foot- and hanging-wall side of the fault the

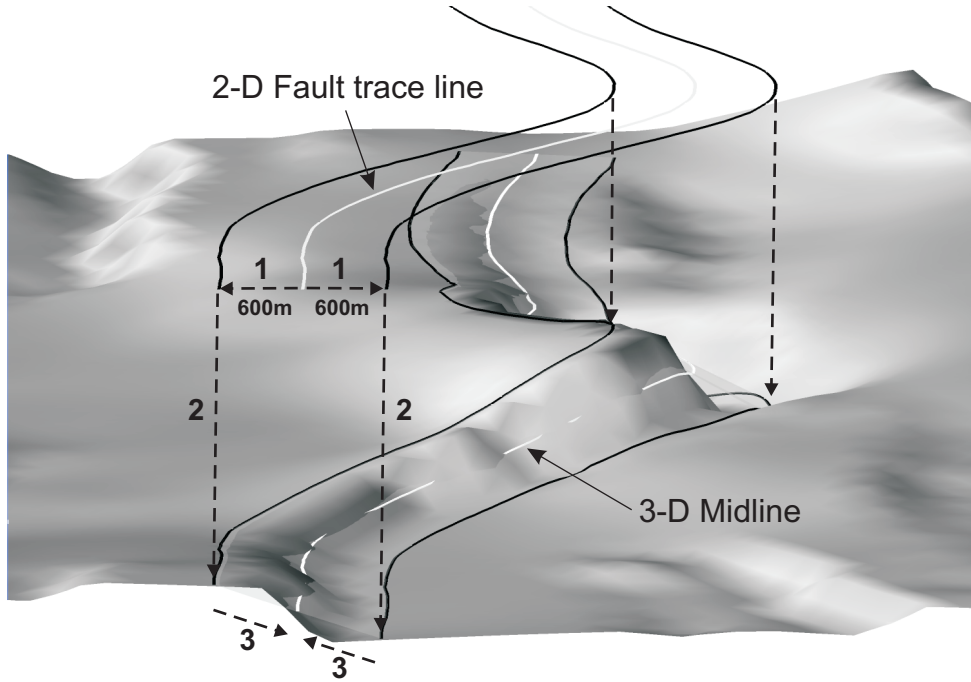


Figure A.2: Projection of a fault-trace line onto the corresponding key horizon using the midline method. Numbers are representing the order of steps.

geological horizon is generally smooth (Fig. A.2 and Fig. A.6). By shifting the input lines out of the irregular zone in both directions with the same offset and by projecting them vertically onto the surface, two smooth 3-D lines are obtained on each side of the fault. Taking the co-ordinate-wise average of these lines results in a line (the midline), which is much smoother than that obtained by a direct projection, and whose lateral co-ordinates are the same as those of the original line. This line can be considered as a good 3-D representation of the intersection of the fault and the relevant surface. Using the 3-D lines created this way as the 3-D skeleton of the fault model results in a surface with much better quality.

A.1.2 Implementation of the midline method

The algorithm proposed above (Fig. A.2) was inserted into a series of operations organised into three stages (Fig. A.3). The 3-D fault models are produced at the end of these operations. In the first stage a GIS application (ArcInfo) is used to prepare the fault-trace lines created using conventional mapping techniques. Data preparation includes the horizontal smoothing of the faults lines (discussed later), aiming to remove any high frequency component.

During the second stage the 3-D midlines are calculated using a newly developed computer software written in Java2 language. The software uses the algorithm proposed in figure A.2. The inputs of the software are the geological horizons and the fault-trace lines. Beside the calculation of the 3-D midlines quality-improving steps (i.e resampling and vertical smoothing) are also applied in order to maximise the quality of the 3-D skeleton (see below). During the third stage the 3-D fault models are created using the build-in functionality of GOCAD (Worum, 2001 NITG internal report; Fig. A.1). The final fault models are represented by triangulated surfaces.

It must be emphasised that regional geological knowledge and a continuous quality check must play a key role during fault modelling. In a regional mapping campaign faults often cut only two or three of the mapped horizons. In the case of a complex tectonic zone, where more individual faults are involved, which in addition might have been reactivated several times, the number and real geometry of the fault surfaces are difficult to determine using only a limited number of 3-D midlines. In these situations regional geological knowledge as well as the study of available seismic surveys are key factors in constructing a geologically consistent, high quality fault model.

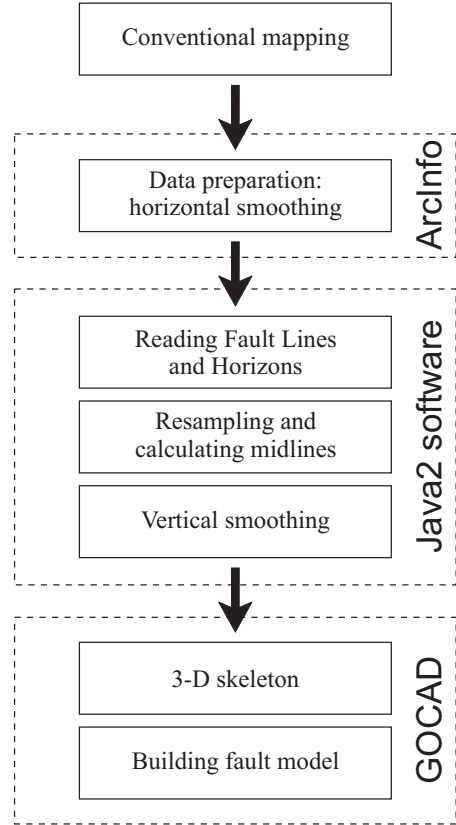


Figure A.3: Flowchart of creating 3-D fault models using fault trace lines obtained from conventional mapping.

A.1.3 Disadvantages and errors of the midline method

With respect to the 3-D fault creation the conventional mapping procedure and also the midline method itself have several disadvantages, which all have an effect on the final quality of the models. Good quality models not only have high quality surfaces (smooth etc.), but also are reliable in a sense that they provide a good geometrical correspondence of the real fault they are representing. There are three main sources of errors: (1) mapping errors; (2) errors of the midline method; (3) data and processing errors.

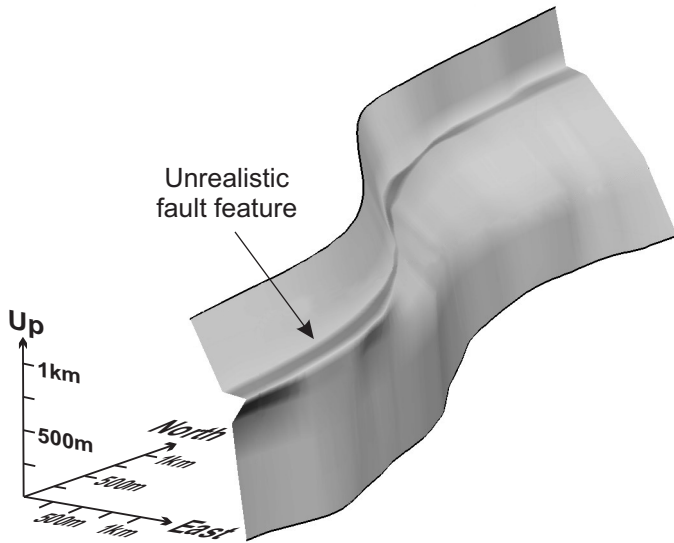


Figure A.4: Example of an unrealistic fault model resulting from an inconsistent input data set.

Mapping errors

Among the three sources of error mapping errors are by far the most important, since inconsistent input data may result in unreliable fault models. The input to the midline method is originated from conventional mapping campaigns, which is in practice a 2-D procedure. It works in a layer-by-layer manner and is most suitable for horizon/layer mapping. As faults are sub-vertical 3-D surfaces, their mapping requires a true 3-D or a vertical rather than a horizontal approach. For example, faults often vanish between two key horizons, so that with conventional mapping their full geometry may remain undetected. In addition the interpreter does not always consistently map the relative position of the fault trace according to the dip of the fault. Creating 3-D surfaces from inconsistent fault lines may result in unacceptable fault models (Fig. A.4).

3-D fault creation using conventional mapping products therefore has to be performed in an iterative and, consequently, time consuming manner. A particular fault model is built iteratively several times, comparing its consistency with seismic and geological data in every loop. Common line operations between loops include the shifts, partial or total redraws or the deletion of the problematic fault line.

Errors of the method

As the midline method is a geometrical approach, the resulting 3-D skeleton greatly depends on the surface onto which the projection takes place. In a real world scenario let us consider a 3-D line on the fault surface, which points are halfway (in dip direction) between the foot- and hangingwall breakpoints (Fig. A.5) This is called the centerline, which accurately defines the 3-D skeleton of the fault. If the lateral co-ordinates of the centerline are projected onto the surface using the midline method the 3-D midline is obtained, which in a real world scenario may not coincide with the 3-D centerline (see Fig. A.5).

In other words, it is not always possible to exactly recreate the 3-D fault surface using the midline method. This model error however is acceptable, since it is much less than the error arising from the inconsistency of the fault-trace lines. Applying a smaller shifting distance can reduce the model error, but by doing so the processing error increases, since we get closer to the irregular zone. Parameter sensitivity studies allow one to find an optimum shifting distance, when both the model and the processing error are small enough to be removed during processing (see later). By doing so the geometrical quality of the fault models can be maximised.

Another limitation of the midline method is a typical 3D problem related to branching faults. If the midline of the branching fault is calculated then it can significantly deviate vertically from the theoretical centerline near the branch point (Fig. A.6). The reason for this is that if this line is shifted toward the master fault (e.g., left) then the first few hundred meters of the line will be projected onto the footwall of the master fault, while the line shifted to the right will stay “low”. As the midline inherits shape both from left and right this will end up in a deviation shown on figure A.6. By applying smaller shifting distance (and filtering) this effect can be reduced.

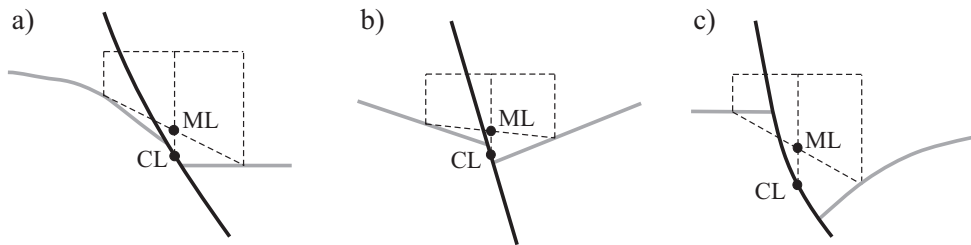


Figure A.5: Cartoons illustrating the discrepancy between the midline (ML) and the centerline (CL) in realistic scenarios. a) Eroded footwall block. b) Rotated fault blocks. c) Listric fault with considerable offset.

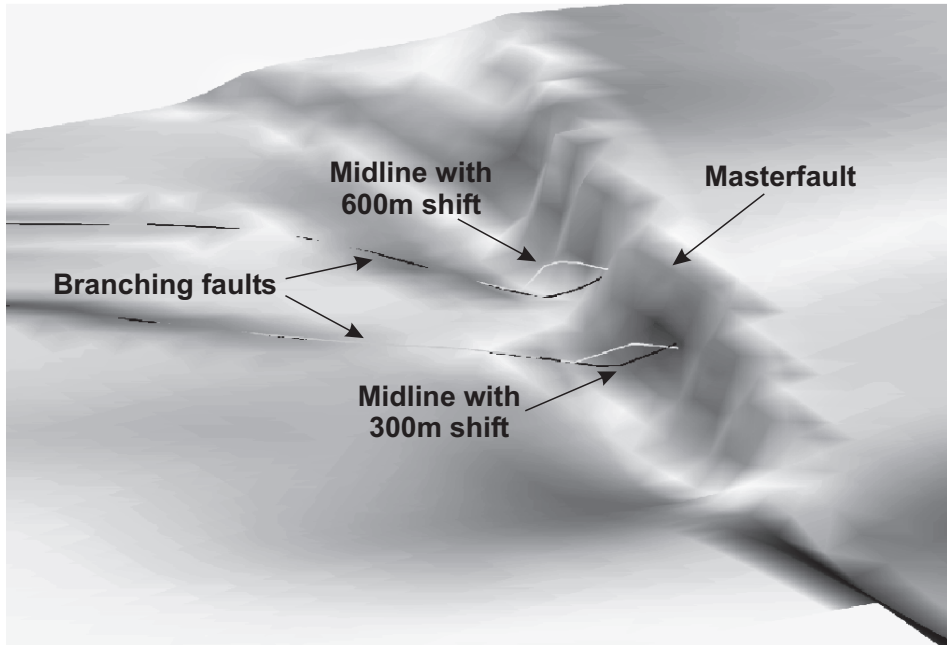


Figure A.6: Artefacts of the calculated 3-D midlines of a branching fault system. Using smaller shifting distance the effect can be reduced (see text for explanation).

Processing errors

For applications using the fault models the geometrical quality of the surfaces is an important issue. As explained earlier the midline method itself can provide an undesirable, high frequency spatial noise if the shifting distance is small. Noise (lateral) can also be produced during mapping of the faults, whose source is mainly the drawing and/or digitisation of the fault lines. These processing and artificial features have to be removed or minimised, since they can manifest themselves in undesirable, high frequency waves and bulges in the final fault model. Thus, attention has to be paid to quality control during every step of the fault creating procedure, that is during data preparation (ArcInfo software), during calculation of the midlines and during creating the surfaces in GOCAD. In the following those steps implemented into the midline procedure are discussed, with the aim to improve the quality of the fault models (see Fig. A.3).

In figure A.7 the result of the smoothing operations is shown, which is performed during data preparation and using the built-in functions of ArcInfo (see Worum, 2001 NITG 02-013-A internal report for details). These operations aim to remove lateral noise from the input data. The smoothed line is much more appropriate as input for the midline calculations and for the fault creation.

If either direct projection or the midline method with small shifting distance are used, high frequency noise is generated, but it affects only the z (depth) component of the midlines (Fig. A.8). The reduction or removal of this noise is targeted using a 1-D mathematical filter, whose coefficients are convolved with the z co-ordinates of the calculated midlines (e.g., Byerly, 1965; Meskó, 1989). Since the filter is dimensionless, the fault lines are resampled equidistantly in the x – y plane prior to filtering (Fig. A.3). As filter the Gauss filter is used since it has the characteristic of being short in both the frequency and the space domains (e.g., Meskó, 1989; Duijndam and Schonewille, 1999). The optimal combination of cut-off-frequency (and consequently the length of the filter) and shifting distance is determined by parameter tests. Figure A.8 quantitatively demonstrates that without using the midline method (direct projection) the calculated 3-D line is of poor quality (oscillating z values) even if it

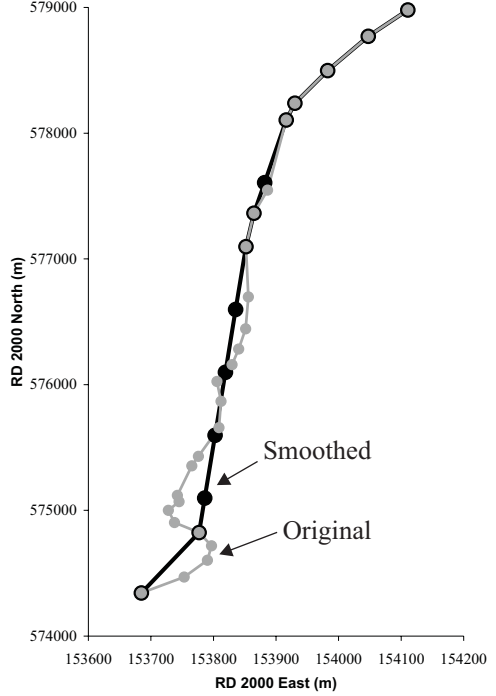


Figure A.7: Lateral smoothing of a fault trace line having unrealistic features. The maximum deflection of the two lines is 60 m .

is smoothed with a short (i.e., weak) filter. An acceptable result is obtained only if a stronger filter is used. Using the midline method with 500 m shift produces a smooth midline, which however deviates from the desired position, especially near the left end of the fault (branch point; see also Fig. A.6). Applying a shorter shifting distance, on one hand provides a better midline compared to the theoretical centerline, which on the other hand is affected by moderate-amplitude high frequency noise. This noise, however, can easily be reduced/removed even with a weak filter, resulting in an optimal, noise-free midline. In the case of a key horizon with 250 m grid size, for the optimal results it is proposed to equidistantly resample the input lines by 140 m , use 200–300 m shifting distance and filter the calculated midlines with the following coefficients: $c_0 = 0.22156$; $c_1 = 0.18989$; $c_2 = 0.11956$; $c_3 = 0.0553$; $c_4 = 0.01879$; $c_5 = 0.00469$; $c_6 = 0.00086$; $c_7 = 0.00012$.

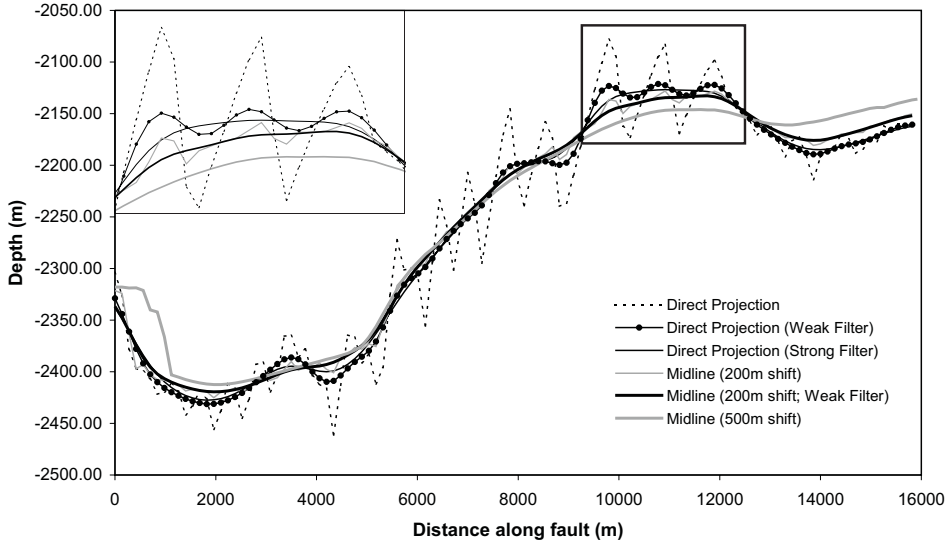


Figure A.8: The effect of processing parameters on a 3-D midline. The most pleasing result is obtained if the midline method using small (200–300 m) shifting distance is combined with a filter (see text for discussion).

The third level of smoothing is applied in GOCAD. During this step the DSI (Direct Smooth Interpolation) algorithm of GOCAD (Mallet, 1992) is used in order to fit a triangulated surface onto the 3-D skeleton instead of using direct triangulation. Creating the surface by interpolation further enhances the smoothness of the surface and results in uniform triangle sizes across the whole surface.

A.2 The direct method

As apparent from the previous section the greatest disadvantage of the midline method is that there is no adequate possibility to check the reliability of the fault models. The input data generally comes from conventional mapping campaigns, which operate on a 2-D level and are not ideal for mapping faults. In addition, the 3-D fault surfaces cannot be directly compared with the seismic data, on which the mapping is based. Still, most of the time this method has to be used, since the available input database is generally based on conventional mapping. For modern and future fault modelling campaigns a more reliable, direct method is proposed, which was successfully applied in the West Netherlands Basin.

A.2.1 Principles of the direct method

The principle of the direct method is the observation that on modern, good quality 3-D seismic surveys the faults can be easily recognised and correlated throughout the seismic survey. As the seismic surveys are deliberately oriented perpendicular to the main structural elements (consequently to the faults) the trace and shape of a particular fault can be easily mapped on subsequent slices of the 3-D survey (Fig. A.9). The interpreted series of sub-vertical lines are exported from the seismic interpretation software into the fault-modelling environment (GOCAD), where the model of the fault can be created using similar steps to those discussed earlier. The greatest advantage of the method is that if the modeller is not satisfied with the final fault model he/she can go directly back to the source of the models (the seismic survey) and modify the interpretation (of course always within a range justified by the seismic data). By doing so the reliability of the fault models can be kept high. In addition, faults in complex fault zones can be more easily distinguished compared to the case when fault-trace lines of several key horizons are used.

As the z co-ordinates of the seismic surveys are in seismic travel time, so are those of the resulting fault models. Compared to the midline method this requires an extra step, namely the depth conversion of the fault models. Since modern seismic surveys are migrated (x,y) during processing, 1-D depth conversion algorithms are suitable for the conversion. In other words during depth conversion the fault models are stretched only in the z direction, the x and y co-ordinates are not changed. In the case of the West Netherlands Basin the faults were depth-converted using the v_0 - K method, which assumes that the interval velocity of the geologic layers defined by the key horizons of the mapping campaign linearly increases with depth. For the conversion the same v_0 and K parameters were used as for depth conversion of the horizons, resulting in fault models adequately matching the horizons (TNO-NITG, 2002).

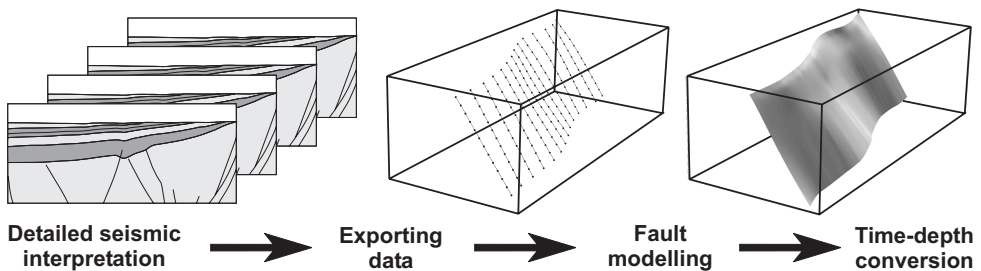


Figure A.9: The main steps of fault modelling using the direct method.

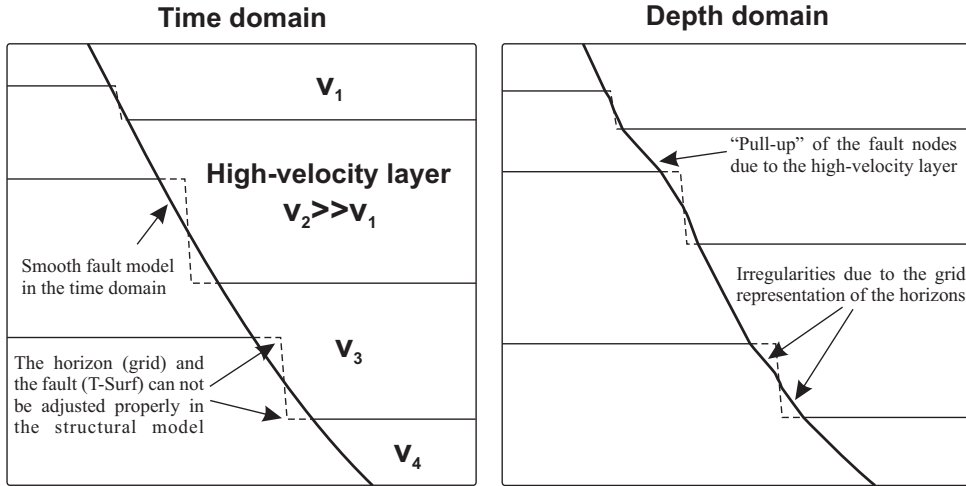


Figure A.10: Geometrical artefacts resulting from the depth conversion of a smooth 3-D fault model.

A.2.2 Errors of the direct method

The direct method is much faster than the midline method, however it is not without errors. The step having the biggest impact on the final quality of the fault surfaces is the time–depth conversion. The source of the error is the fact that fault interpretations on the seismic surveys are smooth and have generally constant dips or slight curvatures. The velocity field used for the depth conversion however is not uniform. Across key geological horizons the interval velocity often jumps resulting in an irregularly increasing average velocity. Converting the smooth time models with such a velocity field may result in irregular (wavy) dip angles in the depth models (Fig. A.10). These “pull-ups” are superimposed on irregularities, that are produced by the fact that triangulated surfaces (i.e., the fault models) cannot be properly adjusted to grids. Fortunately the irregularities are significant only if the geological succession contains a thick, high velocity layer (limestone for example). Nevertheless, a final smoothing operation is usually applied in GOCAD to enhance the quality of the final fault models.

Figure A.11: a) Available 3-D fault models in the southern Netherlands. b) Details of a 3-D fault system in the north–western part of the West Netherlands Basin. The point of view is indicated in panel “a”. A: Amsterdam; U: Utrecht; E: Eindhoven.

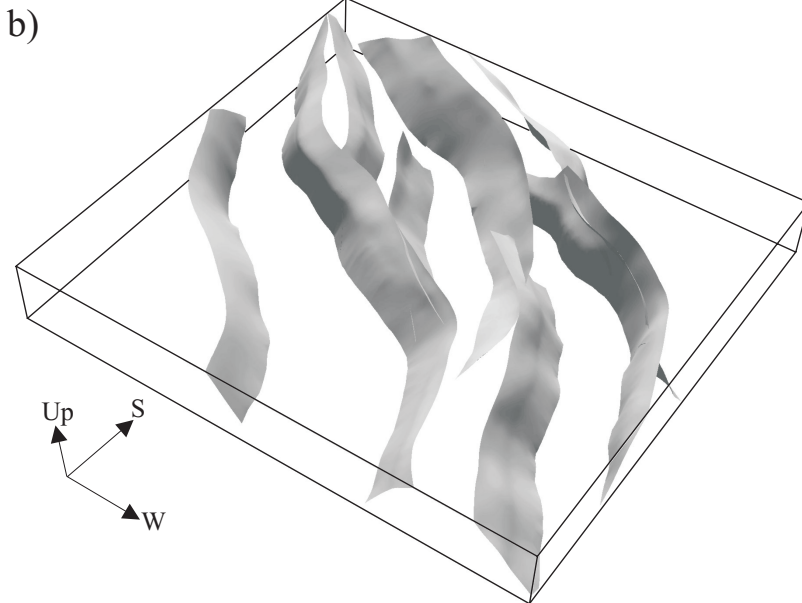
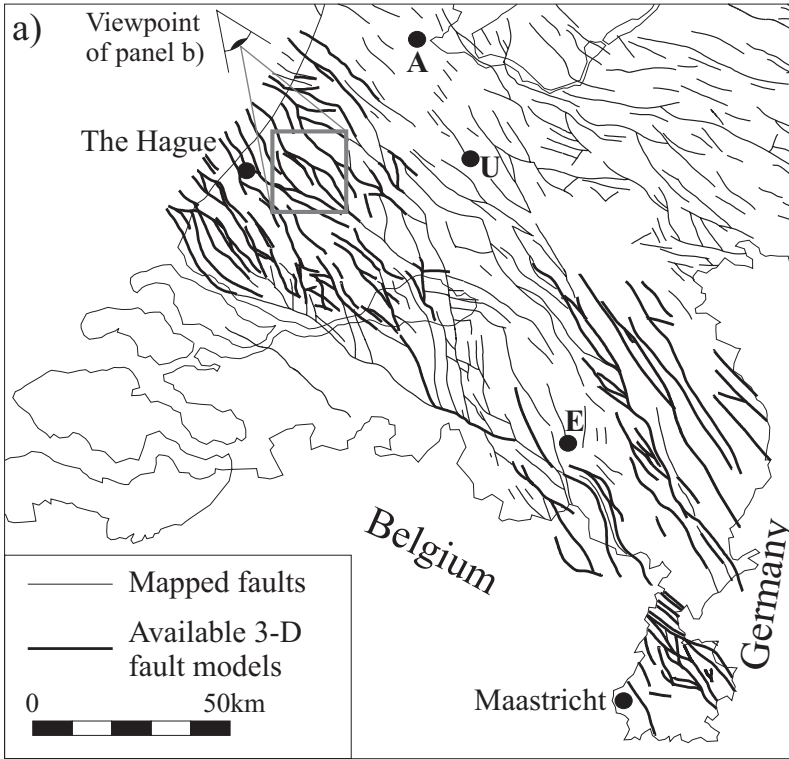


Table A.1: Advantages and disadvantages of the midline- and direct methods

Midline method		Direct method	
Advantage	Disadvantage	Advantage	Disadvantage
operates only in depth domain	sometimes rather slow	fast and delivers very reliable models	requires 3-D seismic surveys
requires general mapping data	less possibilities for quality control	continuous quality control possible	requires a step of depth conversion

A.3 Summary, 3-D digital fault database of the Netherlands

For several geological studies, including studies evaluating the reactivation potential of fault-systems, the detailed, three-dimensional geometry of the faults is very important. With the increasing use of computers in geosciences these surfaces are required to be available in a digital format. In this chapter two fault-modelling methods were discussed, which are extensively used in TNO–NITG Dutch Geological Survey, and which deliver high quality 3-D fault surfaces suitable as inputs for further studies. The midline method is more frequently used, since the regional mapping campaign, which provides the input for the fault creation, is already at a developed stage. This method is an effective, but sometimes rather slow procedure (Table A.1). The other, direct procedure is faster and produces more reliable results. However this procedure is sometimes limited to a smaller area, since 3-D seismic data are required during the process. Therefore the direct method is more suitable for modern and future mapping campaigns.

Today more than 100 3-D fault models are available from various parts of the Netherlands, which were created using the two techniques presented in this chapter. Areas with interesting structural features, with pronounced Quaternary fault activity or where high quality 3-D seismic surveys are available (West Netherlands Basin and Roer Valley Graben) were favoured during the process (Fig. A.11). These fault models serve as inputs for the fault reactivation analysis presented in *Chapters 3* and *4*. Besides these two areas fault models are also available from the westernmost part of the Lower Saxony Basin (NE Netherlands) and from the Vlieland Basin (NW Netherlands). Considering the number of available faults however, these latter areas are of secondary importance compared to the southern Netherlands. Preference among the faults also had to be established, since the fault density, especially in the basin system in the southern Netherlands, is very high. Only primary faults were modelled, along which the offset is high, or those which played an important role in the geological history of the Netherlands (e.g., multiple reactivation).

Appendix B: Colour plates

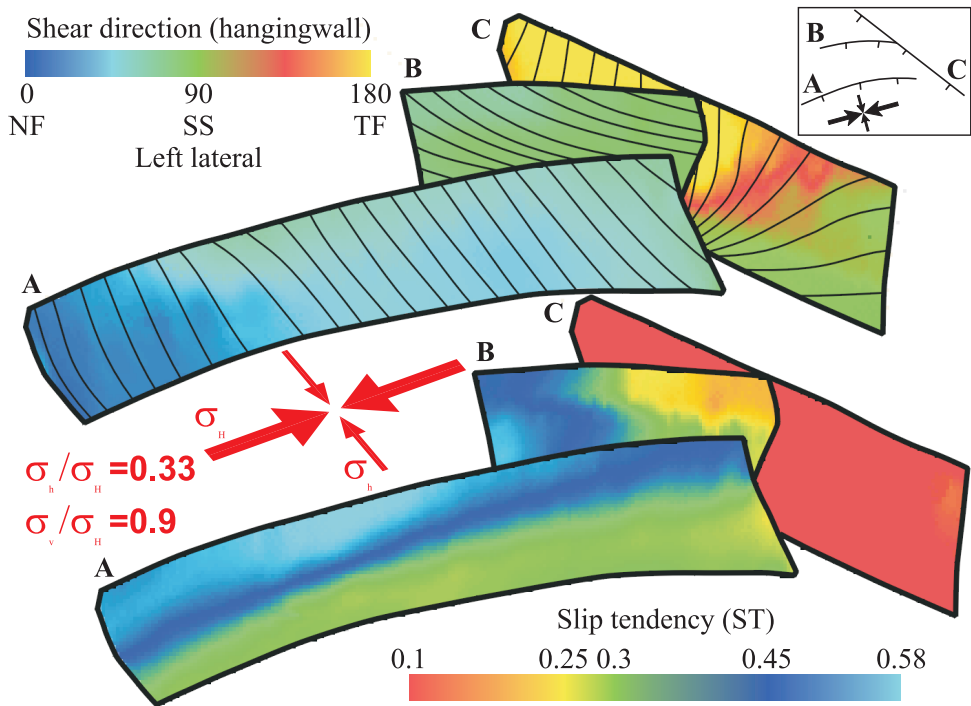


Figure 2.4: Reactivation analysis of a fictional fault system in a synthetic strike slip stress scenario. The inset shows the map view of the modelled faults A, B and C. The lower and upper panel shows the calculated slip tendency and shear directions, respectively. Shear trajectories are also shown (thin lines). NF, SS and TF denote normal faulting, strike slip faulting and thrust faulting, respectively. See text for further discussion.

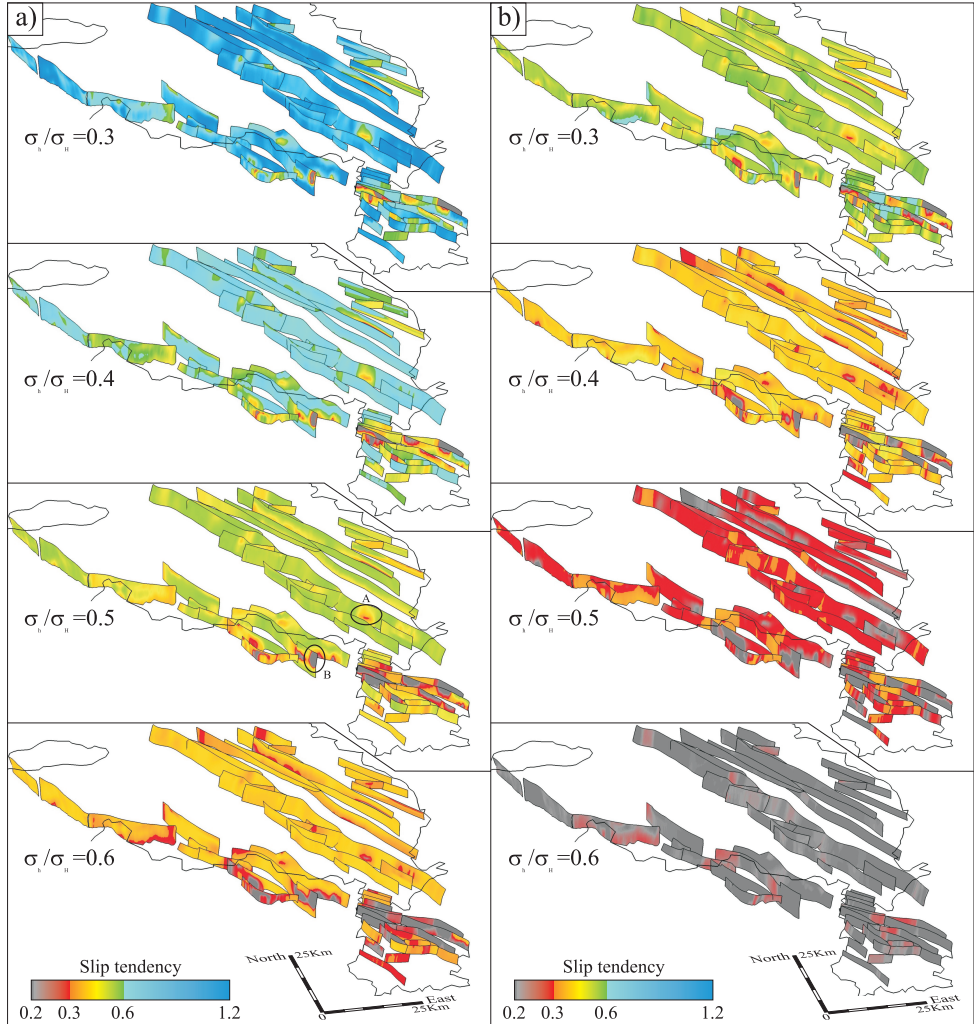


Figure 3.3: Perspective view of the 3-D faults with slip tendency patterns calculated for stress tensors having different σ_v/σ_H ratios and σ_H directions of N145°. Vertical scale is 4x exaggerated. Panel “a” is for stress tensors describing a normal faulting regime, panel “b” is for strike-slip-faulting stress tensors. The R -value of the stress tensor was modelled as 0.45 for panel “a” and as 0.25 for panel “a” representing the maximum slip tendencies within the modelled R -value range.

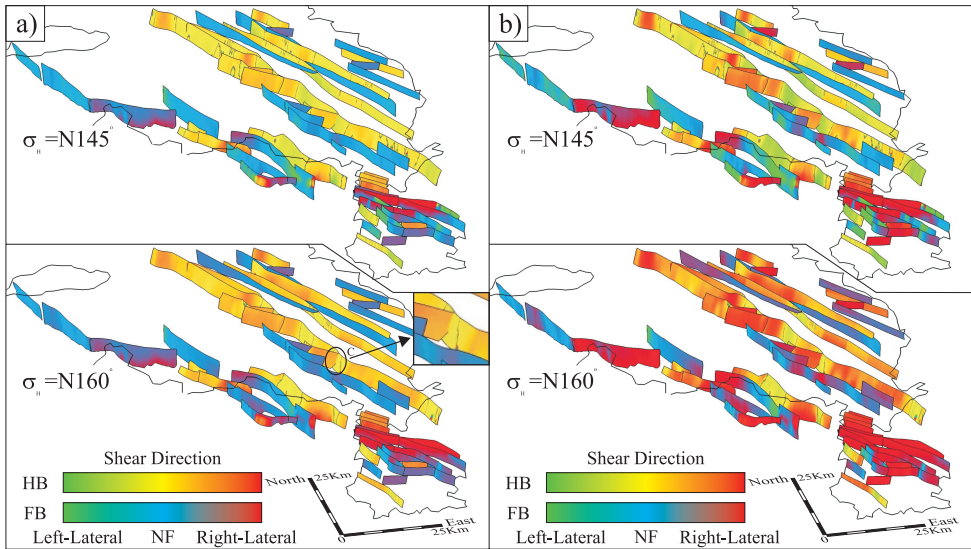


Figure 3.4: Perspective view of the 3-D faults with shear direction patterns calculated for stress tensors having different σ_H directions of N145° and N160°. Vertical scale is 4x exaggerated. Panel “a” is for stress tensors describing normal faulting regime, panel “b” is for strike-slip-faulting stress tensors. The R -value of the stress tensor was modelled as on figure 3.3. HB: hangingwall-block; FB: footwall-block; NF: normal faulting (dip slip shear direction).

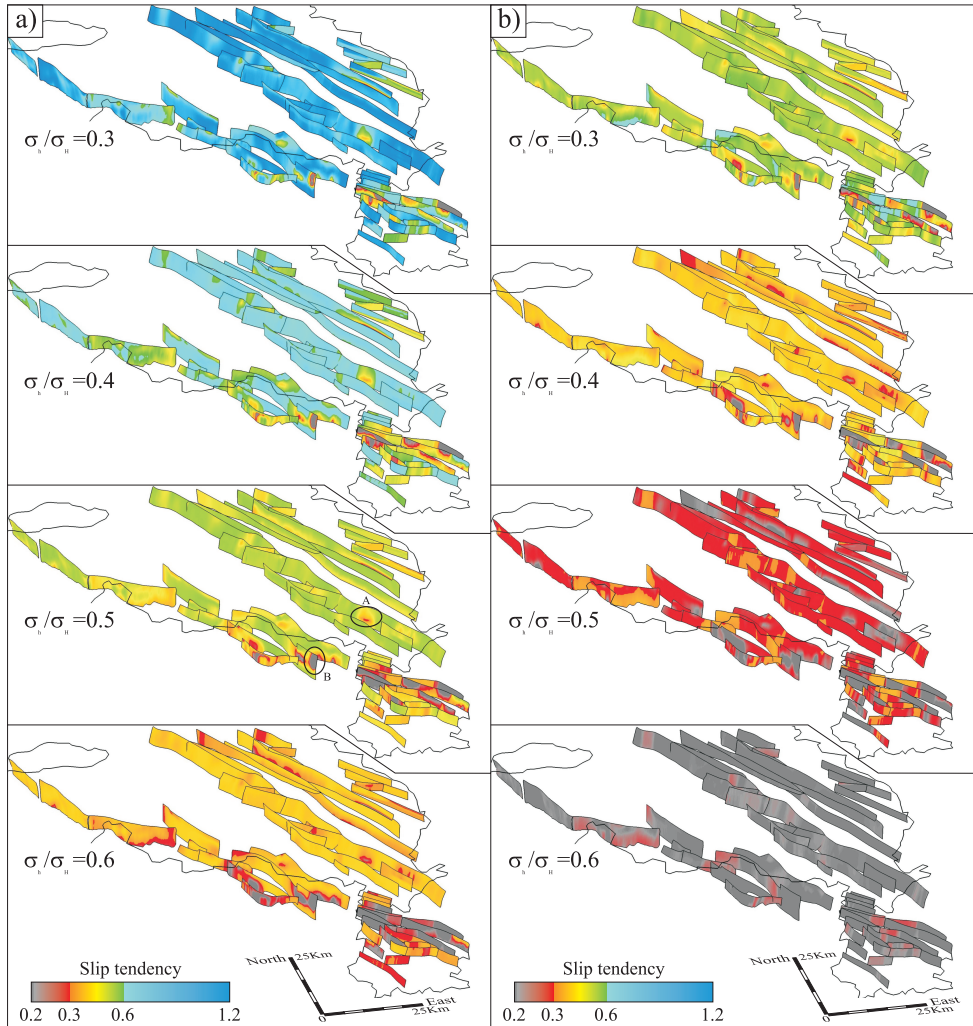


Figure 3.3: Perspective view of the 3-D faults with slip tendency patterns calculated for stress tensors having different σ_h/σ_H ratios and σ_H directions of $N145^\circ$. Vertical scale is 4x exaggerated. Panel “a” is for stress tensors describing a normal faulting regime, panel “b” is for strike-slip-faulting stress tensors. The R -value of the stress tensor was modelled as 0.45 for panel “a” and as 0.25 for panel “a” representing the maximum slip tendencies within the modelled R -value range.

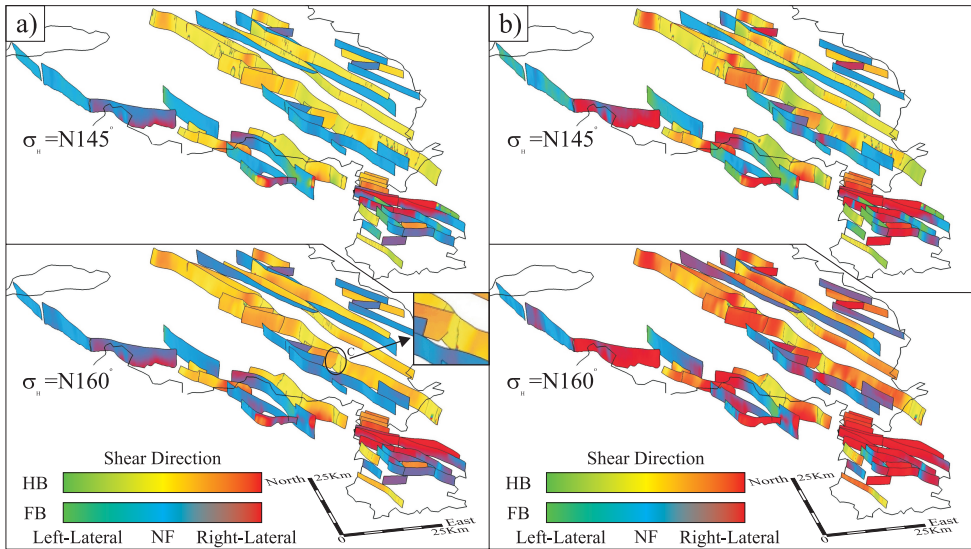


Figure 3.4: Perspective view of the 3-D faults with shear direction patterns calculated for stress tensors having different σ_H directions of $N145^\circ$ and $N160^\circ$. Vertical scale is 4x exaggerated. Panel “a” is for stress tensors describing normal faulting regime, panel “b” is for strike-slip-faulting stress tensors. The R -value of the stress tensor was modelled as on figure 3.3. HB: hangingwall-block; FB: footwall-block; NF: normal faulting (dip slip shear direction).

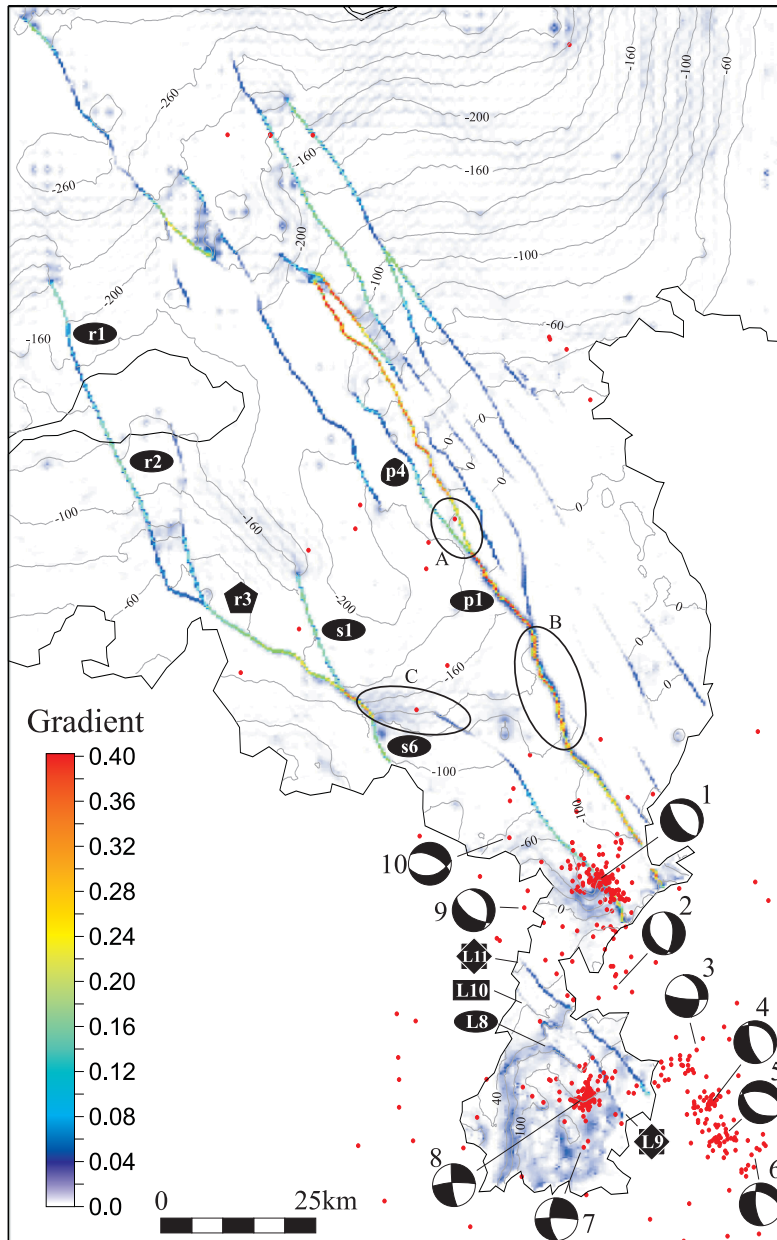


Figure 3.5: Depth map of the base Quaternary horizon (contours; after De Mulder et al., 2003) and its gradient map. Higher gradients imply larger offsets. Earthquakes of the last century are shown in red. Focal mechanisms are from Camelbeeck and van Eck (1994).

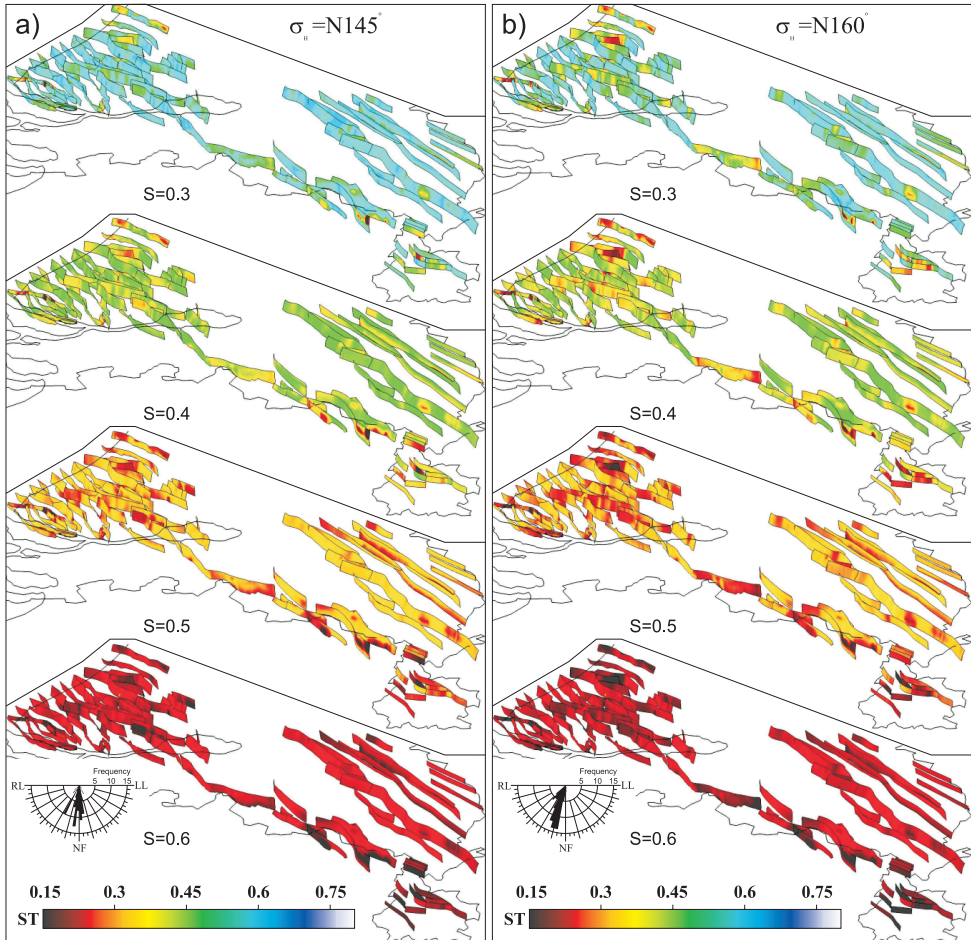


Figure 4.9: Calculated 3-D slip tendency (ST) patterns of the modelled faults for different stress tensors having σ_H direction of a) N145° and b) N160°. The polar histograms display the number of faults along which the average of the shear vectors point into the given direction. (NF: normal faulting (dip slip); LL: left lateral slip; RL: right lateral slip; $S = \sigma_h/\sigma_v$).

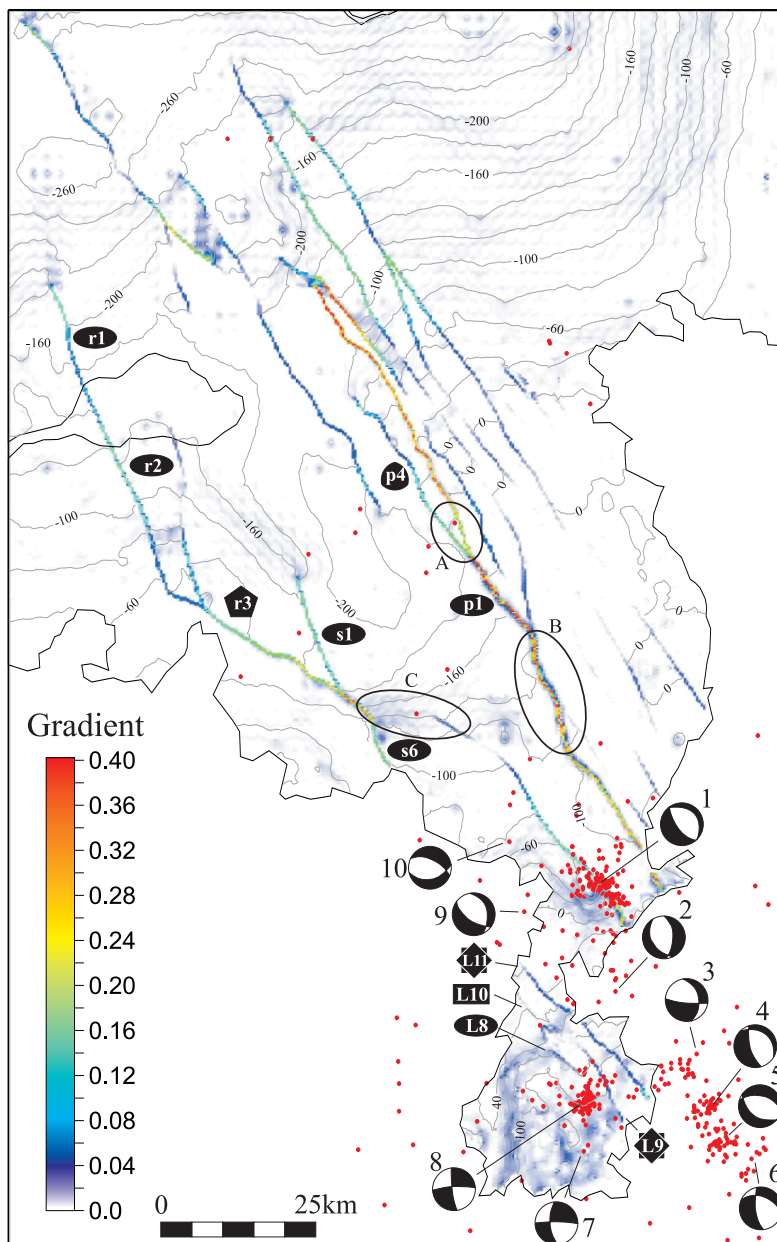


Figure 3.5: Depth map of the base Quaternary horizon (contours; after De Mulder et al., 2003) and its gradient map. Higher gradients imply larger offsets. Earthquakes of the last century are shown in red. Focal mechanisms are from Camelbeeck and van Eck (1994).

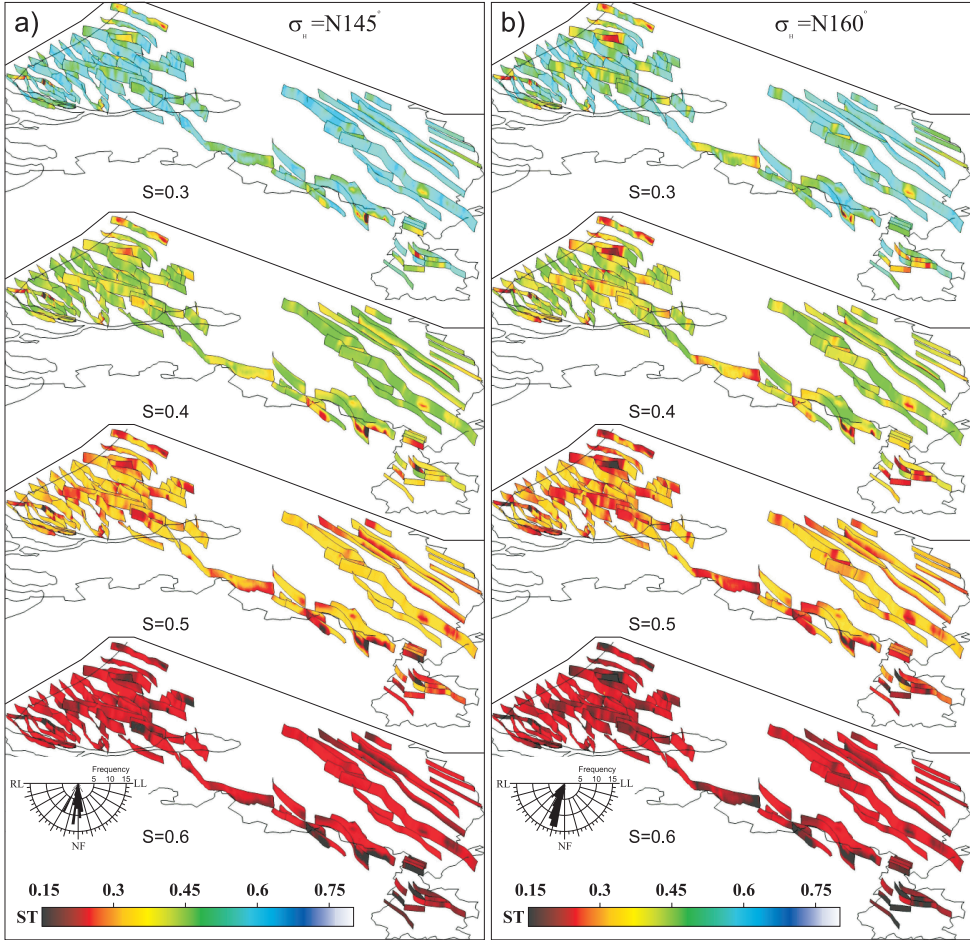


Figure 4.9: Calculated 3-D slip tendency (ST) patterns of the modelled faults for different stress tensors having σ_H direction of a) $N145^\circ$ and b) $N160^\circ$. The polar histograms display the number of faults along which the average of the shear vectors point into the given direction. (NF: normal faulting (dip slip); LL: left lateral slip; RL: right lateral slip; $S = \sigma_h/\sigma_v$).

References

- Ahorner, L. 1975 Present-day stress field and seismotectonics block movements along major fault zones in Western Europe. *Tectonophysics* 29: 233–249
- Alaniz-Alvarez, S.A., Tolson, G. and Nieto-Samaniego, A.F. 2000 Assessing fault reactivation with the Re-Activa Program. *Journal of Geoscience Education* 48: 651–657
- Alexander, L.L. and Handschy, J.W. 1998 Fluid flow in a faulted reservoir system; fault trap analysis for the Block 330 Field in Eugene Island, south addition, offshore Louisiana. *AAPG Bulletin* 82(3): 387–411
- Anderson, E.M. 1951 The dynamics of faulting. Oliver and Boyd, Edinburgh, UK, 206p
- Andriessen, P.A.M. 1995 Fission-track analysis; principles, methodology and implications for tectonothermal histories of sedimentary basins, orogenic belts, and continental margins. *Geologie en Mijnbouw* 74(1): 1–12
- Angelier, J. 1984 Tectonic analysis of fault slip data. *Journal of Geophysical Research* 89: 5835–5848
- Angelier, J. 1990 Inversion of field data in fault tectonics to obtain the regional stress; part 3. A new rapid direct inversion method by analytical means. *Geophysical Journal International* 103: 363–376
- Angelier, J. 2002 Inversion of earthquake focal mechanisms to obtain the seismotectonic stress; IV, A new method free of choice among nodal planes. *Geophysical Journal International* 150(3): 588–609
- Anselmetti, F.S. and Eberli, G.P. 1993 Controls on sonic velocity in carbonates. *Pure and Applied Geophysics* 141(2–4): 287–323
- Aochi, H., Madariaga, R. and Fukuyama, E. 2003 Constraint of fault parameters inferred from nonplanar fault modelling. *Geochemistry, Geophysics, Geosystems* (G3) 4(2): doi: 10.1029/2001GC000207
- Bada, G. 1999 Cenozoic stress field evolution in the Pannonian Basin and surrounding orogens. Ph.D. Thesis, Netherlands Research School of Sedimentary Geology (NSG), publ. no. 990101, Vrije Universiteit, Amsterdam, 204p
- Baldschuhn, R., Best, G. and Kockel, F. 1991 Inversion tectonics in the north-west German basin. In: Spencer, A.M. (ed.): *Generation, accumulation and production of Europe's hydrocarbons*, Special Publication of the European Association of Petroleum Geoscientists, 1, Oxford University Press, Oxford, UK, pp. 149–159
- Beekman, F., Badi, M. and Van Wees, J.D. 2000 Faulting, fracturing and in situ stress prediction in the Ahnet Basin, Algeria — a finite element approach. *Tectonophysics* 320: 311–329
- Bell, J.S. and Babcock, E.A. 1986 The stress regime of the Western Canadian Basin and implications for hydrocarbon production. *Bulletin of Canadian Petroleum Geology* 34(3): 364–378
- Bergerat, F. 1987 Stress field in the European platform at the time of Africa–Eurasia collision. *Tectonics* 6: 99–132.
- Biju-Duval, B., Dercourt, J. and Le Pichon, X. 1977 From the Tethys ocean to the Mediterranean seas; a plate tectonic model of the evolution of the western Alpine system. In: Biju-Duval, B. and Montadert, L. (eds.): *Structural history of the Mediterranean basins*. Ed. Technip, Paris, France, pp. 143–164
- Blundell, D.J. 2002 Cenozoic inversion and uplift of southern Britain. In: Doré, A.G., Cartwright, J.A., Stoker, M.S., Turner, J.P. and White, N. *Exhumation of the North Atlantic Margin: timing mechanisms and implications for petroleum exploration*. Geological Society, Special Publication No. 196, London, UK, pp. 85–101
- Bodenhause, J.W.A. and Ott, W.F. 1981 Habitat of the Rijswijk oil province, onshore, The Netherlands. In: Illing, L.V. and Hobson, G.D. (ed.): *Petroleum geology of the continental shelf of NW Europe*. Institute of Petroleum (London), pp. 301–309
- Bodine, J.H., Steckler, M.S. and Watts, A.B. 1981 Observations of flexure and the rheology of the oceanic lithosphere. *Journal of Geophysical Research* B86(5): 3695–3707
- Bott, M.H.P. 1959 The mechanics of oblique slip faulting. *Geological Magazine* 96: 109–117
- Bott, M.H.P. 1991 Ridge push and associated plate interior stress in normal and hot spot regions. *Tectonophysics* 200: 17–32
- Bouw, L. and Oude Essink, G.H.P. 2003 Fluid flow in the northern Broad Fourteens Basin during Late Cretaceous inversion. *Netherlands Journal of Geosciences/Geologie en Mijnbouw* 82(1): 55–69
- Brace, W.F. and Kohlstedt, D.L. 1980 Limits on lithospheric stress imposed by laboratory experiments. *Journal of Geophysical Research* 85(B11): 6248–6252
- Brudy, M., Zoback, M.D., Fuchs, K., Rummel, F. and Baumgärtner, J. 1997 Estimation of the complete stress tensor to 8 km depth in the KTB scientific drill holes: Implications for crustal strength. *Journal of Geophysical Research* 102(B8): 18453–18475
- Buck, W.R. 1991 Modes of continental lithospheric extension. *Journal of Geophysical Research* 96(B12): 20161–20178
- Bulat, J. and Stoker, S.J. 1987 Uplift determination from interval velocity studies, UK southern North Sea. In: Brooks, J. and Glennie, K. (eds.): *Petroleum Geology of North West Europe*, Graham and Trotman, pp. 293–305
- Byerlee, J.D. 1978 Friction of rocks. *Pure Applied Geophysics* 116: 615–626
- Byerly, P.E. 1965 Convolution filtering of gravity and magnetic maps. *Geophysics* 30(2): 281–283
- Camelbeek T. and van Eck, T. 1994 The Roer Valley Graben earthquake of 13 April 1992 and its seismotectonic setting. *Terra Nova* 6: 291–300
- Camelbeek, T., Van Eck, T., Pelzing, R., Ahorner, L., Loohuis, J., Haak, H.W., Hoang-Trong, P. and Hollnack, D. 1994 The 1992 Roermond earthquake, the Netherlands, and its aftershocks. *Geologie en Mijnbouw* 73: 181–197
- Cameron, T.D.J., Crosby, A., Balson, P.S., Jeffery, D.H., Lott, G.K., Bulat, J. and Harrison, D.J. 1992 United Kingdom offshore regional report: the geology of the southern North Sea. HMSO for the British Geological Survey, London, UK
- Cashman, P.H. and Ellis, M.A. 1994 Fault interaction may generate multiple slip vectors on a single fault surface. *Geology* 22: 1123–1126

References

- Chadwick, R.A. 1985 Cenozoic sedimentation, subsidence and tectonic inversion. In: Whittaker, A. (ed.) Atlas of onshore sedimentary basins in England and Wales: post-Carboniferous tectonics and stratigraphy. Blackie & Son, Glasgow, UK, pp. 61–63
- Chadwick, R.A. 1993 Aspects of basin inversion in southern Britain. *Journal of the Geological Society*, London, 150: 311–322
- Cloetingh, S. and Burov, E.B. 1996 Thermomechanical structure of European continental lithosphere; constraints from rheological profiles and EET estimates. *Geophysical Journal International* 124(3): 695–723
- Cloetingh, S. and Wortel, R. 1986 Stress in the Indo-Australian plate. *Tectonophysics* 132: 49–67
- Cloetingh, S., Wortel, R. and Vlaar, N. 1982 Evolution of passive continental margins and initiation of subduction zones. *Nature* 297: 139–142
- Cloetingh, S., Burov, E. and Poliakov, A. 1999 Lithosphere folding: Primary response to compression? (from central Asia to Paris basin). *Tectonics* 18: 1064–1083
- Cloetingh, S.A.P.L. (editor) 2000 Environmental tectonics and climate; the Netherlands Environmental Earth System Dynamics Initiative (NEESDI). *Global and Planetary Change* 27
- Cornet, F.H. and Burlet, D. 1992 Stress field determinations in France by hydraulic tests in boreholes. *Journal of Geophysical Research* 97(B8): 11829–11849
- Cornet, F.H. and Hudson, J.A. (eds.) 2003 Rock stress estimation. *International Journal of Rock Mechanics and Mining Sciences* 40(7–8): 955–1276
- Cornu, T., Schneider, F. and Gratier, J.P. 2003 3D discrete kinematic modelling applied to extensional and compressional tectonics. In: Nieuwland, D. (ed.): New insights into structural interpretation and modelling. *Geological Society Special Publication*, 212, Geological Society of London, London, UK, pp. 285–294
- Curry D. 1992 Tertiary. In: Duff, P.M.D. and Smith, A.J. (eds.) *Geology of England and Wales*. Geological Society, London, UK, pp. 389–408
- Dahlen, F.A. 1981 Isostasy and the ambient state of stress in the oceanic lithosphere. *Journal of Geophysical Research* 86: 7801–7806
- Daley, B. and Edwards, N. 1971 Palaeogene warping in the Isle of Wight. *Geological Magazine* 108(5): 399–405
- De Batist, M. and Henriët, J.P. 1995 Seismic stratigraphy of the Palaeogene offshore of Belgium, southern North Sea. *Journal of the Geological Society*, London, 152: 27–40
- De Batist, M. and Versteeg, W.H. 1999 Seismic stratigraphy of the Mesozoic and Cenozoic in northern Belgium: main results of a high-resolution reflection seismic survey along rivers and canals. *Netherlands Journal of Geosciences/Geologie en Mijnbouw* 77: 17–37
- De Jager, J., Doyle, M.A., Grantham, P.J. and Mabilard, J.E. 1996 Hydrocarbon habitat of the West Netherlands Basin. In: Rondeel, H.E., Batjes, D.A.J. and Nieuwenhuijs, W.H. (eds.), *Geology of Gas and Oil Under the Netherlands*. Kluwer Academic Publishing, Dordrecht, pp. 191–209
- De Lugt, I.R., Van Wees, J.D. and Wong, Th.E. 2003 The tectonic evolution of the southern Dutch North Sea during the Palaeogene: basin inversion in distinct pulses. *Tectonophysics* 373(1–4): 141–159
- De Mulder, E.F.J., Geluk, M.C., Ritsema, I., Westerhoff, W.E. and Wong, Th.E. 2003 De ondergrond van Nederland. *Nederlandse Organisatie voor toegepast-natuurwetenschappelijk onderzoek TNO*, 379p
- Den Hartog Jager, D.G. 1996 Fluvio-marine sequences in the Lower Cretaceous of the West Netherlands Basin: correlation and seismic expression. In: Rondeel, H.E., Batjes, D.A.J. and Nieuwenhuijs, W.H. (eds.), *Geology of Gas and Oil Under the Netherlands*. Kluwer Academic Publishing, Dordrecht, pp. 229–241
- Dirkzwager, J.B. 2002 Tectonic modelling of vertical motion and its near surface expression in the Netherlands. PhD Thesis, Netherlands Research School of Sedimentary Geology (NSG), Publ. No. 20020901, Vrije Universiteit, Amsterdam, 156p
- Dirkzwager, J.B., Van Wees, J.D., Cloetingh, S.A.P.L., Geluk, M.C., Dost, B. and Beekman, F. 2000 Geo-mechanical and rheological modelling of upper crustal faults and their near-surface expression in the Netherlands. *Global and Planetary Change* 27: 67–88
- Dronkers, A.J. and Mrozek, F.J. 1991 Inverted basins of the Netherlands. *First Break* 9(9): 409–425
- Duijndam, A.J.W. and Schonewille, M.A. 1999 Nonuniform fast Fourier transform. *Geophysics* 64(2): 539–551
- Dupin, J.M., Sassi, W. and Angelier, J. 1993 Homogeneous stress hypothesis and actual fault slip: a distinct element analysis. *Journal of Structural Geology* 15; 8: 1033–1043
- England, P. 1996 Geophysics; the mountains will flow. *Nature* 381: 23–24
- Fabricius, I.L. 2003 How burial diagenesis of chalk sediments controls sonic velocity and porosity. *AAPG Bulletin* 87(11): 1755–1778
- Ferrill, D.A. and Morris, A.P. 2003 Dilational normal faults. *Journal of Structural Geology* 25: 183–196
- Fleitout, L. and Froidevaux, C. 1982 Tectonics and topography for a lithosphere containing density heterogeneities. *Tectonics* 1: 21–56
- Foley, L., Daltaban, T.S. and Wang, J.T. 1998 Numerical simulation of fluid flow in complex faulted regions. In: Coward, M.P., Daltaban, T.S. and Johnson, H. (eds.): *Structural geology in reservoir characterization*. Geological Society Special Publication, 127, Geological Society of London, London, UK, pp. 121–132
- Ford, M., Lickorish, W.H. and Kusznir, N.J. 1999 Tertiary foreland sedimentation in the Southern Subalpine Chains, SE France: a geodynamic appraisal. *Basin Research* 11: 315–336
- Gale, A.S., Jeffery, P.A., Huggett, J.M. and Conolly, P. 1999 Eocene inversion history of the Sandown Pericline, Isle of Wight, southern England. *Journal of the Geological Society*, London, 156: 327–339
- García-Castellanos, D., Cloetingh, S.A.P.L. and Van Balen, R.T. 2000 Modelling the Middle Pleistocene uplift in the Ardennes–Rhenish Massif: thermo-mechanical weakening under the Eifel? *Global and Planetary Change* 27: 39–52
- Geluk, M.C., Duin, E.J.Th., Duser, M., Rijkers, R.H.B., Van den Berg, M.W. and Van Rooijen, P. 1994 Stratigraphy and tectonics of the Roer Valley Graben. *Geologie en Mijnbouw* 73: 129–141
- Geluk, M.C., Plomp, A. and Van Doorn, Th.H.M. 1996 Development of the Permo-Triassic succession in the basin fringe area, southern Netherlands. In: Rondeel, H.E., Batjes, D.A.J. and Nieuwenhuijs, W.H. (eds.), *Geology of Gas and Oil Under the Netherlands*. Kluwer Academic Publishing, Dordrecht, pp. 57–78
- Gephart, J.W. 1990 Stress and the direction of slip on fault planes. *Tectonics* 9(4): 845–858
- Gephart, J.W. and Forsyth, D.W. 1984 An improved method for determining the regional stress tensor using earthquake focal mechanism data: application to the San Fernando earthquake sequence. *Journal of Geophysical Research* 89: 9305–9320
- Gerling, P., Geluk, M.C., Kockel, F., Lokhorst, A. and Nicholson, R.A. 1999 “NW European gas atlas”; new implications for the Carboniferous gas plays in the western part of the southern Permian Basin. In: Fleet, A.J. and Boldy, S.A.R. (eds.): *Petroleum geology of Northwest Europe — Proceedings of the fifth conference*. Geological Society of London, London, UK, pp. 799–808
- Gillcrist, R., Coward, M.P. and Mugnier, J.L. 1987 Structural inversion and its controls: examples from the Alpine foreland and the French Alps. *Geodynamica Acta*, 1(1): 5–34

- Gölke, M. 1996 Patterns of stress in sedimentary basins and the dynamics of pull-apart basin formation. Ph.D. Thesis, Netherlands Research School of Sedimentary Geology (NSG), Publ. No. 961002, Vrije Universiteit, Amsterdam, 167p
- Gölke, M. and Coblenz, D. 1996 Origins of the European regional stress field. *Tectonophysics* 266: 11–24
- Gras, R. and Geluk, M.C. 1999 Late Cretaceous–Early Tertiary sedimentation and tectonic inversion in the southern Netherlands. *Geologie en Mijnbouw* 78: 1–19
- Grauls, D.J. and Baleix, J.M. 1994 Role of overpressures and in situ stresses in fault-controlled hydrocarbon migration: a case study. *Marine and Petroleum Geology* 11: 734–742
- Green, P.F., Duddy, I.R., Laslett, G.M., Hegarty, K.A., Gleadow, A.J.W. and Lovering, J.F. 1989 Thermal annealing of fission tracks in apatite: 4. Quantitative modelling techniques and extension to geological timescales. *Chemical Geology; Isotope Geoscience Section* 79(2): 155–182
- Groenewoud, W., Lorenz, G.K., Brouwer, F.J.J., Molendijk, R.E. 1991 Geodetic determination of recent land subsidence in The Netherlands, In: Johnson, A.I. (ed.), *Land Subsidence*. IAHS publ. 200: 463–471
- Grünthal G. and Stromeyer, D. 1994 The recent crustal stress field in Central Europe sensu lato and its quantitative modeling. *Geologie en Mijnbouw* 73: 173–180
- Grützner, J. and Mienert, J. 1999 Physical property changes as a monitor of pelagic carbonate diagenesis: An empirically derived diagenetic model for the Atlantic Ocean basins. *AAPG Bulletin* 83: 1485–1501
- Haenel, R. 1983 Geothermal investigations in the Rhenish Shield. In: Fuchs, K., von Gehlen, K., Mälzer, H., Murawski, H. and Semmel, A. (Eds.), *Plateau uplift, The Rhenish Massif, a Case History*. Springer-Verlag, Berlin, pp. 228–247
- Haimson, B. and Fairhurst, C. 1967 Initiation and extension of hydraulic fractures in rocks. *SPEJ, Society of Petroleum Engineers Journal* 7(3): 310–318
- Hansen, S. 1996 A compaction trend for Cretaceous and Tertiary shales on the Norwegian shelf based on sonic transit times. *Petroleum Geoscience* 2: 159–166
- Haq, B.U., Hardenbol, J. and Vail, P.R. 1987 Chronology of fluctuating sea levels since the Triassic. *Science* 235: 1156–1167
- Hardebeck, J.L. and Hauksson, E. 2001 Crustal stress field in southern California and its implications for fault mechanics. *Journal of Geophysical Research* 106 (B10): 21859–21882
- Heasler, H.P. and Kharitonova, N.A. 1996 Analysis of sonic well logs applied to erosion estimates in the Bighorn Basin, Wyoming. *AAPG Bulletin* 80(5): 630–646
- Heybroek, P. 1974 Explanation to tectonic maps of the Netherlands. *Geologie en Mijnbouw* 53(2): 43–50
- Hillis, R.R. 1991 Chalk porosity and Tertiary uplift, Western Approaches Trough, SW UK and NW French continental shelves. *Journal of the Geological Society, London* 148: 669–679
- Hillis, R.R. 1993 Quantifying erosion in sedimentary basins from sonic velocities in shales and sandstones. *Exploration Geophysics* 24: 561–566
- Hillis, R.R., Thomson, K. and Underhill, J.R. 1994 Quantification of Tertiary erosion in the Inner Moray Firth using sonic velocity data from the Chalk and the Kimmeridge Clay. *Marine and Petroleum Geology* 11(3): 283–293
- Hobbs, B.E., Ord, A. and Marone, C. 1990 Dynamic behaviour of rock joints. In: Barton, N. and Stephansson, O. (Eds.) *Rock Joints*. A. A. Balkema, Rotterdam, Netherlands, pp. 435–445
- Houtgast, R.F. and Van Balen, R.T. 2000 Neotectonics of the Roer Valley Rift System, the Netherlands. *Global and Planetary Change* 27: 131–146
- Houtgast, R.F., R.T. van Balen, C. Kasse and J. Vandenberghe 2003. Late Quaternary tectonic evolution and postseismic near surface displacements along the Geelen Fault (Feldbiss Fault Zone – Roer Valley Rift System, the Netherlands), based on trenching. *Netherlands Journal of Geosciences / Geologie en Mijnbouw* 82(2): 177–196
- Houtgast, R.F., Van Balen, R.T., Bouwer, L.M., Brand, G.B.M. and Brijker, J.M. 2002 Late Quaternary activity of the Feldbiss Fault Zone, Roer Valley Rift System, the Netherlands, based on displaced fluvial terrace fragments. *Tectonophysics* 352: 295–315
- Huckenholz, H.G. 1983 Tertiary volcanism of the Hocheifel area. In: Fuchs, K., von Gehlen, K., Mälzer, H., Murawski, H. and Semmel, A. (Eds.), *Plateau uplift, The Rhenish Massif, a Case History*. Springer-Verlag, Berlin, pp. 121–128
- Huyghe, P. and Mugnier, J.L. 1995 A comparison of inverted basins of the southern North Sea and inverted structures of the external Alps. In: Buchanan, J.G. and Buchanan, P.G. (eds.) *Basin inversion*. Geological Society, Special Publications No. 88, London, UK, pp. 339–353
- Illies, J.H. and Fuchs, K. 1983 Plateau uplift of the Rhenish Massif — introductory remarks. In: Fuchs, K., von Gehlen, K., Mälzer, H., Murawski, H. and Semmel, A. (Eds.), *Plateau uplift, The Rhenish Massif, a Case History*. Springer-Verlag, Berlin, pp. 1–8
- Isaac, K.P. and Plint, A.G. 1983 Discussion on Eocene sedimentation and tectonics in the Hampshire Basin and reply. *Journal of the Geological Society, London*, 140(2): 319–320
- Ito, T. and Zoback, M.D. 2000 Fracture permeability and in situ stress to 7 km depth in the KTB Scientific Drillhole. *Geophysical Research Letters* 27(2): 1045–1048
- Jaeger, J.C., and Cook, N.G.W. 1976 *Fundamentals of rock mechanics*. Chapman and Hall, London
- Japsen, P. 1993 Influence of lithology and Neogene uplift on seismic velocities in Denmark: implications for depth conversion of maps. *AAPG Bulletin* 77: 194–211
- Japsen, P. 1994 Retarded compaction due to overpressure deduced from a seismic velocity/depth conversion study in the Danish Central Trough, North Sea. *Marine and Petroleum Geology* 11(6): 715–733
- Japsen, P. 1998 Regional velocity—depth anomalies, North Sea Chalk; a record of overpressure and Neogene uplift and erosion. *AAPG Bulletin* 82(11): 2031–2074
- Japsen, P. 1999 Overpressured Cenozoic shale mapped from velocity anomalies relative to a baseline from marine shale, North Sea. *Petroleum Geoscience* 5: 321–336
- Japsen, P. 2000 Investigation of multi-phase erosion using reconstructed shale trends based on sonic data; Sole Pit axis, North Sea. *Global and Planetary Change* 24(3–4): 189–210
- Japsen, P. and Chalmers, J.A. 2000 Neogene uplift and tectonics around the North Atlantic: overview. *Global and Planetary Change* 24: 165–173
- Jones, D.K.C. 1980 The Tertiary evolution of southeast England with particular reference to the Weald. In: Jones, D.K.C. (ed.) *The shaping of Southern England*, Institute of British Geographers Special Publication 11: 13–47
- Jones, M.E., Bedford, J. and Clayton, C.J. 1984 On natural deformation mechanisms in the chalk. *Journal of the Geological Society, London*, 141: 675–683
- Kenter, J.A.M., Podladchikov, F.F., Reinders, M., Van der Gaast, S.J., Fouke, B.W. and Sonnenfeld, M.D. 1997 Parameters controlling sonic velocities in a mixed carbonate–siliciclastics Permian shelf-margin (upper San Andreas Formation, Last Chance Canyon, New Mexico). *Geophysics* 62(2): 505–520
- Klein, R. and Barr, M. 1987 Regional state of stress in western Europe. In: O. Stephansson (ed.):

References

- Proceedings of the International Symposium on Rock Stress and Rock Stress Measurements, Centek, Lulea, Sweden, pp. 33–45
- Kooi, H., Hettema, M. and Cloetingh S. 1991 Lithospheric dynamics and the rapid Pliocene–Quaternary subsidence phase in the southern north sea basin. *Tectonophysics*, 192(3–4): 245–259
- Kooi, H., Johnston, P., Lambeck, K., Smither, C. and Molendijk, R. 1998 Geological causes of recent (~100 yr) vertical land movements in the Netherlands. *Tectonophysics* 299: 297–316
- Krantz, R.W. 1991 Measurements of friction coefficients and cohesion for faulting and fault reactivation in laboratory models using sand and sand mixtures. *Tectonophysics* 188: 203–207
- Kuszniir, N.J. and Bott, M.H.P. 1977 Stress concentration in the upper lithosphere caused by underlying visco-elastic creep. *Tectonophysics* 43: 247–256
- Lake, S.D. and Karner, G.D. 1987 The structure and the evolution of the Wessex Basin, southern England: and example of inversion tectonics. *Tectonophysics* 137: 347–378
- Langanaecker, V. 1998 The Campine Basin, stratigraphy, structural geology, coalification and hydrocarbon potential for the Devonian to Jurassic. Ph.D. thesis Katholieke Universiteit Leuven, Leuven, Belgium
- Letsch, W.J. and Sissingh, W. 1983 Tertiary stratigraphy of The Netherlands. *Geologie en Mijnbouw* 62: 305–318
- Lippolt, H.J. 1983 Distribution of volcanic activity in space and time. In: Fuchs, K., von Gehlen, K., Mälzer, H., Murawski, H. and Semmel, A. (Eds.), Plateau uplift, The Rhenish Massif, a Case History. Springer-Verlag, Berlin, pp. 112–120
- Lister, C.R. 1975 Gravitational drive on oceanic plates caused by thermal contraction. *Nature* 257: 663–665
- Liu, L. and Zoback, M.D. 1997 Lithospheric strength and intraplate seismicity in the New Madrid seismic zone. *Tectonics* 16(4): 585–595
- Lokhorst, A. (ed.) 1998 The Northwest European gas atlas. Netherlands Institute of Applied Geosciences TNO, Haarlem, The Netherlands, ISBN 90-72869-60-5
- Magara, K. 1976 Thickness of removed sedimentary rocks, paleopore pressure, and paleotemperature, southwestern part of Western Canada basin. *AAPG Bulletin* 60: 554–566
- Mallet, J.L. 1992 GOCAD; a computer aided design program for geological applications. NATO ASI Series, Series C: Mathematical and Physical Sciences 354: 123–141
- Mallon, A.J. and Swarbrick, R.E. 2002 A compaction trend for non-reservoir North Sea Chalk. *Marine and Petroleum Geology* 19(5): 527–539
- Malservisi, R., Gans, C. and Furlong, K.P. 2003 Numerical modeling of strike-slip creeping faults and implications for the Hayward fault, California. *Tectonophysics* 361: 121–137
- Martinez-Diaz, J.J. 2002 Stress field variation related to fault interaction in a reverse oblique-slip fault: the Alhama de Murcia fault, Betic Cordillera, Spain. *Tectonophysics* 356: 291–305
- Mathiesen, A., Bidstrup, T. and Christiansen, F.G. 2000 Denudation and uplift history of the Jameson Land Basin, East Greenland — constrained from maturity and apatite fission track data. *Global and Planetary Change* 24: 275–301
- Meskó, A. 1989 Bevezetés a geofizikába. Tankönyvkiadó, Budapest, Hungary, 510p
- Michon L. and Van Balen, R.T. 2004 Characterisation and quantification of active faulting in the Roer Valley Rift System based on high precision Digital Elevation Models. *Quaternary Science Reviews*, in press
- Michon, L., Van Balen, R.T., Merle, O. and Pagnier, H. 2003 The Cenozoic evolution of the Roer Valley Rift System integrated at a European scale. *Tectonophysics* 367: 101–126
- Monié, P. and Philippot P. 1989 Mise en évidence de l'âge Eocène moyen du métamorphisme de haute pression dans la nappe ophiolitique du Mont Viso (Alpes occidentales) par la méthode 39Ar—40Ar, *C. R. Acad. Sci. Paris*, 309: 245–251
- Monsen, K. 2001 Acoustic velocity in fractured rock. *Journal of Geophysical Research* 106(B7): 13261–13267
- Moos, D. and Zoback, M.D. 1983 In situ studies of velocity in fractured crystalline rocks. *Journal of Geophysical Research* 88(B3): 2345–2358
- Morris, A., Ferrill, D.A. and Henderson, D.B. 1996 Slip-tendency analysis and fault reactivation. *Geology* 24(3): 275–278
- Müller, G., Zoback, M.L., Fuchs, K., Mastin, L., Gregersen, S., Pavoni, N., Stephansson O. and Ljunggren, C. 1992 Regional patterns of tectonic stress in Europe. *Journal of Geophysical Research* 97: 11783–11803
- Nalpas, T., Le Douaran, S., Brun, J.P., Unternehr, P. and Richert, J.P. 1995 Inversion of the Broad Fourteens Basin (offshore Netherlands), a small-scale model investigation. *Sedimentary Geology* 95: 237–250
- Nieto-Samaniego, A.F. and Alaniz-Alvarez, S.A. 1997 Origin and tectonic interpretation of multiple fault patterns. *Tectonophysics* 270: 197–206
- Nieuwland, D.A. and Walters, J.V. 1993 Geomechanics of the South Furious Field; an integrated approach towards solving complex structural geological problems, including analogue and finite-element modelling. *Tectonophysics* 226(1-4): 143–166
- Nyland, B., Jensen, L.N., Skagen, J., Skarpnes, O. and Vorren, T. 1992 Tertiary uplift and erosion in the Barents Sea: magnitude, timing and consequences. In: Larsen, R.M., Brekke, H., Larsen, B.T. and Talleraas, E. (eds.) Structural and tectonic modelling and its application to petroleum geology. NPF Special Publication 1, Norwegian Petroleum Society (NPF), pp. 153–162
- Oudmayer, B.C. and De Jager, J. 1993 Fault reactivation and oblique-slip in the southern North Sea. In: Parker, J.R. (ed.): Petroleum geology of Northwest Europe — Proceedings of the fourth conference. Geological Society of London, London, UK, pp. 1281–1290
- Pace, B., Boncio, P. and Levecchia, G. 2002 The 1984 Abruzzo earthquake (Italy): an example of seismogenic process controlled by interaction between differently oriented synkinematic faults. *Tectonophysics* 350: 237–254
- Pascal, C. 1998 Etude mécanique et modélisation de la fracturation en extension, application au domaine de la Mer du Nord. Unpublished Ph.D. Thesis, Sciences de la Terre, Univ. P. and M. Curie, Paris, 410pp
- Pascal, C. and Angelier, J. 2003 Sortan, an analytical method to determine fault slip as induced by stress. *Mathematical Geology* 35(5): 627–642
- Pascal, C. Angelier, J. Seland, R.T. and Lepvrier, C. 2002 A simplified model of stress-slip relationships: application to the Frøy field, northern North Sea. *Tectonophysics* 357: 103–118
- Pettijohn, F.J. 1984 Sedimentary rocks, 3rd edition, CBS Publishers and Distributions, Delhi, India, pp. 628
- Plenefisch, T. and Bonjer, K.P. 1997 The stress field in the Rhine Graben area inferred from earthquake focal mechanisms and estimation of frictional parameters. *Tectonophysics* 275: 71–97
- Plint, A.G. 1982 Eocene sedimentation and tectonics in the Hampshire Basin. *Journal of the Geological Society, London*, 139: 249–254
- Poix, O. 1998 Sonic anomalies, a measure to quantifying overpressures. — Overpressures in petroleum exploration; Proc. Workshop, Pau, April 1998. — Bull. Centre Rech. Elf Explor. Prod., Mém. 22: 207–211
- Pollard, D.D., Saltzer, S.D. and Rubin, A.M. 1993 Stress inversion methods: are they based on faulty assumptions? *Journal of Structural Geology*, 15: 8:

- 1045-1054
- Prodehl, C., Mueller, St., Glahn, A., Gutscher, M., and Haak, V. 1992 Lithospheric cross sections of the European Cenozoic rift system. *Tectonophysics* 208: 113-138
- Racero-Baena, A. and Drake, S.J. 1996 Structural style and reservoir development in the West Netherlands oil province. In: Rondeel, H.E., Batjes, D.A.J. and Nieuwenhuis, W.H. (eds.) *Geology of gas and oil under the Netherlands*. Royal Geological and Mining Society of the Netherlands (KNGMG), Kluwer Academic Publisher, Dordrecht, The Netherlands, pp. 211-227
- Ramaekers, J.J.F. 1991 The Netherlands. In: Hurgtig, E., Cermak, V., Haenel, R. and Zui, V. (Eds.), *Geothermal Atlas of Europe*. Hermann Haack Verlagsgesellschaft mbH, Gotha.
- Ranalli, G. 1987 Rheology of the Earth. Deformation and flow processes in geophysics and geodynamics. Allen & Unwin, Boston
- Ranalli, G. 1992 Average lithospheric stress induced by thickness changes: a linear approximation. *Physics of the Earth and Planetary Interiors* 69: 263-269
- Ranalli, G. 1995 Rheology of the Earth. Chapman and Hall, London, UK, 413p
- Rebañ, S., Philip, H. and Taboada, A. 1992 Modern tectonic stress field in the Mediterranean region; evidence for variation in stress directions at different scales. *Geophysical Journal International* 110: 106-140
- Reches, Z. 1987 Determination of the tectonic stress tensor from slip along faults that obey the Coulomb yield criterion. *Tectonics* 6: 849-861
- Richardson, G., Vorren, T.O. and Tørudbakken, B.O. 1993 Post-Early Cretaceous uplift and erosion in the southern Barents Sea: a discussion based on analysis of seismic interval velocities. *Norsk Geologisk Tidsskrift* 73: 3-20
- Richardson, R.M. and Coblenz, D.D. 1994 Stress modelling in the Andes: constraints on the South American intraplate stress magnitudes. *Journal of Geophysical Research* 99: 22015-22025
- Richardson, R.M., and Solomon, S.C. 1979 Tectonic stress in the plates. *Reviews of Geophysics and Space Physics* 17(5): 981-1019
- Rijkers, R.H.B. and Duin, E.J.Th. 1994 Crustal observations beneath the southern North Sea and their tectonic and geological implications. *Tectonophysics* 240: 215-224
- Ritter, J.R.R., Jordan, M., Christensen, U.R. and Achauer, U. 2001 A mantle plume below the Eifel volcanic fields, Germany. *Earth and Planetary Science Letters* 186: 7-14
- Rohrman, M., Van der Beek, P., Andriessen, P. and Cloetingh, S. 1995 Meso-Cenozoic morphotectonic evolution of southern Norway: Neogene domal uplift inferred from apatite fission track thermochronology. *Tectonics* 14: 700-714
- Rondeel, H.E. and Everaars, J.S.L. 1993 Spanning in noordoost Nederland, een breakoutanalyse. In: Eindrapport multidisciplinair onderzoek naar de relatie tussen gaswinning en aardbevingen in Noord-Nederland. Het Koninklijk Nederlands Meteorologisch Instituut (KNMI)
- Rummel F. 1986 Stresses and tectonics of the upper continental crust — a review. In: Stephansson, O. (Ed.) *Rock stress and rock stress measurements [international symposium on rock stress and rock stress measurements [Stockholm, September 1-3], proceedings]*: Centek Publishers, Stockholm, p. 177-184
- Sassi, W. and Faure, J.L. 1997 Role of faults and layer interfaces on the spatial variation of stress regimes in basins: inferences from numerical modelling. *Tectonophysics* 266: 101-119
- Sassi, W., Colletta, B., Bale, P. and Paquereau, T. 1993 Modelling of structural complexity in sedimentary basins; the role of pre-existing faults in thrust tectonics. *Tectonophysics* 226(1-4): 97-112
- Scholle, P.A. 1977 Chalk diagenesis and its relation to petroleum exploration; oil from chalks, a modern miracle? *AAPG Bulletin* 61: 982-1009
- Schreiber, U. and Rotsch, S. 1998 Cenozoic block rotation according to a conjugate shear system in central Europe — indications from palaeomagnetic measurements. *Tectonophysics* 299: 111-142
- Slater, J.G. and Christie, P.A.F. 1980 Continental stretching: an explanation of post-mid-Cretaceous subsidence of the central North Sea Basin. *Journal of Geophysical Research* 85(B7): 3711-3739
- Sibson, R.H. 1974 Frictional constraints on thrust, wrench and normal faults. *Nature* 249: 542-544
- Sibson, R.H. 1985 A note on fault reactivation. *Journal of Structural Geology* 7(6): 751-754
- Sibson, R.H. 1994 Crustal stress, faulting and fluid flow. In: Parnell, J. (Ed.) *Geofluids: Origin, Migration and evolution of Fluids in Sedimentary Basins*. Geological Society Special Publications 78: 69-84
- Skagen, J.I. 1992 Methodology applied to uplift and erosion. *Norsk Geologisk Tidsskrift* 72: 307-311
- Skar, T. 2000 The influence of intraplate stresses on basin subsidence and fluid pressure; Evolution of Haltenbakken, Mid-Norwegian margin. Ph.D. Thesis, Netherlands Research School of Sedimentary Geology (NSG), Publ. No. 20000802, Vrije Universiteit, Amsterdam, 147p
- Small, R.J. 1980 The Tertiary geomorphological evolution of south-east England: an alternative interpretation. In: Jones, D.K.C. (ed.) *The shaping of Southern England*, Institute of British Geographers Special Publication 11: 49-70
- Suppe, J. 1985 Principles of structural geology. Prentice-Hall, Inc, New Jersey.
- Talwani, M. and Eldholm, O. 1977 Evolution of the Norwegian-Greenland sea. *Geological Society of America Bulletin* 88(7): 969-999
- Tenthorey, E., Cox, S.F. and Todd, H.F. 2003 Evolution of strength recovery and permeability during fluid—rock reaction in experimental fault zones. *Earth and Planetary Science Letters* 206: 161-172
- Tilton, G.R., Schreyer, W. and Schertl, H.P. 1991 Pb-Sr-Nd isotopic behavior of deeply subducted crustal rocks from the Dora Maira Massif, Western Alps, Italy: II. What is the age of the ultrahigh-pressure metamorphism? *Contributions to Mineralogy and Petrology* 108: 22-33
- TNO-NITG, 1999 Geological Atlas of the Subsurface of the Netherlands: Explanation to mapsheet XV: Sittard-Maastricht, Utrecht, 127pp
- TNO-NITG, 2001 Geological Atlas of the Subsurface of the Netherlands: Explanation to mapsheets XIII and XIV: Breda-Valkenswaard and Oss-Roermond, Utrecht, 149pp
- TNO-NITG, 2002 Geological Atlas of the Subsurface of the Netherlands: Explanation to mapsheets VII and VIII: Noordwijk-Rotterdam and Amsterdam-Gorinchem. Utrecht, 135pp
- TNO-NITG, 2003 Geological Atlas of the Subsurface of the Netherlands: Explanation to mapsheets XI and XII: Middelburg-Breskens and Roosendaal Terneuzen, Utrecht, 107pp
- Twiss, R.J. and Moores, E.M. 1992 Structural geology. Freeman Co., New York
- Underhill, J.R. and Paterson, S. 1998 Genesis of tectonic inversion structures: seismic evidence for the development of key structures along the Purbeck-Isle of Wight Disturbance. *Journal of the Geological Society, London*, 155: 975-992
- Vågnes, E., Gabrielsen, R.H. and Haremo, P. 1998 Late Cretaceous-Cenozoic intraplate contractional deformation at the Norwegian continental shelf: timing, magnitude and regional implications. *Tectonophysics* 300: 29-46
- Van Adrichem Boogaert, H.A. and Kouwe, W.F.P. 1997 Stratigraphic nomenclature of the Netherlands, revision and update by RGD and NOGEP. Mededelingen Rijks Geologische Dienst, Haarlem, The Netherlands
- Van Balen, R.T., Houtgast, R.F. and Cloetingh, S.A.P.L. 2004 Neotectonics of The Netherlands.

References

- Quaternary Science Reviews, in press
- Van Balen, R.T., Van Bergen, F., de Leeuw, C., Pagnier, H., Simmelink, H., Van Wees, J.D. and Verweij, J.M. 2000 Modelling the hydrocarbon generation and migration in the West Netherlands Basin, the Netherlands. *Geologie en Mijnbouw/Netherlands Journal of Geosciences* 79(1): 29–44
- Van Balen, R.T., Verweij, J.M., Van Wees, J.D., Simmelink, H., Van Bergen, F. and Pagnier, H. 2002 Deep subsurface temperatures in the Roer Valley Graben and the Peelblock, the Netherlands — new results. *Netherlands Journal of Geosciences/Geologie en Mijnbouw* 81(1): 19–26
- Van den Berg, M.W. 1994 Neotectonics of the Roer Valley rift system. Style and rate of crustal deformation inferred from syn-tectonic sedimentation. *Geologie en Mijnbouw* 73: 143–156
- Van den Berg, M.W., Groenewoud, W., Lorenz, G.K., Lubbers, P.J., Brus, D.J. and Kroonenberg, S.B. 1994 Patterns and velocities of recent crustal movements in the Dutch part of the Roer Valley rift system. *Geologie en Mijnbouw* 73: 157–168
- Van Hoorn, B. 1987 Structural evolution, timing and tectonic style of the Sole Pit inversion. *Tectonophysics* 137: 239–284
- Van Wees, J.D. and Cloetingh, S. 1996 3D flexure and intraplate compression in the North Sea basin. *Tectonophysics* 266: 343–359
- Van Wees, J.D. and Stephenson, R. 1995 Quantitative modelling of basin and rheological evolution of the Iberian Basin (central Spain); implications for lithospheric dynamics of intraplate extension and inversion. *Tectonophysics* 252: 163–178
- Van Wees, J.D., Orlic, B., Van Eijs, R., Zijl, W., Jongerius, P., Schreppers, G.J., Hendriks, M. and Corriu, T. 2003 Integrated 3D geomechanical modelling for deep subsurface deformation; a case study of tectonic and human-induced deformation in the eastern Netherlands. In: Nieuwland, D. (ed.): *New insights into structural interpretation and modelling*. Geological Society Special Publication, 212, Geological Society of London, London, UK, pp. 313–328
- Van Wijhe, D.H. 1987 Structural evolution of inverted basins in the Dutch offshore. *Tectonophysics*, 137: 171–219
- Van Wijhe, D.H., Lutz, M. and Kaasschieter, J.P.H. 1980 The Rotliegend in The Netherlands and its gas accumulations. *Geologie en Mijnbouw* 59(1): 3–24
- Vandenbergh, N., Laga, P., Steurbaut, E., Hardenbol, J. and Vail, P.R. 1998 Tertiary sequence stratigraphy at the southern border of the North Sea Basin in Belgium. *Mesozoic and Cenozoic Sequence Stratigraphy of European Basins*, SEPM Special Publication No. 60: 119–154
- Vernik, L. and Nur, A. 1992 Petrophysical classification of siliciclastics for lithology and porosity prediction from seismic velocities. *AAPG Bulletin* 76: 1295–1309
- Verweij, J.M. 2003 Fluid flow systems analysis on geological timescales in onshore and offshore Netherlands. Ph.D. Thesis, Netherlands Institute of Applied Geoscience TNO, Utrecht, The Netherlands, 278p
- Wallace, R.E. 1951 Geometry of shearing stress and relation to faulting. *Journal of Geology* 59: 118–130
- Winstanley, A.M. 1993 A review of the Triassic play in the Roer Valley Graben, SE onshore Netherlands. In: Parker, J.R. (ed.): *Petroleum geology of Northwest Europe — Proceedings of the fourth conference*. Geological Society of London, London, UK, pp. 595–607
- Woodridge, S.W. and Linton, D.L. 1955 Structure, surface and drainage in south-east England. George Philip, London, UK
- Worum, G. and Michon, L. 2004 Implications of continuous structural inversion in the West Netherlands Basin for understanding controls on Palaeogene deformation in NW Europe. *Journal of the Geological Society*, London, in press
- Worum, G., Michon, L., Van Balen, R.T., Van Wees, J.D., Cloetingh, S. and Pagnier, H. 2004 Pre-Neogene controls on present-day fault activity in the West Netherlands Basin and Roer Valley Rift System (southern Netherlands): role of variations in fault orientation in a uniform low-stress regime. *Quaternary Science Reviews*, in press
- Worum, G., Van Wees, J.D., Bada, G., Van Balen, R.T., Cloetingh, S.A.P.L. and Pagnier, H. 2004 Slip tendency analysis as a tool to constrain fault reactivation: a numerical approach applied to 3-D fault models in the Roer Valley Rift System (South-east Netherlands). *Journal of Geophysical Research* (109), B02401, doi: 10.1029/2003.JB002586
- Yamaji, A. 2000 The multiple inverse method: a new technique to separate stresses from heterogeneous fault-slip data. *Journal of Structural Geology* 22: 441–452
- Yin, Z.M. and Ranalli, G. 1992 Critical stress difference, fault orientation and slip direction in anisotropic rocks under non-Andersonian stress systems. *Journal of Structural Geology* 14(2): 237–244
- Yin, Z.M. and Ranalli, G. 1995 Estimation of the frictional strength of faults from inversion of fault-slip data: a new method. *Journal of Structural Geology* 17(9): 1327–1335
- Zagwijn, W.H. 1989 The Netherlands during the Tertiary and the Quaternary: a case history of Coastal Lowland evolution. *Geologie en Mijnbouw* 68: 107–120
- Ziegler, P.A. 1987 Late Cretaceous and Cenozoic intraplate compressional deformations in the Alpine foreland — a geodynamic model. *Tectonophysics* 137: 389–420
- Ziegler, P.A. 1990 Geological Atlas of Western and Central Europe, second and completely revised edition. Shell Int. Petr. Mij, The Hague, The Netherlands
- Ziegler, P.A. 1992 North Sea rift system. *Tectonophysics* 208: 55–75
- Ziegler, P.A. 1994 Cenozoic rift system of western and central Europe: an overview. *Geologie en Mijnbouw* 73: 99–127
- Ziegler, P.A., Schmid, S.M., Pfiffner, A. and Schönborn, G. 1996 Structure and evolution of the Central Alps and their northern and southern foreland basins. In: Ziegler, P.A. and Horvath, F. (eds) *Peri-Tethys Memoir 2: Structure and Prospects of Alpine Basins and Forelands*. *Mém. Mus. natn. Hist. nat.* 170: 211–233
- Ziegler, P.A., Van Wees, J.D. and Cloetingh, S. 1998 Mechanical controls on collision-related compressional intraplate deformation. *Tectonophysics* 300: 103–129
- Zijerveld, L., Stephenson, R., Cloetingh, S., Duin, E. and Van den Berg, M.W. 1992 Subsidence analysis and modelling of the Roer Valley Graben (SE Netherlands). *Tectonophysics* 208: 159–171
- Zoback, M.L. 1992 Stress field constraints on intraplate seismicity in Eastern North America. *Journal of Geophysical Research* 97 (B8): 11761–11782
- Zoback, M.D. and Haimson, B.C. (eds.) 1983 Hydraulic fracturing stress measurements; proceedings of a workshop, December 2-5, 1981. *Natl. Acad. Press*. Washington, DC, United States, 269p
- Zoback, M.D. and Healy, J.H. 1992 In situ stress measurements to 3.5 km depth in the Cajon Pass scientific research borehole; implications for the mechanics of crustal faulting. *Journal of Geophysical Research* 97(B4): 5039–5057
- Zoback, M.L. and Zoback, M.D. 1980 Faulting patterns in north-central Nevada and strength of the crust. *Journal of Geophysical Research* 85: 275–284
- Zoback, M.L., Anderson, R.E. and Thompson, G.A. 1981 Cainozoic evolution of the state of stress and style of tectonism of the Basin and Range Province of the Western United States. In: Vine, F.J. and Smith, A.G. (Eds.), *Extensional Tectonics Associated with Convergent Plate Boundaries*. *Philos. Trans. R. Soc. Lond. Ser. A: Math. Phys. Sci.*, vol. 300. Royal Society of London, London, U.K., 1454p